AGARD-CP-481

AGARD-CP-481

AD-A229 161

AGARD

ADVISORY GROUP FOR AEROSPACE RESEARCH & DEVELOPMENT

7 RUE ANCELLE 92200 NEUILLY SUR SEINE FRANCE

AGARD CONFERENCE PROCEEDINGS No.481

Applications of Superconductivity to Avionics

(Les Applications de la Supraconductivité
dans le Domain de l'Avionique)

DTIC
ELECTE
DEC 0 3 1990
S B D

NORTH ATLANTIC TREATY ORGANIZATION

DISTRIBUTION AND AVAILABILITY
ON BACK COVER

NORTH ATLANTIC TREATY ORGANIZATION

ADVISORY GROUP FOR AEROSPACE RESEARCH AND DEVELOPMENT

(ORGANISATION DU TRAITE DE L'ATLANTIQUE NORD)

AGARD Conference Proceedings No.481

Applications of Superconductivity

to Avionics

(Les Applications de la Supraconductivité
dans le Domain de l'Avionique)

The Mission of AGARD

According to its Charter, the mission of AGARD is to bring together the leading personalities of the NATO nations in the fields of science and technology relating to aerospace for the following purposes:

— Recommending effective ways for the member nations to use their research and development capabilities for the common benefit of the NATO community;

— Providing scientific and technical advice and assistance to the Military Committee in the field of aerospace research and development (with particular regard to its military application);

— Continuously stimulating advances in the aerospace sciences relevant to strengthening the common defence posture;

— Improving the co-operation among member nations in aerospace research and development;

— Exchange of scientific and technical information;

— Providing assistance to member nations for the purpose of increasing their scientific and technical potential;

— Rendering scientific and technical assistance, as requested, to other NATO bodies and to member nations in connection with research and development problems in the aerospace field.

The highest authority within AGARD is the National Delegates Board consisting of officially appointed senior representatives from each member nation. The mission of AGARD is carried out through the Panels which are composed of experts appointed by the National Delegates, the Consultant and Exchange Programme and the Aerospace Applications Studies Programme. The results of AGARD work are reported to the member nations and the NATO Authorities through the AGARD series of publications of which this is one.

Participation in AGARD activities is by invitation only and is normally limited to citizens of the NATO nations.

Theme

Recent advances in developing high temperature superconductors have renewed interest in the entire superconductivity field. Modern techniques in materials preparation are making it possible to fabricate a number of new superconducting components which promise significant improvements in the performance of avionics systems. The almost daily revelation of advances in this area attests to its importance as an emerging technology. This Specialists' Meeting brought together device scientists and avionics engineers to explore the possibilities for exploiting all aspects of superconductivity in avionics systems.

Thème

Les dernières réalisations dans le domaine des supraconducteurs à haute résistance thermique sont à l'origine d'un renouveau d'intérêt dans le sujet de la supraconductivité pris dans son ensemble

Les techniques modernes de préparation des matériaux permettent de fabriquer un certain nombre de nouveaux composants supraconducteurs qui devraient amener des améliorations importantes en ce qui concerne les performances des systèmes avioniques.

Les annonces presque quotidiennes d'avances dans ce domaine témoignent de son importance en tant que technologie naissante.

Cette réunion de spécialistes a rassemblé les experts en composants et les ingénieurs en avionique pour qu'ils puissent examiner ensemble les possibilités qui existent d'exploiter tous les aspects de la supraconductivité dans les systèmes avioniques.

A-1

Avionics Panel

Chairman: Dr Richard Klemm
FFM—FGAN
Neuenahrer Str. 20
D-5307 Wachtberg 7
Germany

Deputy Chairman: Eng. Jose M.G.B.Mascarenhas
C-924
c/o Cinciberlant Hq
2780 Oeiras
Portugal

TECHNICAL PROGRAMME COMMITTEE

Chairman: Mr William E.Howell
Advanced Transport Operating Systems Program Office
NASA Langley Research Center
Mail Stop 265
Hampton, VA 23665
United States

Mr Jean Michel Brice
Directeur Technique
B.P. 123
38521 St. Egreve Cedex
France

Col. F.Corbisier
Hq AAFCE (BE) PART
Ramstein Air Base
D-6792 Ramstein-M3
Germany

Mr Jean Dansac
Directeur Scientifique
Thomson-CSF. Division Activités
   Optroniques (D.A.O.)
52, rue Guynemer
92132 Issy-les-Moulineaux
France

Dr Geoffrey H.Hunt
ADRMS
Royal Aerospace Establishment
Farnborough, Hants. GU14 6TD
United Kingdom

Dr Ron W.MacPherson
A/DS POL
Dept. of National Defence
MGen George R.Pearkes Bldg
Ottawa, Ontario, K1A 0K2
Canada

Dr R.Voles
Chief Scientist
Thorn EMI Electronics Ltd
120 Blythe Road
Hayes, Middx, UB3 1DJ.
United Kingdom

Dr David C.Baird
Dean of Science
Royal Military College
Kingston, Ontario K7K 5L0
Canada

Mr P.K.Blair
Racal Decca Advanced Dev. Ltd
North Weylands Industrial Est.
Molesey Road
Walton-on-Thames
Surrey KT12 3PL
United Kingdom

Dr Jerry A Wilson
Santa Barbara Research Center
75 Coromar Drive
Goleta, CA 93117
United States

Dr Gérard Creuzet
Chef du Laboratoire d'Analyse
   Physique
Thomson CSF LCR
91404 Orsay Cedex
France

Mr P.Nedellec
Centre de Spectrometrie Nucleaire
   et Spectrométrie de Masse
Bâtiment 108
91405 Orsay
France

Dr Patrick Hemenger
AFWAL MLPO
Wright Research & Development
   Center
OH 45433-6533
United States

Dr Martin M.Sokoloski
NASA Headquarters
Code RC
Washington D.C. 20546
United States

AVIONICS PANEL EXECUTIVE

Lt Colonel James E.Clay

Mail from Europe:
AGARD—OTAN
Attn: AVP Executive
7, rue Ancelle
92200 Neuilly sur Seine
France

Mail from US and Canada:
AGARD—NATO
Attn: AVP Executive
APO New York 09777

Tel: 33(1) 47 38 57 65
Telex: 610176 (France)
Telefax: 33(1) 47 38 57 99

Contents

---

† Not available at time of printing

SESSION V — SUMMARY

---

† Not available at time of printing.

TECHNICAL EVALUATION REPORT ON THE NATO/AGARD

AVIONICS PANEL'S SPECIALISTS' MEETING

APPLICATIONS OF SUPERCONDUCTIVITY TO AVIONICS

Bath, England, May 7-8, 1990

Dr. Louis C. Ianniello
Deputy Associate Director for
Basic Energy Sciences
U.S. Department of Energy
Washington, D.C. 20585

SUMMARY

This meeting on superconductivity was very timely in view of the discovery of a new class of higher temperature superconductors in 1986. All of the relevant topics relating to potential applications of interest to AGARD were covered, although in limited depth. The papers were mostly well prepared and provided the participants with an excellent overview of the field. The discussion revealed that substantial superconductivity applications for avionics continue to be in the future and that some difficult long-term research is required before the superconductivity potential can be realized.

THEME OF THE MEETING

Since the discovery in 1986 of high temperature oxide superconductors by Bednorz and Muller, for which they later received the Nobel Prize in Physics, there has been a great deal of increased activity in superconductivity. The objective of this meeting was to bring together device scientists and avionics engineers to review recent progress made and to explore the possibilities for exploiting superconductivity in avionics systems. The field of superconductivity, which is not a new field, having been created in 1911 with the discovery of the phenomenon by K. Onnes, has seen alternating periods of optimism and pessimism. During the euphoric period following the discovery of high temperature superconductors, with materials being discovered with superconducting temperatures as high as 125K, many potential applications were discussed. In planning the meeting, it was believed that the modern techniques of materials preparation and characterization would enable some relatively rapid progress towards device applications and, therefore, the purpose of the meeting was to expose elements of the avionics community to this progress in a timely manner. As the meeting demonstrated and this report indicates, the field of superconductivity once again is in a period of intense research with slower than expected progress towards applications.

TECHNICAL INFORMATION

The meeting was logically organized over a 2-day period. Twenty-two papers were listed on the program, and twenty were presented. There were sessions on: (1) An Introduction to Superconductivity; (2) Status of Superconducting Electronic Devices; (3) Use of Superconductivity in Sensors; (4) Superconducting Large Scale Devices; and (5) A Summary Panel Discussion.

In the first session, the speakers provided the science foundation for superconducting applications for both the newer high temperature materials and the low temperature superconductors. It was pointed out that the oxide superconductors are more complex, and not fully understood, but basically behave similarly to the older metallic low temperature superconductors. One important feature of the new high temperature superconductors is that they are anisotropic, which introduces problems in conductor or film preparation. A present obstacle is the low critical current density; but progress is being made, although slower than had been expected. Cryogenic temperatures are still required despite progress in high temperature superconductivity. An interesting new miniature closed cycle refrigerator was discussed, but life test data is limited to date.

The next session explored the use of superconductivity for electronic devices such as microwave antennas, filters, cavities, transmission lines, oscillators, and computer elements. These applications for superconductors all have to compete with existing materials/devices. For microwave applications, although the potential is large, the difficulty with maintaining very low temperatures has presented obstacles to actual applications. With the discovery of high temperature superconductors, the future is more attractive not only because of the decreased problems of low temperature, but also because of the broadening of the energy-gap. This might allow for smaller losses and higher operating frequencies. With regard to computer elements, good progress has been made with the lower temperature materials, and there is some promise for increasing the memory density using multi-layered structures.

The third session focused on sensor applications. Areas reviewed included: accelerometers, gyroscopes, infra-red detectors, and magnetometers. It was pointed out that critical current density is not as important as well prepared films for most of these applications. Characterization of films is an important aspect of present developments in high temperature superconductivity and ac magnetic susceptibility holds some promise for this requirement. Precision accelerometers are possible based on the magnetic shielding effect or the magnetic levitation effect in superconductors. High temperature SQUIDs can be introduced for high sensitivity magnetometers using the natural weak-links of the new oxide materials, it was pointed out.

Large-scale superconducting devices were discussed during the fourth session. Such devices as motors, generators, transformers, and transmission lines would provide advantages over existing devices in energy efficiency, weight, and space. The low temperature superconducting materials have been used to construct many of these devices and they are becoming closer to reality. The new oxide materials will require more research to increase their current carrying capacity and to overcome the brittle nature of the materials.

In the summary session, some pessimism was expressed over the future of superconductivity applications in view of the need for reliable cryogenic equipment and the lack of developments in the electronics area beyond the two-terminal devices. Materials which can be superconducting at ambient temperatures would, of course, change the situation. Additional research may also enhance the usefulness of the present materials, but it appears to require a long-term outlook.

RECOMMENDATION

The subject of superconductivity and potential applications of it is an old subject, but it was worthy of an AGARD meeting to examine the impact of the newly discovered high temperature superconductors. It wasn't possible to foresee the leveling off of progress, but that apparently is what the meeting showed. From now on, unless there are new breakthroughs, there will be some difficult research ahead. The meeting was structured to cover the entire field. In the future, a more focused meeting on special AGARD issues would be more fruitful in view of the already large number of general superconductivity meetings elsewhere.

PROGRESS IN HIGH T_c SUPERCONDUCTORS

R.G.Humphreys, N.G.Chew, S.W.Goodyear, J.A.Edwards, J.S.Satchell, and S.E.Blenkinsop

Royal Signals and Radar Establishment, St Andrews Road, Malvern, Worcs. WR14 3PS, U.K.

SUMMARY.

The high temperature superconductor materials are introduced, and their properties relating to applications reviewed, with particular reference to the prospects for fabrication of devices. Recent results on the factors relating to the growth of smooth high quality $YBa_2Cu_3O_7$ thin films are presented.

1. INTRODUCTION

Since the first high temperature superconductor (HTS) was reported over three years ago[1], much has been learnt about their properties, and many new materials discovered. Other papers at this meeting will discuss the wide range of potential applications in avionics. In this paper, we focus on the materials issues which relate to the fabrication of devices, initially looking broadly at the general state of the art, and then presenting some specific results on the requirements for growth of high quality $YBa_2Cu_3O_7$ films.

2. THE MATERIALS AND THEIR PROPERTIES

A great many high temperature superconducting compounds have now been discovered, and it would serve no useful purpose to attempt to review them all. All are mixed metal oxides, and all contain at least one element whose concentration can be varied to adjust the carrier concentration, analogous to doping in semiconductors. The optimum carrier concentrations of high temperature superconductors are in the region of one carrier per unit cell, so the "doping" levels are very high by semiconductor standards. All the HTS materials with high critical temperatures (T_c) are Cu containing layer compounds, with highly anisotropic properties.

Table 1

Compound	Brief name	T_c
$YBa_2Cu_3O_7$	YBCO	93
$Bi_2Sr_2Ca_2Cu_3O_{10}$	BiSCCO	110
$Tl_2Ba_2Ca_2Cu_3O_{10}$	TIBCCO	125

Each layer contains a metal atom, usually with some oxygen, and the stacking sequence of the metals can be changed by varying the composition and/or the preparation conditions. There are three basic materials systems which are favoured for applications: the highest T_c members of each family are listed in table 1.

Of these, the most developed material is YBCO. This is a relatively simple system: although it can form in two other stacking sequences, it is comparatively easy to control which of them is formed under defined preparation conditions. The other two compounds listed are members of rather complicated materials systems, with many different stacking sequences possible, and the preparation conditions determining which is favoured are rather subtle. It is often quite difficult to obtain phase pure material, therefore. This is perhaps less important in the TIBCCO system than in the BiSCCO system, because many of the members of the TIBCCO system have high T_c's, while formation of the wrong phase in the BiSCCO system leads to a reduction of T_c to around 80K. On the other hand, the TIBCCO system is difficult to work with because of the volatility of the Tl and its high toxicity. At least in the short term, many of the protoype devices will be based on YBCO, because the material is easier to work with, and seems to pin flux more effectively than the others, leading to higher critical current densities (J_c).

The materials systems listed above all have positive Hall coefficients in the normal state, indicating that the carriers are holes. A simplistic view of this observation is encouraged by the fact that they are all highly oxidised. Another class[2] of otherwise similar superconductors has been found with negative Hall coefficients, which are reduced to induce conducting behaviour. These materials at

present have only shown relatively low critical temperatures, but deserve a mention because they indicate another relatively new avenue for searching for new superconductors with high T_c.

Despite enormous theoretical effort to understand the microscopic mechanism responsible for superconductivity in these materials, a consensus solution to the problem has not yet been found. Most theoreticians remain convinced that the mechanism is not the phonon one responsible for low T_c superconductivity. Any hope of predicting the maximum T_c which can be obtained in the future must wait for such an understanding. At present, the most successful inventors of new materials systems are crystal chemists, relying on a feel for valence, bonding and structure.

Nevertheless, it is remarkable that most of the experimentally determined parameters show behaviour close to that predicted by the BCS theory which describes low T_c superconductors. Much of this may be due to the fact that Landau–Ginzburg theory, which depends on little else than the transition to the superconducting state being a second order one with a single (complex scalar) order parameter, predicts similar results, and a knowledge of the mechanism is not essential for a phenomenological understanding of many properties. The second order nature of the transition means that the superconducting properties vary smoothly towards the normal state properties as the temperature approaches T_c. It is therefore necessary to cool superconducting devices significantly below T_c for good performance: the margin required depends on the device, and those applications requiring a large margin will favour using the material with the highest possible T_c.

The critical fields and characteristic lengths of the high T_c superconductors are generally agreed on to within reasonable margins. Table 2 gives approximate values for the characteristic lengths in nm of YBCO at low temperature, taken from Schneider and Frick[3]. The two columns refer to directions with respect to the c axis of the crystal structure.

Table 2

	//c	⊥c
London length	700	140
Coherence length	0.5	2.5

The London length is similar to the skin depth, but is nearly independent of frequency, and is defined with respect to the direction in which the shielding current flows. The coherence length is the "size" of a Cooper pair. The coherence length normal to the planes is less than a unit cell dimension, showing that the superconducting carriers are localised to a particular part of the lattice. All these lengths increase with temperature, and become large near T_c. The short coherence lengths are expected to have consequences for the

performance of tunnel junctions. The theory is not well worked out, but the boundary conditions and quality of the the surface atomic layers may be much more important than in low T_c superconductors. This is compounded by the low carrier densities of HTS, with the consequence that charge trapped at the surface or in the insulator may substantially modify the properties of the surface atomic layers.

Perhaps the most important parameter which has not been unequivocally measured is the magnitude of the superconducting energy gap. Tunneling measurements continue to give poor current–voltage characteristics, with an apparent gap which depends on the preparation conditions[4]. Infra–red experiments do not offer a solution either. This has been interpreted[5] as being due to the very short coherence lengths of the high T_c superconductors, with the consequence that they are in the clean limit, so that any IR absorption is weak.

3. MATERIALS TECHNOLOGIES

There are three broad classes of materials technology which are aimed at different applications areas. The most obvious is the high power regime, where superconducting coils are required to produce high magnetic fields. This demands large amounts of well controlled material (e.g. wire or tape) which can be formed into a desired shape and is capable of sustaining large currents at high magnetic fields. Large currents can only be sustained in superconductors by inhibiting motion of the flux lines which pass through the material. This is dependent on the presence of material defects. The detailed investigation and understanding of flux pinning and flow are still controversial. In particular, the very low critical currents seen in some superconductors at high temperature has been interpreted in a number of ways, and the solution is still uncertain.

Low temperature superconductors are almost invariably made in the form of randomly oriented polycrystals, with no detriment to the superconducting properties. This is not the case for high temperature superconductors. This is a very important difference between the high and low temperature superconductors, and deserves some discussion. Early work using randomly oriented material showed that it was very easy to obtain high T_c's, but the current carrying capacity was limited, and dropped dramatically on applying a magnetic field. Such material would clearly not be useful for making magnets. It has now been shown[6] the the critical current of high quality ceramic wires is limited to these low values by the self field. This is in strong contrast to epitaxial thin films, where values obtained are very much larger than for bulk material (millions of A/cm² at 77K), and are much less sensitive to applied magnetic fields[7]. The weak links in bulk ceramic are the grain boundaries, whose critical current density is a function of the misorientation angle

between grains[8]. Efforts to improve the current carrying capacity have therefore concentrated on producing textured material. This is possible in a large number of ways, and it is not clear which will be the best technique for producing materials for applications. The best values[9] (10^4 A/cm^2 at 77K in 1T) at present come from melt texturing techniques[9,10], which produce nearly single crystal material in centimeter dimensions. It remains to be seen whether these techniques will scale to large sizes.

At the other end of the material technology spectrum, single crystal thin films depositied epitaxially on single crystal substrates are needed for the low power applications in electronics (a wide range of Josephson junction based devices, microwave filters, delay lines). High quality films have been grown by laser ablation, sputtering, evaporation (MBE) and MOCVD. The subject is too extensive to deal with here: we have recently reviewed it elsewhere[11]. Films can be put down either as amorphous material, which is subsequently annealed to give superconducting films, or directly as crystalline material. Post-annealed films can have reasonably high critical current densities and be epitaxial, but such material is polycrystalline and usually has rough surfaces. The high T_c phases of BiSCCO and TIBCCO have only been made in this way. The highest quality HTS films made so far are YBCO, and are single crystal, with smooth surfaces.

In between the two, many applications (e.g. cavities, shields, circuits, antennae) require material in larger sizes than can be envisaged using single crystal substrates, but may still best be filled using material supported on a substrate, and crystallographically oriented on it. This thick film area has not received as much attention as it merits, although progress has been made recently in this area. For example, a novel electrophoretic technique using magnetic field alignment[12] has been shown to give improved microwave properties, and a technique involving partial melting has yielded textured films with critical current densities which are much less sensitive to applied magnetic field than randomly oriented material[13].

As we shall hear later in this conference, many of the applications in avionics will be in passive microwave components. These are expected to be practical rather soon, since the properties that have already been demonstrated represent a large improvement on what can be achieved with normal metals. The surface resistance depends on the square of the frequency, in contrast to normal metals which show an approximate square root dependence, so that a convenient figure of merit for a superconductor is the frequency at which its loss equals that of Cu at 77K (the cross-over frequency). The properties of high quality randomly oriented bulk material are surprisingly good: a number of groups have reported cross-over frequencies in excess of 10GHz, while

values for single crystals and epitaxial thin films imply cross-over frequencies over 200 GHz. The data on this subject are often only reported at conferences, and so are not very accessible; an excellent review has been given by Muller[14].

There is a large range of potential applications using active devices based on Josephson junctions. There is still no report of the manufacture of a deliberately made tunnel junction with good properties. Although many groups are working towards this, it seems probable that to achieve the technology will require sustained effort for some time to come. The first tunneling results on an all-epitaxial high T_c SIS structure have recently been reported[15], and similar SNS structures have also been made[16]. It is encouraging that such complex structures could be made within three years of the material being discovered, and underlines the point that epitaxial growth of these materials is unexpectedly easy. The clarity of the tunneling characteristics were poor, and there were indictions that the material T_c was degraded near the junction. The SNS structures were thicker, and show good electrical properties.

Perhaps the most promising indication that active devices will turn out to have useful performance are the results obtained on SQUID's, which use accidental grain boundaries as their weak links. The best of these show noise levels comparable to commercially available helium temperature SQUID's (17).

4. THE IMPORTANCE OF COMPOSITION CONTROL IN THIN FILM GROWTH

We now move from the general review to the discussion of a particular case of the materials technology from our own work, which gives an idea of the precision which is needed to produce the material needed for devices. Of the techniques used for producing thin films, laser ablation[18] and single target sputtering[19] can both produce films close to the optimum composition from a stoichiometric source, a contributory factor to the rapid progress made using these methods. In contrast, evaporation [20-22] and multiple target sputtering[23,24] require careful stabilization and control of individual metal deposition rates to obtain the required composition, but are then better suited to systematic studies of the effect of composition on film properties. It is important that the effect of small variations in film composition be quantified, since the phase width is unknown and finite deviations from exact stoichiometry are inevitable in all deposition techniques. It is also likely that some non-uniformity will be introduced when processes are scaled to larger area substrates. We have used evaporation from the metals in the presence of activated oxygen to carry out a systematic study of the correlation between composition, transport properties, structure and surface morphology in YBa$_2$Cu$_3$O$_7$ films. The aim is to optimise simultaneously the electrical properties and the

morphology of films.

Films were deposited in an ultra high vacuum evaporator using electron beam heated sources for Y, Ba and Cu metals. Evaporation rates were stabilized using a single multiplexed mass spectrometer to sample each metal flux adjacent to the substrate. The substrates used were polished (001) oriented MgO single crystals. MgO was chosen because of its acceptable dielectric properties, but it has the drawback that it yields lower critical current densities than some other substrates[19]; so far as we are aware the highest value reported to date is $3.5 \ 10^6$ A/cm^2 at $77K^{25}$. The substrate temperature was 690C. The platen was rotated during growth to ensure uniformity. Oxygen (molecular with ~10% atomic) was admitted to the system at the rate of 2sccm and partially confined by a silica cylinder in the region of the substrate to give a pressure of ~2 10^{-4} mbar at the film surface. After growth, the films were cooled in a pressure estimated to be ~10^{-2}mbar, containing ~10 % atomic oxygen. Considerable care is needed in measuring and controlling the substrate temperature and in quantifying the atomic oxygen flux: these issues have been discussed extensively elsewhere[11]. Here it is sufficient to note that the temperature and pressure were chosen to be in regions where the film properties are insensitive to small fluctuations in these parameters. More details of the growth technique will be discussed elsewhere.

Values of critical temperature and critical current density for the films were obtained using four terminal resistance measurements on laser delineated[26] tracks 300um long and 12um wide The voltage criterion for J_c was 1uV. The c axis lattice parameters (c_0) and widths of the 007 reflections were measured using an x-ray diffractometer in Bragg-Brentano geometry. The 007 line shapes were fitted using a pair of Lorenzians to represent the Cu $K_{\alpha 1}$ and $K_{\alpha 2}$ X-ray lines, and are given as the full width at half maximum of the Lorenzian, expressed as an uncertainty in c_0. All the films were epitaxially oriented with respect to their substrates, as shown by reflection high energy electron diffraction (RHEED). They were predominantly c-oriented, as shown by X-ray diffraction. The films were superconducting with high T_c as grown, but all the data presented were measured after annealing at 500C in 1 atmosphere of oxygen, to minimise any scatter in the data due to incomplete oxygenation.

In the absence of information on the phase diagram under the growth conditions, two composition scans were chosen: varying Cu content at constant Ba/Y ratio, and varying Ba/Y ratio at constant Cu content. The absolute calibration of the composition axes is deduced from the data discussed below. We find that the film properties are dependent on variations from the optimum composition that are near or beyond the absolute accuracy limit of commonly used analysis techniques such as Rutherford backscattering
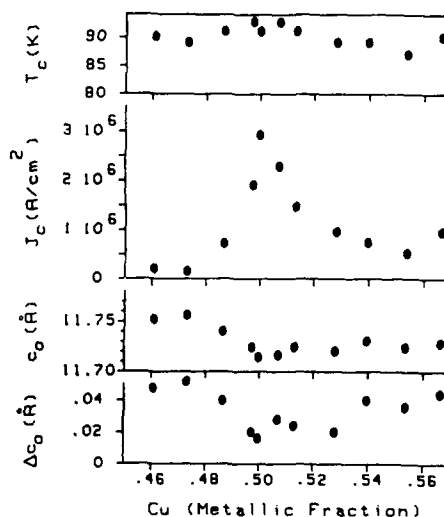
Fig. 1. T_c, J_c, c-axis lattice parameter and width of the 007 X-ray reflection plotted as functions of Cu content expressed as the atomic metallic fraction.

spectrometry (RBS) or energy dispersive x-ray analysis.

The effect of varying the Cu content, for a Ba Y atomic ratio of 2.22 ± 0.05 (on the calibration determined below), is shown in Fig 1. Of the parameters plotted, the critical current density at 77K is the one most sensitive to composition, showing a sharp peak with a value of -3 10^6 A/cm^2. The critical temperature is barely affected by quite large variations in the Cu content. As the Cu content is reduced from the optimum value there is a rapid degradation in J_c and a corresponding rapid increase in c_0 and 007 peak width. An increasing Cu content results in a slower reduction in J_c, a slower increase in 007 peak width, and little change in c_0. Thus excess Cu is less detrimental to film transport and structural properties than Cu deficiency. It has been assumed that the composition which gives the "best" properties corresponds to a Cu atomic metallic fraction of 0.5 in calibrating the horizontal axis of Fig.1.

Corroborative evidence for this assignment is offered by the variation in surface morphology in this region. Fig. 2a shows a scanning electron micrograph of a sample which has a slight excess of Cu The lumps in this image are optically transparent, and not easily detected in X-ray diffraction. We identify them as a randomly oriented Cu rich second phase: a higher density of these precipitates is observed in samples containing
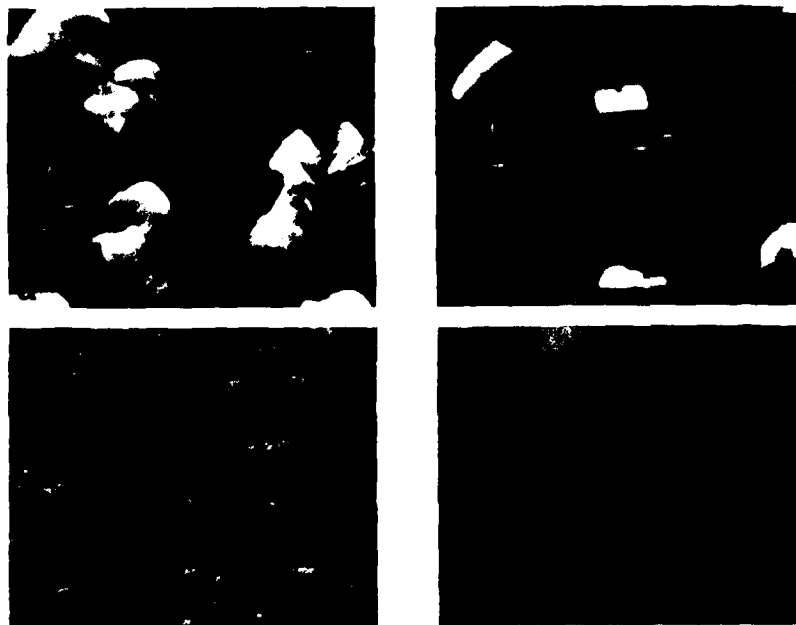
Fig. 2. Scanning electron microscope images of three films with varying Cu content (0.515, 0.5. and 0.485 atomic fraction of the metals for a, b and c respectively). d is an image of a film close to exact stoichiometry.

a greater excess of Cu. Segregation into discrete precipitates is consistent with the insensitivity of T_c and c_0 to large amounts of excess Cu, although some reduction in the critical current density would be expected. Fig. 2b shows the surface morphology of the "best" sample of this scan. A few of the lumps characteristic of excess Cu are still visible. This suggests that this film was slightly Cu rich, and hence that the absolute calibration of Fig. 1 is slightly in error. Fig. 2c shows a sample slightly deficient in Cu. The lumps are no longer present, and a pitted morphology characteristic of all our Cu deficient samples is observed.

The effect of varying the Ba/Y ratio with constant Cu fraction is shown in Fig 3. For these data, as in the case of Fig. 1, the horizontal axis has been translated such that the "best" data points coincide with a stoichiometric metal content, i.e. a Ba/Y ratio of 2. The scan in varying Ba/Y ratio was chosen to be at a Cu fraction corresponding to the peak in Fig. 1 to within $\pm.005$. Second phase lumps characteristic of excess Cu were present at a low number density, similar to Fig. 2b, in all of the samples of Fig. 3. It is evident that the range over which high J_c is observed is much wider than it is in Fig. 1. A sharp decrease

in both T_c and J_c values occurs as the Ba/Y ratio is increased above optimum; this is reflected in increased values of c_0 and 007 peak width. At Ba/Y ratios below the optimum value a more gradual degradation in film properties is observed, until the excess Y content is quite large. Beyond this point, films show drastically reduced J_c, while the other parameters show no marked change in behaviour. This is consistent with a transition to a granular morphology, as observed by Kwo et al. [22]. Surface roughness on a much finer scale was found to correlate with Ba/Y ratio. Smooth surfaces were obtained for Ba/Y$\leq$2, while Ba/Y$>$2 led to inclusion of a-oriented material and surface roughening. Qualitatively similar correlations over a more limited range of Ba/Y ratios were found in ref. 23.

Using the results above, it became apparent that the varying Cu scan had been carried out for a Ba/Y ratio which was non-optimum. This might be the source of the slight disagreement ($\sim.01$ atomic metallic fraction) between the "best" Cu content indicated by transport properties and surface morphology. From the data, it was inferred that the desired combination of good transport properties with smooth surfaces would be obtained with a Ba/Y ratio of 2 on the calibration
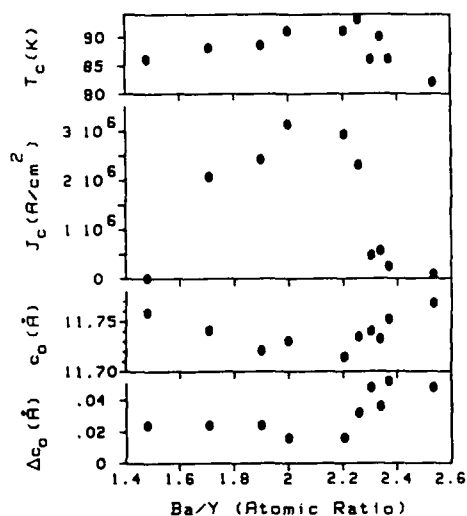
Fig. 3. T_c, J_c, c-axis lattice parameter and width of the 007 X-ray reflection plotted as functions of Ba/Y ratio.

of Fig. 3, and a Cu content very slightly less ($\sim$.01) than that calibrated as 0.5 in Fig. 1. The morphology of a film close to this composition is shown in Fig. 2d. The surface is smooth except for slight pitting, suggesting a very small deficiency of Cu. A streaked RHEED pattern was obtained from this sample. This film had a T_c of 92K and a J_c of 3.2 10^6 A/cm^2 at 77K, the highest value we have measured, and similar to the best reported value for films on MgO substrates.

The data presented above demonstrate that there is a well defined composition where T_c and J_c reach their highest values and c_0, 007 peak width and surface roughness are minimised. Significant degradation from the optimum values can occur for small changes in cation ratios, at the limit of accuracy of the present experiments. These data provide a basis for defining the composition control and uniformity required to produce films with a particular set of properties. Furthermore, with reproducible growth equipment, it is possible using the present results to identify deviations from the optimum composition rapidly and accurately using the surface morphology alone.

References

1. J.G.Bednorz and K.A.Muller, Z. Phys. B 64, 189 (1986)
2. Y.Tokura, H.Takagi and S.Uchida, Nature 337, 345 (1989)
3. T. Schneider and M.Frick, Springer series in Solid State Sciences 89, 176 (1989)
4. J.Geerk, G.Linker, O.Meyer, Q.Li, R.-L.Wang and X.X.Xi, Physica C162-4, 837 (1989)
5. K.Kamaras, S.L.Herr, C.D.Porter, N.Tache, D.B.Tanner, S.Etemad, T.Venkatesan, E.Chase, A.Inam, X.D.Wu, M.S.Hegde and B.Dutta, Phys. Rev. Lett. 64, 84 (1990)
6. N.McN.Alford, T.W.Button, C.E.Gough, F.Wellhofer, D.A.O'Connor, M.S.Colclough, R.J.Pollard and D.G.McCartney, J. App. Phys. 66, 5930 (1989)
7. J.S.Satchell, R.G.Humphreys, N.G.Chew, J.A.Edwards and M.J.Kane, Nature 334, 331 (1988)
8. J.Mannhart, P.Chaudhari, P.Dimos, C.C.Tseui and T.R.McGuire, Phys. Rev. Lett. 61, 2476 (1988)
9. M.Murakami, M.Morita, K.Doi and K.Miyamoto, Japan. J. App. Phys. 28, 1189 (1989)
10. S.Jin, T. H. Tiefel, R.C.Sherwood, M.E.Davis, R.B.van Dover, G.W.Kamlott, R.A.Fastnacht and Keith, App. Phys. Lett. 52, 2074 (1988)
11. R.G.Humphreys, J.S.Satchell, N.G.Chew, J.A.Edwards, S.W.Goodyear, S.E.Blenkinsop, O.D.Dosser and A.G.Cullis. Supercond. Sci Tech 3, 38 (1990)
12. M.Hein, G.Muller, H.Piel, L.Ponto, M.Becks, U.Klein and M.Peiniger, J. App. Phys. 66, 5940 (1989)
13. J.S.Abell, T.C.Shields, F.Wellhofer, K.N.R.Taylor and D.Holland, Physica C162-4,1265 (1989) and N. McN. Alford (private communication)
14. G.Muller Proc. 4th workshop on RF superconductivity, KEK, Tsukuba-Shi, August 1989
15. K.Hirata, K.Yamamoto, K.Iijima, J.Takada, T.Terashima, Y.Bando and H.Mazaki, App. Phys. Lett. 56, 683 (1990)
16. K.Mizuno, K.Hagashino, K.Setsune and K.Wasa App. Pys. Lett. 56, 1469 (1990)
17. R.H.Koch, W.J.Gallagher and B.Bumble, App. Phys. Lett. 54, 951 (1989)
18. T.Venkatesan, X.Wu, B.Dutta, A.Inam, M.S.Hegde, D.M.Hwang, C.C.Chang, L.Nazar and B.Wilkens, App. Phys. Lett. 54, 581 (1989)
19. X.X.Xi, G.Linker, O.Meyer, E.Nold, B.Obst, F.Ratzel, R.Smithey, B.Strehlau, F.Weschenfelder and J.Geerk, Z. Phys. B 74, 13 (1989)
20. N.Missert, R.Hammond, J.E.Mooj, V.Matijasevic, P.Rosenthal, T.H.Geballe, A.Kapitulnik, M.R.Beasley, S.S.Laderman, C.Lu, E.Garwin and R.Barton, IEEE Trans Magnetics, MAG-25,2418 (1989)
21. T.Terashima, Y.Bando, K.Iijima, K.Yamamoto and K.Hirata, App. Phys. Lett. 53, 2232 (1988)

22. J.Kwo, M.Hong, D.J.Trevor, R.M.Fleming, A.E.White, J.P.Mannaerts, R.C.Farrow, A.R.Kortan and K.T.Short, Physica C162-4, 623-4 (1989)
23. Y.Shirakawa and M.Kobayashi, Japan. J. App. Phys. 28, L1405 (1989)
24. K.Kuroda, K.Kojima, M.Tanioku, K.Yokoyama and K.Hamanaka, Japan. J. App. Phys. 28, 1797 (1989)
25. L.Schulz, B.Roas and P.Schmitt, Symposium on Processing of Films for High Temperature Superconducting Electronics, Santa Clara, October 1989, Proc. SPIE vol 1187, to be published.
26. R.G.Humphreys, J.S.Satchell, N.G.Chew and J.A.Edwards, App. Phys. Lett. 54, 75 (1989)

Discussion

Name of Author: Dr. R. Humphreys

Paper No.: 2 -- Progress in High Tc Superconductors

Name of person asking question: M. C. Green

Question

Have you considered the use of the praseodymium analogue of YBCO as an insulator layer, since it gives an excellent lattice match and is not a superconductor?

Answer

Used Y_2O_3 because when they tried it, it worked. Epitaxy very easy to achieve in YBCO system, even on Y_2O_3. Would like to have a single insulator only. Y_2O_3 a good insulator for thick layer devices. PrBCO has been made in very thin epilayers a few atomic layers thick, but people have not yet seen tunneling.

PHYSICS AND APPLICATIONS OF LOW TEMPERATURE SUPERCONDUCTIVITY

by

Dr D.C.Baird
Dean of Science
Royal Military College
Kingston, Ontario K7K 5LO
Canada

My intention is to provide a historically-based introduction to low temperature superconductivity. I shall emphasise those aspects of the basic physics that underlie the practical applications of superconductors and are significant for understanding the properties of the new high temperature superconductors.

Before proceeding we should pause for a moment to remember the founder of the subject. After first liquefying helium in 1908, Kamerlingh Onnes in Leiden, Holland, wished to investigate the electrical properties of metals at the new low temperatures. Early results on the resistivity of many metals showed a linear decrease of resistivity with temperature that ended in a constant value, called the residual resistance, as shown in Fig 1. Only mercury showed deviation from this pattern, and it appeared that, at a particular temperature, the resistance of this metal showed an abrupt change to a very low value. More detailed investigation suggested that, over a very narrow temperature range, the resistance of mercury became essentially zero, as shown in Fig 2.
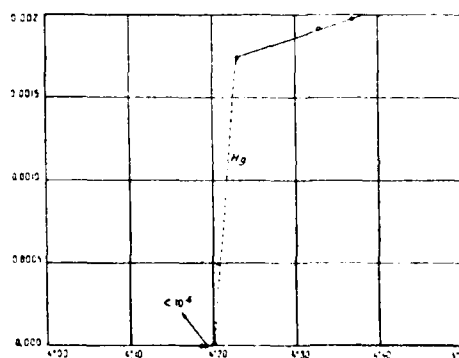
Fig 2
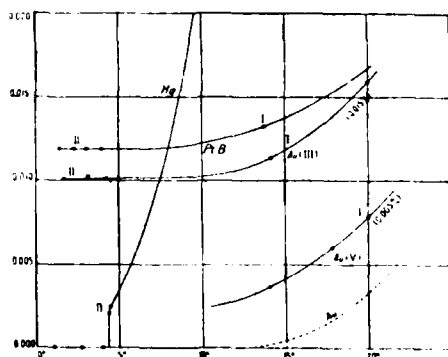
Subsequent investigation showed that the property of zero resistance was exhibited by a number of materials. There are 25 superconducting elements, with transition temperatures, T_c, ranging from 0.1K for iridium to 9.3K for niobium, and dozens of alloys and compounds with transition temperatures ranging (for the low temperature superconductors) up to 23K for Nb_3Ge and including the technologically important NbTi at 9.5K. The distribution of the superconducting elements in the peri-

Fig 1

	1A	2A	3A	4A	5A	6A	7A	← 8A →			1B	2B	3B	4B	5B	6B	7B	8B
	H																	He
	Li	Be											B	C	N	O	F	Ne
	Na	Mg											Al 1·19 99	Si	P	S	Cl	A
	K	Ca	Sc	Ti 0·39 100	V 5·30 1020	Cr	Mn	Fe	Co	Ni	Cu	Zn 0·85 52	Ga 1·09 55	Ge	As	Se	Br	Kr
	Rb	Sr	Y	Zr 0·55 47	Nb 9·15 1960	Mo 0·92 98	Tc 8·2	Ru 0·49 66	Rh	Pd	Ag	Cd 0·55 30	In 3·4 285	Sn 3·72 306	Sb	Te	I	Xe
	Cs	Ba	La 5·91 1600	Hf	Ta 4·48 830	W ~0·01	Re 1·70 198	Os 0·66 65	Ir 0·14 19	Pt	Au	Hg 4·15 412	Tl 2·39 171	Pb 7·19 803	Bi	Po	At	Rn
	Fr	Ra	Ac	Th 1·37 162	Pa	U 0·68												

Be becomes superconducting in thin-film form with T_c 6 8 K.
Bi becomes superconducting in thin-film with T_c 6 K and under high pressure with T_c 4 K.
Te becomes superconducting under high pressure with T_c 3·3 K.
Sb becomes superconducting under high pressure with T_c 2·6 K.
Fe is reported to become superconducting at 4·2 K in thin-film form.
In each box, the upper figure refers to the critical temperature in degree (From 'High-Field Superconductivity and its Applications' by J. A. Catterall, *Metallurgical Review*, Vol. 11, 1966) Kelvin, and the lower figure to the critical field at 0 K in gauss.

Fig 3

odic table is shown in Fig 3. It is obvious that they fall into two general areas of the table. On account of the physical properties of the metals they became known, respectively, as the "soft" superconductors, such as tin, lead and indium, and the "hard" superconductors, like tantalum and niobium. A more significant way of classifying superconducting materials will become clear later.

Since the superconducting state seems to be characterised by a genuinely zero value for resistivity, it is possible to observe persistent currents.
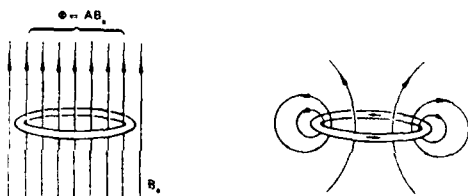
Fig 4

If, as shown in Fig 4, a ring of superconducting material is cooled through its transition temperature in the presence of a magnetic field, the material will become superconducting with a certain value of magnetic flux threading the ring. If, now, the external field is removed, circulating currents will be established in the ring that will preserve the magnetic flux in the ring at its initial value. The presence and value of the circulating currents will be detectable from the external magnetic field, and the undamped persistence of these currents has been veri-

fied over periods of years. The superconducting state seems to be one of genuinely zero resistance.

The superconducting state is, however, characterised by another property that distinguishes it from a state of mere perfect conductivity. The natural consequence of the condition R=0 (which implies E=0) is given by Maxwell's equation

$$\text{curl}\,\vec{E} = -\frac{\partial \vec{B}}{\partial t}$$

For, if E=0, we must have B=constant. This would imply that, if we cool a superconductor through its transition temperature in the presence of a magnetic field and then remove the field, the material would preserve (by circulating surface currents) the original value of the field. Actual observation, however, shows that superconductors behave differently. Rather than preserve the original value of magnetic field, the superconductor responds to the removal of the external field by ejecting the field originally threading it. This unpredicted phenomenon is called the Meissner effect, and it allows us to characterise the superconductor by the additional property B=0. A graphic illustration of the Meissner effect is the floating magnet pictured in Fig 5. The rejection of the field of the permanent magnet from the lead bowl is caused by surface currents in the superconducting lead. These simulate a "mirror" magnet, and give rise to the repulsion between the magnet

and the superconducting sur-face.

Fig 5

It is of interest to note that a magnet floating above a finite slab of traditional superconductor, such as lead, would be in only unstable equi-librium, and the demonstration illustrated in Fig 5 achieves stability from the bowl-shaped form of the lead. On the other hand, the stability of the famous illustrations of the Meissner effect in the new high temperature superconductors makes it obvious immediately that the interaction of these materials with magnetic fields must be more complicated than for lead, and must involve a mixture of flux rejection with flux penetration and trapping.

The foregoing description concerns only the existence of the superconducting state. In addition, however, it is possi-ble to observe that the state can be destroyed, not only by increasing temperature, but also by increasing magnetic field.
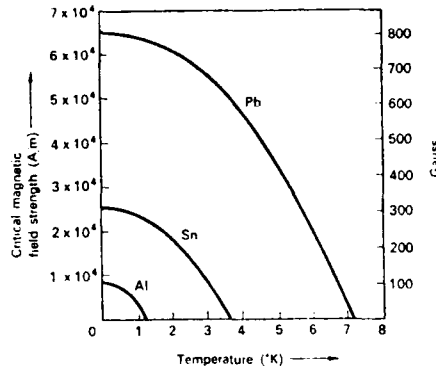
Fig 6

If we observe the resistance of a thin, needle-shaped specimen in a field parallel to its length, we find that the mag-netic field required to destroy superconductivity, H_c, is different for different ele-ments and that it varies with temperature as shown in Fig 6.

The magnetic properties of a thin, superconducting specimen can now be summarised in a B-H or M-H diagram as shown in Fig 7. As H increases from zero, the field is rejected from the specimen, the flux threading the specimen remains zero, and the corresponding magnetization grows linearly. This behaviour continues until $H=H_c$, at which point the specimen makes a sud-den transition into the normal state and the magnetization drops abruptly to zero.

Fig 7

Fig 8
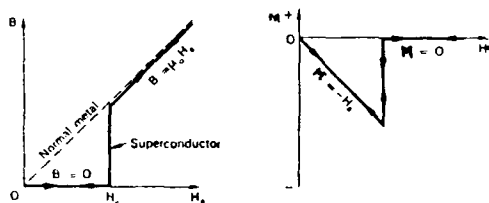
If H decreases from a higher value, the same path on the B-H or M-H diagram would be followed in reverse.

If the specimen does not have the form of a thin needle oriented along the field direction, the situation becomes more complicated. For low external fields the rejection of a magnetic field from a bulk specimen will arise from a complicated distribution of surface currents that gives rise to a field distribution that exactly cancels the field in the interior of the specimen and adds to the external field outside it, leading to the overall field distribution shown in Fig 8. It is obvious that the value of the external field at points close to the surface of the specimen differs from the field at more distant points, and also that it varies over the surface of the specimen. To take a specific example, if the diagram in Fig 8 showed a section through a circular cylinder (instead of the elliptical figure), the field at the two ends of the diameter perpendicular to the field would have a value twice
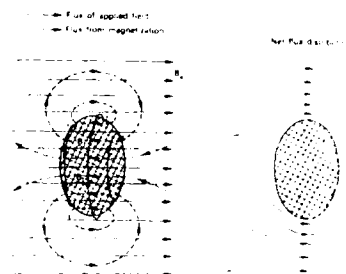
This field variation has direct relevance to the destruction of superconductivity as the external field grows. The field at the points on the diameter will reach H_C when the external field at infinity has the value $H_C/2$. At that point it is not hard to see that an ambiguous condition appears, of which the general outcome is a complicated mixture of normal and superconducting regions known as the intermediate state.

As far as the magnetic energy of the situation is concerned, it would be preferable if the specimen were to subdivide itself into an infinitely fine mesh of superconducting and normal regions. This preference, however, is offset by an additional consideration, the presence of an inter-phase surface energy between the normal and superconducting regions. The existence of this surface energy can be understood if we include in the discussion two additional concepts. The first of these is called the penetration depth, λ. It is obvious that

the surface currents that shield the interior of a super-conductor from a magnetic field cannot flow in an infinitely thin surface layer, and in the mid-1930's the phenomenological London theory for the electro-magnetic properties of super-conductors had included a calculation for the depth of the surface currents.

over a distance of the order of (in his specimens) 10^{-4}cm, and this range he called the coher-ence distance. The concept plays an important role in many aspects of superconductivity, including the properties of the new high temperature supercon-ductors.

We are now able to see how the interplay of the penetra-tion depth and the coherence distance gives rise to a surface energy. Referring to Fig 10, which shows a section through the surface region of a

Fig 9

This is also the depth to which an external magnetic field penetrates, at least to some extent, into a superconductor, and the exponential variation of penetrating field with dis-tance is illustrated in Fig 9.

The second additional con-cept is called the coherence distance, commonly designated by ξ. This concept was intro-duced by Pippard in the early 1950's in order to aid in the interpretation of his measure-ments on rf resistance of superconductors. These measurements had made it clear that the degree of order in the superconducting electrons could not change abruptly, but only

(a) Penetration depth and coherence range at boundary

(b) Contributions to free energy

(c) Total free energy

Fig 10

superconductor, we can see, first, that the demagnetization energy is lowered because the magnetic field is not excluded from the whole specimen and, second, that the electronic energy is higher because the

superconductivity does not extend right to the surface of the material. For the case $\xi > \lambda$ the net result of these two contributions to the total energy is a positive energy associated with the boundary between the superconducting and normal regions. We refer to such superconductors as Type I superconductors.

The role played by a positive surface energy in determining the structure of the intermediate state is similar to that of surface tension in soap bubbles: it limits the degree of subdivision between phases and determines the geometry of the resulting boundaries. In cases of practical importance the exact form of the intermediate state is hard to calculate, and it is best to observe the structures directly. In Fig 11 we see the upper surface of a superconducting cylinder placed in an axial magnetic field. The magnetic field is made visible by an irregularly shaped piece of paramagnetic glass that overlaps the edge of the specimen and extends to the centre of the top surface. The polarized light that is used for illumination experiences rotation of its plane of rotation in any part of the glass traversed by the magnetic field, so that superconducting regions in the pictures are dark and normal regions are bright. In the top picture the field is so low that no penetration has taken place and only the field passing the edge of the specimen is visible.

Fig 11

As the field increases, the first penetration is a static fringe of flux fingers that is followed, at yet higher fields, by flux bundles that separate from the fingers and move towards the centre until the whole specimen is filled with flux and the transition to the normal state is complete.

Many of the gross magnetic properties of superconductors can be described using nothing more than the simple considerations given above. More refined concepts are needed for other, more sophisticated, properties. For example, it had early been deduced from the London theory that the flux threading a superconductor should be restricted to multiples of a certain value. The value of this flux quantum is very low.

$$\Phi = 2 \times 10^{-15} \text{weber}$$
$$= \frac{h}{2e}$$

The quantity 2 in the expression for the flux quantum is significant, as it corresponds to the role of _pairs_ of electrons in the superconducting state, and the importance of this point will become clear when we come to consider the microscopic theory of superconductivity. On account of the smallness of the flux quantum no direct observation of flux quantization was made until the early 1960's by Deaver and Fairbank in the United States and by Doll and Näbauer in Germany. Although much more exact observations of flux quanta can now be made, the historic observations of Deaver and Fairbank are shown in Fig 12.
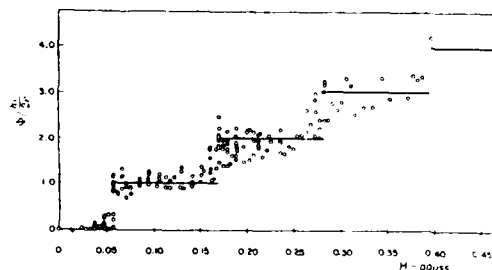
Fig 12

In addition to the destruction of superconductivity by an external magnetic field, the possibility exists that superconductivity can also be destroyed by the field produced by a current flowing in the superconductor itself. Consider a cylindrical superconductor traversed by a current, as shown in section in Fig 13. The radial dependence of the field produced by the current will be given by

$$H \propto \frac{i}{r}$$

and it is obvious that, as the current increases, the magnetic
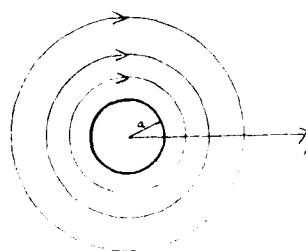
Fig 13

field will first reach the value H_c at the surface of the wire. The current at which this happens is called the critical current, usually designated i_c (with a corresponding current density j_c). When H reaches H_c at the surface of the wire it is easy to see that an unstable situation results. The wire subdivides into a mixture of superconducting and normal regions and the
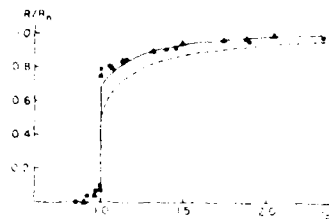
Fig 14

resistance of the wire undergoes an abrupt transition to a resistance intermediate between zero and the fully normal value, as shown in Fig 14. Phase boundaries that satisfy the boundary conditions and give rise to resistance in agreement with the observed values are shown in Fig 15,
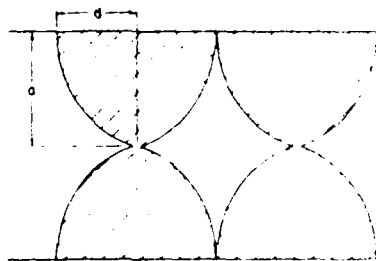
Fig 15

which shows the wire in longitudinal section. Hatched regions are normal and the clear regions are superconducting.

The preceding discussion has been *restricted to Type I* superconductors for which $\xi > \lambda$ and the surface energy is positive. Different properties appear when we consider the case of negative surface energy. If $\xi < \lambda$, as illustrated in Fig 16, the balance between the two contributions to surface energy becomes negative.
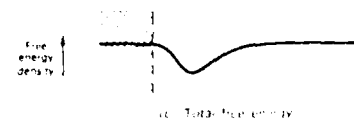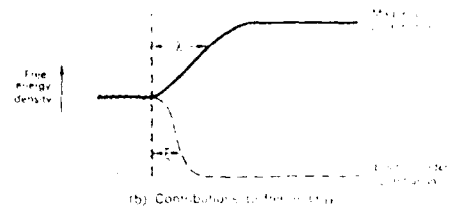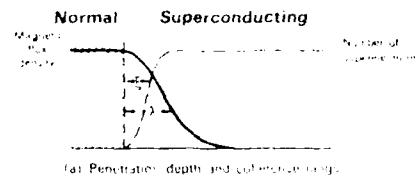
Fig 16

The materials for which this occurs are called Type II superconductors. Type II superconductivity appears in a few elements, like vanadium,

and in many alloys and compounds, of which the new high temperature superconductors are outstanding examples. In these materials it is energetically favourable for the magnetic and normal regions to be as finely subdivided as possible, and this tendency dominates their magnetic properties. The finest subdivision possible occurs when each normal region is traversed by just one flux quantum. In the presence of a magnetic field, therefore, the equilibrium configuration for a Type II superconductor is a flux line lattice, in which the superconducting order varies spatially as shown in Fig 17.
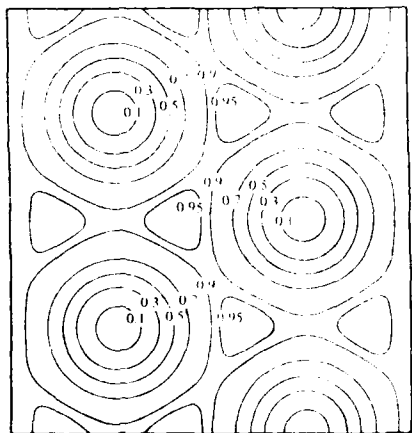
Fig 17

The normal core of each flux line is surrounded by more-or-less superconducting material that carries the supercurrent ring required to maintain the flux line. This is called the mixed state of a Type II superconductor. The flux distribu-

tion in a slab in a transverse field will, therefore, look as shown in Fig 18.
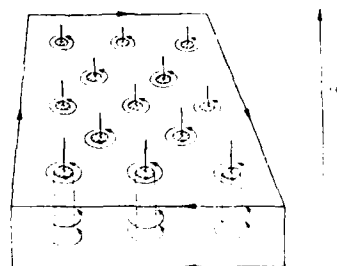
Fig 18

Direct observations of the flux line lattice have been made by many observers. Among the first were Essmann and Träuble in Germany, who used finely divided ferromagnetic particles to show the flux lines at the surface of a superconducting slab (Fig 19).
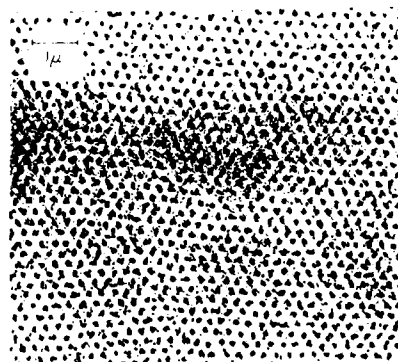
Fig 19

The process of flux invasion into an ideal Type II superconducting slab in a transverse field is now easy to imagine. The only barrier to penetration

would be the mirror image force at the surface, and, once that is overcome, each flux line would enter the material as shown in Fig 20.
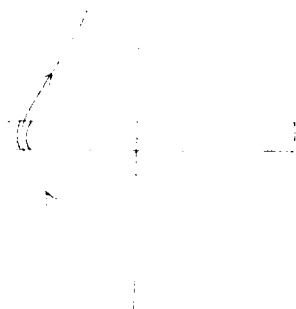
Fig 20

Once past the surface, the flux line would move inwards to take up as central a position as possible and so minimise its magnetic energy. For each value of the external field, therefore, there would arise (on the assumption of free flux line mobility) a certain equilibrium density of flux lines throughout the material. This process, too, can be observed using the magneto-optic viewing method. In Fig 21 we see the upper face of a thin niobium film. In the upper picture, flux lines have been flooding in from those points on the periphery of the film where entry was easiest, and have moved radially inwards to adopt a distribution that is close to an equilibrium structure. As the external field is raised, as shown in the lower picture, the density of the flux line distribution continues to

increase.

Fig 21

Such observations have also been made on high temperature superconductors, for which the detailed behaviour of flux is of great importance.

The magnetic behaviour of Type II superconductors can be summarized in a B-H or M-H diagram as shown in Fig 22.
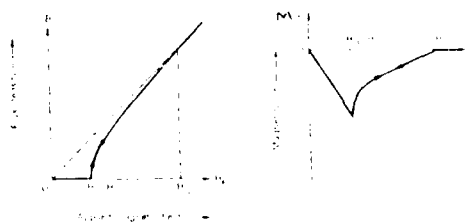
Fig 22

The superconducting state at low values of H is succeeded at a value of field called the first critical field, H_{c1}, by the long region of the mixed state that extends to a value, H_{c2}, after which the material is essentially normal. Superconductivity can, therefore, persist to very high values of magnetic field. Typical values of H_{c2} for commonly used materials are 13 Tesla for NbTi and 20 Tesla for Nb_3Sn.

The ideal magnetic behaviour that has been described for Type II superconductors is modified by factors that limit the free movement of flux lines. Such flux pinning, as it is called, arises from the presence of local areas of the material that impede the passage of a flux line and give rise to non-equilibrium conditions. For example, if flux from an increasing external field is trying to enter a specimen, it may be held up by flux pinning at the point of entry long past the field at which it would normally enter the material. This unstable condition may then be resolved by a sudden inrush of flux, called a flux jump, to a new position of quasi-equilibrium. The process is illustrated in Fig 23 which shows, initially, a specimen with minimal penetration at the edges, followed by two successive flux jumps. Such flux jumps release substantial amounts of stored energy and can be very significant in the practical application of Type II superconductors.
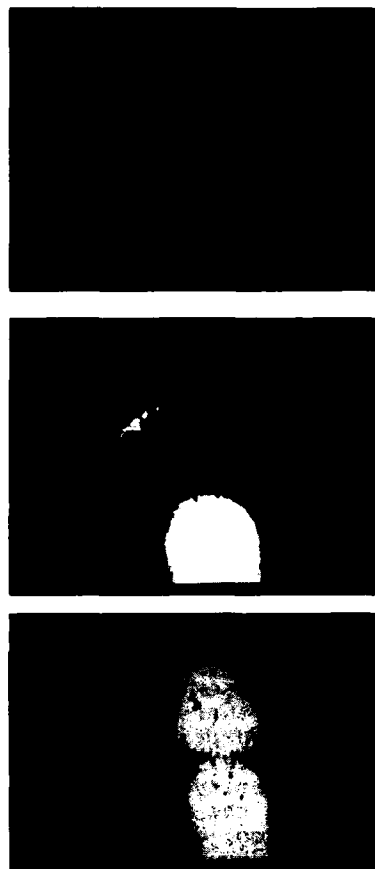
Fig 23

Since many of the applications of superconductivity involve the current-carrying capacity of the materials it is important to understand the interaction of flux lines with currents. Consider a slab, shown in Fig 24, of Type II superconductor that carries a

current and also contains flux from a transverse magnetic field.
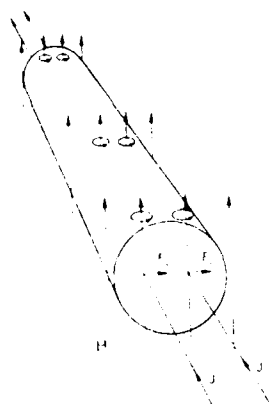
Fig 24

The ring current supporting each flux line will combine vectorially with the main current so that the magnetic field on one side of the flux line is increased and decreased on the other. The result is that the flux line will tend to move in a direction perpendicular to the current. The moving magnetic field of the flux line will, in turn, create an emf. The current flow, therefore, will be dissipative and the material will be useless for such purposes as solenoid construction. If, on the other hand, the flux lines are pinned so that they do not move in the combined presence of the external field and the current, the material will behave, even in the presence of the flux lines, as if it were wholly superconducting and free of dissipation. Such a material will be suitable for solenoid construction, and high-field superconductors were introduced, first, by Kunzler at the Bell Telephone Laboratories in 1961. These materials, notably NbTi and Nb_3Sn, are now extensively in use. Since their usefulness depends on their current-carrying capacity in the presence of a magnetic field, the properties are generally described in terms of a current-field-temperature diagram as shown in Fig 25.
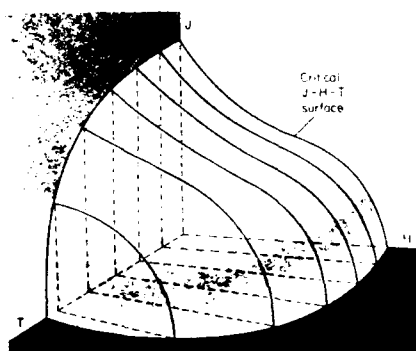
Fig 25

The region of use of the material is defined by the surface in this three-dimensional diagram. Normal conditions of use cover magnetic fields up to 5 or 10 Tesla for NbTi, with higher values for Nb_3Sn, and current densities in the range of 10^4 to 10^5 amps cm^{-2}. These figures will be of interest when we consider the properties of the new high temperature superconductors.

Actual cable for high field solenoids is generally manufactured from twisted strands of the superconducting material embedded in a copper matrix.

As a consequence of the man-
ufacturing processes the mate-
rial is provided with the
internal defects that promote
flux pinning and is also,
through the copper cladding,
protected against quenching,
the catastrophic restoration of
resistance through flux jump-
ing. A typical commercial
cable is shown in cross-section
in Fig 26.
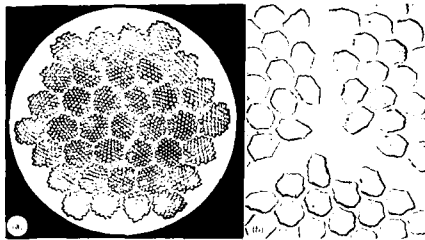
Fig 26

In both parts of the diagram
the darker NbTi filaments can
be seen embedded in the lighter
copper matrix. Superconducting
solenoids, such as those illus-
trated in Fig 27, have been
successfully employed for many
years in scientific research.
The upper picture shows a coil
designed at the Argonne
National Laboratory for use in
magneto-hydrodynamic research
and the lower picture shows the
famous "yin-yang" magnet
designed for fusion research at
the Livermore laboratory.
Superconducting solenoids are
also extensively used in medi-
cal diagnosis, and the Magnetic
Resonance Imaging system
constitutes the largest single
commercial application of
superconductivity.
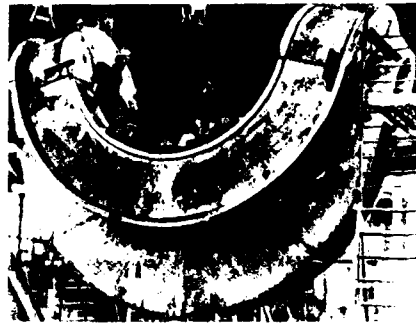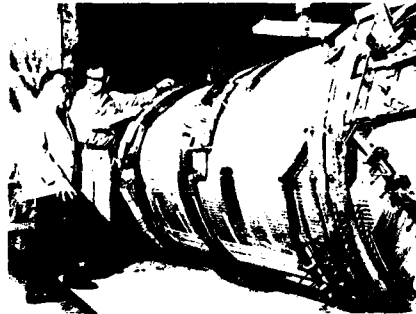
Fig 27

In addition, the development
work in Japan on high speed
ground transportation using
magnetic levitation will soon
reach fulfilment with the con-
struction of the first section
of a new passenger-carrying
link between Tokyo and Osaka
(Fig 28). The upper photograph
in Fig 28 shows the prototype
vehicle and the lower diagram
shows its construction. The
superconducting coils are
mounted in a vertical plane at
the bottom of each side of the
vehicle, and the field produced
by the coils provides both lev-
itation above the horizontal
metal strip and also propulsion

from the linear induction motor coils at the side of the track.
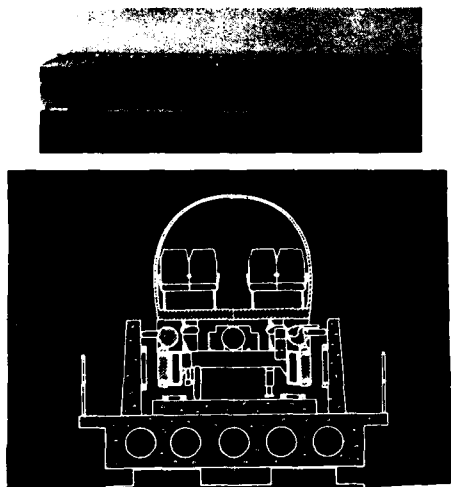
Fig 28

The NbTi coils are cooled by a storage tank of liquid helium and Fig 29 shows, in the upper picture, the self-contained coil and refrigeration unit and, in the lower picture, the coil itself. The liquid helium tank is recharged with liquid helium on a daily basis, and the whole unit is intended to be maintained and serviced by normal railroad personnel. The test vehicle carries passengers and has attained speeds up to 500 km hr^{-1}. In view of the extensive use of solenoids such as those shown above and of the Japanese experience in transportation one can confidently say that superconducting sclenoids have already reached the stage of industrial application.
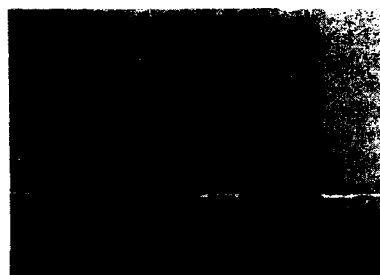
Fig 29

The applications of superconductors that have been described up to this point can be understood using relatively simple electrodynamic theory. Other applications, however, require a more detailed understanding of superconductivity at a microscopic level. The first successful attempt to construct a basic theory of superconductivity was based on work by Cooper who, in 1956, showed that, if there is any attractive interaction between electrons in a metal, no matter how small, it is possible for the electrons, in pairs, to form bound states. The energy of these bound pairs is less than that of unpaired elec-

trons, so that they will con-
stitute the ground state, which
will be separated from the
upper, unbound, states by an
energy gap. The Cooper pairs
of electrons are correlated in
momentum but are separated in
space by a distance ξ, the
coherence distance. The
coherent wave packets of the
electron pairs are immune to
the scattering mechanisms that
give rise to ordinary electri-
cal resistance, so that
resistance-free current flow
and the other familiar proper-
ties of superconductors follow
from the model. On the basis
of Cooper's proposal a detailed
theory was constructed by Bar-
deen, Cooper and Schrieffer
(BCS) in 1957. The BCS model
incorporates a pairing interac-
tion that is supplied by the
metallic lattice which, through
the polarization caused in the
lattice of positive atomic
cores by one electron, would
exercise an attractive force on
another electron as shown in
Fig 30.

from the BCS theory is the
variation of the density of
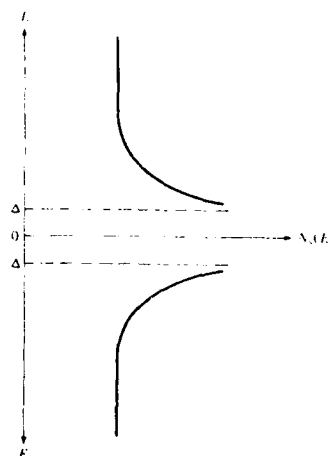
Fig 31

electronic states above and
below the energy gap. The
curve is shown in Fig 31, which
shows the superconducting
states below the energy gap and
non-superconducting states abo-
ve.The energy gap itself is one

Fig 30

One important result derived
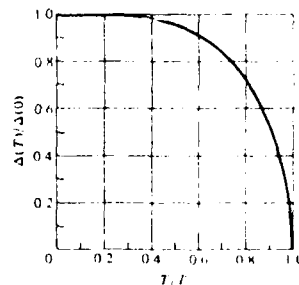
Fig 32

of the most important features of the BCS model. It turns out that the magnitude of the energy gap is dependent on temperature, and the complete curve is shown in Fig 32. The magnitude of the energy gap is also related to the transition temperature, and the well-known BCS equation relates these quantities to the fundamental properties of the lattice.

$$2\Delta(0) = 3.5 kT_c = 4\hbar\nu_D e^{-\frac{1}{N(0)V}}$$

Here $\Delta(0)$ is the magnitude of the energy gap at T=0. The properties of the lattice and the strength of the electron-electron interaction appear through the quantities ν_D, which is the Debye frequency, related to the stiffness of the lattice, and V, the magnitude of the electron interaction. Since lattice movement can be described using the concept of quantized acoustic waves, called phonons, we refer to the BCS model in terms of an electron-phonon interaction. There is no reason to suppose that such an electron-phonon interaction is the only possible interaction that can give rise to superconductivity, but on that basis the BCS model does provide a very accurate description of low temperature superconductors. In addition, it supplies guidance in the search for a model for high temperature superconductors. The equation above shows how the transition temperature is related to the physical properties of the material, and demonstrates that some interaction

stronger than the BCS phonon-mediated interaction is needed to supply the high transition temperatures of the new materials.

Our discussion of the energy gap now makes it possible to consider one of the most important properties of superconductors, electron tunneling, either between normal metals and superconductors (ns) or between two superconductors (ss). In a representation familiar from the descriptions of semiconductors, the state density of electrons (at T=0) in a normal metal (on the left) and a superconductor (on the right) are shown in Fig 33, separated by a thin layer of insulator.
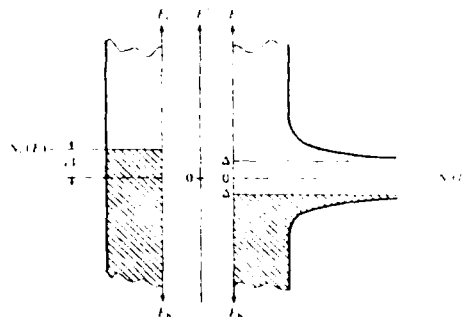
Fig 33

Clearly the variation of tunneling current with bias voltage will reflect the state density functions on the two sides of the barrier, and for the simple ns case the resulting i-v characteristic is shown in Fig 34.

energy gap on the left side of
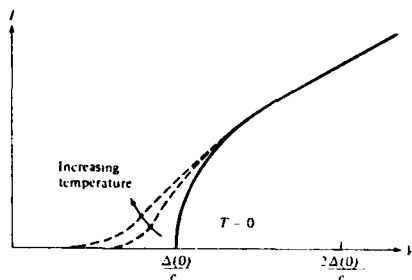
Fig 34

The state density functions for tunneling between two superconductors (at T>0) are shown in Fig 35.
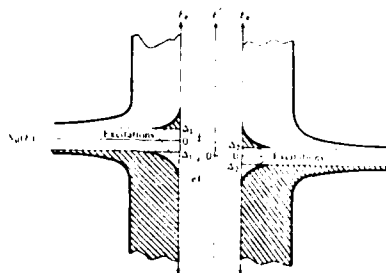
Fig 35

The i-v characteristic for ss tunneling is more complicated than for ns tunneling, and is shown in Fig 36.

Tunneling, either ns or ss, has been of great significance for the study of superconductivity, but the contribution of tunneling to superconducting applications lies in an extension of the simple concept of tunneling. If we look again at the state density curve shown in Fig 35, we can see that electrons from below the

Fig 36

the diagram that make a transition, through tunneling, to the empty states on the right that lie above the gap are making a transition from a superconducting to a normal state. This is referred to as pair breaking, and energy (from the bias voltage) must be supplied for this to take place. In 1962 it was suggested by Josephson that tunneling across an insulating gap between two superconductors could also be accomplished by intact electron pairs. Such a tunnel current would flow without dissipation and without any potential difference across the barrier. Josephson tunneling thus allows a supercurrent to bridge a narrow gap in a superconducting material and maintain coherence of the phase of the wave functions for the superconducting electron pairs across the barrier. It is, however, restricted to a certain magnitude of current, above which dissipation reappears. An idealized variation of current vs. voltage for Josephson tunneling is

shown in Fig 37.
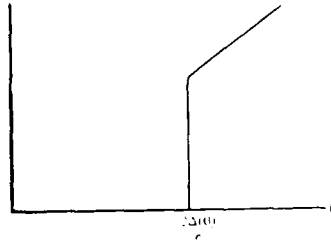
Fig 37

Such Josephson tunneling is of great importance for high temperature superconductors, in which it appears that supercurrents flow in multi-grain specimens as a consequence of Josephson tunneling at the contacts between the grains. Superconductivity can thus be observed in bulk specimens at low currents, but resistance reappears for higher currents.

We refer to the limited contact between two superconductors that can support Josephson tunneling as a weak link. Various manufactured weak links are encountered in devices, and they form an important part of the discussion of high temperature superconductors (Fig 38).
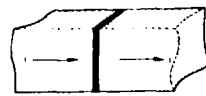
(a) Tunnelling junction
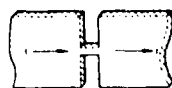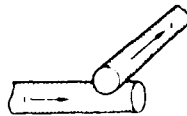
(b) Construction   (c) Point contact

Fig 38

Josephson tunneling is the basis, also, of one of the most significant applications of low temperature superconductivity, the use of Josephson devices to measure very low magnetic fields.   The penetration of a magnetic field into the barrier region, across which a supercurrent is flowing by Josephson tunneling, affects very markedly the i-v characteristic of the junction and also introduces other effects at microwave frequencies. These are brought into practical application in the form of a two-junction circuit known as a Superconducting QUantum Interference Device (SQUID) which is illustrated in Fig 39.
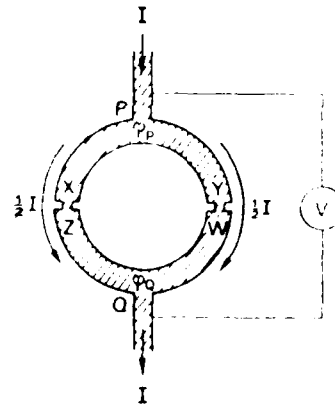
Fig 39

The correlation of phase of the superconducting electrons across each of the weak links XZ and YW allows the detection of interference effects arising from the supercurrent flow in the two separate paths. These

interference effects are highly sensitive to the magnetic flux contained within the loop and provide the most sensitive device available for the measurement of low magnetic fields. Because SQUIDs are so important they will form the subject of separate papers, and they will not be discussed further here.

REFERENCES

1) Rose-Innes and Rhoderick, Introduction to Superconductivity, Pergamon Press, 1978
2) Van Duzer and Turner, Principles of Superconductive Devices and Circuits, Elsevier, 1981
3) Wilson, Superconducting Magnets, Clarendon Press, 1983

Discussion

Name of Author: Dr. D. Baird

Paper No.: 3 -- Physics and Applications of Low Temperature Superconductivity

Name of person asking question: John R. Vig

Question

Have you considered the temperature coefficient and other (environment-dependent) properties of superconducting resonators? It takes more than just high Q to meet or exceed the capabilities of acoustic resonators (which are temperature compensated, work at "normal" temperatures, have high Q, are rugged, small, etc.)

In what applications would superconducting resonators be superior to acoustic resonators (such as SAW, DRO, etc.)?

Answer

The temperature coefficient of a resonator in contact with liquid coolant would not be large. Measuring the Q of a resonator is a convenient way of measuring the loss per unit length of a stripline which allows us to demonstrate and quantify the material properties compared to normal metal. As resonators, I suspect one would be looking at higher frequencies than acoustic resonators can achieve. One will also be looking at resonators as components of stripline filters and more complex structures.

Discussion

Name of Author: Dr. D. Baird

Paper No.: 3 -- Physics and Applications of Low Temperature Superconductivity

Name of person asking question: A. P. Divecha

Question

If defects are needed to increase Jc, why does a thin film of HTS have higher Jc? Thin film is a single XL and highly perfect and epitaxial.

Answer

Current flow in a bulk specimen of HTS material requires passage of the current across the boundaries between adjacent grains of the polycrystalline material. Because of the very low coherence length in HTS material, the Josephson tunneling that carries the supercurrent between the grains is limited to low currents. Such a limitation is not encountered in the more nearly monocrystalline structures that can be achieved in thin films.

Discussion

Name of Author: Dr. D. Baird

Paper No.: 3 -- Physics and Applications of Low Temperature Superconductivity

Name of person asking question: A. P. Divecha

Question

Explain melting of the flux lattice in HTS. How does it differ from lattice in a metallurgical sense? What is flux pinning?

Answer

The term "melting of the flux line lattice" refers to high temperature superconductors rather than low temperature materials. In HTS materials the mixed state exists over an extended temperature range at the lower end of which flux line motion is more susceptible to pinning than it is at the high temperature end. Pinning is a consequence of the arrival of a flux line at a portion of the material where a defect of some sort produces a totally higher value of critical field. Such a barrier to flux movement can be lowered, or eliminated altogether, above a certain temperature, and the resulting mobility of the flux line lattice is referred to as melting.

HIGH TEMPERATURE SUPERCONDUCTING THIN FILMS FOR MICROELECTRONICS: PREPARATION AND PROPERTIES

G.Creuzet, R.Cabanel and A.Schuhl

Laboratoire Central de Recherches Thomson-CSF
91404 Orsay Cedex (France)

INTRODUCTION

The discovery of high temperature superconductors (HTSC) [1] has generated a great deal of activity, both fundamental and towards applications. For the latter, low current devices appear to be particularly interesting. The fundamental building block of superconducting electronics is the Josephson junction, in which two superconducting electrodes are isolated by a thin metallic (SNS) or insulating (SIS) barrier. Due to the extreme low value of the coherence length in these compounds, one has to achieve very thin (a few nm) barriers with sharp interfaces with the superconducting material. This leads first to the major challenge of producing HTSC epitaxial films controlled at the atomic level.

HTSC STRUCTURE

From a microscopic point of view, the high-T_c superconducting oxides appear as a "super" lattice, in the sense that the structure is made up from the superposition of planes along the c direction. Figure 1 shows the structure of the model compound $YBa_2Cu_3O_7$ (1:2:3) [2]. Here the basic alternance is $Y_{1/2}-CuO_2-BaO-CuO-BaO-CuO_2-Y_{1/2}$. Such a description is supported in this case by the fact that the CuO_2 planes play the major role in the conduction process.

This situation is favourable to a layer-by-layer growth of HTSC thin films, as discussed later. The main consequence of this structure is the strong anisotropy, as shown by the superconducting parameters, which have been measured on single crystals [3, 4]. In particular, the coherence length is around 30 Å in the a-b plane but only 6 Å along the c direction (less than half the c parameter). This extremely low value leads to strong constraints for the elaboration of junctions: as the thickness of the barrier in SIS or SNS junctions must be of the order of magnitude of the coherence length, it is clear that one has to control the HTSC thin film growth at the atomic level.
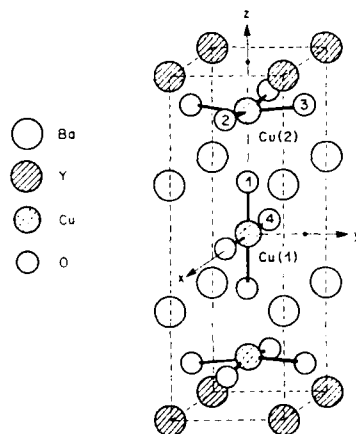
Fig.1 Crystal structure of $YBa_2Cu_3O_7$ (from ref.2).

HTSC THIN FILM GROWTH: GENERAL FEATURES

All the available techniques normally used for other materials have been tested for the preparation of HTSC thin films. Superconducting films have been obtained in all cases more or less, but the film quality is often very bad and still unsatisfactory for realistic applications. Schematically, the results can be classified in three categories: (A) unoriented grains with other phases inside the material, especially in the grain boundaries, and rather bad surface roughness (several hundred Å); (B) juxtaposition of oriented grains without extra phases and better surface roughness than in A (100 Å or less); (C) single crystal films. Most of the available films are in the A category, and only a few groups present reproducible results of the B-type. The best critical current densities ever obtained with HTSC (typically a few 10^6 A cm^{-2} at 77 K and around 10 A cm^{-2} at 4.2 K) have been obtained on B-type thin films. A crucial point is the necessity, or not, of a post-annealing in the fabrication process. Such a step is very often required in order to complete the oxygen stoichiometry, and also to build up the structure if the as-deposited film is amorphous. For the standard compound $YBa_2Cu_3O_7$, "classical" annealing consists of warming in oxygen or inert gas up to 800°C to 900°C, then a plateau in that state (for the structure), followed by a slow cooling in oxygen with or without another plateau around 500°C (for the oxygen content). This kind of annealing usually leads to A type films, with very bad surface roughness, and also interdiffusion between the film and the

substrate. B-type films often require a short post-annealing at moderate temperature in order to complete the oxygen stoichiometry. It is expected that "perfect" C-type films need to be obtained as-deposited, without any kind of annealing. This is to avoid any interdiffusion with the substrate and hence any defect at the interface, but mainly because, as in single crystals, a perfect lattice does not allow oxygen diffusion into the structure.

THIN FILMS PREPARED BY LASER ABLATION

The laser ablation technique reveal to be of high interest for HTSC thin film growth. It is very versatile, and it allows a lot of important features, as the easy use of different targets for multilayer deposition. The best results are B-type films, with typical transition of 1 K width around 90 K, and critical current density well above 10^6 A/cm^2 at 77 K. Recently, very good results have been obtained on such films grown on LaAlO$_3$ substrate [5]: microwave surface resistance values at 77 K between 1 and 10 GHz were found to be more than one or two orders of magnitude lower than for copper at the same temperature. Thus laser ablation appear to be a well adapted technique for application which do not require the extreme perfection of C-type films.

THIN FILMS PREPARED BY MBE AND ALE

In the challenge towards perfect C-type films, coevaporation and MBE appear to be very promising [6-8]. Good films have been obtained at Bell labs by standard MBE growth, followed by a short annealing at 550°C [6]. Recently, the same group also managed to eliminate this final post-treatment [7]. The first results using a modulation of the Ba and Dy flux were reported by the Stanford group [8]. The method needs to be optimized, but they obtained as-deposited superconducting films. The major problems in MBE deposition are the introduction of atomic oxygen, the optimization of substrate temperature and the control of atomic flux during growth.

Although our final objective is direct epitaxy of YBaCuO films, samples have been first produced using the "standard" process i.e. amorphous deposition at low temperature following by an in-situ annealing under oxygen in order to achieve both structure and oxygen stoichiometry. Good films of about 2000 Å thickness have been obtained on SrTiO$_3$ and ZrO$_2$ substrates. The coevaporation was made from pure Ba, Cu and Dy sources, using atomic oxygen produced by a dc plasma source which is described elsewhere [9]. Typical resistive transitions in the 90 K range present 2 K width, but the process was not optimized to obtain high critical current densities.

The second step was to achieve successfully the codeposition of Dy$_1$Ba$_2$Cu$_3$O$_7$ superconducting films without any post treatment after improvement of the atomic oxygen cell. The growth was performed at higher temperature, say between 450°C and 600°C. The oxygen pressure during the cooling (i.e. 2.10^{-5} Torr) was the same as during the

growth. We used various substrates, i.e. $SrTiO_3$, ZrO_2 or MgO. This way routinely leads to superconducting films with zero resistance in the 80 K range (sample S3 on figure 2). X-Ray diffraction study demonstrates that the films are c-axis oriented. Such results have been obtained on films with thicknesses from 200 to 5000Å. Scanning Electron Microscopy study revealed than the grain size (less than 500 Å) and roughness of the films strongly depends on the cation stoichiometry. A better in-situ control of film composition could lead to higher quality surfaces and superconducting properties as pointed out by Kwo et al. [10].
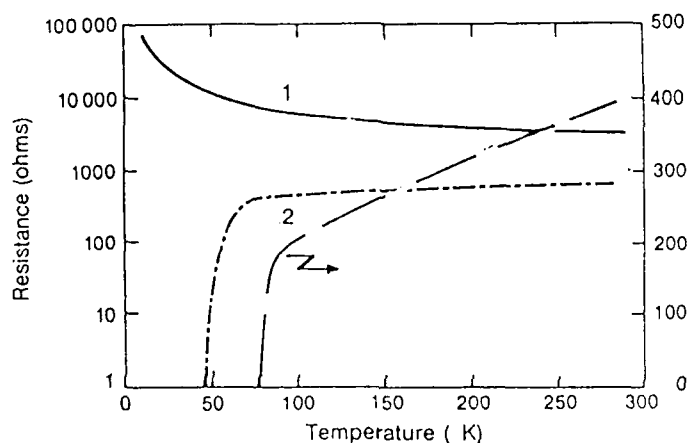
Fig 2: resistance as a function of temperature for as-deposited films on MgO (001). S1 and S2 are 150 Å ALE grown samples (see text), and S3 is a 2000 Å film obtained by codeposition.

In the view to producing perfect epitaxial films, and furthermore controlled Josephson junctions, the Atomic Layer Epitaxy (ALE) technique is one of the most promising. The sources are basically the same as above, but the atomic fluxes are modulated by a shutter computer control procedure, in order to achieve layer-by-layer growth of the desired structure.

Using this ALE technique we have achieved epitaxial growth of 300 Å films of $Dy_1Ba_2Cu_3O_{6.2}$ at relatively low substrate temperature (480°C). No post-annealing was performed. We are able to control a two-dimensional growth mode, as is required for controlled Josephson junction epitaxy, up to at least 400 Å (32 atomic cells and 5 hours deposition).

This growth mode was checked by RHEED (Reflection High Energy Electron Diffraction) pattern observation (Figure 3): in particular,

interruptions are necessary after each cell (or better after each dense CuO_2 plane) to recover a RHEED image characteristic of 2D surface. Moreover, we do not observe any diffusion between the film and the substrate for temperatures as high as 500°C, as checked by RBS analysis [11]. However at this stage the films were not oxidized enough to be superconducting directly after growth.

Fig 3: RHEED pattern of ALE film after completion of the 20th cell.

Recently, we obtained our best ALE films, which are superconducting as-deposited. In these films, the total thickness is typically of the order of 240 Å (20 atomic cells). The substrate temperature is maintained at 600°C. As expected, the oxygen content of the films has been considerably enhanced by increasing slightly the total oxygen flux, and by optimizing the substrate temperature during growth. The high temperature onset of the resistive transition, as well as X-ray diffraction show the presence of the superconducting 1:2:3:7 phase. Since the films present zero resistance at low temperature (zero resistance is observed above 45 K which is the highest T_c obtained by ALE growth on 1:2:3 films to date), the 1:2:3 phase represents at least 50% of the film.

We emphasize that the quality of the as-grown films is essentially limited by the control of their stoichiometry, which is not precise enough. Indeed, the best results corresponds to a situation (S1) which is closed to the sticking of precisely one monolayer for each atomic plan. This is supported by RHEED patterns which are 2D-like until the end of deposition. On the contrary, when the number of sticked atoms is intentionnally fixed to more than one monolayer (1.2 monolayer for each species in S2), 3D growth is observed on RHEED patterns after the fourth cell (in this case), and the sample is semiconducting-like (figure 2). X-Ray diffraction study let us

say that both films are c-axis oriented and present the same amount of 1:2:3 phase. However, other phases are also observed, although the overall composition is very closed to the optimum one in both cases. As the transport properties are crucially different, that means that the ALE process performed around 600°C induces weak diffusion of the species in the direction of the growth. To overcome this problem, a flux control technique during growth is now under development.

JUNCTIONS BY ATOMIC SUBSTITUTION

Assuming that C-type films are available, we can then imagine growing superlattices. In this context, the first step will be the sandwich structure which is precisely a controlled-layer SNS or SIS junction, depending on the nature of the material in the middle. Considering the fact that, for example, the $PrBa_2Cu_3O_7$ compound presents a semiconducting-like behaviour, but is isostructural with any other 1:2:3 material, we can envisage a sandwich of the type $YBa_2Cu_3O_7$ -$PrBa_2Cu_3O_7$ -$YBa_2Cu_3O_7$ grown in epitaxial conditions, with c-axis perpendicular to the substrate. As the thickness of the barrier in SNS or SIS junctions must be of the order of magnitude of the coherence length, we deduce that the praseodynium substitution must be limited to a few unit cells. This requirement supports the use of the ALE technique for thin film deposition.

Recently, preliminary results were reported on such sandwiches [12,13]. For the Jülich group using a sputtering technique [12]. the growth was not fully epitaxial, but the lattice orientation was not affected by the substitution of Pr to Y. However, only very small deterioration of the transport properties of the final heterostructure was observed, which is probably due to large uncertainties in the microstructure. On the other hand, the Bellcore work using laser deposition [13] obtained current-voltage characteristics similar to those of traditional SNS components. However, these are preliminary results as the barrier is not fully controlled and is too thick.

Nevertheless, the $YBa_2Cu_3O_7$-$PrBa_2Cu_3O_7$-$YBa_2Cu_3O_7$ structure appears to be very promising for HTSC devices. In future, multilayered structures from this fundamental building block may be also of interest for advanced superconducting components.

Recently, the Berkeley group succeeded in producing $YBCO/SrTiO_3/YBCO$ structures [14] on MgO using laser ablation. In this trilayer structure, both YBCO films present a sharp resistive transition, and the barrier is highly resistive with a thickness around $0.4\mu m$. This structure do not present the classical I-V characteristics, but it is an important step for junction fabrication using $SrTiO_3$ as a barrier.

CONCLUSION

For HTSC thin film preparation, reasonable good films are now available routinely using the laser ablation technique. In particular, these films present high frequency characteristics which are good enough to develop superconducting components like microstrips for delay lines. For Josephson Junction electronics, the requirements, especially for the barrier thickness control, are much more ambitious. In this context, Molecular Beam Epitaxy, and furthermore Atomic Layer Epitaxy, appear to be very promising.

REFERENCES

[1] J.G. Bednorz and K.A. Muller, Z.Phys. B **64**, 189 (1986).

[2] M. Stavola, D.M. Krol, W. Veber, S.A. Sunshine, A. Jayaraman, G.A. Kourouklis, R.J. Cava and E.A. Rietman, Phys. Rev. B **36**, 850 (1987).

[3] T.K. Worthington, W.J. Gallagher and T.R. Dinger, Phys. Rev. Lett. **59**, 1160 (1987).

[4] A. Umezawa, G.W. Crabtree, J.Z. Liu, T.J. Moran, S.K. Malik, L.H. Nunez, W.L. Kwok and C.H. Sowers, Phys. Rev. B **38**, 2843 (1988).

[5] A. Inam, X.D. Wu, L. Nazar, M.S. Hegde, C.T. Rogers, T. Venkatesan, R.W. Simon, K. Daly, H. Padamsee, J. Kirchgessner, D. Moffat, D. Rubin, Q.S. Shu, D. Kalokitis, A. Fathy, V. Pendrick, R. Brown, B. Brycki, E. Belohoubek, L. Drabeck, G. Gruner, R. Hammond, F. Gamble, B.M. Lairson and J.C. Bravman, Appl. Phys. Lett. **56**, 1178 (1990).

[6] J. Kwo, M. Hong, D.J. Trevor, R.M. Fleming, A.E. White, R.C. Farrow, A.R. Kortan and K.T. Short, Appl. Phys. Lett. **53**, 2683 (1988).

[7] J. Kwo, M. Hong, D.J. Trevor, R.M. Fleming, A.E. White, J.P. Mannaerts, R.C. Farrow, A.R. Kortan and K.T. Short, M^2S-HTSC 89 Proceedings, Physica **162-164**, 623 (1989).

[8] D.G. Schlom, J.N. Eckstein, E.S. Hellman, S.K. Strieffer, J.S. Harris, Jr., M.R. Beasley, J.C. Bravman, T.H. Geballe, C. Webb, K.E. von Dessonneck and F. Turner, Appl. Phys. Lett. **53**, 1660 (1988).

[9] M.Touzeau, D.Pagnon, P.Luzeau, A.Barski, A.Schuhl, R.Cabanel, S.Koch, J.P.Hirtz and G.Creuzet, to appear in MRS Fall meeting 89 Proceedings.

[10] J. Kwo, T.A. Fulton, M. Hong and P.L. Gammel, Appl. Phys. Lett. **56**, 788 (1990).

[11] A.Schuhl, R.Cabanel, S.Koch, J.Siejka, M.Touzeau, J.P.Hirtz and G.Creuzet, M²S-HTSC 89 Proceedings, Physica **162-164**, 627 (1989).

[12] U. Poppe, P. Prieto, J. Schubert, H. Soltner, K. Urban and Ch. Buchal, submitted to Solid State Comm.

[13] C.T. Rogers, A. Inam, M.S. Hedge, D. Dutta, X.D. Wu and T. Venkatesan, Appl. Phys. Lett. **55**, 2032 (1989).

[14] J.J. Kingston, F.C. Wellstood, P. Lerch, A.H. Miklich and J. Clarke, Appl. Phys. Lett. **56**, 189 (1990).

Discussion

Name of Author: Dr. G. Creuzet

Paper No.: **4** -- Films Minces de Supraconducteurs a Haute Temperature Critique

Name of person asking question: R. Humphreys

Question

We grow films consistently on the "unstable" side of the Bormann and Molbone stability line. This is done both with and without atomic oxygen. We believe the line is in the wrong place.

Answer

It is probably very difficult to know precisely either the sample temperature (as used in MBE systems) or the atomic oxygen pressure in any experiment. Nevertheless, perhaps you are right in your case. Anyway, the main point is that such a line exists and, therefore, the problem is arising from the fact the MBE-like systems must work at low oxygen pressure. Then rather high growth temperatures are impossible, except if we use active oxygen.

SUCCESS CRITERIA FOR OXIDE SUPERCONDUCTOR WIRES - MEASURING THE PRESENT, PREDICTING THE FUTURE

Carl J. Russo
American Superconductor Corp
149 Grove Street
Watertown, Massachusetts USA 02172-2828
telephone 617-923-1122

Abstract

Successful application of oxide superconductor wires to large-scale applications requires: high critical current in long lengths at high fields; adequate mechanical properties for handling; a process technology scalable to production quantities; corrosion resistance; adequate strength at low temperatures in high fields; superconducting joints; cryostability; and low AC losses.

The present state of conductor development will be discussed in terms of several figures of merit. Historical data will be evaluated, technology challenges will be investigated, and predictions for the future of oxide superconductor wire development will be examined.

Introduction

A number of superconducting oxide materials ($YBa_2Cu_3O_{7-x}$, $Bi_2Sr_2Ca_1Cu_2O_{8-x}$, $Bi_2Sr_2Ca_2Cu_3O_{10-x}$, $T_2Ba_2Ca_2Cu_3O_{10-x}$, etc.) have been recently discovered. These oxide materials possess higher transition temperatures and higher critical fields than non-oxide superconductors, which may lead to enhanced performance in wire-type applications. These superconducting oxides are also brittle and thus susceptible to cracking during loading[1]. Since it is likely that stresses will be applied during the manufacture, installation, and use of superconducting wire, it will be necessary to "toughen" the oxide wire. Enhancement of fracture toughness can be achieved through the use of a superconducting oxide/metal composite.

For power applications, only two classes of the new oxide materials appear to have promise when large quantities of material are required. These families, which are based on rare earth and bismuth perovskites, have as their most common members $YBa_2Cu_3O_{7-x}$ (YBCO) and $Bi_2Sr_2CaCu_2O_{8-x}$ or $Bi_2Sr_2Ca_2Cu_3O_{10-x}$(BSCCO). The thallium-based oxides are not considered here largely because of the scarcity of thallium which has limited their use to thin-film applications.

The great challenge in using polycrystalline oxide superconductors has been to improve: critical currents in magnet fields, electrical contact, and mechanical characteristics. Without adequate electrical and mechanical properties, bulk-processed, oxide superconductors cannot be used in practical power applications.

Most of these challenges have been met by using microcomposite structures which mix a normal metal, such as silver, with the superconducting oxide. Below is a description of how conventionally processed, oxide-superconductors and metal-oxide superconductor microcomposites are being developed by the oxide superconductor community.

Electrical Properties of the Superconductor

The electrical properties of superconductors are the driving force for applications. The ability of super-conductors to carry very high current densities compared to copper enable applications like high-field, air-core magnets. The basic parameters which describe a superconductor are: the critical temperature, T_c; the critical current density, J_c; and the critical field, H_c. These are briefly described below and a more detailed discussion is available in texts like Rose-Innes[2].

Critical Properties - T_c, J_c, and H_c

Superconductors operating below their critical temperature, T_c, are characterized by their lack of DC electrical resistivity, ρ. In the best low-T_c superconductors, $\rho < 10^{-18}$ Ω-cm is the limit of the measurement capability by persistent current techniques. The ability of a high-field magnet to operate in persistent-mode with no external electrical connections is important in high stability applications where very constant fields are required.

Resistivities measured in highly-oriented, polycrystalline, thin films of $Tl_2CaBa_2Cu_2O_x$ and single-crystal samples of $Bi_2Sr_2Ca_1Cu_2O_{8-x}$ for $26<T<100K$ have been several orders of magnitude higher than those measured in low-T_c superconductors, and the resistivity has shown strong magnetic-field orientation dependence[3]. Resistivity values will need to improve if oxide superconductors are to be used in persistent-mode.

The superconductor will stay superconducting until a critical field is applied or a critical current is passed through the sample at a given temperature and field. Most of the discussion of superconducting properties focuses on improving the critical current.

The Meissner effect is the property of superconductors that excludes externally imposed magnetic fields from the interior of the superconducting body. The Meissner effect is important in the consideration of AC losses and the use of superconductors as shielding material.

All superconductors can be categorized as either Type I or Type II. Besides the usual zero resistance criteria, Type I superconductors exhibit the Meissner effect whenever they are in the superconducting state (below H_c or H_{c1}). Type II superconductors exhibit the Meissner effect in low magnetic fields (below H_{c1}), and a mixed state in slightly higher magnetic fields ($H_{c1}<H<H_{c2}$), with discrete flux quanta causing localized normal regions surrounded by material still in the superconducting state. The material still shows zero resistance to steady currents, but any motion of these flux lines causes energy dissipation in the conductor.

Since H_{c1} is less than 500 gauss in all cases, only a few superconductors are of technical importance for applications in magnetic fields. These are all Type II superconductors. The commonly used metal superconductors are NbTi and Nb_3Sn, and the ceramic oxide superconductors are YBCO and BSCCO.

The J_c vs B characteristics of oxide superconductors in bulk form will be a major component in determining their usefulness. Most of the practical, large-scale manufacturing techniques produce polycrystalline materials. Therefore, critical current properties must be adequate in these forms for the applications of interest. In general, this corresponds to $J_c>10,000$ A-cm^{-2} in magnetic fields characteristic of the application.

The Present State of Conductor Development

Currently, the oxide superconductor community is producing superconducting-oxide wire, and metal, superconducting-oxide microcomposite wire and ribbon conductors by the following techniques:

(1)   the coating of wire substrates with ceramic superconductors;

(2)   the oxidation of metallic precursors made by mechanically alloying and by deformation processing;

(3)   the deformation processing of oxide powders in metal tubes;

(4)   the mixing of oxide with binder, then extruding, spinning, or shaping it in the green state with subsequent binder burnout, sintering, and oxidation.

The issues involved in wire, magnet, and cable development and manufacture (e g., oxide powder production, wire shaping, wire annealing treatments and microstructure development, wire bundling techniques, etc.) are also emerging.

YBCO vs BSCCO - Recent Results

To date, bulk-processed YBCO, has had poor performance in magnetic fields. The knee in the critical current vs field curves typically occurs in the 10-20 gauss range, independent of temperature, and the critical current usually drops to unacceptably low values when the fields reach 100-1000 gauss. YBCO will not be used in high-field applications until the poor performance in high magnetic fields is solved.

Tapes made of $YBa_2Cu_3O_{7-x}$ on a silver substrate have been produced with J_c (77K, 0 Applied Field) values of 2000 A/cm^2, [4]. Silver-sheathed coils of $YBa_2Cu_3O_{7-x}$ and $Tl_2Ba_2Ca_2Cu_3O_y$, produced by drawing and cold-rolling followed by annealing, have yielded Jc (77K, 0 Applied Field) values of 3,330 and 6700 A/cm^2, respectively[5,6]. It is anticipated that these results will improve by an order of magnitude within a year.

The critical current in magnetic field performance of YBCO thin-films, single-crystals, and melt-textured forms approach 1,000,000 A-cm^{-2} even at 77K in fields as high as 1 tesla. These bulk materials have exhibited properties approaching the theoretical limits. Materials where the c-axis of the material is aligned perpendicular to the substrate, as demonstrated by thin film, tend to show the highest critical currents.

Tenbrink[7] et al, and a variety of Japanese workers have demonstrated exciting results for BSCCO materials at 4K. Recent results by Carter et. al. have shown similar results at 20K. The advent of a superconductor material which can handle currents higher than 10,000 A-cm^{-2} in fields higher than 20 tesla leads to exciting prospects for the production of high-field magnets.

Polycrystalline BSCCO materials have shown limited current densities in magnetic field for temperatures above 20-30K. High critical current operation at higher temperatures in high field will be possible when adequate pinning mechanisms are found. Encouraging data[8] on critical current improvements of oxide superconductors under neutron and proton irradiation show the direction required for finding good pinning centers in these materials. Figure 1 shows data normalized to $J_{co}(T=4.2 K, B=0)=100$[9] showing the effects of temperature on current density in magnetic field for material where no effort has been made to improve pinning or texture.

Figure 1. Normalized Critical Current vs Field for BSCCO. oco=100

Figure 1. Normalized Critical Current vs Field for BSCCO. oco=100
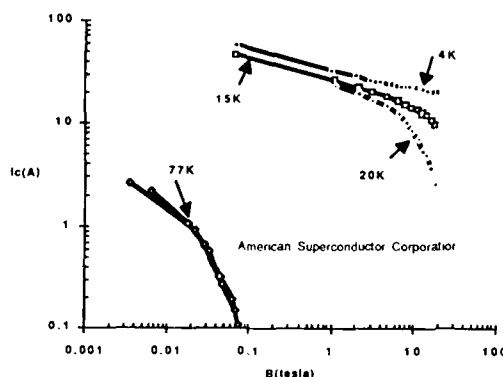
Silver-sheathed $(Bi,Pb)_2Sr_2Ca_2Cu_3O_x$ wires have attained $J_c(77K, B=0)$ values of 15,000 A/cm^2,[10] with recent improvements to 17,400 $A\text{-}cm\text{-}2$,[11]. Subsequent work on $Bi_2Sr_2Ca_1Cu_2O_{8\text{-}x}$ have shown current densities approaching 320,000 $A\text{-}cm^2$, at 4.2 K[12]. This material class is generally abbreviated as BSCCO.

Table 1. Comparison of some recent results on bulk polycrystalline $Bi_2Sr_2Ca_2Cu_3O_{10=x}$ (2223) and $Bi_2Sr_2Ca_1Cu_2O_{8=x}$ (2212) powder-In-tube processed oxide superconductor.

Hikata (Sumitomo) 2223			Uno (Furakawa Electric) 2212		
T (K)	H (Tesla)	J_c (A-cm-2)	T (K)	H (Tesla)	J_c (A-cm-2)
77	0	2.5×10^4	77	0	3.5×10^4
77	0.1	1.2×10^4			
4.2	0	$>5.0 \times 10^4$	4.2	1	3.2×10^5
4.2	23	3.8×10^4	4.2	10	1.7×10^5

Silver is one of few metals that does not seriously degrade the electrical properties of copper, oxide-based superconductors. Because oxygen diffusion through silver is relatively fast compared with oxygen diffusion through the superconducting oxides, a silver sheath does not inhibit the achievement of the proper oxygen stoichiometry in copper, oxide-based superconductors[13],[14]. Thus, silver is a desirable metal for use in a superconducting-oxide/metal composite.

AC Losses

In a Type II superconductor in the mixed state, a steady current can be passed through the conductor without any energy dissipation. The lines of magnetic flux created by the current passing though the conductor are pinned by defects in the crystal structure. An alternating current causes the flux lines in the superconductor to continually undergo an acceleration due to the Lorentz force, JxB.

The Lorentz acceleration manifests itself as a voltage required to drive the current through the superconductor. This flux motion dissipates energy as heat in the conductor. Therefore, a Type II superconductor exhibits resistive-like behavior due to hysteretic AC losses in the mixed state.

Oxide superconductors operate at higher temperatures than metallic superconductors. Oxide superconductors with similar energy dissipation due to AC losses will operate more efficiently due to smaller refrigeration requirements. While NbTi has been produced in wire forms which have very low AC losses, the liquid helium loss in NbTi magnets operating under AC conditions tends to be very large.

These NbTi conductors designed for AC operation are composites of fine filaments of superconductor (< 10 µm diameter) embedded in a resistive metal matrix. In these conductors, there are three sources of AC losses: hysteretic, filament coupling, and eddy current. Hysteretic losses are intrinsic to the superconductor, as explained above, and are minimized by reducing the diameter of the superconductor - hence the use of very fine filaments.

Filament coupling losses occur due to time variant magnetic fields causing currents that move from filament to filament through the resistive matrix. These currents are reduced by twisting the conductor and using a high resistivity matrix such as CuNi instead of pure copper. The twisting causes the filaments to follow a helical path through space resulting in the flux threading alternately in the positive and negative sense through a surface bounded by the filaments. The net result of this is a cancellation of the inductive component of the driving force for the filament coupling currents. The higher matrix resistivity further reduces the amount of currents induced in the matrix. Copper-nickel also takes advantage of the ferromagnetism of the nickel to shield the magnetic flux.

Eddy currents, the third loss mechanism, are the result of high frequency currents induced in the matrix at the surface of the conductor. These eddy currents cause a loss that is relatively small and generally ignored, unless the frequency of operation is very high (> 10 kHz).
Although there are three decades of experience behind metallic superconductors, the prediction of AC

losses is still far from being a science. In general, the prediction of AC losses is hindered by the complexity of the conductor geometry and the interaction of the conductor and the materials surrounding it in any given application. As an example, the Brookhaven National Laboratory superconducting transmission line predicted AC losses to be 20-50% of the actual measured values depending on the system parameters. They were unable to fully account for the sources of the additional losses[15].

Ceramic, oxide superconductors are Type II superconductors and thus exhibit the behavior outlined above. Understanding of the AC loss issue in these materials is complicated by their weak-link (YBCO) and flux flow (BSCCO) behavior.

Cryostability

As discussed in the section above, the motion of flux in a superconductor causes energy dissipation. Motion of the conductor itself can cause similar dissipation. Regardless of the cause, if the energy dissipation cannot be removed from the superconductor rapidly enough, then the superconductor will convert to a normal zone in the area where the dissipation occurs.

If the current cannot be shunted around the normal zone, and there is a substantial amount of energy stored in the superconducting device, then the normal zone will heat until the material melts. Therefore, it is important to provide a current shunt around the superconductor to handle the current, and to provide a method for the removal of heat. This is especially the case when superconductors are in devices with large amounts of stored energy, such as high field magnets.

Cryostability implies the ability of a conductor to return to the superconducting state after a small to moderate perturbation. Cryostability depends on a fairly low resistivity, an alternate path or shunt around the normal zone, and a mechanism to absorb the heat dissipated in the normal zone and the resistive path. The addition of silver to oxide superconductors improves cryostability, especially when the material is processed by the metal precursor route. Note however, that the larger amounts of normal metal included usually reduce the available critical current in a given cross-section.

Normal Zone Propagation

The stored energy in a superconducting device which begins dissipating in the normal zone must be able to propagate through the wire at a fast enough rate to prevent the wire from destroying itself. Usually, this is only a problem in superconducting devices with large, stored energy, such as magnets. The normal-zone, propagation velocity is related to the heat capacity, the thermal conductivity, and the configuration of the wire in a given device. If the dissipated heat in the normal zone cannot be re-

moved, then the normal zone heats up, and through thermal conduction the normal zone propagates. At cryogenic temperatures, the heat capacity of all materials decreases rapidly as a function of temperature. This allows the normal zone to propagate rapidly thus limiting the stress due to thermal gradients and uniformly dissipating the stored energy in the coil volume.

The operating temperature of superconducting devices with large stored energy is governed to a large extent by the ability of the cryogenic system to limit damage in the event of a quench. This drives the desired operating temperatures to lower values.

Mechanical Properties

In order to use oxide superconductors effectively, they must have mechanical properties which allow their fabrication and their use with thermal cycling when they are superconducting.

A useful empirical method for measuring the fracture toughness of a superconducting-oxide/metal composite is to measure the critical current of the superconducting-oxide as a function of strain and/or applied stress. A plot of the of most common superconductors' critical current performances as a function of strain is shown in figure 2. The properties of conventionally processed YBCO are not adequate for use in applications where thermal or mechanical stress in the superconducting state is required. However, YBCO where silver has been added has superior mechanical properties in the superconducting state. Similarly, mechanical properties in the normal state, as exhibited by the fracture toughness, have also been significantly improved with the addition of a noble metal such as silver. The mechanical properties with BSCCO materials are similar.

Figure 2. Normalized critical current (Jn) vs strain for high and low temperature superconductors
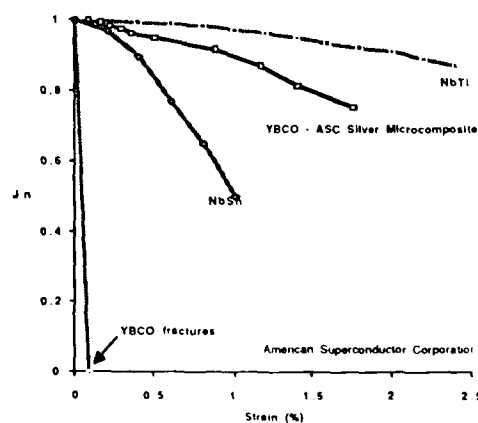
Corrosion Resistance

There has been concern that oxide superconductors would not have sufficient chemical stability[16] to be useful in a variety of applications. This concern is related to the decomposition of YBCO while in the presence of water, oxygen, hydrocarbons, or carbon dioxide. Most of this decomposition is due to barium in an oxide state tending to barium carbonate. This problem is generally handled by sheathing YBCO in a nonreactive metal such as silver. BSCCO does not react as readily as YBCO, and it appears to have better stability over time.

Joints

The manufacture of superconducting joints in oxide superconductors has been demonstrated when using metal precursor technology[17]. The inability to make low-loss connections in conventionally processed, oxide superconductors will limit their applicability to lower current applications.

Processing to Long Lengths

Several processing technologies give superior critical current performance to bulk processed materials, but are not capable of giving reasonable current handling capacity over long lengths. These technologies include melt-textured growth and most of the thin-film processing technologies. If a processing technology is to be useful for power applications, then it must provide current handling capability over 10's of meters to 1000's of kilometers depending on the application.

Figures of Merit

Given the number of conflicting requirements needed for different applications, it is useful to have several figures of merit which can be used to show the progress of oxide superconductors for different applications. It is also useful to plot these figures of merit vs time as they may be useful predictive tools.

J x L:
Providing high critical currents is of little use unless they can be demonstrated over a significant length. For example, a 10km long transmission line operating at $J \approx 10,000$ A-cm^{-2} requires $J \times L \approx 10^{10}$ A-cm^{-1} Presently 10^6 A-cm^{-1} are achievable and may increase as fast as a few orders of magnitude per year. Therefore, large-scale applications should have oxide superconductor wire available by the mid 1990s.

B^{2}r ~ Stress:
Large magnets for use in motors, particle physics, or energy storage are usually limited by mechanical stresses, not the properties of the superconductor. Therefore, the ability of a superconductor-plus-support structure to maintain a high critical current while under stress may be an appropriate figure of merit. In the relatively simple case of a solenoidal magnet, the

stress is proportional to B^2r, where r is the radius of the magnet[18].

$J_cV \approx Br^2$:
The current density and the volume of a conductor determine the magnetic field which can be produced in a given bore for a solenoidal magnet. This figure of merit is useful for determining the trade-off of magnet bore, required conductor amount, and critical current.

Cost vs Performance

Cost-performance trade-offs are useful for the economic feasibility studies usually developed for large-scale power engineering projects. Below are a few examples of the type of measures which may be useful.

$/l x L:
In low-field applications, such as transmission lines, the cost per length for a given current capacity may be the correct measure. Superconductors need to do considerably better than copper in order to compete in this type of application.

$/l x L x B:
For magnets, the cost per field generated is a useful cost-performance measure. Clearly, one uses the least expensive material consistent with the field which needs to be generated. John Williams[19] uses a variant of the formula below for estimating this figure of merit.

$$f(\text{¢/[tesla-amp-meter]}) = [J_c(\text{A-cm}^{-2}) \, L(\text{m/\$}) \, A(\text{cm}^2) \, B(\text{tesla})]^{-1}$$

Table 2 shows f for copper and a variety of superconductors. It is assumed that the copper is operating water cooled. Note that an approximate diameter in mils, ø, is given for an 1800 A conductor based on the current density in field. Even $50/m BSCCO is cost competitive for high-field magnets and can be cost competitive at 10 tesla at $25/m.

Table 2. Price performance factor, f, for high-field magnet conductor. The diameter of an 1800 A conductor, ø, is given in mils.

Material	ø	Assumptions	f
copper	600	$ 20/m for 1800 A, 2 tesla, 1kA-cm^{-2} Stranded and insulated	0.55
NbTi	74	$2.34/m for 254 A, 7.6 tesla. (insulated multi-filament only, no sheath)	0.07-0.14
Nb(Ta)Sn	81	$ 10.17/m for 215 A 14 tesla (insulated multi-filament only, no sheath)	0.17-0.34
BSCCO	60	$50/m for 1820 A, 20 tesla, 100 kA-cm^{-2} Pure silver is $ 4.4/m at $ 100/# Ag.	0.14

For space- or undersea-based, magnetic field applications, the field per weight or the field per volume may be an appropriate measure. Several others can be developed to help determine which material technology is appropriate for a given application.

Maintaining Specification Over Length

Serial processes such as wire, yarn, and optical fiber production are most cost effective if the total output of a process can be profitably sold without selecting parts of the output after production. Besides increasing the cost of selected material, the continuous length of material which can be produced within a given specification is usually compromised during the selection process.

In-situ process control tools are usually required to maintain given specifications to tight-tolerance standards. These tools need to be developed for the oxide superconductor industry.

Conclusions

In the last two years, great progress has been made in the production and manufacture of polycrystalline, bulk-processed, oxide superconductors. Current densities in high fields are now available. Processing by inexpensive methods is also available now.

BSCCO electrical properties are of sufficient quality to enable high field applications at 20K, a temperature accessible to conventional cryocooler technology. Enhanced mechanical properties in oxide superconductor/metal microcomposites ensure enough robustness for economical manufacturing processes.

While many of the fundamental problems have been solved, a few, such as the weak links in YBCO and flux pinning in BSCCO, need innovative solutions for many applications to evolve.

Acknowledgements

[1] N. McN. Alford, J.D. Birchall, W.J. Clegg, M.A. Harmer, K. Kendall, and D.H. Jones, "Physical and Mechanical Properties of YBa$_2$Cu$_3$O$_{7-x}$ Superconductors," J. Mat. Sci., Vol. 23, No. 3, pp. 761-68, 1988

[2] A. C. Rose-Innes and E. H. Rhoderick, Introduction to Superconductivity, 2nd ed., Pergamon Press, Oxford England, 1978

[3] D. H. Kim, K. E. Gray, R. T. Kampwirth, and D. M. McKay, "Possible Origins of Resistive Tails and Critical Currents in High Temperature Superconductors in a Magnetic Field", submitted to Phys. Rev B

[4] S. Matsuda, M. Okada, T. Morimoto, and K. Aihara, "Superconducting Tape-Shaped Wire by YBa$_2$Cu$_3$O$_y$ with Jc = 2000 A/cm^2," MRS Symposium Proceedings, "High Temperature Superconductors," Vol. 99, ed. by M. B. Brodsky, et. al, pg. 695, MRS, Boston, MA, 1987

[5] M. Okada, A. Okayama, T. Morimoto, T. Matsumoto, K. Aihara, and S. Matsuda, "Fabrication of Ag-Sheathed Ba-Y-Cu Oxide Superconductor Tape," Jap. J. Appl. Phys., Vol. 27, No. 2, pg. L185, 1988

[6] M. Okada, R. Nishiwaki, T. Kamo, T. Matsumoto, K. Aihara, S. Matsuda, and M. Seido, "Ag-Sheathed Tl-Ba-Ca-Cu-O Superconductor Tape with Tc = 120K," Jap. J. Appl. Physics, Vol. 27, No. 12, pg. L339, 1988

[7] J. Tenbrink, K. Heine, H. Krauth, A. Szulcyzk and M. Thöner, "Entwicklung von Hoch-T$_c$Supraleiterdrähten", VDI Berichte Nr. 733,1989, p 399-404

[8] van Dover et al on neutron and protons.

[9] W. Carter et al, unpublished.

[10] T. Hikata, T. Nishikawa, H. Mukai, K. Sato, H. Hitotsuyanagi, "Electromagnetic Properties and Morphology of Ag-Sheathed Bi-Pb-Sr-Ca-Cu-O Superconducting Wires," Jap. J. Appl. Phys., Vol. 28, No. 7, pp. L1204-6, 1989

[11] Ken-ichi Sato, Takeshi Hikata, Hidehito Mukai, Takato Masuda, Munetsuga Ueyama, Hajime Hitotsuyanagi, Tsutomo Mitsui and Maumi Kawashima, "Electromagnetic Properties and Structures of BiPbSrCaCuO Superconducting Wires," presented at International Symposium on

Superconductivity '89 at Tsukuba, Japan, November 14-17, 1989.

[12]Naoki Uno, Noritsuga Enomoto, Hiroyuki Kikuchi, Kaname Matsumoto, Masanao Mimura and Minoru Nakajima, "The Transport Critical Current Property of High Tc Superconducting Wires", presented at International Symposium on Superconductivity '89 at Tsukuba, Japan, November 14-17, 1989.

[13]T. A. Ramanarayanan, and R. A. Rapp, "The Diffusivity and Solubility of Oxygen in Liquid Tin and Solid Silver and the Diffusivity of Oxygen in Solid Nickel," Met. Trans., Vol. 3, No. 12, pg. 3239, 1972

[14]S. J. Rothman, J. L. Routbort, L. J. Nowicki, K. C. Goretta, L. J. Thompson, J. N. Mundy, and J. E. Baker, "Oxygen Diffusion in High-Tc Superconductors," Preprint from Argonne National Laboratory, 1989

[15]E. Forsythe and R. A. Thomas, "Performance Summary of the Brookhaven Superconducting Power Transmission System", Cryogenics, (26):11, pp 599-613, 1986.

[16]Claudia P. Ostertag, Francis Beech, Edwin R. Fuller, Jr. "Chemical Modifications of the Orthorhombic Superconductor $Ba_2YCu_3O_{7-x}$", Ceramic Transactions Volume 1 Ceramic Powder Science II., G. L. Messing, H. Hausner, ed. American Ceramic Society, October 1988.

[17]patent pending, American Superconductor Corporation.

[18]D. Bruce Montgomery, Solenoid Magnet Design - The Magnetic and Mechanical Aspects of Resistive and Superconducting Systems. John Wiley and Sons, New York, 1969.

[19]John Williams, National Magnet Laboratory, Cambridge, MA, private communication.

MINIATURE CLOSED CYCLE REFRIGERATORS
by
T W Bradshaw and A H Orlowska
Rutherford Appleton Laboratory
Chilton, Didcot, Oxon
OX11 0QX
UK

SUMMARY

This paper describes a closed cycle cooler
suitable for long-life space applications.
The development heritage and the mechanical
design are described and the inherently
long life-time characteristics of the
cooler are explained. Many types of cooler
have been developed from the original
concept: this paper concentrates on those
developed at the Rutherford Appleton
Laboratory (RAL).

1.   INTRODUCTION

Many space instruments require cooling to
cryogenic temperatures. This may be to
improve the signal to noise ratio of
infra-red detectors at long wavelengths or
to extend the lifetime of a cryostat by
actively cooling the radiation shields and
thereby reducing the parasitic heat load on
the cryogen.

These requirements have previously been met
by the use of solid or liquid cryogens.
Despite the simplicity of this approach
there are disadvantages; the lifetime is
limited and there are severe mass and
volume penalties. Many of the cryogens
used in these types of coolers are
inflammable or noxious and pose a safety
problem. There is therefore room for a
small lightweight, long-life closed cycle
cooler. The closed cycle coolers that have
been used suffered from performance
degradation due to wear of sliding seals,
leakage of the working gas and
contamination from lubricants used in the
motor mechanism[1].

The cooler described in this paper contains
no sliding seals and has a space proven gas
containment system used in pressure
modulators that have been flown on the
Nimbus satellites[2] and on Pioneer Venus
probe[3]. The pressure modulators are used

to make measurements of the concentration
of various key gases in the upper
atmosphere using a limb-sounding technique.
The modulators contain a piston moving in a
cylinder alternately compressing and
expanding the gas of interest in a
transparent test cell. The infra-red
signal from the atmosphere is viewed
through this cell and is modulated by the
gas in the test cell enabling the
concentration to be determined.

The piston, driven by a linear motor, has a
clearance of a few tens of microns between
it and the cylinder wall. At the frequency
of operation (around 20 Hz in the
modulator) this acts as a seal to the
alternating pressure wave. The piston is
prevented from touching the wall by
diaphragm springs which are very stiff
radially but allow free movement in a
longitudinal direction. The motor drive is
very similar to a loudspeaker with a moving
coil and a permanent magnet providing a
strong radial magnetic field. There is
also a position sensor which is used in a
servo system to provide accurate
positioning of the piston. There are no
rubbing parts.

The pressure modulator performs a similar
function to that required of a compressor
in a Stirling cycle. This fact was
recognised and development of a Stirling
cycle cooler based on the pressure
modulator linear drive and spring
suspension system proceeded at Oxford
University. The displacer unit is driven
by a smaller linear motor than the
compressor.

The cooler has since been developed for
space use by RAL and Oxford University in
support of the Improved Stratospheric and
Mesospheric sounder (ISAMS)[4]. This
single stage cooler is now being
manufactured and marketed by British
Aerospace at Filton. Other versions of
this type of cooler are being manufactured
by Lucas Aerospace. A version was also
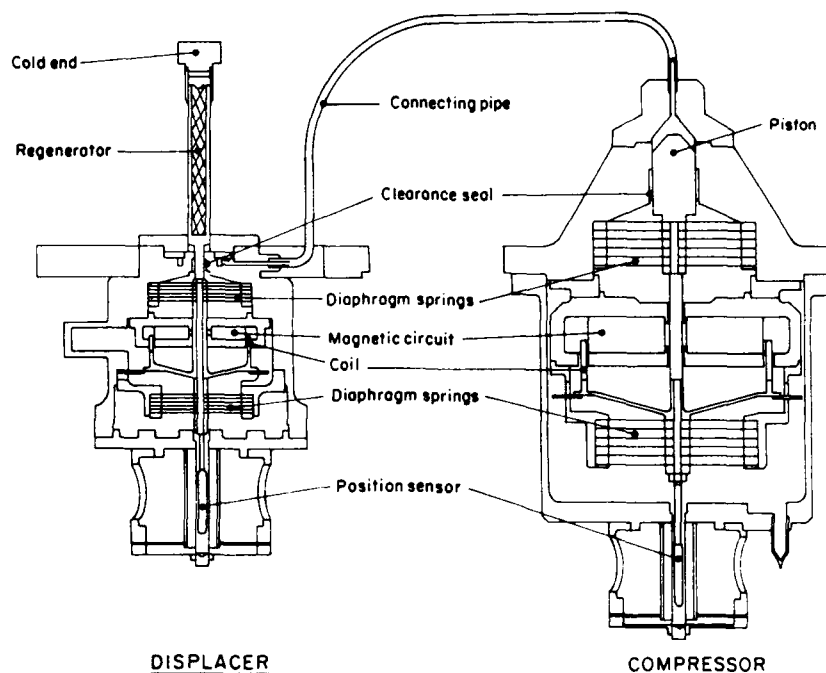
Figure 1. Cross-section of the single stage cooler

used in the infra-red reconnaissance system (Linescan) built by British Aerospace, Stevenage[5].

Several variations of the pressure modulator have been used in space instruments, these have used two different sizes of diaphragm springs which are the same sizes that are now used for the suspension systems of the compressor and displacer in the Stirling cycle cooler. The pressure modulator in the Nimbus 6 PMR experiment contained diaphragm springs, similar to those now used in the cooler compressors, which accumulated 2×10^9 cycles operating at a stroke of +/- 5 mm. The diaphragm springs are made from beryllium-copper which does not fatigue if operated below a certain stress level (a large margin of safety is included in the stress calculations). Confirmation that the material is operating below its fatigue failure limit is reached after approximately 10^8 cycles. The Stirling

cycle cooler operates at approximately 40 Hz so this region is reached after 700 hours of running (1 month). This has been proved many times - a life test cooler has operated for 2.5 years another over 1 year and several have operated for over a thousand hours with no diaphragm spring failure. Spring types have also been routinely tested on a purpose built test bed up to 10^8 cycles.

2. THE SINGLE STAGE COOLER

The single stage cooler has the layout shown in Figure 1. The compressor unit consists of a piston mounted on a drive shaft. The drive shaft is constrained radially by two sets of diaphragm springs. This enables a small clearance to be maintained between the piston and the cylinder. The linear drive is provided by

a moving coil motor. The radial magnetic
field is provided by a magnetic circuit
containing a permanent magnet. A soft iron
slug is mounted on the drive shaft at the
opposite end to the piston, this is part of
the inductive position sensor. The
pressure vessel is in the form of a thin
wall tube around this item. The sensing
coils are mounted around this tube and are
outside the working gas.

The bodies of the cooler are made from
titanium which has a good strength to
weight ratio. Plastics are used for
certain parts of the cooler (the drive
coil and the displacer, for instance) but
their use is kept to a minimum to avoid
contamination of the working gas by
outgassing.

The working gas is helium at approximately
14 bar pressure and is contained in the
cooler using the same sealing methods used
successfully in the pressure modulator
design. This is a system using gold 'O'
rings and tested jointing methods.

The cooler has been vibration tested to
typical levels of 8 g r.m.s for the single
stage cooler. During the vibration testing
it has been possible to observe the
movements of the compressor and displacer
mechanisms by looking at the position
sensor outputs as the test proceeds. It
was found that the movements were very
small and in no case were the mechanisms
driven near the end stops.

The performance of the single stage cooler
is given in Figure 2.[6] The cold end

Figure 3. Cross-section of the two-stage displacer

temperature is shown as a function of power
supplied to the cold end using an
electrical heater and therefore represents
the cooling power available after parasitic
losses have been overcome. The three
curves in this figure represent the
performance for different input powers.
The power referred to on the figure (W -
i^2R) is the total input power less the term
due to Joule heating in the compressor
drive coil. This is the power going in to
the thermodynamic cycle so it is convenient
to express the performance in this way as

TEMPERATURE (K)

POWER TO COLD END (WATTS)

Figure 2. Single stage cooler performance

it permits comparison of the results obtained when the compressor is run off resonance. (The compressor is run on or near resonance and the motor efficiency is generally around 66%.) The displacer unit drive motor does not run on resonance but takes a relatively small amount of input power which is generally around 1 W depending on the precise operating conditions.

The coolers have undergone life tests; one has run for approximately two years to date and another for 2.5 years. The performance of the second cooler did degrade rapidly after 2.5 years due to a bush used as a clearance seal in the displacer having worked loose. The problem has been rectified in subsequent versions and this cooler has been reassembled without disturbing the spring suspension and is back on life test.

3. TWO STAGE COOLER

Many detectors require temperatures lower than those achieved by single stage coolers (typically above 50 K^7). Cooling at low temperatures is very power consuming due to the increase in parasitic losses and the decreasing theoretical maximum (Carnot) coefficient of performance (COP). It can be advantageous to intercept some of the parasitic heat loads at an intermediate temperature, where the COP is high, in order to reduce the total input power required.

The single stage cooler described above can be adapted to provide refrigeration at an intermediate temperature by means of a
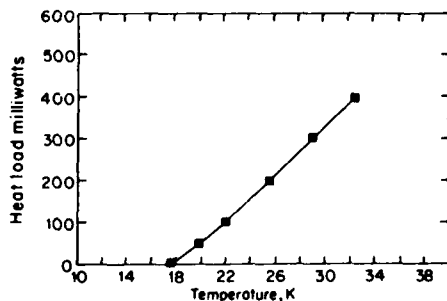
Figure 4   Two stage cooler performance

stepped displacer. This displacer, shown in Figure 3 runs in a stepped cold finger, providing an additional annular expansion space. In order to provide a sufficient pressure swing in the larger dead volume of the two stage displacer two compressors are used. Although the resulting cooler is larger than a single stage it has the advantage of momentum balanced compressors since these are mounted head-to-head and are driven in phase and with the same stroke (controlled by a servo system). All the major features, diaphragm springs, clearance seals, linear motors and gold O-ring seals of the single stage machine are preserved in this development.[8]. Some changes have been made in order to simplify manufacture and assembly; for example the inductive position sensors at the end of the piston and displacer shafts have been replaced by capacitative sensors which allow the shafts to be made shorter and thicker.

The performance of such a two stage refrigerator built at RAL is shown in Figure 4, where it can be seen that the cooler gives around 200 mW of useful refrigeration at about 26 K, and will give over 50 mW at 20 K, for approximately 80 W into the compressors. A base temperature of 16.3 K has been reached with no cooling load. This level of performance is not only useful for detector cooling but could also find application in the cooling of shields in helium cryostats in order to prolong their life.

4. JOULE-THOMSON SYSTEM FOR LOWER TEMPERATURES

Regenerative systems such as the Stirling cycle coolers described here tend to be very inefficient at temperatures much below 20 K. As the temperature decreases the heat capacity of most regenerator materials also decreases while the volumetric heat capacity of the gas passing through the regenerator matrix increases. The resulting regenerator ineffectiveness severely limits the available cooling power.

One phenomenon which is often exploited to achieve lower temperatures is the Joule-Thomson (J-T) expansion of a gas. If the gas is below its inversion temperature this expansion will result in cooling. The

maximum inversion temperature for helium is around 40 K.

RAL has been awarded a contract by the European Space Agency (ESA)[9] to build a closed cycle 4 K cooler, using the two stage Stirling cycle refrigerator described above to precool the helium for a J-T stage. High pressure helium for the expansion is supplied by two compressors identical to those used in the Stirling cycle with valves incorporated in the head to rectify the gas flow. A simplified layout of the 4 K cooler is shown in Figure 5. The high pressure helium passes through three coaxial heat exchangers and two matrix heat exchangers before reaching the expansion orifice. High effectiveness coaxial heat exchangers are required to minimise the heat load on the precooler. The cold matrix heat exchangers and a hot reactive getter will trap impurities and prevent blockage of the expansion orifice.

A J-T stage has been built and mounted on a small development model two stage cooler (similar to those described here). This stage has been run 'open-loop' using high pressure helium from a gas bottle and with a rotary pump on the low pressure side. The gas is precooled to about 28 K by the small two stage cooler but notwithstanding this relatively high temperature the J-T stage has reached 3.5 K.

In the closed cycle J-T cooler the high pressure helium for expansion will be provided by two compressors. These have been built and tested and found to give pressure ratios greater than 10 for the flowrate required.

5.   REFERENCES

1. A.L. Johnson, "Spacecraft borne long life cryogenic refrigeration status and trends", Cryogenics, 23, 339-347, (1983).
2. P. Curtis et al, "Remote Sounding of Atmospheric Temperature from Satellites V. The Pressure Modulator Radiometer for Nimbus F", Proc. R. Soc. Lond. A 337, 135-150, (1974).
3. F.W. Taylor et al, "Infrared radiometer for the Pioneer Venus orbiter 1 :
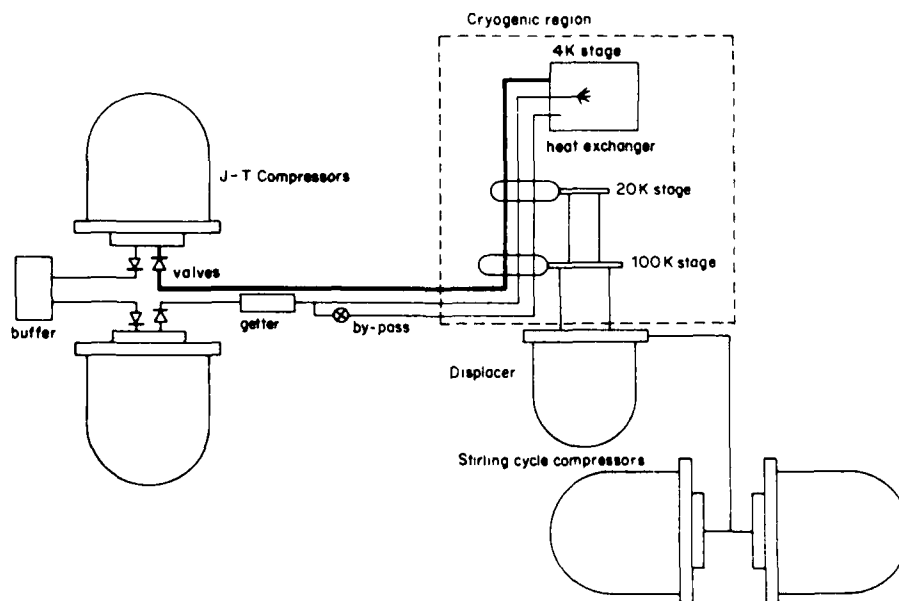
Figure 5.   4 K Cooler layout

Instrument description", Appl. Opt., 18, 3893-3900, (1979).

4. S.T. Werrett et al., "Development of a Small Stirling Cycle Cooler for Spaceflight Applications", Adv. Cryo. Eng. vol. 31, 791-799, (1986).

5. D. Marsden, "Sytem design requirements for infra-red detector Cryocoolers",Proceedings of the fourth International Cryocoolers Conference, Easton, Maryland, 229-240.

6. T.W. Bradshaw et al, "Performance of the Oxford Miniature Stirling cycle Refrigerator",Adv. Cryo. Eng. vol. 31, 801-809 (1986).

7. G. Davey and A.H. Orlowska, "Miniature Stirling cycle cooler" Cryogenics Vol. 27, 158-161, (1987).

8. T.W. Bradshaw and A.H. Orlowska "Miniature mechanical refrigerators for space use", SPIE Vol. 513 pt 1, (1988).

9. ESA contract number 7198/87/NL/MA(SC)

Discussion

Name of Author: Dr. T. W. Bradshaw

Paper No.: 6 -- Miniature Closed Cycle Refrigerators

Name of person asking question: E. Lassiter

Question

Do you have life test data on the two-stage cooler?

Answer

We have no life-test data on the two-stage cooler. We are building a unit for life test at the moment. The single stage cooler has demonstrated 2-5 years of operation.

Discussion

Name of Author: Dr. R. Bradshaw

Paper No.: 6 -- Miniature Closed Cycle Refrigerators

Name of person asking question: P. Encrenaz

Question

There is rapid progress on pulsed tubes, some of them being very efficient.
Do you see them as potential competition to your refrigeration?

Answer

The current state of the art in pulse tubes may make them competitive above
~60K. These devices do require a compressor -- the one I have just described
for use with the stirling cycle is suitable for this application.

Passive Microwave Devices Using High Temperature Superconductors

M.J. Lancaster, T.S.M. Maclean, Z. Wu, C.E. Gough, N. McN. Alford

Birmingham University, Department of Electronic & Electrical Engineering, P.O. Box 363, Birmingham, B15 2TT, United Kingdom

Summary

Passive microwave devices that benefit from the inclusion of a superconducting element are listed. Three devices out of the list; a superconducting loop antenna, a superconducting filter and a cavity resonator have been designed, built and tested. This paper briefly reviews the advantages of each of these components and presents results of their performance.

Introduction

Since the discovery of the new high temperature superconductors in 1986 there has been great effort world wide to optimise the processing techniques and to increase both the critical temperatures and currents. The material processing is now at a stage where many applications can be both demonstrated and in the near future included in systems. Many passive microwave devices have been suggested that will improve in performance if they are wholly or partially made out of a superconducting material. Table 1 gives a list of those passive devices which will benefit significantly. For the majority of devices the improvement in performance comes about because of the reduced surface resistance of the superconductor over conventional materials such as copper. At present the high temperature superconductor has superior surface resistance over copper for frequencies below about 20GHz for the bulk ceramic YBCO and about 200GHz for thin film material [3]

Table 1   Passive Microwave Applications of superconductors.

Resonators	Frequency references [1]
	Oscillators [2]
	Characterisation [3]
	Cavity resonators [3]
	Helical resonators [2]
	Planar resonators [4]
	Tunable resonators
	Coaxial resonators
Delay lines	
Dispersive delay lines [5]	
Filters [see text]	
Antenna	Dipole [6]
	loop [see text]
	Array
Matching networks	
Combiners	
Coaxial transmission lines [7]	
Duplexers	
Screening	
Switches	

The intention of this paper is to give a brief review of the performance of three of the devices in table 1 constructed out of high temperature superconductors. The devices discussed will be a superconducting antenna, a superconducting bandpass filter and a superconducting resonant cavity. All three devices were made to demonstrate and investigate the potential of high temperature superconductors in microwave applications All three applications are made of bulk ceramic material developed at ICI Advanced Materials Division at Runcorn U.K. The material preparation is discussed elsewhere [6]

Superconducting Antenna

Figure 1 shows the efficiency of a copper loop antenna verses its size. It can be seen that for small antennas the efficiency is substantially reduced. This is because as the size of the antenna is reduced the radiation resistance also decreases. When this radiation resistance becomes comparable with, or less than, the loss resistance then the majority of the input power is dissipated in the loss resistance. A simple equivalent circuit for the loop antenna is shown in figure 2. When a small antenna is made out of superconductor the loss resistance is significantly reduced and the efficiency is increased substantially.

For a transmitting antenna the maximum power transmitted will be limited by the critical current of the superconductor. At present only low power applications are possible but it is expected that critical currents in the new materials will improve in the future.

A superconducting receiving antenna will only be practical provided that the noise produced by the loss resistance is significantly lower than the equivalent noise produced by the radiation resistance: i.e. the antenna received noise. The signal to noise ratio for a receiving antenna is [8]
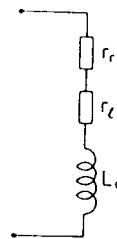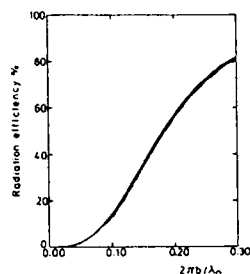
Figure 1 Efficiency of copper loop antenna   Figure 2 Equivalent circuit for loop antenna

$$S:N = \frac{E^2 G_D \lambda^2}{Z_o k 8\pi B} \left\{ \frac{\eta}{\eta T_{sky} + (1-\eta)T_{amb}} \right\} \tag{1}$$

where E is the incident electric field, G_D is the antenna gain, Z_o the impedance of free space, k boltzmans constant and η the antenna efficiency. The noise power received by the antenna and produced by the loss resistance are represented by the sky (T_{sky}) and ambient (T_{amb}) temperatures respectively. For a given antenna the terms outside the square brackets in equation (1) are constant and the signal to noise can be represented by the bracketed term, this is shown in figure 3.
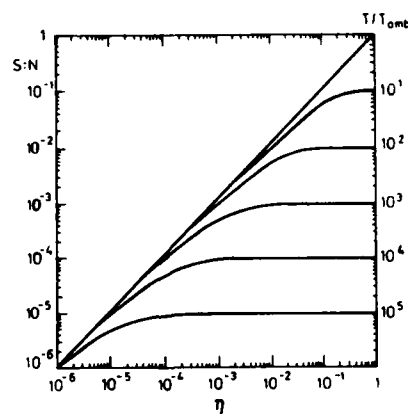
Figure 3 Received signal to noise ratio verses antenna efficiency for some different received noise levels

      For low frequencies (< 30MHz) the sky temperature can be very high [9] so that the use of a superconducting antenna to increase the efficiency has little effect except for very inefficient conventional antennas. However, as the frequency is increased the sky temperature is significantly reduced and above about 500MHz, the ratio T_{sky}/T_{amb} is generally of the order of 1. Here there will be significant improvement in using the efficient superconducting antenna in the receiving mode.

      A few superconducting antennas have been demonstrated using the low temperature superconductors [10, 11]. Walker and Haden [10] demonstrated a loop antenna made out of lead; the antenna showed an increase in gain of 27db between room temperature and 4.2K

      Recently both a dipole [6, 12] and loop antenna [8] made out of high temperature

superconductor have been shown to *improve in efficiency* over a conventional copper antenna. Figure 4 shows a comparison between a high temperature superconducting loop antenna and a copper antenna of the same size. The antenna consists of a small loop of area 19.5cm^2 and a matching circuit. The matching circuit is a transmission line with a shunt capacitance at the end; a diagram of the antenna is shown in figure 5. The experimental results of figure 4 show a 9db increase in radiated power of the superconducting antenna over the copper one at *room temperature and a* 5db *improvement* over copper at liquid nitrogen temperatures.
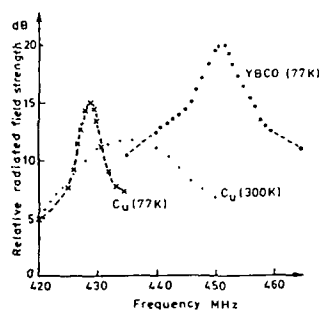
Figure 4   Comparison of output field strengths for copper and superconducting antennas
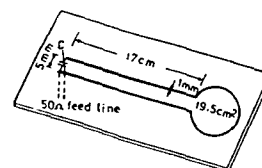
Figure 5   The loop antenna

Analysis has shown that the contact resistance between the YBCO and its feed line is significant and the output level could be further improved if this resistance were reduced.

Superconducting bandpass filter

The reduced surface resistance of the superconductors allows filters to be produced with *significantly lower loss and* higher Q's. Low loss filters are particularly useful for front end applications in sensitive receiver systems. For example filters made out of conventional superconductors have been produced for communication with deep space probes [13] where receiver sensitivity is critical. The filters described in reference [13] were of 150MHz bandwidth at a centre frequency of 8.45GHz, and were constructed out of both NiTi and lead. Results showed that a copper filter had a loss of 0.5db and both superconducting filters had a loss of 0.1db ± 0.6db, this loss being mainly attributed to the SMA connectors and contacts.
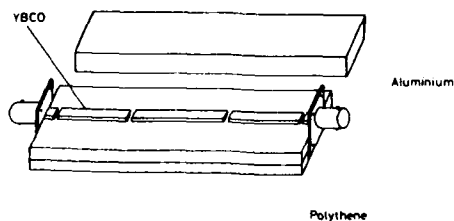
Figure 6   The stripline filter
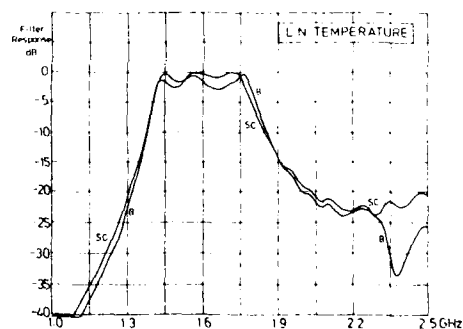
Figure 7   Frequency response of the stripline filter for brass and YBCO elements at 77K

A high-temperature superconducting bandpass filter has been demonstrated at Birmingham University. The filter is of the stripline form in order to minimise the radiation loss. The design was for a 333MHz bandwidth filter at a centre frequency of 1.65GHz, and a Tchebyscheff response with a 1db ripple. The filter was constructed using two aluminium ground planes, with the centre conductors made out of YBCO bars. The design required 3 resonant bars separated by a capacitive gap as shown in figure 6. An identical filter was constructed with brass bars replacing the superconducting ones. Figure 7 shows the response of the YBCO and brass filters, and a significant improvement in loss is seen over the brass filter at 77K. *The mean loss of the superconducting filter is 0.5db and for the brass 1.8db over the passband region.* The shape of the response in both cases is not perfect because of the slight shrinkage of the conductors with temperature altering the gap capacitance.

Superconducting cylindrical cavity

Because of the reduction in surface resistance, resonant devices can be made which have substantially higher Q's than conventional conductor resonators. Table 1 lists some of the different types of resonant devices. This section will discuss one of these; a cylindrical cavity.

There are a number of applications for superconducting cylindrical cavities including oscillators, stable frequency references, filter elements, accelerator cavities and maser cavities. The applications of stable frequency references and accelerators require an improvement in the surface resistance and critical current density respectively. At present use is made of low temperature superconductors for these applications.

A cylindrical cavity has been constructed totally out of bulk YBCO ceramic superconductor. The cavity was designed to operate in TE_{011} mode at 13GHz with the intention of measuring the surface resistance of YBCO at this frequency. A diagram of the cavity is shown in figure 8 where the radius is given as 15mm and the length as 34mm. Coupling of the signal to the cavity was through a small hole in the centre of the cylinder where a small loop antenna was inserted. The unloaded Q of the cavity was deduced from reflection measurements.
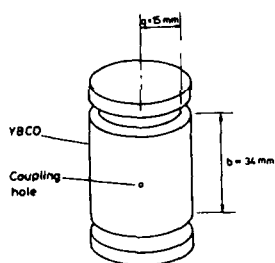
Figure 8   The cylindrical cavity
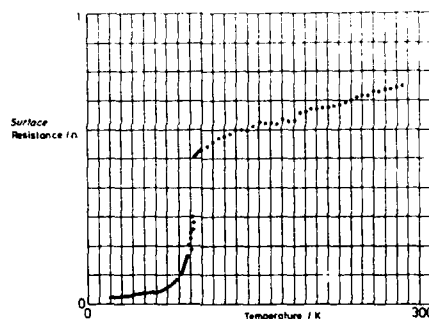
Figure 9   Surface resistance of the superconducting cylindrical versus temperature.

The maximum unloaded Q obtained from the cavity was 34,000 at a temperature of 20K and this fell to 10,000 at 77K. The surface resistance of the cavity can be deduced directly from the Q measurements by the expression

$$Q = \frac{g}{R_s} \qquad (2)$$

where g is a geometrical factor which can be worked out from the dimensions of the cavity which in this case was 778. A graph of surface resistance verres temperature is given in figure 9 showing values of 23mΩ at 20K and 70mΩ at 77K. At this frequency these values at 77K are not quite as good as copper at the same temperature. However, surface resistance of the high temperature superconductors has been shown to vary as ω^2 [3] whereas with copper the increase in surface resistance is $\omega^{1/2}$. This implies that at some lower frequency the superconductor will be superior to copper. This frequency is 7GHz for the bulk YBCO used in the cavity. Further details of this cavity can be found in reference [14].

Conclusion

Three types of microwave device made out of YBCO have been discussed. For each device the reduction in surface resistance over a conventional conductor has been

crucial to its operation. The antenna showed a 5db improvement in output power over a copper antenna. The average insertion loss of the filter improved from 1.8db to 0.5db. The cavity resonator resulted in a crossover frequency of 7GHz between the YBCO and copper materials.

These devices not only have useful applications in themselves but also represent the basis of a new generation of components which can be built using superconductors. The advantage of an antenna made out of a superconductor has been shown but further gain can be obtained if superconducting elements are formed into small arrays to give super gain or super directivity. The advantage of the low loss filter is greater if the bandwidth is reduced or if a sharp cut-off in the characteristic is required. By the use kinetic inductance filters can be made which are tuneable.

In addition, there are a number of other components listed in table 1 which show a large potential for superior performance if they are made out of high temperature superconductors. These have yet to be investigated.

References

[1] Gallop J. "Applications of Low and High T_c Thin Film Devices in Metrology" Institute of Physics Conference on "New Materials and their Applications" University of Warwick, U.K. April 1990.

[2] Everard J.K.A. et al. "High Q Helical Resonator for Oscillators and Filters in Mobile Communication Systems", Electronics letters V25(4), pp. 1648-1650, Nov. 1989.

[3] Klein N. et al. "Millimetre wave surface resistance of epitaxially grown $YBa_2 Co_3 O_{7-x}$ thin films", Appl. Phys. lett., 54(8), Feb. 1989, pp. 757-759.

[4] Lancaster M.J. "Passive Microwave Devices Applications of High Temperature Superconductors", Institute of Physics Conference on "New Materials and their Applications", University of Warwick, U.K., April 1990.

[5] Ralston R.W. "Signal Processing: opportunities for superconductive circuits", IEEE Trans. Magnetics V21(2), pp. 181-185, March 1985.

[6] Khamas et al. "High-T_c superconducting short dipole antenna", Electronics letters, V24, pp. 460-461, 1988.

[7] Allen R.S. and Nahman W.S. "Analysis and performance of superconductive coaxial transmission lines", Proc. IEEE, V52, pp. 1147-1154, October 1964.

[8] Maclean T.S.M., Wu Z., Lancaster M.J., Gough C.E., Alford N. "High temperature superconducting antennas", British Electromagnetic Conference, National Physics Laboratory, 7-9 Nov. 1989.

[9] Jordan E.C. "Electromagnetic waves and radiating systems", Prentice-Hall, New Jersey, 1968.

[10] Walker G.B. and Haden C.R. "Superconducting Antennas", J. Appl Phys., V40(5), pp. 2035-2039, April 1969.

[11] Adachi S. et. al. "Experiments on superconducting electric dipole and its array", Int. Symp. on Antennas and Propagation, Sendai, Japan, Aug. 1978

[12] Fujinaka M et al. "Trial Manufacture of Dipole Antenna Using $Y_1Ba_2Cu_3O_{7-x}$ Ceramic Wire", Int. J. Electronics, V67(2), pp. 245-249, 1989.

[13] Bantista J.J. and Petty S.M. "Superconducting NbTi and Pb(Cu) Bandpass Filters", IEEE Trans. on Magnetics, V21(2), pp 640-643, 1985.

[14] Lancaster M.J. et al "High temperature superconducting cavity for measurement of surface impedance", Int. Conf. on "Low Temperature Electronics", Berkely California, April 1990 to be published in Cryogenics

DISCUSSION FORM

Name of Author: Dr. M. Lancaster

Paper No.: 7 -- Passive Microwave Devices Using High Temperature
            Superconductors

Name of person asking question: Divecha

Question

1.   What is the thickness of the thick film?

2.   What is the heat treatment

Answer

1.   ~30μ.

2.   Do not know.

MICROWAVE SUPERCONDUCTING ELECTRONIC DEVICES.

P. Hartemann.
Thomson-CSF, Laboratoire Central de Recherches.
Domaine de Corbeville - 91404 - Orsay Cedex (France).

SUMMARY.

The present and future applications of superconductors to the small-scale microwave electronics are reviewed by taking into account the results obtained with the conventional superconductors and the potentialities of the new high-temperature superconductors. The signal transmission by superconductive planar waveguides is surveyed. Then the effect of the electrode thickness on the propagation loss and velocity along superconductive microstrip waveguides is pointed out. The use of Josephson junctions in mixers or amplifiers or generators of periodic signals is considered. Examples of signal processing devices including linear or nonlinear superconducting elements are given. Their main characteristics are compared to those feasible by other techniques.

I - INTRODUCTION.

The small-scale electronic applications of superconductors involve the analog or digital signal processing, the electromagnetic wave detection and the magnetometry. Since the discovery of high critical temperature superconductors (critical temperature $\gtrsim$ 90 K), the potential impact of superconductivity on electronics is strongly enhanced. Recently the microwave quality of one of these new materials($YBa_2Cu_3O_7$)has been spectacularly improved by succeeding in fabricating epitaxially grown films [1] and passive devices demonstrating the capabilities of high-temperature superconductors (HTS) will be carried out in the near future. This paper concerns the current status and prospects about the microwave analog processing based on superconductive components. The first section deals with the signal transmission through superconducting planar waveguides and the second one is devoted to the functions performed by Josephson junctions. Examples of devices implemented with linear or nonlinear superconducting elements are described in the last section and their main characteristics are compared to the results obtained with devices fabricated by different techniques.

II - SIGNAL TRANSMISSION.

Modern electronic devices are achieved by stacking films on substrates. Then the microwave features of superconducting thin layers are firstly surveyed.

In contrast to the DC situation an alternative wave induces losses in superconductors. The losses result from the dissipative motion of normal electrons generated by thermal excitation and by Cooper-pair breakings due to the incident photon energy. This electron motion is produced by the electric field necessary to impose the alternative circulation on the Cooper-pairs.

Two theoretical approaches are used to evaluate the microwave losses : these are the two fluid model [''] and the more realistic Mattis-Bardeen method (MB). The last one deduced from the BCS theory involves the energy gap [2]. Both introduce an imaginary part in the conductivity σ for taking into account the superconductivity. The behavior of a superconductive layer is driven by the surface impedance Z_S. If the displacement currents are neglected, the expression of Z_S for a layer deposited on a non conducting substrate is :

$$Z_S = \left(\left(j\mu_0\frac{\omega}{\sigma}\right)^{1/2}\right) \coth\left[d(j\mu_0\omega\sigma)^{1/2}\right] = R_s + jX_s$$

with ω = angular frequency ($\omega = 2\pi f$).
        d = thickness of the superconducting layer.

The results obtained from the two approaches are not very different for thermal and photon energies smaller than the energy-gap.

A superconducting layer behaves differently according to the value of the product $d(\mu_0\omega\sigma)^{1/2}$. When this product is much smaller than one (the layer is thinner than the magnetic field penetration depth λ_L), the kinetic inductance L_k accounting the kinetic energy of electron-pairs becomes large and must be added to the conventional magnetic inductance.

$$L_k = \frac{\mu_0\lambda_L^2}{W.d}$$

with W.d = the superconducting strip section.

λ_L^2 is proportional to the reciprocal of the pair density. Then this inductance is tunable by variation of the pair number. Thermal or magnetic or optical or electronic means can be used to induce a kinetic inductance change. The electronic process consists of injecting a current in the strip to increase the pair velocity and adjust the pair density by the depairing effect.

Signal transmitting waveguides with a coplanar or microstrip configuration are implemented using superconducting electrodes. In the case of microstrips, the two electrodes are separated by a thin dielectric slab with a thickness H. The dielectric losses are supposed negligible. The guide losses and the propagation velocity depend upon the surface impedance. After the TF model the delay per length-unit is given by R/v (W >> H) where R is the kinetic - inductance - induced delaying factor ($R = \left[1 + 2\frac{\lambda}{H} \coth \left(d/\lambda_L \right) \right]^{1/2}$)and v the free propagation velocity in the dielectric material. The impedance of such a guide is Z_c :

$$Z_c = Z_{co}R$$

where Z_{co} is the impedance of the guide formed with normal electrodes. The same kind of formulas is found by the MB theory. When the aspect ratio W/H is smaller than about 15, a fringe factor is introduced. It reduces the impedance without great influence on the delay for ratio W/H $\geq$ 5. It reaches about 1.6 for W/H equal to 5 and d/H close to 1.

Then the main advantages of superconducting planar waveguides are :

low conduction losses.

The propagation losses per length-unit depend on the real and imaginary parts of the surface impedance. If the dielectric and electrode thicknesses are much larger than the penetration depth, the losses are proportional to the ratio R_S/H, the strip being much wider than H. In figure 1, experimental values of R_S versus frequency for different superconducting materials ($YBa_2Cu_3O_7$ and Nb thin films, Nb_3Sn) are compared to those for pure copper. For instance the 10 GHz surface resistance of niobium films cooled at 4.2 K is equal to 10^{-4} $\Omega/\square$. For $YBa_2Cu_3O_7$ at 77 K after recent results, it is close to 5 x 10^{-4} $\Omega/\square$ that is 20 times weaker then R_S for bulk copper at the same temperature. R_S is practically proportional to the squared frequency f whereas for a normal conductor it is proportional to the square root of the frequency. Then the increase of R_S with the frequency is for a superconductor steeper than for a normal conductor.

Fig. 1 : Experimental surface resistance versus frequency for bulk copper and different superconducting materials. The results for $YBa_2Cu_3O_7$ (– – – –) are very recent and could be improved.
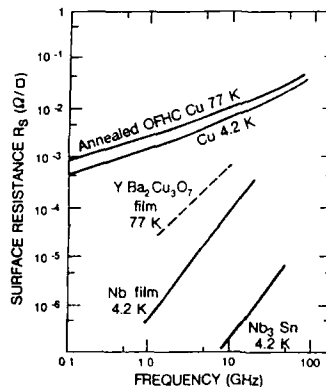
The table 1 shows the estimated unloaded quality factor (Q_{uc}) resulting from conductor loss alone for low impedance microstrip resonators. By comparison, Q_{uc} for a cylindrical copper cavity cooled at 77 K would be 2.08 x 10^5 at 2 GHz (TE011 mode) and 7.9 x 10^4 at 10 GHz. Then the advantage given by high-temperature superconductors is enhanced at low frequencies and the microstrip resonator quality factor at 77 K could be higher than that of a copper cavity cooled at the same temperature.

Electrodes	Frequency	Q_{uc}	
		2 GHz	10 GHz
Cu (300 K)		1 700	750
Cu (77 K)		5 200	1 970
$YBa_2Cu_3O_7$ (77 K)		9.9 x 10^5	39 500

Table 1 : Estimated unloaded conductor quality factor (Q_{uc}) for low impedance microstrip resonators (ratio of the cut-off frequency over the operating frequency = 5, relative permittivity of the dielectric = 9.5).

For microstrip waveguides with superconducting electrodes, the losses per length-unit is proportional to the product f^2 λ^3_L/H according to the TF model. For niobium at 4.2 K,

the losses are about 0.2 dB/cm for a 5 μm wide guide operating at 10 GHz with an impedance close to 10 Ω (W/H = 10). With copper electrodes, the losses are 8 dB/cm at 4.2 K and 12 dB/cm at 77 K. As a consequence of the frequency dependence, the losses at 100 GHz for niobium and copper would be about 20 dB/cm. That is prohibitive. With high-T_C superconductors a reduction of the losses around 100 GHz is expected as a consequence of the great energy-gap broadening and planar guides operating at millimeter wavelengths would be practicable.

. frequency independent propagation velocity.

In these dispersionless guides, very short pulses can propagate without shape degradation along relatively great length.

. slow-wave propagation in very thin films.

When the dielectric thickness is small with respect to the penetration depth, the propagation velocity is reduced. As a consequence of the kinetic inductance effect, the delay increases very much if the electrode thickness is also thin. As shown in figure 2 the delaying factor R reaches a few tens for electrode thicknesses which would be practicable. R values close to 30 were observed at 4.2 K with niobium nitride electrodes. In these conditions, the losses per length-unit are proportional to the expression $f^2 \lambda_L^3/(H.d)^{1/2}$ whereas the losses per delay-time-unit are proportional to $f^2 \lambda_L^2$ and remain finite versus electrode thickness (figure 2). As pointed out previously, the extra delay introduced by the kinetic inductance is tunable by various means.
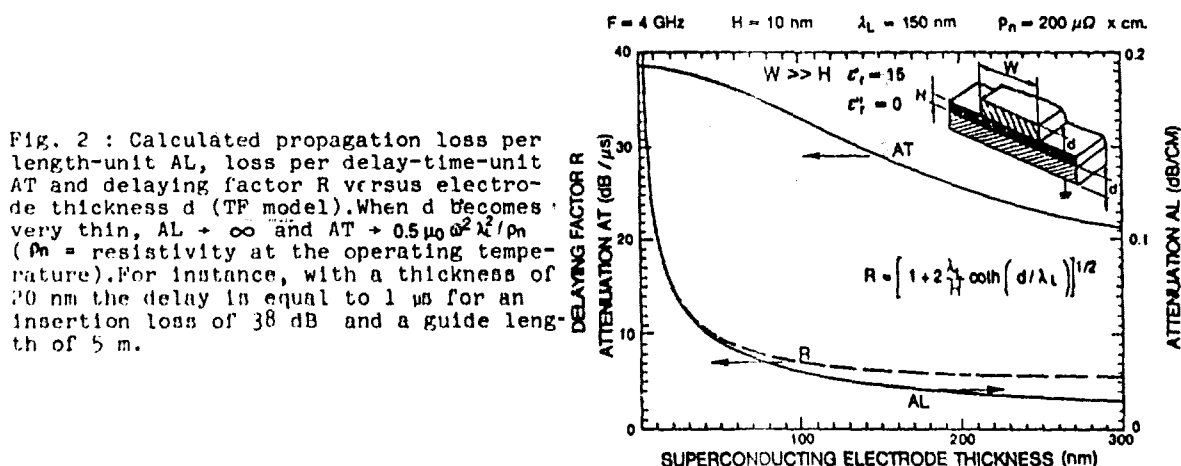
Fig. 2 : Calculated propagation loss per length-unit AL, loss per delay-time-unit AT and delaying factor R versus electrode thickness d (TF model).When d becomes very thin, AL → ∞ and AT → $0.5 \mu_0 \omega^2 \lambda^2/\rho_n$ (ρ_n = resistivity at the operating temperature).For instance, with a thickness of 20 nm the delay is equal to 1 μs for an insertion loss of 38 dB and a guide length of 5 m.

F = 4 GHz   H = 10 nm λ_L = 150 nm ρ_n = 200 μΩ x cm.

$$R = \left[1 + 2\frac{\lambda_L}{H} \coth\left(d/\lambda_L \right) \right]^{1/2}$$

III - FUNCTIONS PERFORMED BY JOSEPHSON JUNCTIONS.

Different signal processing functions can be performed by exploiting the nonlinear features of Josephson junctions.

. Mixing.

A very efficient multiplication of two signals has been obtained by taking advantage of the Josephson junction nonlinearity. An efficiency factor (ratio of the multiplied signal power over the product of the two input signal powers) close to - 40 dBm was measured at 3 GHz with niobium junctions. To increase the saturation level, arrays of junctions in series have been employed.These multipliers are basic components of correlators (see section IV).

Frequency down - converters are often necessary for signal processing. With SIS (Superconductor-Insulator-Superconductor) junction mixers, the conversion efficiency is higher than one and a gain of about 10 dB has been reached for a mixer cooled at 1.3 K. A supplied local oscillator power between a few nW to a few ten nW is sufficient at 100 GHz, whereas the Schottky diode mixers exhibit losses of 3 to 7 dB and the required local oscillator power must be about a mW for room temperature mixers and 0.1 mW at 15 K.

. Amplification.

The non-linear variation of the Josephson junction inductance versus supercurrent is exploited to implement low noise parametric amplifiers with a gain of about 10 dB (see Fig. 7).

. Periodic signal generation.

According to the AC Josephson effect, a periodic signal is generated by applying a voltage V to Josephson junctions. The frequency of this signal is proportional to V

(483.6 MHz/µV). This perfect linear voltage dependence of the frequency suggests the use of junctions to generate frequency modulated signals. Tunable local oscillators operating up to about one terahertz can be implemented with junctions made of low-temperature superconductors. But the junction impedance is low ($< 1 \Omega$) and the coupling between a junction and a practical impedance is very inefficient. Only a weak power (10^{-10} to 10^{-9} W) is available.

An other approach to achieve oscillators consists of exploiting the fluxon dynamic in long Josephson junctions operating at resonant or flux-flow type mode. As for a short junction the impedance of a long junction is low.

Two methods are studied to overcome this large impedance mismatch between the junctions and the useful loads. In the first one, an impedance transformer is used. For instance a flux-flow type Josephson oscillator has been coupled by kinetic inductance to a stripline operating as an impedance transformer. In the second method, arrays of phase-locked junctions (short or long) are implemented. As an example, a power of 1 µW deliverable on a load ranging from 20 to 60 Ω has been obtained between 350 and 450 GHz with an array made of 40 short SIS junctions [3] (figure 3). These junctions are parallel DC biased and in series along a serpentine microstrip. But both methods reduce greatly the oscillator tunability. However in such conditions, Josephson junctions may be used as generators.
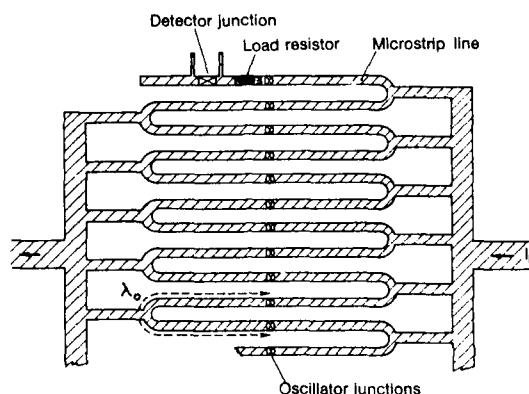
Fig. 3 : Josephson junction array oscillator.

IV - EXAMPLES OF MICROWAVE SUPERCONDUCTING DEVICES.

Devices including linear or nonlinear superconducting elements are shortly described and their main characteristics are discussed.

IV.1. Linear devices.

These passive devices are based on propagation lines.

a) Simple delay lines.

The superconducting materials allow to fabricate low loss and dispersionless planar waveguides with few micrometer wide strips. Then it is possible :

. to realize several meter long monolithic planar guides wound in meanders or spirals for inducing delay-time.

. to obtain slow-waves using thin dielectric and superconductive layers. The propagation velocity would be reduced up to some thousands km/s and maximum delay would be about 1 µs. Moreover the delays are electronically controlled and could be used for instance in scanning array antennas.

. to interconnect semiconductor chips on modules. As a consequence of the very narrow width of superconducting links, the packing density can be increased without introduction of high losses.

The figure 4 shows the predicted bandwidth-delay diagram for simple analog delay lines fabricated by three different techniques. The performances of optical fiber delay lines overlap in great part the superconductive delay line characteristics. However the potentialities of superconductors for complex processing are much heavier because the possible tunability and the capabilities of Josephson junctions.
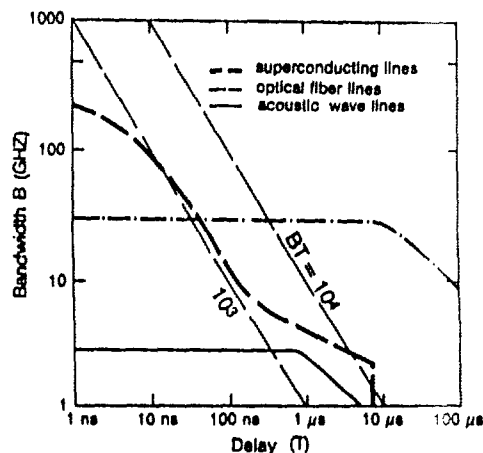
Fig. 4 : Forseen bandwidth-delay diagram for simple analog delay lines.

b) Dispersive delay lines.

As the superconducting waveguides are dispersionless, the delay variation versus frequency is obtained by a distribution of frequency selective couplers along delay lines. With this geometry, insertion losses of 5 dB for a delay variation of 37.5 ns in a bandwidth of 2.6 GHz around 4 GHz have been measured for 3.3 m-long and 39 μm-wide niobium striplines deposited on silicon disks. For practical use (spectrum analysis) this delay must be increased by stretching the strip length or exploiting the kinetic inductance effect [4].

c) Filters and oscillators stabilized by resonators.

As suggested in table 1, very selective filters can be advantageously implemented with coupled superconducting planar resonators. Superconducting cavities may be used also for filtering. At present time the fabrication of strong Q cavities based on high-temperature superconductors don't seem feasible in the near future.

Transversal filters can be performed with tapped delay lines and resistive parts for weighting. By kinetic inductance variation, theses filters would be programmable.

d) Small antennas.

Electrically small antennas fabricated with superconducting materials can operate efficiently, the ohmic loss resistance of antennas and associated matching networks becoming by superconductivity much weaker than the radiation resistance.

IV.2. Nonlinear devices.

Two examples are given.

a) Correlators.

The figure 5 shows the schematic of a proposed time-integrating signal correlator which is completely formed with superconductive elements. At the output, the correlation function is given with a number of samples equal to the tap number. Such a correlator consisting of 128 taps with a bandwidth of 2.5 GHz is studied at present time in USA [4].
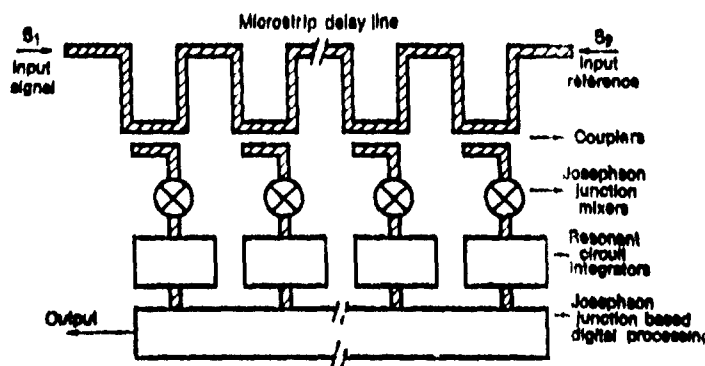
Fig. 5 : Schematic of a time-integrating correlator implemented with superconducting elements.

b) Heterodyne receivers.

SIS Josephson junctions operate as mixers in heterodyne receivers of radiotelescopes to detect (sub)millimeter waves. They work in photon-assisted quasiparticle tunneling mode. An example of receiver configuration is shown in figure 6.
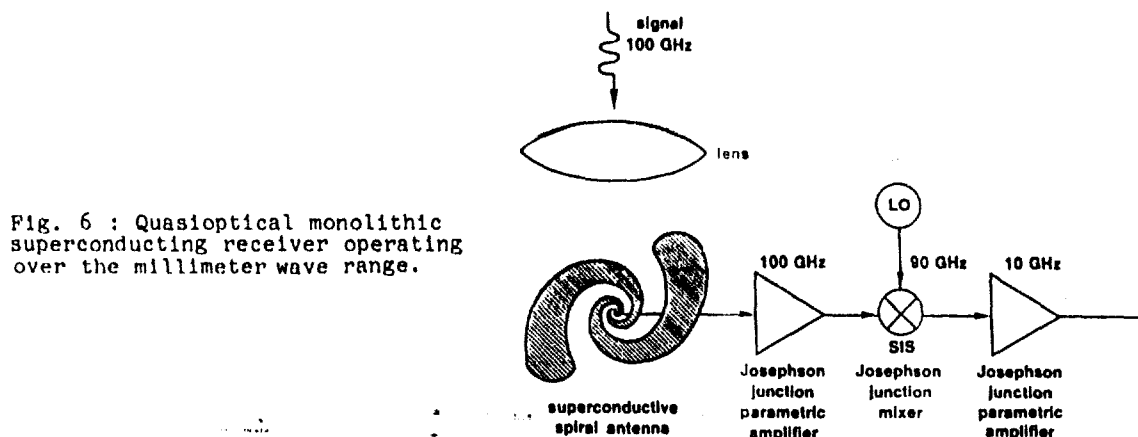
Fig. 6 : Quasioptical monolithic superconducting receiver operating over the millimeter wave range.

Recently a noise temperature of 41 K at 114 GHz has been reached in laboratory with a receiver cooled à 2.5 K and an antenna at 298 K [5]. The estimated contribution of the SIS mixer is smaller than 5.6 K. These noise temperatures were measured by a double-sideband set-up. With a single-sideband, the noise temperature of this receiver type is close to 60 K at 100 GHz, 200 K at 230 GHz and 400 K at 400 GHz. By comparison, for Schottky diodes cooled at 15 K, the noise temperature is 140 K at 100 GHz, 400 K at 230 GHz and 800 K at 400 GHz (see Fig. 7).
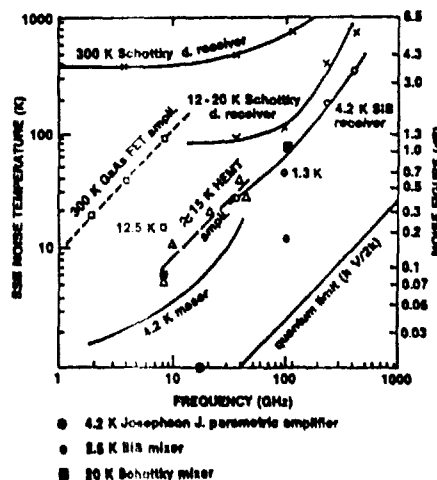
Fig. 7 : Single-sideband noise temperature for receivers, amplifiers and mixers.

The amplifiers used in receivers can be also superconducting. As shown in figure 7, over the 10 GHz frequency range, the cooled semiconductor devices (HEMT) compete with superconducting parametric amplifiers.

With conventional superconductors the highest frequency which can be detected is about one terahertz (Nb N) according to the energy-gap value. With high-T_c superconductors, the frequency limit could reach about 10 terahertz. But at 77 K the thermal noise is increased by a factor 20. Then it would be preferable for radio-astronomy applications to use large energy-gap superconductors cooled at lower temperature.

With high-temperature superconductors, SNS (Superconductor-Normal metal-Superconductor) Josephson junctions seem easier to fabricate than SIS junctions. At present time only embryonic HTS junctions have been achieved [6].

V - CONCLUSION.

While the electronic potentialities of superconductors are extensive, their present impact on the microwave electronics is very weak. Only heterodyne receivers effectively operate in radiotelescopes. The non-development of devices based on conventional superconductors is attributed to the difficulty for maintaining cryostats at the liquid helium temperature in systems. Moreover the device performances have to be improved and works about low-temperature superconductors are pursued in laboratories. However the future prospects are much more attractive through the recent strong raising of the critical temperature ($T_c \gtrsim 90$ K). The most advantageous feature of new high-T_c superconductors is the broadening of the energy-gap by an order of magnitude. With this

enlarged gap it would be possible with respect to the conventional superconductors to obtain a :

. smaller loss for given frequency and reduced temperature, or

. higher operating frequency for given loss and reduced temperature, or

. higher operating reduced temperature for given loss and frequency.

With the new superconductors, the millimeter wave frequencies would be reached without prohibitive losses and complex analog signal processings could be achieved in this frequency range. Moreover the large gap allows the use of neon at 27 K and nitrogen at 77 K as cooling liquids. In these conditions, the maintenance of the operating temperature is easier, the latent heat of vaporization being 61 times larger for nitrogen and 41 times for neon than for helium. The cryogenic environment is simpler, less costly and can be extensively used in all areas of high performance electronics. At present time, the 10 GHz surface resistance of high-T_C superconductor films ($YBa_2Cu_3O_7$) at 77 K is about the value measured for Nb films at 4.2 K, that is much lower that one of copper at 77 K. Then microwave passive devices based on HTS films are coming in few years. A technique for fabricating Josephson junctions must be carried out to take advantage of all capabilities of high-temperature superconductors. However the intensity of efforts achieved around the world about these topics is very impressive and the high -T_C superconductor technology is progressing rapidly.

REFERENCES.

[1]   A. Inam, X.D. Wu, L. Nazar, M.S. Hegde, C.T. Rogers, T. Venkatesan, R.W. Simon, K. Daly, H. Padamsee, J. Kirchgessner, D. Moffat, D. Rubin, Q.S. Shu, D. Kalokitis, A. Fathy, V. Pendrick, R. Brown, B. Brycki, E. Belohoubek, L. Drabeck, G. Gruner, R. Hammond, F. Gamble, B.M. Lairson, J.C. Bravman. Microwave properties of highly oriented $Y_1Ba_2Cy_3O_{7-x}$ thin films, Appl. Phys. Lett., 56, 1990, p.1178.

[2]   J. Bardeen, L.N. Cooper and J.R. Schrieffer. Theory of superconductivity. Phys. Rev., 108, 1957, p. 1175.

[3]   K. Wan, A.K. Jain and J.E. Luckens. Submillimeter wave generation using Josephson junction arrays, Appl. Phys. Lett., 54, 1989, p. 1805.

[4]   R.S. Withers and R.W. Ralston. Superconductive analog signal processing devices, Proc. IEEE, 77, 1989, p. 1247.

[5]   S.K. Pan, A.R. Kerr, M.J. Feldman, A.W. Kleinsasser, I.W. Stasiak, R.L. Sandstrom, W.J. Gallagher. An 85-116 GHz SIS receiver using inductively shunted edge junctions, IEEE Transac, MTT, 37, 1989, p. 580.

[6]   M.A.M. Gijs, D. Scholten, Th. van Rooy and R. IJsselsteijn. Superconducting proximity effect in $Y_1Ba_2Cu_3O_{7-\delta}$ -Ag-Pb trilayer structures. Solid State Communications, 71, 1989, p. 575.

High Tc Superconductors for Microwave Filters

J.C. MAGE, D. DIEUMEGARD

THOMSON-CSF Laboratoire Central de Recherches

Domaine de Corbeville 91404 ORSAY Cedex (France)

Abstract :

Passive microwave components will probably be the first application of high Tc superconductors. Devices such as multi-pole filters, delay lines, transversal filters with improved performances can easily be developped as soon as reliable high quality superconducting thin films are available. The basic constituent of these devices is a microwave line which consists of a superconducting layer deposited on a dielectric substrate then patterned. At the present time, the accurate characterization of both superconducting and dielectric materials is the main topic of the research activities in co-operation with the improvement of deposition techniques.

Introduction

The improvement of the performances of some passive microwave components is a significant challenge. For many years the specifications have been limited by the resistance of normal metals (copper, gold, silver, aluminium). This implies the use of bulky cavity filters and impedes the integration of many components, which would be desirable in the present technological context. Moreover this limitation makes some devices- such as transversal filters - inoperative by standard microwave circuit design. It is necessary to resort to other techniques such as CCD or acoustic waves which are somewhat frequency limited. On the other hand, the feasability of compact long delay lines and chirp filters has been demonstrated by the use of Niobium film at liquid Helium temperature (Ref. 1). It is very interesting to test these latter concepts with high Tc superconductors because they make possible either to operate at a more convenient temperature (liquid Nitrogen for instance) or to improve outstandingly the performances of these devices.

We can predict that this kind of device will probably be the first real application of high Tc superconductors. At the present time, the highest quality available materials are quasi single crystal pure YBCO thin films grown on a 10 x 10 mm dielectric substrate. This is ideally suited for demonstrating the great interest of such a new family of components.

I. Microwave filters and lines

Microwave filters are purely passive components. They do not require any non-linear element. Their principle of operation relies on wave propagation laws deduced from Maxwell equations. Two main kinds can be distinguished :

· Pole filters are made of resonant elements which can be RLC circuits, metallic cavities, dielectric resonators or lenghts of lines (typically half wavelength long). These resonators are coupled to each other by mutual inductance or capacitance in order to get a specified transfer function.

· Transversal filters are made of long con-tinuous transmission lines which can be bifilar line, coaxial line, waveguide, coplanar and microstrip line or even acoustic waves and optical fibers. The design includes internal and external couplings obtained by proximity effect in order to modify the transmission properties. When there is no coupling, it results in a simple delay line. With convenient couplings it is possible to obtain a frequency dependent transmission and to make dispersive delay lines, chirp filters...

Standard design uses bulky metallic cavities and coaxial line coils in order to get low insertion loss. This is not compatible with the evolution of the technology which makes Microwave Integrated Circuits prevail. The interest of superconductors is to avoid encumbering components by using integrated microwave lines. This is possible because the microwave resistance of superconduc-

tors is much lower than that of normal conductors and thus permit to get low attenuation and high performances in a compact package (Ref. 1).

The basic element of the components we are interested in, is the integrated microwave line (Ref. 2). Two examples are presentend in figure n°1 :

a) Microstrip line .
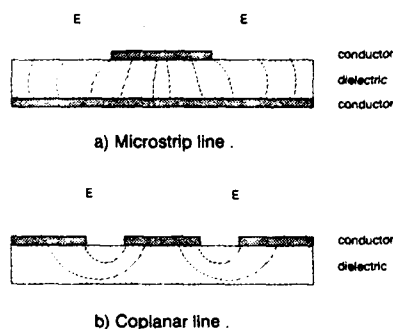
b) Coplanar line .

Figure N° 1 : Microwave lines (electric field) .

- Coplanar lines can be patterned from a single conducting layer deposited on a dielectric substrate.
- Microstrip lines require two conducting layers. The lower layer, generally non patterned, is the ground plane, and the upper layer is patterned into the designed circuit.

In both cases, it must be noticed that some of the electric field lines which go from one conductor to the other, cross the dielectric material. This is a very important point. It means that, in order to get very low attenuation lines, it is necessary to use not only a conductor with low resistance - that is the reason why we plan to use superconductors - but also a dielectric material with low loss. Both of these points are equally important.

Some designs can reduce the role of the dielectric material, substituting it by air or vacuum. Waveguides for instance consist of hollow pipes, but they cannot be integrated because their section must contain at least one half wavelength.

Inverted striplines (where the dielectric is above the circuit) and suspended striplines (where the dielectric is thinned and partly substituted by air) can reduce the contribution of dielectric loss to attenuation but these lines are more breakable and much more vibration sensitive than coplanar and microstrip lines.

The only way to get low attenuation integrated lines is to study simultaneously superconducting and dieletric materials. Material science is the basis of any technology. It is parted between chemical skill for the synthesis of materials and physical competences for the analysis of the resulting samples. Microwave characterization will only be considered further.

II. Characterization Methods

We have to measure both the surface resistance Rs of superconductors (definition in paragraph IV) and the dielectric loss tangent tan δ of dielectric materials (definition in Paragraph III). Two kinds of methods can be considered :

- Transmission methods consist in measuring the insertion loss and phase shift of a propagating structure. Accurate measurements require a high sensitivity microwave analyser, long lines, low resistance superconductor to normal metal contacts, low Standing Wave Ratio connections.

- Resonant methods consist in measuring the resonant frequency and the linewidth of a resonating structure. It requires a stable microwave generator, half wavelength structures, contactless couplings.

Resonant methods are much more accurate because it can be considered that the wave goes to and fro inside the resonator Q times. Q is the quality factor of the resonance (inverse of the relative linewidth) and is typically 10^4 to 10^5. Consequently, transmission methods would require kilometers long line (= Q x wavelength) in order to compete with resonant methods. Moreover, resonant methods avoid the problem of contacts and connections. On the other hand, they permit only discrete frequency values measurements.

Several resonant methods can be used. The quality factor can be measured either by direct half height linewidth for Q lower than 10^5 or by a temporal decrement method for Q higher than 10^5.

The accuracy is typically 1 to 0.1 %, and is more limited by thermal stability problems and spurious resonances which distort the peak than by the microwave test equipment. Several set-up can be considered :

1° Rectangular waveguide copper cavity

This geometry corresponds to usual Electron Spin *Resonance Spectrometers. They are often used to carry out Arbitrary Units characterization in order to estimate the qualitative behaviour of* materials versus a magnetic bias.

It is possible to get a more quantitative result by *use of the perturbation theory.* Let fo and Qo be the resonant frequency and the quality factor of the empty cavity (typical values fo = 10 GHz - Qo = 6000).

They turn into f and Q when the sample is introduced in the cavity. Let x be the quantity to be measured - either the permittivity or the surface impedance. It is a complex value. From the perturbation theory, the real and imaginary parts can be expressed as :

$x' = 2 A (fo - f)/fo$
$x'' = A (Q^{-1} - Qo^{-1})$
with
$A = A' Fm^2/Fs^2$

Fm is the mean field (electric or magnetic) in the cavity
Fs is the field at the location of the sample
A' is the volume or surface ratio cavity to sample

These formulae are a good approximation as far as the sample is smaller than one tenth of the wavelength - which implies that A is large (typically 10^3 - 10^4) and that the field lines are not altered by the presence of the sample- which supposes that the field lines are tangent to the surface of the sample everywhere.

The limits of this method (corresponding to an error of 100 %) are :

$\tan \delta \simeq Qo^{-1} \simeq 2 \times 10^{-4}$
$Rs \simeq Rs \; copper \simeq 10 \; m\Omega \; at \; 10 \; GHz$

2° Cylindrical copper TE$_{011}$ cavity

The principle is the same as the previous method, but the use of a cylindrical cavity instead of a rectangular one brings several advantages :

- the quality factor is much higher (typ : 33000 at 10 GHz)

- the TE_{011} mode where field lines are tangent to the surfaces avoid any discontinuity problem (either contact or depolarising effects) as far as the cylindrical symmetry is preserved.

- the cylindrical symmetry (of the cavity and the sample) permits exact solution instead of perturbation formulae - which authorizes larger samples and improves the sensitivity.

Large superconductivity samples can be measured by substituting them to one end of the cavity (diameter = 40 mm at 10 GHz). *Dielectric* substrates can be measured by introducing them in a split cavity.

The limits of this method are :

$\tan \delta \simeq 3 \times 10^{-6}$
$Rs \simeq 0.05 \times Rs \; copper \simeq 0.5 \; m\Omega \; at \; 10 \; GHz.$

3° Cylindrical Niobium TE$_{011}$ cavity

This method keeps all the advantages of the previous one, but the use of superconducting Niobium at liquid helium temperature (or below) leads to much higher quality factors (more than 10^7 at 10 GHz).

The limits are therefore divided by one thousand

$\tan \delta \simeq 10^{-9}$
$Rs \simeq 10^{-6} \; \Omega$

This method is technically much heavier than the previous ones because the cavity must be kept superconducting in liquid Helium. Characterizations of samples versus temperature are somewhat ticklish and require a carefully designed sample holder in order to heat the sample without heating the cavity (Ref.3)

4° Dielectric Resonator Method

This method is very similar to the method n°2 except that the metallic cylinder of the cavity is replaced by a non metallized dielectric cylinder. This modification is interesting :

- this cylindrical geometry still admits a simple analytical solution (Ref.4)
- the diameter of the resonator is divided by the refraction index of the dieletric material, which means that small samples can be measured without loss of sensitivity
- this method can be used either to measure the loss tangent of a dielectric material or the surface resistance of a superconducting sample, in a co-operative way. The limits of the method are set only by the quality of the available materials

An experimental set-up is presented in the figure n°2. The quality factor of this resonant cell depends on the loss tangent and on the surface resistance Rs in the following way :

$$Q^{-1} = A \tan \delta + B_1 Rs_1 + B_2 Rs_2 + B_3 Rs_3$$
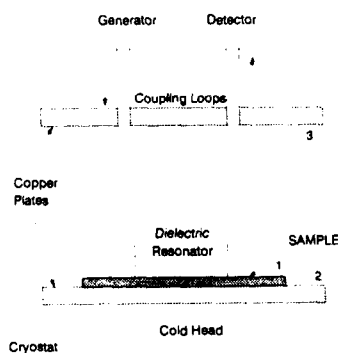
Figure N° 2 : Dielectric Resonator Measuring Cell

The indices 1, 2, 3 correspond to the different conductors as numbered on figure n°2. The coefficients A and Bi depend on the geometry and have to be calculated by suitable means (Ref.4). Several geometries must be measured in order to separate the different unknown quantities : in the figure n°2, the copper plate is separated from the dielectric in order to reduce B_3, the value of B_1 increases when the dielectric resonator gets flat- which favours the measurement of Rs_1.

The distance between the plates must be kept smaller than the half wavelength at the operating frequency in order to avoid radiating energy (under cut-off condition).

5° Lines

The final object - the coplanar or the microstrip line - can be used to determine the properties of its constituents. This proceeding can be very powerful. Coaxial and bifilar lines were commonly used to characterize the surface resistance of metallic wires. For the present time, thin films are concerned, so that patterning is required to achieve a line. It needs specific technical means and it can damage the surface resistance of the sample. These are the two drawbacks of this method.

The strength of this method consists in the possibility of varying the width of the line. The quality factor of a resonant length of line can be expressed as :

$$Q^{-1} = A \tan \delta + Rs \, \lambda/\pi W Zc$$

with $A \simeq 1$

λ = wavelength at the operating frequency = c/f

W = width of the line

Zc = characteristic impedance of the line (Zc is geometry dependent but scale independent)

For wide lines, the second term is small and the measurement is sensitive to tanδ. For narrow lines, the second term is predominant and the measurement is sensitive to Rs. So if we can engrave arbitrarily narrow lines, we are able to measure any surface resistance however small it could be. A surface resistance 43 times lower than that of copper has been measured by this method for YBCO deposited on Lanthanum Aluminate (Ref. 5)

III. Dielectric Materials

Dielectric materials are characterized by their complex relative permittivity $\varepsilon^* = \varepsilon' - j\varepsilon''$

The real part ε' determines the velocity V of the wave along the line :

V = c/n   with

c = velocity in vacuum = 3×10^8 m/s

n = refraction index = $\sqrt{\varepsilon'}$

The imaginary part ε'' contributes to the attenuation α of the wave along the line :

$\alpha = \pi \varepsilon'' f/c$ with α = expressed in Neper/m
                                        f = operating frequency

The loss tangent is $\tan \delta = \varepsilon''/\varepsilon'$

The choice of the dieletric material depends on the application :

- LOW PERMITTIVITY -ε'- material are convenient for CHIP TO CHIP INTERCONNECT. The shortest propagation time is required, so the highest velocity, hence the lowest permittivity Polymers, silica, cordierite and fosterite can be considered.

_ HIGH PERMITTIVITY -ε'- materials are convenient for DELAY LINES and FILTERS. The higher the permittivity, the slower the velocity. So it is possible to get a longer delay or to use a shorter line.

IN ANY CASE, THE LOWEST LOSS -ε''- IS REQUIRED.

Furthermore, dielectric materials for superconductors deposition must fulfil several conditions :

- lattice matching : the interatomic distances must suit those of superconducting materials in order to promote epitaxy

- chemical stability : there must be neither chemical reaction nor even physical diffusion between the dielectric and the superconductor

- thermal expansion matching to avoid cracking or peeling

The systematic study of dielectric loss for many materials and various operating conditions reveals several interesting points :

- Most of pure crystals exhibit a linear dependence of tanδ on the frequency in the microwave range. This behaviour has been observed for the materials of the table I from about 1 GHz up to 100 GHz. The quality factor Q is the inverse of tanδ. The linear variation of tanδ versus f implies that the product Q x f is constant. So this parameter Qf is the most apposite quantity to characterize high quality dielectric materials.

- The materials of table I also exhibit a consistent behaviour versus temperature -an example is given in figure n'3. The curve is approximately linear around room temperature but it turns to a typical knee around 100 K. For lower temperatures, the loss tends to zero with an horizontal slope, but the residual value is very dependent on the purity of the material.

This quasi universal behaviour of dielectric loss versus frequency and temperature can be modelled thanks to the infrared absorption theory involving multi-phonons mechanisms. The theoretical infrared spectrum of a pure crystal, when neglecting anharmonic effects, contains only narrow discrete lines corresponding to Transversal Optical Phonons which interact with infrared photons. The real spectrum includes wide lines, secondary peaks and continuous background which can be explained by taking into account the anharmonic effects. This quantum mechanics problem can be solved by using a phonon collision formalism. In the zero frequency limit (which corresponds to the microwave range) it is possible to write down a simplified formula (Ref.6).

$$\varepsilon'' \sim \frac{hf}{kT}\left(\sinh \frac{hf_0}{kT}\right)^{-2}$$

with   h = Planck constant $= 6.62 \times 10^{-34}$ J/Hz

f = operating microwave frequency

k = Boltzmann constant $= 1.38 \times 10^{-23}$ J/K

fo = mean optical phonon frequency

This law accounts for :

- linearity of tan δ versus frequency

- linearity of tan δ versus temperature between 200 - 400 K

delta microradians

Figure N°3 :Dielectric loss of rutile vs T

TABLE I

Material	Permittivity	Q*f THz
1 Mg O	9	250
2 Al₂O₃	9.5	300
4 Mg Ti O₃	18	180
3 La Al O₃	24	220
5 Ba₃Mg Ta₂O₉	25	330
6 (Zr,Sn,Ti)O₂	36	45
7 Ti O₂	86	50

TABLE II

Material	loss at 300 K	loss at 77 K
Sr Ti O₃	5*10⁻⁴	4*10⁻⁴
Y S Zirconia	45*10⁻⁴	26*10⁻⁴

- rounding of the curve near To = h fo/k
- horizontal slope for T = 0 K

The materials of table I converge satisfactorily to this theoretical law. Unfortunately, some materials fail (Table II). Yttria stabilized Zirconia and Strontium Titanane exhibit unusually high loss at room temperature, and these losses do not vary consistently versus temperature. This can be explained for Strontium Titanate by several phase transitions (cubic to tetragonal, tetragonal to orthorhombic) occuring between 0 and 300 K.
Both of these materials have been widely used as substrates for depositing high Tc superconductors, especially Strontium Titanate because of a good lattice matching with superconducting perovskites. Unfortunately the high value of the dieletric loss prohibits their use for microwave line application.

It must be noted that Strontium Titanate has also a high value of permittivity ($\varepsilon' \simeq$ 300 at R.T. >10 000 at low temperature). This can be very interesting for delay lines but it would be necessary to reduce ε'' first by some wise chemical substitution.

At the present time, Lanthanum Aluminate seems to be the best candidate. Its loss tangent at low temperature is much lower than 10^{-5} and lattice matching is good. Its only drawback consists in heavy twinning due to the rhomboedral structure. Lanthanum Gallate may avoid this problem. Sapphire has also been studied, but results were poor because of structural and chemical incompatibility. The use of the crystallographic plane 1012 may revive its interest (Ref.7).

IV. Superconducting materials

In the microwave range, superconductors are characterized by their surface impedance Zs. Mattis and Bardeen have carried out the calculation resulting from the BCS theory (Ref. 8). The real part of Zs corresponds to the surface resistance Rs which is defined for a square and is independent of its side. The imaginary part corresponds to an inductance and is strictly correlated to the London penetration depth.

In the figure n°4, the decimal logarithm of Rs expressed in Ohms is plotted versus the reduced temperature T/Tc where Tc is the critical temperature. Different cases are presented :
  a) Niobium

b) YBCO with the BCS relation for the energy gap (13,8 meV)
c) YBCO with the most probable value for the gap (20 meV).

When the energy of the microwave photon is higher than the energy gap, the superconductor turns back to normal state (about 600 GHz for Nb and 6000 GHz for YBCO). The same when T is above Tc.

It must be noted that for the superconductor state, the surface resistance tends to zero when the temperature tends to zero, while it tends to a finite value for the normal state (as for any normal metal, due to ano malous skin effect). This is due to the disapperance of normal electrons which occurs only at T = 0K. Then all the electrons are paired. This means that as far as the material quality and the cryogeny can be mastered, outstanding performances can be expected from superconducting devices.

The reference point, when considering the figure n°4 or the experimental results, is the surface resistance of pure copper (OFHC) which is about ten milliohms at low temperature and 10 GHz. It varies like the square root of the frequency while the surface resistance of superconductors varies about like the square of the frequency.

High Tc Superconductors are only four years old. The progress has been rapid since the discovery of the BaLaCuO phase with Tc = 13 K in January 86 (Ref. 9), then the LaSrCuO phase with Tc = 33 K in April 86 (Ref.10) and the YBaCuO phase with Tc = 93 K in February 87 (Ref.11). Many other phases containing Bismuth, Thallium, etc... with Tc up to 125 K have been discovered later on, but the main effort concerning thin films deposition and microwave characterization has been focussed on YBaCuO because this phase is relatively well known, easy to synthesize, stable and harmless.

In May 87, it was known that the surface resistance of YBCO ceramics was comparable to that of copper at 10 GHz. This was disappointing but could be explained by the poor microstructure of such samples. At the same time, many laboratories tried to deposit thin films by a wide variety of methods : co-evaporation sputtering, laser ablation...(Ref.12). During the following months, several trends emerged:
  - some substrates were inappropriate : silicon, silica or alumina react with YBCO and inhibit

a) Niobium

$E_0 = 1.52$ meV
$r_0 = 5.3$ uö.cm
$T_c = 9.46$ K

b) YBCO

$E_0 = 13.8$ meV
$r_0 = 58$ uö cm
$T_c = 91$ K

c) YBCO

$E_0 = 28$ meV
$r_0 = 58$ uö.cm
$T_c = 91$ K
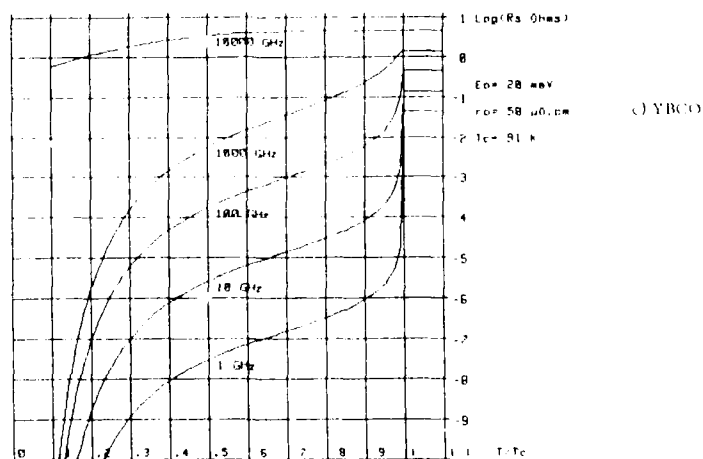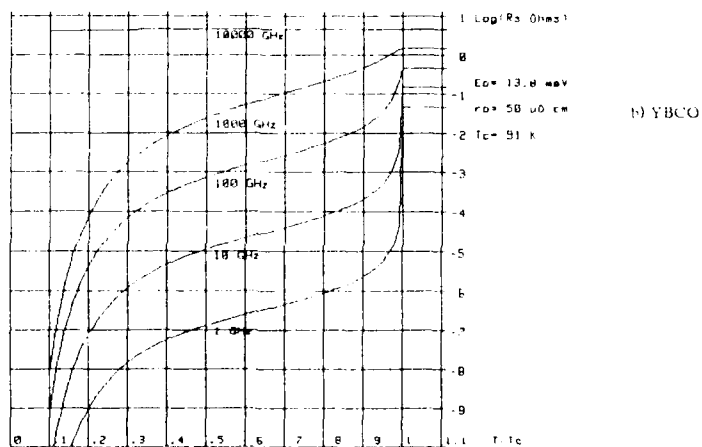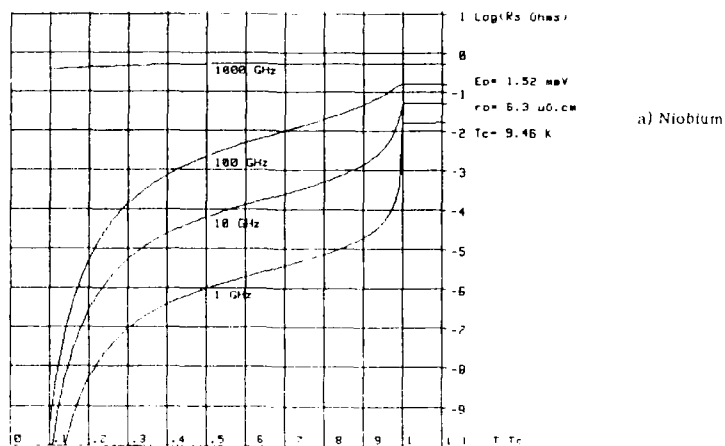
Figure n°4 : THEORETICAL VALUES OF SURFACE RESISTANCE

superconductivity.

- some substrates like magnesia, yttria stabilized zirconia could be used satisfactorily.

- one substrate - strontium titanate - seemed ideal because of lattice matching.

- the stoechiomety of the film was very important for its electrical properties.

- the surface resistance of polycrystalline, room temperature deposited, post annealed films was similar to that of ceramics.

- the surface resistance of highly textured films deposited at 750°C on Strontium Titanate could be ten times lower than that of copper at 86 GHz (Ref.13).

This last result was obtained during Summer 88, only one year and a half after the discovery of YBCO, but then it appeared that Strontium Titanate which was quite successful for laboratory purposes, was inadequate for microwave applications. Fortunately, some foreseeing researchers simultaneously demonstrated the advantage of Lanthanum Aluminate (Ref. 14) which was confirmed later (Ref.5). At the present time the best films have a surface resistance one hundred times lower than that of copper at 77 K and 10 GHz - i.e. 10^{-4} Ohm, which is very near the theoretical value of the figure n°4b.

Conclusion

For many years, the microwave filter technology has stumbled upon the basic limit of copper resistance. The low Tc superconducting metals (Niobium etc...) have permitted to demonstrate that original components were feasible, but the application field was limited by cryogenic requirements. The occurence of high Tc oxide superconductors will permit to improve the performances of this kind of devices while requiring lighter cryogenic means.

The most typical applications will be delay lines and transversal filters which are often impracticable by usual technology, but the first demonstrators will probably be multi- pole filters with improved performances. The recent progress of cryogeny with small closed cycle Helium refrigerators will favour the take-off of these new components.

References

1.   R.S. Withers, R.W. Talston : Proc IEEE Vol 77 n°8 (Aug.1989) p.1247

2.   R.E. Matick "Transmission lines for digital and communication networks" Mc Graw-   Hill Book COMPANY.

3.   D.L. Rubin et al Phys.   ν B Vol 38 n°10 (Oct 1988) p. 6538

4.   D. Kahjfez, P. Guillon "Dielectric Resonators" Artech House Microwave Library

5.   A.A. Valenzuela, B. Daalmans, B. Roas Electronic Letters Vol 25 n°21 (Oct 1989) p.1435

6.   J.C. Mage Rapport DAII n°80.35.174

7.   K. Char et al. Appl. Phys. Lett. Vol 56 n°8 (Feb.1990) p.785

8.   D.C. Mattis J. Bardeen Phys. Rev. Vol 111 n°2 (July 1958) p.412

9.   J.C. Bednorz, K.A. Muller Z. Phys. B n°64 (1986) p.189

10.   R.J. Cava et al Phys. Rev. Lett. n°58 (1987) p.408

11.   M.K. Wu et al Phys. Rev. Lett. n 58 (1987) p.908

12.   M.R. Beasley Proc. IEEE Vol 77 n 8 (Aug 1989) p.1155

13.   N. Klein at al Appl. Phys. Lett. Vol 54 n 8 (Feb 1989) p 757

14.   R.W. Simon et al Appl. Phys. Lett. Vol 53 n°26 (Dec 1988) p. 2677

THE STATUS-QUO AND PROSPECT OF SUPERCONDUCTING DIGITAL DEVICES

Ushio Kawabe
Superconducting Electronics Research Center
Central Research Laboratory, Hitachi, Ltd.
Kokubunji, Tokyo-185, Japan

1. Introduction

Superconducting digital devices, featuring high-speed, small size and low power dissipation, are expected to be one of key components of future computer system.

Currently, research and development are continued to demonstrate the possibility of the superconducting computer system above 1 GHz clock using highly reliable Nb/AiO$_x$/Nb Josephson junctions with small size and high current density[1], [2] and further to explore new digital devices capable with higher speeds and higher levels of integration[3],[4]. The striking feature is that superconducting digital devices have a small switching energy below 0.1 fJ and that they can be connected with a lossless superconducting wiring. From this good performance, a giga-scale integration type parallel-processing computer is promising through the heat flux and cooling power in cryogenic environment are taken into consideration.

The status-quo and prospect of superconducting digital devices will be discussed.

2. Progress of Josephson devices

The performance of high speed devices is expressed by the product of delay time, τ, and power dissipation, p, as shown in Fig. 1. Josephson junction (JJ) devices have the smallest switching energy of below 0.1 fJ in high speed devices and they are connectable with a lossless superconducting wiring. The fastest delay time is 1.5 ps for the Josephson junction device [5].

The delay time of JJ devices has been renewed year by year, as shown in Fig 2. The JJ devices were developed with unreliable but easily obtainable Pb alloy junctions before 1989, after which they were replaced from Pb alloy to Nb junctions with the progress of vacuum technology, and at the same time from the wet (lift-off) to the dry (ion-etching) processes. Afterwards, Josephson technologies made rapid progress. The fastest delay time attains at about one ps/gate, which value is obtained by dividing the full delay time of multi-stage JJ devices into the number of stages. This value corresponds to the case of a light load with one fan-in and one fan-out.

Figure 3 shows the cross section view of a JJ integration circuit. A current can flow from the superconducting upper electrode through a tunneling barrier to the superconducting lower electrode without generating any voltage if there is some phase difference between both superconducting electrodes. When a signal current is given to the control line, the current can not flow through the tunneling barrier, but can bypass another circuit of a MoNx resistor because there is no phase difference. Then, a voltage appears across the superconducting electrodes. This voltage is an output signal enough to kick the next stage. How to make a good tunneling barrier[6], [7] is, in this meaning, an important key for JJ technology because the scattering in area and thickness of the tunneling barrier depends on the margin of LSI and its operation.

Also in Fig. 4, the integration level for JJ logic LSI was developed with a steer gradient in comparison with the IC level of Si MOS and Si bipolar transistors. After 1988, many LSIs with various functions were tested to realize a gigahertz-cycle-time Josephson computer.

3. Demonstration of Josephson microcomputer

A GIPS microcomputer has been developed in order to demonstrate the feasibility of JJ technology. This computer is composed of a 4-bit data processor chip and a 1K-bit RAM (random access memory) chip, as shown in Figs 5 (a) and (b)[8], [9]. The system can operate in 1ns cycle with 40 mW power dissipation. The following key technologies are were developed to realize the microcomputer.

1) Good uniform of threshold current of Nb/AlOx/Nb junctions was obtained

2) High speed operation was attained by 3-stage pipeline architecture

3) Non-syncronized access capability was obtained by employing a full dc-powered memory system.

4) Low impedance superconducting packaging technology was developed for high seed operation

As listed in Table 1, the Josephson Logic circuits are composed of plural Josephson

junctions. Bistable switching operation is done either by magnetic coupling or current injection. Since the Josephson junction device is a latching one, it has to be driven by means of periodically cutting down. The Josephson interferometer logic (JIL) gate was chosen for the combinational logic circuits in our system because it is most reliable for the input-output separation. However, the dc-driven operation is very important for sequential and memory circuits. The old dc-driven devices had a problem of latch-up. We solved it only by putting a passive resistor for a constant voltage source across the old Huffle (Unltaching flip-flop logic element) circuit. This latch-up-free modified Huffle circuit was employed for the memory and sequential circuits in our system.

Fig. 6 shows the block diagram of a 4-bit data processor chip. In the chip with a size of 7 mm X 7mm, 3665 gates are integrated with 14960 Nb/AlOx/Nb junctions on the 2.5 μm design rule and with 1546 MoNx resistors. The minimum gate delay is 9 ps for the OR gate of the three-junction- interferometer type and 19.4 ps for the AND gate of the wired type. The maximum power dissipation amounts to 40 mW (including the 18 mW power consumed in the 8 regulators) for the whole chip which is not designed optimally. It was difficult to design the large scale circuits of more than 1K-gates manually. We employed a serial-fan-out CAD tool for the large scale circuits. At the left side of the chip shown in Fig. 6, the input and dc-output buffers are arranged. At the right side, the regulators for ac power are prepared. The upper portion has the arithmetic logic unit (ALU) and the accumulator (ACC). At the central portion, the control unit, the register, the read only memory (ROM), the instruction decoder(DEC), the program counters (PC1 and PC2) and the memory buffer register(MBR) are laid out. At the lower portion, three resister files (RF) are arranged for data, operation code and address. The 128 bits of the three RFs serve for the instruction cache, and the rest 64 bits serve for data. The external memory connected to the data processor has 256 words x 4 bits, and the address is done by 8 bit program counter (PC1 and 2). The external memory is driven with the dc power without any timing signal and the timing signal required is given from the data processor of the heart core. The 88 input and output pines are prepared around all sides of the chip. Table 2 lists the features of the data processors. The ALU RF, and I/O buffers form the data path. The ALU is composed of the 8-bit ACC, the 4-bit shift register (which is denoted by [S]), the 4

bit X 4 bit parallel multiplier, the 4 bit full adder and the eight 4-bit multiplexer. The ALU can execute the 6 instructions of MUL (parallel multiplication), ADD (addition), SUB(subtraction), DIV(fixed-floating-point division), PASS and SHIFT, as shown in Table 3. The rest instructions are for the RF and the external memory.

The 16 X 30-bit ROM stores the previously described 16 instructions. The instruction fetch, the data fetch and the the decode /execution were made by a three-stage pipeline architecture. Further one cycle time is needful to load data from the external memory. In Fig.7, the operation of 1-GHz clock was realized under the 70% duty of the ac current amplitude. The critical path is a case of MUL. The instruction path of the MUL has the path length of 22.5 mm. The number of the fan-out and gate stage are 29 and 24. The total delay for the MUL amounts to 725 ps. The average line delay is 9.0 ps/mm. An increase in one fan-out equals to what a signal is propagated for the length of 165 μm. The average gate delay per a gate is 20 ps.

The maximum machine cycle time of our microcomputer was 1 ns, which is composed of 0.6 ns for the circuit and wiring delay time, 0.3 ns for the ac-power-transition time, and 0.07 ns for the clock margin time. The superconducting packaging delay time was not taken under consideration. Considering the punch through phenomenon [10] and selecting the ac- power-transition time to be 0.3 ps, the critical path delay time was obtained to be 700 ps at the clock time of 1GHz. Since an average of 1 cycle are required for one instruction, this 1 GHz-clock cycle corresponds to 1 GIPS (10^9 instructions per second). This performance is 15 times better than that of ordinary semiconductor computers. As the first candidate of applications of this high performance JJ microcomputer. a parallel processor is expected. The second candidate is expected to be a signal processor like A/D convertor and FFT.

4. Sprouts of superconducting devices

Table 4 lists Josephson junctions and new superconducting devices supporting the progress of supercomputers. The Si-MOS IC level has been year by year developed with fine patterning of 0.8 μm for 4Mb-RAM, 0.5 μm for 16Mb-RAM, and 0.2 μm for 256Mb-RAM. However, the fine patterning approaches to 0.1 μm, near which a quantum limit appears in case of the semiconductor devices at 300K. It is superconducting devices having a different principle from that of the Si devices to break through this limit We have three superconducting devices. The

first device is such the Josephson junction device as previously described, which is a diode due to the superconducting tunneling effect. The second device is a three-terminal one due to the superconducting proximity effect, which was proposed by Clarke et. al, Sussex University in 1980 [11], and which was first verified by our Group in 1984 [12].The third device is a new electron-wave one [4] due to the Andeev reflection [13], in which parallel processing and analog neural processing are possible. As compared with size between these superconducting devices, the three terminal and new electron-wave devices will be one fifth and one sixtieth smaller than the junction size of the Josephson junction, respectively, which are expected to high density devices for the future computer if a Josephson junction is within 1 square μm.

5. SUMMARY

Research and development have been developed to demonstrate the possibility of the superconducting computer system above 1-GHz clock using highly reliable Nb/AlO$_x$/Nb Josephson junctions with small size and high current density, and further to explore new digital devices capable with higher speeds and higher levels of integration.

Consequently, Realization of a gigahertz-clock JJ computer was attained by employing reliable Nb/AlOx/Nb junction technology. Under the JJ technology, sprouts of promising concept devices beyond the quantum limit of ordinary semiconductor devices was brought up. To obtain the performance advantages that can compensate for disadvantage of cryogenic cooling, we have to realize further many breakthroughs in circuitry, powery, and packaging technologies. The superconducting computer will appear in the 21 C.

References

[1] Y. Hatano, S. Yano, H. Mori, H. Yamada, M. Hirano, and U. Kawabe: IEE J. Solid-State Circuit, SC-24 (1989) pp.1312/Y. Hatano, S. Yano, H. Mori, H. Yamada, M. Hirano, U. Kawabe: IEEE Micro, 8 (1988) 40.

[2]H. Mori, M. Hirano, H. Yamada, Y. Tarutani, Y. Hatano, and U. Kawabe: J. IECE Jpn. , J72-C-II (1989) 672.

[3]T. Nishino, M. Hatano, H. Hasegawa, F. Murai, T. Kure, A. Hiraiwa, K. Yagi, and U. Kawabe: IEEE Electron Device Lett., EDL-10 (1989) 61.

[4]T. Nishino, M. Hatano, H. Hasegawa, F. Murai, and T. Kure: Phys. Rev. Lett. B41(1990)

[5]S. Kotani et. al: Tech. Digest IEDM, (1988) 884.

[6]Y. Tarutani, M. Hirano, and U. Kawabe: Proceedings of the IEEE, 77 (1989) 1164.

[7]N. Miyamoto, Y. Tarutani, M. Hirano, T. Shimotsu, and U. Kawabe: J. Appl Phys 60 (1986) 2187.

[8]Y. Hatano, S. Yano, H. Mori, H. Yamada, and K. Nakahara: IEICE Technical Report (in Japanese), SCE89-60 (1990) 49.

[9]S. Yano, Y. Hatano, H. Mori, H. Yamada, K. Nakahara: IEICE TEchnical Report (in Japanese), SCE89-61 (1990) 55.

[10]H. P. Harris and W. H. Chang: IEEE Trans Magn., MAG-17 (1981) 603

[11]T.D. Clark, R. J. Prance, and A.D C Grassie: J. Appl. Phys 51 (1980) 2736

[12]T. Nishino, M. Miyake, Y. Harada, and U. Kawabe: IEEE Electron Device Lett. EDL-6 (1985) 297.

[13] A. F. Andreev: Zh. Eksp. & Teor. Fiz . 46 (1964) 1827.

Fig. 1. Performance of high speed devices.

Fig. 2. Year trends in the delay time of Josephson junction devices

Fig. 3. Cross sectional view of a Josephson junction circuit

Fig. 4. Year trnds in the integration level of Josephson junction logic LSIs.

Fig. 5. Microphotographs of a 4 bit data processor and a 1K bit RAM chip.

Fig. 6. Block diagram of a 4-bit data processor chip

Fig. 7. Operation waveforms of the 8-bit program counter (PC1 and PC2) in the data processor.

Table 1. Various Josephson junction devices.

Table 2. Features of the data processor.

Table 3. Instruction sets of the data processor

Table 4. Delay times for each instruction.

Table 5. Lists of Josephson junction and new superconducting devices

Fig. 1. Performance of High Speed Devices

Fig. 1. Performance of High Speed Devices

Fig. 2. YEAR TREND IN DELAY TIME OF JJD
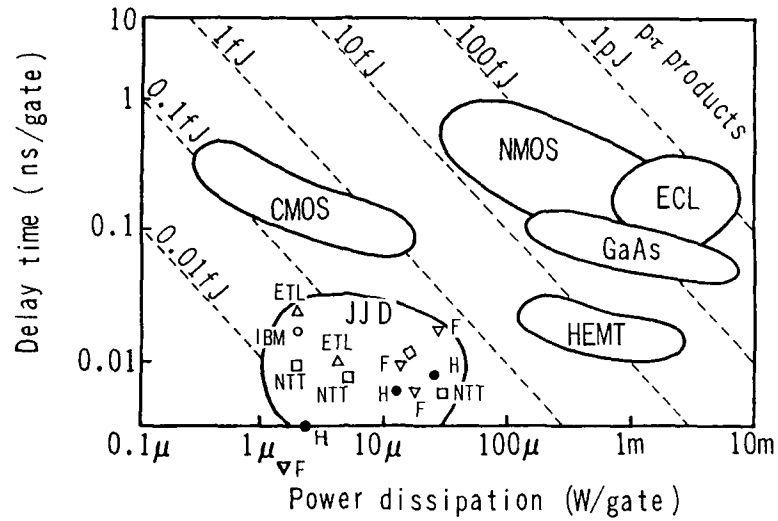
Fig. 2. YEAR TREND IN DELAY TIME OF JJD
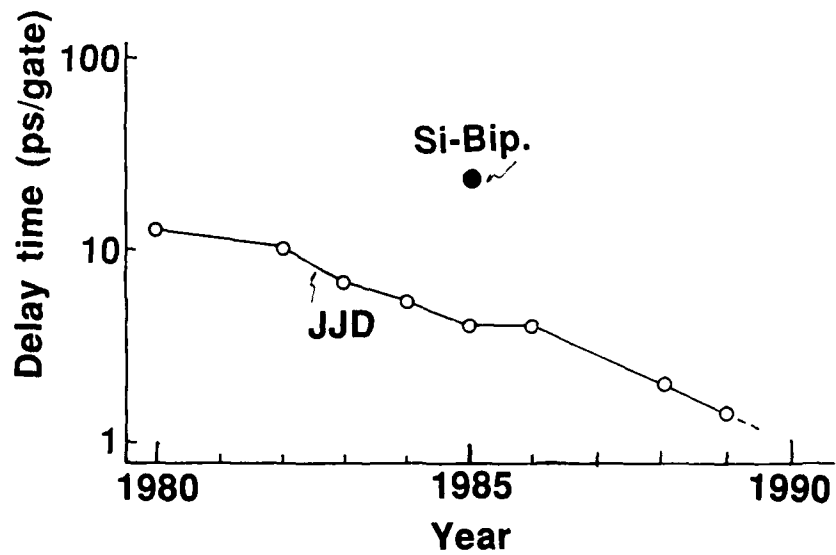
Fig. 3.   JJ Integration technology

Insulator
(SiO:600nm)
Insulator
(Si:380nm)

Control line
(800nm)

SC electrode
(Nb:100nm)

Connection area
(420nm)

Insulator
(SiO:350nm)

SC electrode
(Nb:200nm)

Tunnel barrier
(AlOx: 5nm)

Resistor
(MoNx:100nm)

Substrate(Si)

Grandplane
(Nb:300nm)
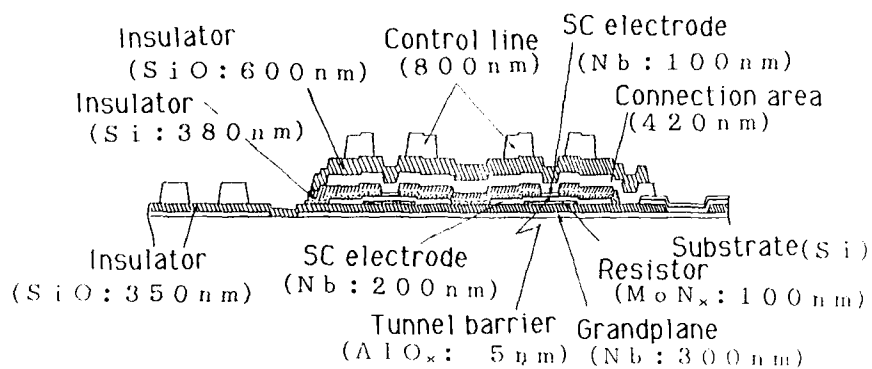
Fig. 4. YEAR TREND OF JJ LOGIC LSI

Si-MOS

Si-Bip.

JJD

IC level (gates/Chip)

100K

10K

1K

100

10

1975 1980 1985 1990 1995

Year

Fig. 5.

1 mm   1 mm
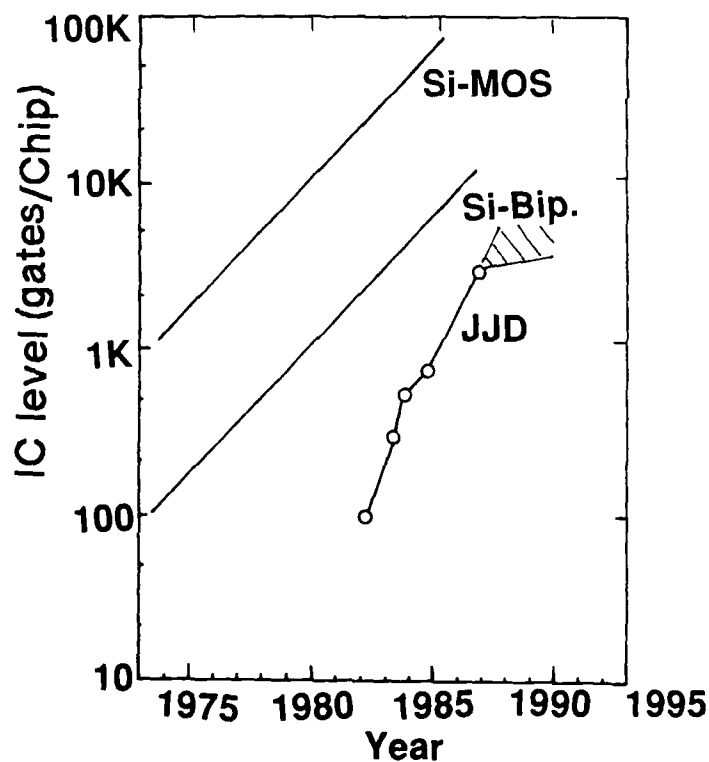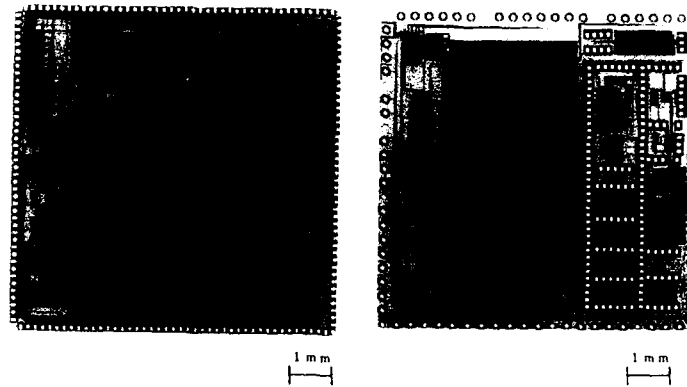
Fig. 6. BLOCK DIAGRAM OF THE DATA PROCESSOR
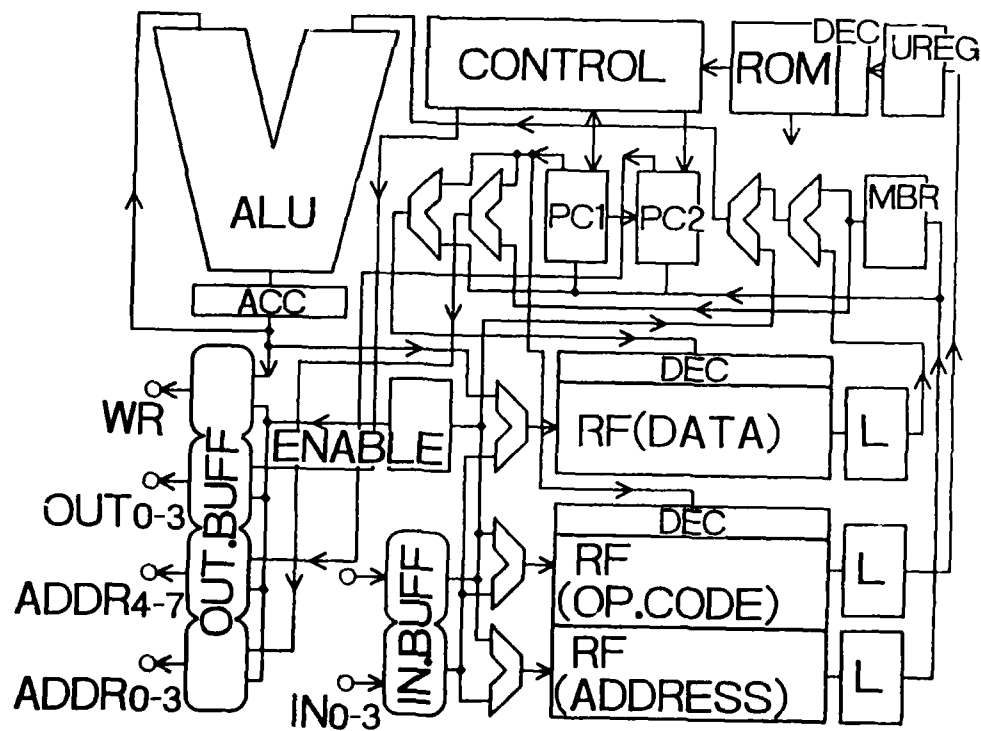
Fig. 7. OPERATION OF THE PROGRAM COUNTER

(a)20MHz   (b)1GHz
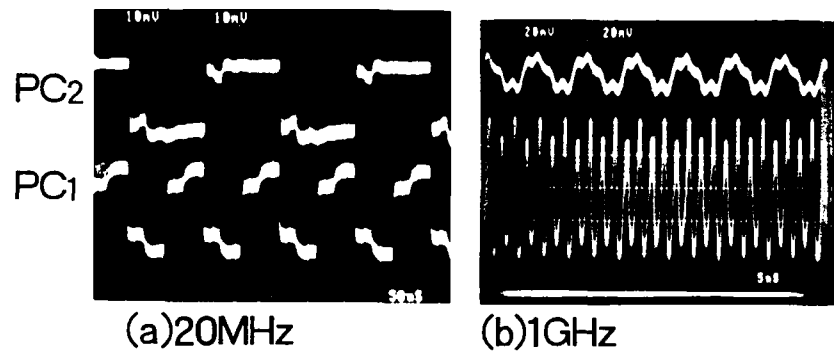
Table 1. JOSEPHSON LOGIC CIRCUITS

1 → 0 \ 0 → 1		Magnetic coupling	Current injection
DC-drive	Return to the SC state	o JTL ckt o Complementary ckt	
	Transition Phenomena	o Current-steering ckt o new Huffle	o Huffle ckt
AC-drive	Periodic cutting down	o JTL o JIL	o CIL o DCL o JAWS o 4JL o MVTL o RCJL o JTHL o RCL

Table 2. Features of the data processor

Instructions	16
ROM	480b
Register File	16×4b×3
Gates	3665
Junctions	14960
Resistors	15462
Process	Nb／AlOx／Nb
Design Rule	2.5um
Chip Size	7.0mm×7.0mm
Clock Rate	1GHz
Power Dissipation	40mW
I／Opins	88

Table 3. Instruction sets of the data processor.

INSTR.	OP.CODE	FUNCTIONS
NOP	0 0 0 0	
DIV0	0 0 0 1	BITSHIFT(Acc − MBR) →Acc, Acc[4] →S[0]
DIV1	0 0 1 0	if S[0]=0 then BITSHIFT(Acc − MBR) →Acc
		if S[0]=1 then BITSHIFT(Acc + MBR) →Acc
		BITSHIFT(S) →S, Acc[4] →S[0]
DIV2	0 0 1 1	S→Acc
ADD	0 1 0 0	Acc + MBR→Acc
SUB	0 1 0 1	Acc − MBR→Acc
MUL	0 1 1 0	Acc × MBR→Acc
SHIFT	0 1 1 1	Acc[7]~Acc[4]→Acc[3]~Acc[0]
LOAD	1 0 0 0	RF[α]→Acc
STORE	1 0 0 1	Acc→RF[α]
CLOAD	1 0 1 0	α →Acc
EXSET	1 0 1 1	α →PC2
EXLOAD	1 1 0 0	α →PC1, M[PC2, PC1]→Acc
EXSTORE	1 1 0 1	α →PC1, Acc→M[PC2, PC1]
EXPGM	1 1 1 0	M[PC2, 0]~M[PC2 + 1, 0]→I_Cache
BNLZ	1 1 1 1	if Acc[3]=1 then α →PC1

M[α]:register file of address α

Table 4. Delay time for each instruction

Instruc-tion	path length [mm]	fan-out	gate stages	total delay [ps]
MUL	22.5	29	24	725
ADD	20.3	17	22	648
LOAD	23.3	26	16	568
STORE	21.7	26	12	474

delay : 9.0ps/mm, 1 fan-out =165 μ m, 1 gate=20ps

Table 5. JJ AND NEW SC DEVICES

Years (micron)	Si-MOS IC level (bit/chip)	Superconducting devices			
		Devices	Quantum effect	Element	Appli cation
1990 0.8 -	4M	J J	SC tunnel ing	Diode	Analog /Digital
1992 0.5 -	16M	SC Tr.	Proxi mity effect	Tran sistor	
1998 0.2 -	256M				
2002 0.1 -	?	AR devices	Andeev reflec tion	Parallel Process ing	Analog /Neural

Discussion

Name of Author: Dr. U. Kawabe

Paper No.: 11 -- The Status Quo and Prospect of Superconducting Digital
Devices

Name of person asking question: MacPherson

Question

How well does the 1 GIPS processor survive thermal cycling between room
temperature and the 4.2K LHe temperature? In other words, have you been able
to cycle it many times without failure of the processor.

Answer

Any performance of our 1 GIPS processor does not change even though thermal
cycling between RT and 4.2K is given many times to it.

Discussion

Name of Author: Dr. U. Kawabe

Paper No.: 11 -- The Status Quo and Prospect of Superconducting Digital
                 Devices

Name of person asking question: R. Humphreys

Question

Have you measured the electrical properties of the YBCO-La$_{1.5}$Ba$_{1.5}$Cu$_3$O$_7$-YBCO
structure?

Answer

DC and AC I-V characteristics were measured at 4.2 K and 35 K for a
superconducting proximity YBCO-La$_{1.5}$Ba$_{1.5}$Cu$_3$O$_7$-YBCO device, respectively.

Discussion

Name of Author: Dr. U. Kawabe

Paper No.: 11 -- The Status Quo and Prospect of Superconducting Digital
            Devices

Name of person asking question: P. Ryan

Question

What is your opinion on the 1 K bit maximum memory density obstacle in low
temperature superconductivity? Do you feel it will be solved to enable low
temperature superconductivity to become a competitor with semiconductor
technology in computing?

Answer

Yes, I believe the problem can and will be solved by multilayer structures and
much R&D effort.

ANALOG SUPERCONDUCTIVE ELECTRONICS FOR AVIONICS

by
A. H. Silver and A. D. Smith
TRW Space & Technology Group
One Space Park
Redondo Beach, CA 90278
USA

ABSTRACT

Superconductive electronics may solve critical problems in avionic sensors and signal processing. This results from both fundamental considerations such as low RF loss and power dissipation, flux quantization, and the Josephson effect. Because new physical mechanisms can be applied, new device configurations can be employed. This presentation will describe the state-of-the-art and project near-term applications. Examples of high leverage superconductive technology in analog signal processing, analog-to-digital converters, low noise receivers, and phased array components will be presented. Both high temperature copper-oxides and low temperature metallic superconductors will be discussed.

PREFACE

Superconductivity is a distinct state of certain conductors that exists below a critical transition temperature (Tc) that is unique for each material[1]. This state is characterized by zero DC resistance, macroscopic magnetic flux quantization, and new nonlinear phenomena that can generate new families of electronic circuits. Before 1986, only the low temperature superconductors (LTS), notably lead (Pb), niobium (Nb), and niobium nitride (NbN), were available for circuit development. The Tc values and operating temperatures of the LTS materials are close to that of liquid helium (LHe), as shown in Table 1. Since 1986, the discovery of high temperature superconductor (HTS) copper oxides such as yttrium barium cuprate $YBa_2Cu_3O_7$, or 1-2-3), bismuth strontium calcium cuprate (BiSrCaCuO compositions), and thallium calcium barium cuprate (TlCaBaCuO) have elevated the transition temperatures and projected circuit operating temperatures nearly an order of magnitude.

Superconductor	Tc	Operating temperature
Niobium	9 kelvin	4 kelvin
Niobium nitride	14	9
$YBa_2Cu_3O_7$	93	70
TlCaBaCuO	125	90

Table 1. Transition temperatures and operating temperatures of technologically important superconducting compounds

In this paper, we describe the fundamental properties and features that lead to a high performance SCE technology for avionics applications. We use LTS examples to describe the state-of-the-art and project future systems. We briefly assess the state-of-the-art in HTS and summarize the problems that remain to be solved.

PASSIVE MICROWAVE DEVICES

Performance is the motivation for developing superconducting electronics (SCE) for avionic systems. Important aspects of SCE devices include:

- operating frequency and signal bandwidth of tens to hundreds of GHz
- detector sensitivity approaching quantum and thermal limits.
- picosecond switching speeds
- sub-microwatt power requirements

The key features of superconductive electronics develop from two distinct phenomena of the superconducting state: the low loss properties of superconducting materials and the unique quantum mechanical behavior of the Josephson junction.

While physicists still debate the microscopic details of the superconducting state, many of the basic phenomena of superconductivity have been accepted for some time. In 1911 Kammerlingh Onnes discovered the disappearance of resistance in superconductors. The famous "zero resistance" property of superconducting materials is, strictly speaking, only true at DC[1]. Nevertheless, for a wide range of frequencies the resistive losses in superconductors fall orders of magnitude lower than the best normal metals, copper, silver, and gold (See Fig. 1)
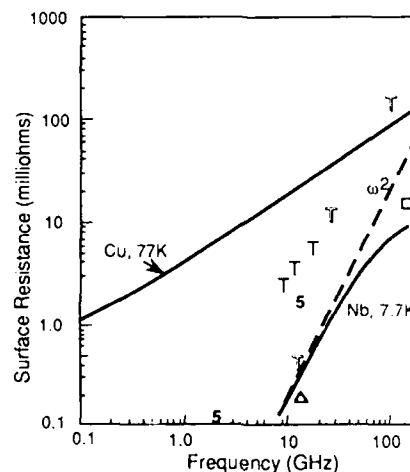
Figure 1. Surface resistance measured for normal metal copper, superconducting niobium at 7.7 kelvin, and a compendium of data points for HTS thin films with the lowest reported surface resistance. Data points include TRW films on lanthanum aluminate substrates (T and shadowed-T), Bellcore (5), and Stanford (Δ). Simple physical arguments suggest an ω^2 dependence on frequency, as shown.

Microwave electronic circuits, key elements of modern avionic systems packages, are highly amenable to the improvements possible with low resistivity conductors. Presently, microwave circuit designers face a fundamental dilemma in microstrip design as avionic systems push to higher frequencies and increased circuit density. Designers who chose standard thickness substrates must face large radiation losses, cross-talk between neighboring circuits, geometrical dispersion, and potential multi-mode propagation. On the other hand, those designers choosing thinner substrates must cope with large resistive losses and resistive dispersion. These problems are particularly severe in long delay lines, and wideband signal processing.

(2a)

(2b)
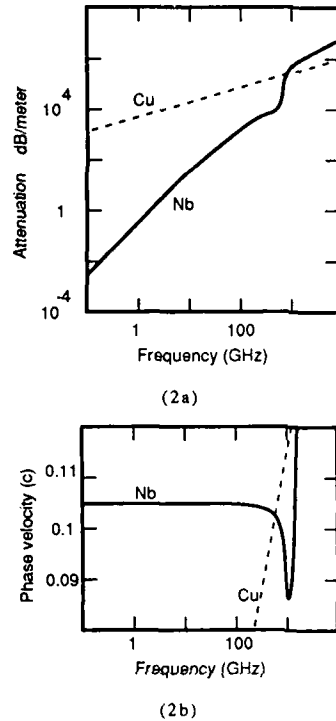
Figure 2. The attenuation (2a) and phase velocity (2b) for both normal metal copper (Cu) and superconducting niobium (Nb) microstrip, after Kautz[2]. Niobium predictions are for a 4 kelvin conductor 0.1 microns above a niobium groundplane.

Superconductivity offers a path around the resistivity roadblock. The low resistive loss in superconducting materials translates directly into low propagation loss in superconducting films (See Fig. 2a), even in thin dielectric geometries. Superconducting microstrip competes favorably with waveguide for low loss, while maintaining the size and weight advantages of microstrip structures. In addition, superconducting microstrip is essentially dispersionless up to 500 GHz, a property unmatched by either conventional microstrip or waveguide.[2] Figure 2b compares the frequency dependence of wave velocity for normal and superconducting lines.

Radar signal processing is one area where the combination of bandwidth and long propagation times lead to high device performance. Scientists at M.I.T./Lincoln Laboratory have built several fundamental building blocks for radar signal processing, including a microstrip chirp filter. The chirp filter consisted of a dispersively coupled delay line on thin silicon substrates[3]. By spiraling 3 meters coupled microstrip, experimenters achieved 2.3 GHz of chirp bandwidth, potentially providing 0.1 meter range resolution in a radar systems.

As superconducting materials progress to higher operating temperatures, lower surface resistances, and more stable chemistry, an entirely new architecture of superconducting microwave and millimeter wave integrated circuits (S-MMIC) microwave circuits is spreading. In order to take full advantage of the miniaturization possible with superconductivity, very thin dielectrics are required. S-MMIC replaces substrate dielectrics

with deposited thin films (See Fig. 3). The resultant structure enables very densely packed circuits, with line spacings of 2 microns without cross-talk.
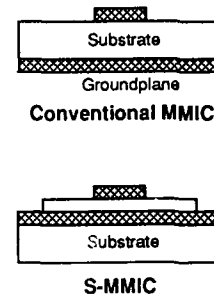
Figure 3. Geometries for standard MMIC (top) and Superconducting MMIC (bottom). In conventional MMIC the substrate material serves as the dielectric for wave propagation. Substrates are typically 0.5 mm thick. In the superconducting version, the groundplane is deposited on top of the substrate. Wave propagation is through a deposited thin film, typically 0.5 microns thick.

Superconducting delay lines have been demonstrated in S-MMIC technology using niobium nitride films at liquid helium temperatures[4]. Delay lines require maximum electrical line lengths in a minimum volume package, while maintaining low signal attenuation. S-MMIC architectures are attractive due to the high packing densities for microstrip lines. In addition, designers are aided by another peculiarity of superconductivity: kinetic inductance. The inertial energy of the superconducting electrics contributes an inductance-like term to the microstrip wave equation. Inductive slowing of propagating waves adds electrical length and additional delay to microstrip lines. Researchers at the U.S. Naval Research Laboratory report velocities as low as 0.01 c (corresponding to an effective dielectric constant of 10,000) with only 0.01 dB/cm attenuation at 2 GHz[4].

Josephson electronics
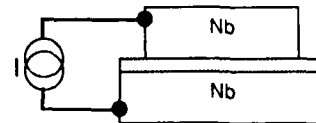
Figure 4. Josephson junction, the active element of superconducting electronics. The Josephson junction consists of two thin film films of superconductor, typically a few thousand angstroms thick, separated by an dielectric barrier 10-20 angstroms thick. Quantum mechanical tunneling transports electrons across the dielectric to produce current flow.

The second element of superconductive electronics, the Josephson element, has no direct equivalent in conventional electronics. Figure 4 shows a tunnel junction type of Josephson element. Current flow of superconducting electron pairs ("supercurrent") through a Josephson element can be described by the simple current-voltage relationship given by

$$I = I_c \sin \theta$$

$$d\theta/dt = 2\pi/\Phi_o \, V$$

where I_c is the maximum pair supercurrent and θ is the quantum mechanical phase difference across the junction. The flux quantum, Φ_o, is a fundamental constant given by

$$\Phi_o = h/2e \cong 2 \times 10^{-15} \, volt\text{-}sec$$

where h is Planck's constant and e is the electronic charge.

Despite the simplicity of the Josephson equations, the applications of Josephson devices are widely varied. Engineers harness the Josephson tunnel junction as threshhold-detecting current switches (limiting at I_c), voltage-controlled oscillators, variable inductor, and magnetometers.

JOSEPHSON JUNCTION OSCILLATORS

The Josephson tunnel junction is a natural voltage-to-frequency converter. Biased at a constant DC voltage, the Josephson junction spontaneously oscillates at a frequency, f, given by

$$f = V_{bias} / \Phi_o = V_{bias} \, X \, 484 \, GHz/mV$$

The frequency agility and line shape of Josephson voltage-controlled oscillators is demonstrated in Fig. 5. Stepwise adjustment of the junction bias voltage shifts the oscillator frequency from 9 to 10 GHz with only a few dB amplitude variation[5]. Josephson junction oscillators operate from to rf to sub-millimeter frequencies.

One area of concern is power. Individual junction oscillators can produce at most a nanowatt of microwave power. Recently devised oscillator arrays produce microwatt level oscillator power at sub-millimeter wave frequencies[6]. These levels of power, in an integrated circuit geometry, present interesting new possibilities for integrated superconducting mixer/local oscillator circuits up to 435 GHz. Figure 6 shows the output power measured for a 40 junction Josephson array.
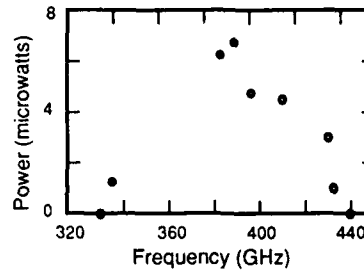
Figure 6. Measured sub-millimeter wave output power for Josephson oscillator array, demonstrated at Stony Brook (see Ref. 6).

ANALOG-TO-DIGITAL CONVERTERS

Circuit architectures handle a larger and larger fraction of signal processing using digital techniques. Pipelined digital signal processors now handle cycle times approaching 10 nsec, and superconductive microprocessors have been demonstrated faster than 1 nsec[7].

Interfacing our rapidly developing computer power to real-time avionic environment focuses critical performance requirements on a specific subcircuit: the analog-to-digital (A/D) converter. We task A/D converters with the difficult job of translating the inherently analog world of electromagnetic fields into a binary format recognizable by digital processors.

Superconducting electronics offers unique possibilities for high speed A/D conversion. These capitalize on the unique quantization inherent in the Josephson junction and SQUID (superconducting quantum interference device). The SQUID is the simplest superconducting circuit, consisting of one or more Josephson junctions in a circuit closed with superconducting inductors. The SQUID has an infinite number of discrete magnetic states that differ by precisely one flux quantum. Transitions between these states can be made by switching a Josephson junction in the circuit.

Designers are pursuing two basic approaches, each of which use the high speed and precise linearity of SQUIDs, to perform analog-to-digital conversion. First, parallel conversion uses multiple identical SQUIDs, fed with successively divided input current. The parallel approach is illustrated in Fig. 7. Circuit designers use the periodic response of the SQUID detect inputs modulo a flux quantum. Each SQUID produces one bit of output, with the first SQUID producing the least significant bit.

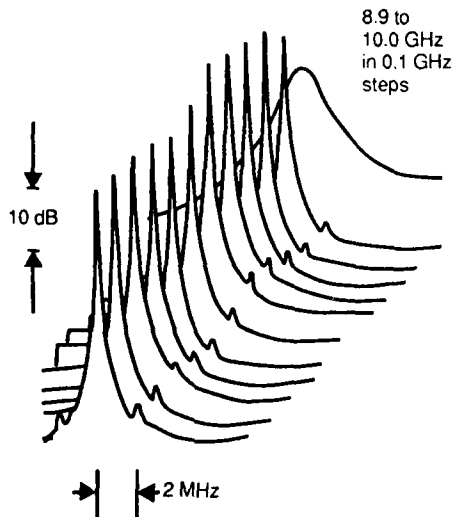8.9 to 10.0 GHz in 0.1 GHz steps

10 dB

2 MHz

Figure 5. Josephson voltage-controlled oscillator output power. DC voltage across the Josephson junction was varied stepwise to produce output power from 8.9 to 10.0 GHz. Linewidths are less than 200 kHz to 3 dB points. (See Ref. 5.) Extraneous peaks 2 MHz from the carrier are due to frequency modulation of an external signal.

Figure 7. Parallel SQUID A/D converter architecture. Input current applies magnetic field to a series of SQUIDs. Each SQUID produces a logic zero for nearly integer applied flux ($|\Phi/\Phi_0 - n| < 1/4$). Successive division by two reduces sensitivity of the downstream converters, thus producing a binary weighted output.

The second superconducting A/D approach, shown in Fig. 8, relies on a single SQUID quantizer to detect transitions between magnetic states induced by an input current. Each additional quantum of flux applied to the SQUID produces an additional pulse output. A chain of high speed, Josephson counters generates the digital output. The multiple SQUID type is being developed for very high sampling rates at modest resolution (4-6 bits). The latter, single quantizer approach appears more suitable for high resolution converters.
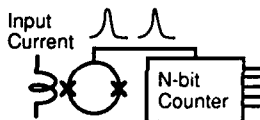
Figure 8. Single quantizer superconducting A/D approach. The quantizing SQUID is designed to produce a voltage pulse for every additional flux quantum introduced into the SQUID loop. A superconducting counter produces the final A/D output.

The performance of these converters is limited by the speed of the SQUID threshold devices in responding to an analog signal and making the required magnetic transitions. These should approach 1 picosecond. This results in projected performance limited by the standard aperture uncertainty relation with the aperture uncertainty given by the switching time.

Key features of these A/D converters include low gate count and ultra-low power dissipation. The gate count increases linearly with the number of bits, compared with approximately 2^N for high performance semiconductor converters. Figure 9 shows a compendium of conventional and superconducting A/D converter performances. Projected power dissipation is less than 20 microwatts, independent of sampling rate. For comparison, the fastest semiconductor A/D converters plotted on figure 9 require up to 20 watts to operate. The power advantage of superconductors becomes significant for processing information from antenna arrays with wide bandwidth, where the large number of A/D converters required places a heavy emphasis on low individual converter power consumption.

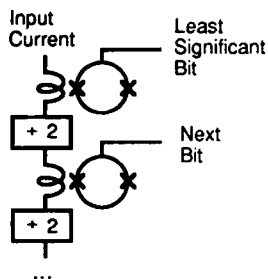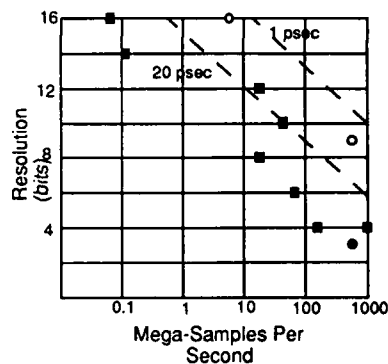
Key
■ Semiconducting - Bipolar and Hybrid
● Superconducting
○ Superconducting under development

Figure 9. Comparison of superconducting and semiconducting A/D converter performance. Ultimate speed-resolution products are limited by aperture times. Limits for 1 picosecond and 20 picosecond technology are shown. In addition to being faster, superconducting A/D converters dissipate 3 to 5 orders of magnitude less power than semiconductor devices.

Prospects for High Temperature Superconductors

For now, scientists take advantage of mature, liquid helium-based LTS technology in demonstrating the full capability of superconducting circuits in laboratory environments. Looking outside the laboratory, the avionic environment adds such harsh requirements on size, weight, reliability, and power that airborne helium liquefiers may never be practical. Until quite recently, the unavoidable cryogenic costs of superconductivity always outweighed the potential performance in systems trade-off studies. The discovery and development of high T_c materials has caused system engineers to reconsider earlier cost-benefit assumptions.

Where do HTS materials stand in early 1990? Earlier papers in this conference have concentrated in quantitative assessment of both DC and microwave properties of the new superconductors. HTS materials now stand 1 to 2 orders of magnitude lower resistivity than copper at key microwave frequencies. In avionic systems, this allows direct substitution of HTS for normal metals to improve microwave filter performance. Dispersive delay lines which are impractical with copper become feasible with present HTS materials.

Microwave resistivities continue to fall as material scientists improve the HTS materials. Ultra-compact S-MMIC circuits will be practical in HTS materials in the near future. Researchers are actively developing the multi-layer films with low resistivity required to make such items as S-MMIC delay lines and feed networks.

HTS development of Josephson device electronics lags somewhat behind pure film development, although scientists are making progress. Individual HTS Josephson elements have been demonstrated operating up to millimeter wave frequencies. In order to tackle circuits such as Josephson voltage-controlled oscillators or A/D converters, significant advances will be

required on junction quality, reproducibility, uniformity, and yield.

REFERENCES

1 For an introductory overview of superconducting technology, see Superconductors: Conquering Technology's New Frontier, by R. W. Simon and A. D. Smith, Plenum Press (1988).

2 R. L. Kautz, "Miniaturization of Normal-State and Superconducting Striplines, Journal of Research of the National Bureau of Standards 84, 247-259 (1979). See also R. L. Kautz, "Picosecond Pulses on Superconducting Striplines," J. Appl. Phys. 49, 308-314 (1978).

3 R. S. Withers, "Signal Processing: Opportunities for Superconductive Circuits", IEEE Trans. Magn. MAG-21, 181-185 (1985). See also Superconducting Devices, S. T. Ruggiero and D. A. Rudman (eds.), Academic Press (1990).

4 J. M. Pond, J. H. Claassen, and W. L. Carter, "Kinetic Inductance Microstrip Delay Lines", IEEE Trans Magn. MAG-23, 903-906 (1987).

5 A. D. Smith, R. D. Sandell, A. H. Silver, and J. F. Burch, "Chaos and Bifurcation in Josephson Voltage-Controlled Oscillators," IEEE Trans. Magn. MAG-23, 1267-1270 (1987).

6 K.-L. Wan, A. K. Jain, and J. E. Lukens, "Submillimeter Wave Generation Using Josephson Junction Arrays." IEEE Trans. Magn. MAG-25, 1076-1079 (1989).

7 For a review of superconducting computing, see H. Hayakawa in Superconducting Devices, S. T. Ruggiero and D. A. Rudman (eds.), Academic Press (1990)

Fabrication and Characterization of High T·mperature Superconducting Thin Films for Sensors and Electronics

P.M. Hemenger, T.L. Peterson, and R. Fletcher
Materials Laboratory (WRDC/MLPO)
Wright Research & Development Center
Wright-Patterson AFB, OH, 45433-6533

I. Maartense and P.T. Murray
University of Dayton Research Institute
Dayton, OH, 45469

D.W. Chung
San Jose State University
San Jose, CA, 95912

ABSTRACT

Superconducting thin films of $YBa_2Cu_3O_{7-x}$ that do not require post-annealing have been deposited on $SrTiO_3$ substrates using laser ablation. The electrical, magnetic, optical, and structural properties of the films have been analyzed in order to identify and control the processing parameters which lead to optimization of the material's properties.

The laser deposition process using an ArF excimer laser to grow high temperature superconducting (HTS) films is described. Detailed characterization of the films using ac magnetic susceptibility measurements is emphasized, because this technique is valuable as a screening tool. In one temperature scan from 4.2 to 125 K the critical temperature, T_c, the width of the transition, the presence of additional superconducting phases, the film's response to magnetic fields, and the critical current, J_c, are obtained. The susceptibility results are correlated with transport measurements of $J_c (T)$ and $T_c (R=0)$.

Process control is essential when fabricating HTS materials for avionics applications. A process optimized to produce the best properties for one particular application such as high J_c, for interconnects will probably not be an optimal process for producing sensor material. High current-carrying capability is generally not important for sensors, but rather good optical properties and low noise characteristics. The material requirements will also differ depending upon the type of sensor, e.g. bolometric or non-equilibrium. Some applications will require more stringent control of surface morphology, grain structure, and crystallographic orientation than will other applications. For these reasons a parametric study of the process is required in order to fabricate material with properties optimized for each application.

INTRODUCTION

High temperature superconducting ceramic (HTS) thin films with high critical current densities and good microstructures have been fabricated in the Y-Ba-Cu-O system using a variety of deposition techniques, including vacuum evaporation with either a barium [1] or a barium fluoride [2] source, metallo-organic chemical vapor deposition (MOCVD) [3], molecular beam epitaxy (MBE) [4], multi-source sputtering [5], single-source off-axis sputtering [6], laser ablation [7], and variations on these processes. Laser ablation and off-axis sputtering have produced the best $YBa_2Cu_3O_{7-x}$ (YBCO) films which have transition temperatures near 90 K and critical current densities of over one million amperes per square centimeter at 77 K. These properties open the door to a multitude of applications [8-10] which may include, in the near term, passive elements such as integrated circuit interconnects and strip lines, high frequency antennas, and microwave filters. In the future, active devices may become available for superconductive electronic circuits, when reliable processes are developed for building junctions and gates.

Some applications, for example infrared detectors, probably will not require material with a high current density; they will most likely be limited by reliable producibility of materials with the optimum microstructures and transition temperatures. Infrared detectors based upon the bolometer concept are considered a near-term application of the HTS materials [11-13] because of their high sensitivity when compared to other bolometric materials, operating temperatures near or above 77 K, and the relative ease with which it should be possible to produce the material over large areas and in arrays. Detectors based upon a non-equilibrium or pair-breaking response offer the potential for much faster and possibly more sensitive devices [14], but the material requirements appear to be far more demanding. Performance optimization will require a better understanding of the detection mechanisms, which is currently the subject of vigorous research.

This paper describes results from YBCO films with a range of properties, processed in-situ on strontium titanate substrates, using laser ablation for deposition. Electrical and magnetic measurements are compared with microstructural and surface morphology data. The films' properties have been found to depend strongly upon growth parameters such as substrate temperature and oxygen pressure during deposition as well as oxygen pressure during cool-down.

MATERIAL PROCESSING

The films were fabricated in a laser ablation system, as shown schematically in Fig 1. Pulses from an ArF excimer laser (wavelength = 0.193 μm) strike the stoichiometric $YBa_2Cu_3O_{7-x}$ polycrystalline bulk target which has been prepared from high purity (>99.999) starting materials. The substrate is single crystal strontium titanate oriented with the <001> direction (c-axis) normal to the surface. The substrate and target are spaced about 6 cm apart. Prior to deposition the substrate is heated to about 850°C for 30 minutes in O_2 for cleaning and then cooled to the deposition temperature of about 750°C. The laser beam striking the target is pulsed at 20 Hz with an energy of 20 mJ/pulse and an energy density of ~1.5 J/cm². The target is rotated and the laser beam is rastered in order to remove material uniformly from the target's surface. During deposition a stream of high purity oxygen flows across the rotating substrate and a background oxygen pressure of 100 to 200 mTorr is maintained in the chamber. The growth rate is about 4 Å/s so that about 30-45 minutes are required to grow a 1 μm thick film. Upon completion of deposition the chamber is back-filled with pure oxygen, generally to one atmosphere, and the substrate is cooled to room temperature in 1.5 hours. The resulting films are superconducting as processed and those used for the analyses described below have received no additional treatment. Similar processing has been used to fabricate superconducting films on magnesium oxide substrates, however the processing parameters must be adjusted to achieve optimum properties.
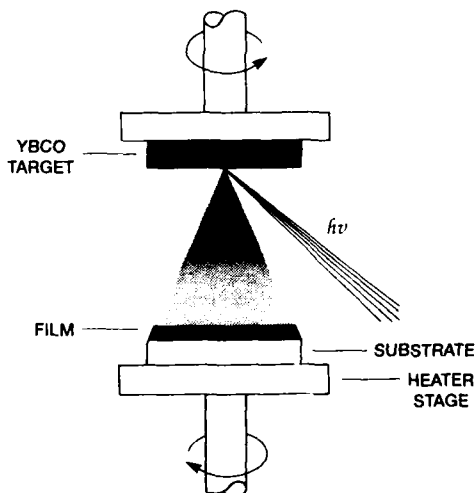
Figure 1. Schematic diagram of the laser ablation system.

Changes in the oxygen pressure and/or the substrate temperature during growth strongly affect the resulting films' properties, which include their microstructures as well as their electrical and magnetic performance. Three films, named A, B, and C, have been selected from different growth runs to illustrate the variations in properties that result from changes in the processing parameters. The major differences among the films are their critical currents as functions of temperature, the widths of their transition regions, and their microstructures. Films A and B have high critical currents relative to film C as well as sharper transitions and more uniform microstructures. The transition temperatures of the films do not vary widely, indicating that their phase compositions are probably similar and therefore that their microstructures, i.e. granularity and orientation, are primarily responsible for the measured differences in properties. The qualitative definition of "best" in describing film properties is dependent upon the application for which the material is intended. For example, film A with the highest critical current density, J_c, is best for transmission lines, but another of the films may be best for a bolometric detector in which the broader transition region relaxes temperature control requirements at the expense of somewhat reduced sensitivity. For non-equilibrium radiation detection, agreement has not yet been reached on optimum material properties. In all cases, however, device performance is material limited which necessitates extensive characterization combined with controlled processing so that material properties can be accurately defined and then custom designed for their end use.

ANALYSES

The principal tools used for characterizing the materials are ac magnetic susceptibility [15, 16] and electrical transport, both as functions of temperature, which give information on the current carrying capability of a film as well as the transition temperature and the transition width, x-ray diffraction which establishes the crystallographic orientation, and scanning electron microscopy which reveals the surface morphology and in some cases the granularity. Both x-ray diffraction and ac susceptibility will indicate other phases if they are present in quantities over a few percent, but none were observed in the films described below. The susceptibility and transport analyses are quite different experiments but the results are complementary. For example, information about the current-carrying capacity of the films can be obtained from both analyses and therefore they are used to corroborate each other. The susceptibility gives an indication of how the films perform over their surface areas while the transport measurement can be quite localized depending upon how the film has been patterned and contacted. For example, if the film's properties vary over the surface, a temperature scan of the susceptibility will generally show structure that is not present in the data from uniform films, such as those shown in Figures 2, 3, and 4.
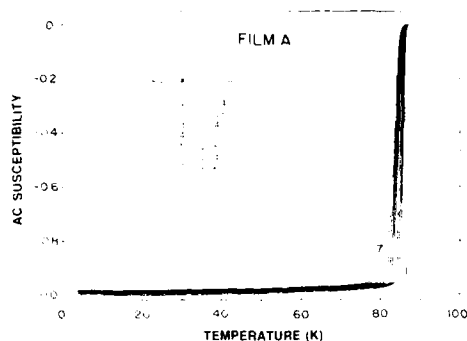
Figure 2. Sample A. Diamagnetic susceptibility as a function of temperature for eight values of ac field, h.
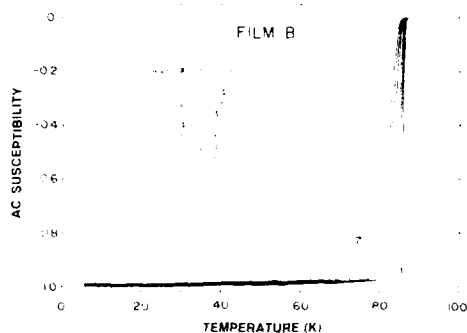
Figure 3. Sample B. Diamagnetic susceptibility as a function of temperature for eight values of ac field, h.
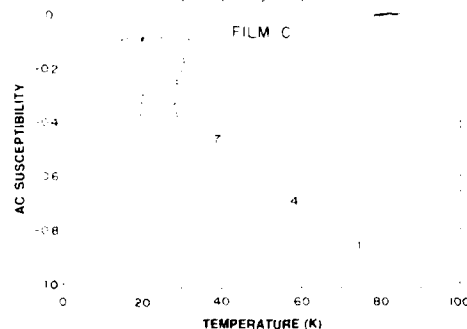
Figure 4. Sample C. Diamagnetic susceptibility as a function of temperature for eight values of ac field, h.

Figures 2, 3, & 4 are plots of the diamagnetism (real part of the complex magnetic susceptibility) for films A, B, & C, respectively, over the temperature range of 4-100 K. Each figure contains a family of curves which result from using ac probe fields, h, of different magnitudes from 0.02 to 3.6 Oe. When the diamagnetic susceptibility equals -1, the film fully shields the probe field, h, at that temperature, but

when it has a value between 0 and -1 the film cannot sustain a sufficiently large current to shield against h and the film is driven normal. The curves from sample A in figure 2 show less separation than do the curves for sample B which in turn show less separation than the sample C curves. This indicates that sample A can carry larger currents at higher temperatures than can samples B and C. This qualitative observation is verified by the plots in figure 5 obtained from transport measurements of critical current densities, J_c (in A/cm^2), as functions of temperature, for samples A, B, and C. The J_c (T) data in figure 5 are obtained by using standard dc 4-point probe equipment to monitor the voltage drop across the sample as the current is increased. The critical current is defined as the current at which 1 µV/cm is measured between the probes. This criterion is arbitrary, but is commonly used for J_c measurements and gives data that is valuable for comparing different materials. The transition temperature, T_c, for each film is estimated from figures 2, 3, and 4, using the smallest ac field, as the temperature of maximum slope. The T_c values for samples A, B, and C are approximately 86 K, 86 K, and 82 K, respectively, which agree with values obtained from the more common transport measurements where T_c is defined, using a small current, as the temperature at which the resistance goes to zero.
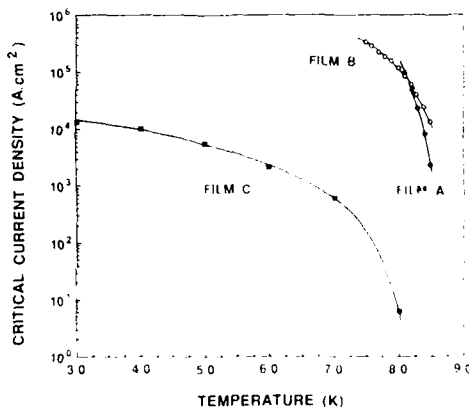
Figure 5. Transport critical current densities as functions of temperature for samples A, B, and C.

Likewise, transition widths determined from susceptibility and resistance measurements produce similar values. The principal advantages of using susceptibility rather than resistance measurements for initial evaluation are that it is completely non-destructive since no contacting is required, it gives rapid turnaround, and one temperature scan produces a complete matrix of data over the full temperature range for up to 20 different ac magnetic probe fields. For these reasons, ac magnetic susceptibility is employed to evaluate all of the as-grown materials and the results are used to determine what additional experiments, if any, should be performed. It also furnishes quick feedback for defining the optimum processing parameters.

A temperature scan of the susceptibility simultaneously produces a matrix of data from the loss (imaginary part of the magnetic susceptibility) in the sample; a typical data set (for sample B) is shown in figure 6. As with the diamagnetism, the separate
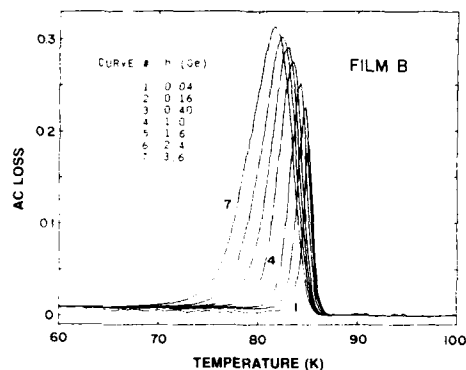
Figure 6. Loss as a function of temperature in sample B for eight values of ac field, h.

curves result from applying different magnitudes of the ac probe field. The amount of separation between loss peaks for different fields again gives an indication of the current-carrying capability of the film. These data can also be used more quantitatively since the magnitude of the magnetic field, h, producing each loss peak is proportional to the critical current density at the peak temperature, T_m. Therefore, plotting h as a function of T_m yields the temperature dependence of the critical current density, J_c. A plot of data from sample B is shown in figure 7. Also plotted in figure 7
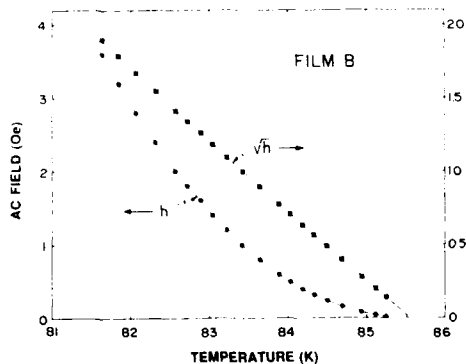
Figure 7. Magnitude of the ac probe field, h, as a function of the loss peak temperature, T_m (curve h). Square root of the ac probe field, $\sqrt{h}$, as a function of loss peak temperature, T_m (curve $\sqrt{h}$).

is the square root of h as a function of T_m. This curve is used to determine the critical temperature, T_c, at which $J_c \approx 0$ by extrapolating the data to zero h. Choosing the square root or some other dependence does not affect the value of T_c but it aids in obtaining an accurate extrapolation. Using susceptibility loss

data to obtain T_c at $J_c=0$ and the temperature dependence of J_c removes the arbitrariness that is inherent in defining T_c as the temperature at which the resistance equals zero and defining $J_c(T)$ values using a voltage criterion, since both of these definitions are dependent, to some degree, upon the experimental set-up. The validity of these concerns has been reinforced by the wide variations researchers have observed in the temperature dependences of critical current densities [2, 17, 18] and their strong dependence upon the values chosen for T_c [19, 20].

X-ray diffraction was used to determine the crystallographic orientation of the films. No phases other than $YBa_2Cu_3O_{7-x}$ were observed in any of the films. The x-ray data for films A & B show strong <00ℓ> peaks beside two superimposed substrate reflections, indicating a preferential orientation of the c-axis perpendicular to the surface of the film. However, very weak <100> and <200> peaks are also observed which may be due to the presence of small minority domains with their c-axes parallel to the substrate. Grazing incidence scans were performed for the three films to look for the presence of a-b planes perpendicular to the substrate surface; films A & B show no major peaks for reflections of the c-axis parallel to the substrate, confirming that these films are strongly oriented with the c-axis perpendicular to the substrate. The x-ray data from film C, however, show several major diffraction peaks that correspond to a low degree of perpendicular c-axis orientation with respect to the substrate surface.

Scanning electron microscopy was used to examine the films' surfaces. Films A and B have relatively smooth and continuous surfaces with no visible granular features. They also contain features which appear to be inclusions about 1 μm in diameter. These are believed to result from nucleated growth of clusters on the growth surface. Further investigations of these surface features, and methods for avoiding their formation, are in progress. Film C consists of small (~0.5 μm diameter) irregularly shaped grains which visually do not appear to have good intergranular connectivity, an observation that correlates with the low critical current densities observed for this film.

DISCUSSION

The temperature dependences of the critical current densities, $J_c(T)$, are quite different for the three films, as seen in figure 5. Film C shows a low value of J_c (only about 1 A/cm^2) at 81 K, whereas films A and B show J_c's as high as 10^5 A/cm^2 at 81 K. The low value of J_c for film C is probably the result of the unfavorable grain alignment (as shown by the x-ray data), the granularity (as seen in the scanning electron micrographs), and the low quality of the intergranular weak links (as shown by the susceptibility data, figure 4). Since no secondary structure was seen in the susceptibility results, this low J_c is unlikely to result from non-uniformities or secondary phases in the film. The values of J_c for films A and B are similar to those found by others in highly aligned films processed with sufficient oxygen during deposition.

The critical current densities for all three films are plotted in Figure 8 in the form of $\log(J_c)$ vs $\log(1-T/T_c)$. The straight lines in the figure are the least-squares fits near T_c to a power law: $J_c = \alpha(1-T/T_c)^n$ where α is a constant. All the films give n values near 2 or greater. The results are sensitive to the value of J_c which is the reason we have analyzed the data using T_c values obtained from susceptibility loss data (figure 7) as well as T_c values obtained from transport data. T_c at $J_c = 0$ is determined from the transport data by extrapolating $J_c(T) \rightarrow 0$. The tendency to a square-law dependence of J_c near T_c seen in cur films would suggest that their electric transport mechanism is dominated by proximity effect (S-N-S) junctions [17, 19, 20]. In any case, the data do not support tunneling in S-I-S type junctions as the primary conduction mechanism, where a n~1 behavior is predicted near T_c. It should be noted that the square-law dependence applies to these films even though their overall properties are quite different. AC susceptibility measurements have yielded an exponent n~2 in all of our other laser processed films as well as in films deposited by several other methods by other groups including co-evaporation, sputtering, and chemical vapor deposition. It therefore appears that this near-quadratic temperature dependence of J_c is intrinsic to the film's overall conduction mechanism, and is not governed by the specific nature of the film structure and the presence of defects or inhomogenieties, although these factors do affect the superconducting transition temperature. Our data therefore support the arguments of Deutscher and Müller[21], who propose that the very short coherence length in the HTS materials will always result in n~2 near T_c.
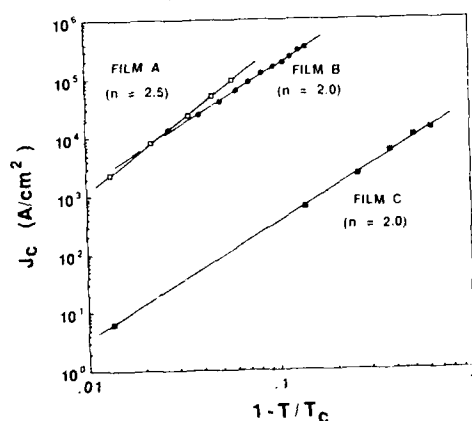
Other groups have shown that n varies widely depending upon the value chosen for T_c and upon the criterion used for determining J_c in transport measurements. In our analysis, T_c was chosen to be the temperature at which $J_c \rightarrow 0$, using the susceptibility loss data as discussed above and illustrated in figure 7. This selection procedure eliminates ambiguities and experimentally-based variability in the T_c criterion, which we believe has contributed to some of the disagreements on the value of n.

ACKNOWLEDGEMENTS

REFERENCES

1. D. D. Berkley, B. R. Johnson, N. Anand, K. M. Beauchamp, L. E. Conroy, A. M. Goldman, J. Maps, K. Mauersberger, M. L. Mecartney, J. Morton, M. Tuominen, and Y-J. Zhang, Appl Phys. Lett. 53, 1973 (1988)

2. A. Mogro-Campero, L. G. Turner, and E. L. Hall, J Appl. Phys. 65, 4951 (1989)

3. J. Zhao, K-H. Dahmen, H. O. Marcy, L. M. Tonge, T. J. Marks, B. W. Wessels, and C. R. Kannewurf, Appl. Phys. Lett. 53, 1750 (1988)

4. J. Kwo, M. Hong, D. J. Trevor, R. M. Fleming, A. E. White, R. C. Farrow, A. R. Kortan, and K. T. Short, Appl. Phys. Lett. 53, 2683 (1988).

5. M. Scherermann, C. C. Chi, C. C. Tsuei, D. S. Yee, J. J. Cuomo, R. B. Laibowitz, R. H. Koch, B. Braren, R. Srinivasan, and M. M. Plechaty, Appl Phys. Lett. 51, 1951 (1987)

6. H. Myoren, Y. Nishiyama, H. Nasu, T. Imura, Y. Osaka, S. Yamanaka, and M. Hattori, Jpn. J. Appl. Phys., 27, L1068, (1988).

7. S. Witanachchi, H. S. Kwok, X. W. Wang, and D. T. Shaw, Appl. Phys. Lett., 53, 234 (1988).

8. H. Kroger, C. Hilbert, D. A. Gibson, U. Ghoshal, and L.N. Smith, Proc. IEEE 77, 1287 (1989)

9. P. H. Carr, Microwave Journal, p.91 (December, 1987).

10. W. J. Gallagher, Solid State Technology, p.151 (November, 1989).

11. P. L. Richards, J. Clarke, R. Leoni, Ph. Lerch, S. Verghese, M. R. Beasley, T. H. Geballe, R. H. Hammond, P. Rosenthal, and S. R. Spielman, Appl. Phys. Lett. 54, 283 (1989).

12. Q. Hu and P. L. Richards, Appl. Phys. Lett. 55, 2444 (1989).

13. P. L. Richards and Q. Hu, Proc. IEEE 77, 1233 (1989).

Figure 8. Dependence of the critical current densities upon (1-t) for samples A, B, and C, where T is the reduced temperature, T/T_c. The n-values are the slopes determined from least-squares fits to the data.

14. H. S. Kwok, J. P. Zheng, and Q. Y. Ying, Appl. Phys. Lett. 54, 2473 (1989).

15. A. K. Sarkar, I. Maartense, T. L. Peterson, and B. Kumar, J. Appl. Phys. 66, 3717 (1989).

16. A. K. Sarkar, B. Kumar, I. Maartense, and T. L. Peterson, J. Appl. Phys. 65, 2392 (1989).

17. S. S. Yom, T. S. Hahn, Y. H. Kim, H. Chu, and S. S. Choi, Appl. Phys. Lett. 54, 2370 (1989).

18. L. H. Allen, P. R. Broussard, J. H. Claassen, and S. A. Wolf, Appl. Phys. Lett. 53, 1338 (1988).

19. S. Y. Lee, Y. H. Kim, J. H. Park, and S. S. Choi, Appl. Phys. Lett. 56, 403 (1990).

20. J. W. C. de Vries, M. A. M. Gijs, G. M. Stollman, T. S. Baller, and G. N. A. van Veen, J. Appl. Phys. 64, 426 (1988).

21. G. Deutscher and K. A. Müller, Phys. Rev. Lett. 59, 1745 (1987).

Discussion

Name of Author: Dr. P. Hemenger

Paper No.: 13 -- Fabrication and Characterization of High Temperature Superconducting Thin Films for Sensors and Electronics

Name of person asking question:

Question

How accurate is the temperature control required for a bolometric detector?

Answer

It is dependent upon the width of the transition region near Tc. This is an adjustable parameter where the films are fabricated. A sharper transition will give a more sensitive detector, but require more precise temperature control.

Discussion

Name of Author: Dr. P. Hemenger

Paper No.: 13 -- Fabrication and Characterization of High Temperature
Superconducting Thin Films for Sensors and Electronics

Name of person asking question:

Question

Is the susceptibility dependent upon the Jc criterion?

Answer

Yes, and also the choice of Tc. This is the reason we have attempted to make
the measurement of Tc less arbitrary.

Discussion

Name of Author: Dr. P. Hemenger

Paper No.: 13 -- Fabrication and Characterization of High Temperature
                 Superconducting Thin Films for Sensors and Electronics

Name of person asking question:

Question

How long does it take to collect the susceptibility data?

Answer

About 2 hours, 1 hour to load and cool and 1 hour to collect data.

Application of High-Temperature Superconductors to High-Precision Accelerometers

James Lenz, Quark Chen,
James McArdie, Tom Werner, Wayne Castleman

Honeywell
3660 Technology Drive
Minneapolis, MN 55418
(Work sponsored by DARPA and ONR, Washington, D.C.)

Abstract

Superconducting materials offer unique capabilities to high-precision acceleration sensing. Two specific aspects are shielding of magnetic fields and magnetic levitation due to the Meissner Effect. The basic configuration and operation of accelerometers using superconducting materials are reviewed. Physical properties such as conductivity, permeability, trapped magnetic flux, and material uniformity are correlated to shielding and levitation performance. Measurements of these properties for the YBaCuO superconductors are included.

Introduction

Inertial accelerometers have become essential components in advanced guidance and navigation systems. Table 1 shows four general categories of these applications, strategic, navigation, tactical, and automotive, and the required bias stability and accuracy for the associated accelerometer. Aircraft, spacecraft, and long-range missile guidance and navigation applications require high-precision accelerometers. A vehicle's position can be determined by combining accelerometers, which sense the changes in the velocity of the vehicle, with gyros, which determine heading and attitude.

The performance parameters of the accelerometer used in Honeywell's standard military navigation system are shown in Table 2. The key parameters are the long-term bias stability, scale factor accuracy, and orthogonality (the alignment of the input axis with the outside casing of the accelerometer). For navigation applications, where three accelerometers are used, it is also important that crosstalk between the three accelerometers either be modeled or, preferably, eliminated.

Table 1. Accelerometer Applications and Performance Parameters

		Required Performance		
Category	Major Application	Bias Stability*	Accuracy (ppm)**	Comment
Strategic	Intercontinental missiles Submarines	1 to 10 µ-g	<0.1	High stability along acceleration direction
Navigation	Aircraft Spacecraft	10 to 100 µ-g	10 to 200	
Tactical	Short-range missiles Aircraft attitude reference	500 to 1000 µ-g	200 to 1000	High-g survivability
Automotive	Active suspension systems Antilock brakes	10 to 100 m-g	>1000	

*Measured in terms of the drift of the null over the duration of the mission.
**Includes minimum resolution and scale factor accuracy.

Table 2. Accelerometer Parameters for Honeywell's H-423 Inertial Navigation System

Performance Parameter	Performance of the H-423
Turn-on transient	7 µ-g
Long-term bias stability	30 µ-g
Scale factor accuracy	175 ppm
Scale factor linearity asymmetry	20 ppm
Orthogonality	5 arc-sec
Random noise	0.0025 fps/√hr

Accelerometer Design

The two basic approaches for designing and fabricating accelerometers, the spring force method and the precession method, are illustrated in Figure 1. The spring force method uses a technique where a proof mass is hinged from the outside casing of the accelerometer. Under an acceleration the proof mass undergoes a displacement from its rest position. This response follows the dynamics of a spring. The displacement of this proof mass is sensed and, for higher precision, a feedback technique is used to immediately null this displacement. In this design the critical factors are the long-term bias stability and hysteresis associated with the spring constant, the damping coefficient, and the nonlinearity terms. The stability of the hinge is the key parameter for producing an accelerometer of this design. The pickoff mechanism for sensing the displacement is often not the leading error source for long-term stability.

$$F = ma = -kx + \gamma \dot{x} + \lambda x^2 + \epsilon(x)$$

k = Spring constant
γ = Damping coefficient
λ = Nonlinearity
ε(x) = Additional error terms

a Spring Force

Torque
$$\vec{\tau} = \vec{r} \times \vec{F}$$
$$\vec{F} = m\vec{a}$$
$$\therefore \vec{a} \propto \vec{\tau}$$

b Precession (pendulum gyro)
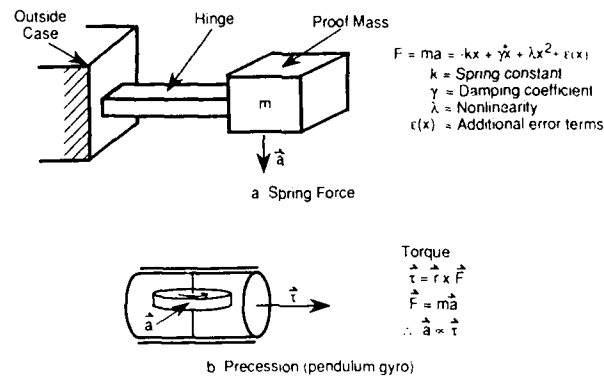
Figure 1. General Design Methods for an Accelerometer

In the precession design method, an apparatus is built such that a high angular momentum wheel can be spun inside of a frictionless supported system. Under the force of acceleration, a torque is introduced into the device that results in a precession. This angular precession is measured by applying a countering force to hold a null position. This type of accelerometer design is employed for applications where high stability or accuracy is needed in the direction of a high acceleration such as along the launch direction of a rocket.

The spring force design, the most common method for building accelerometers, consists of four separate pieces: the style of the accelerometer, the hinge, the pickoff mechanism that senses the displacement, and a driver or rebalance mechanism. Table 3 shows a technical matrix of options for this type of design. The pickoff mechanism and drive/rebalance mechanism are options for any accelerometer design. Often, closed-loop feedback techniques are used to offset hysteresis or nonlinearity effects in the proof mass movement. The style can be broken into two categories. The first uses a beam or diaphragm of either quartz, silicon, or a metal. These materials are used because of their near perfect elastic properties. The second style is based on levitation where electric fields, magnetic fields, or flotation techniques are used for the suspension mechanism of the proof mass.

Table 3. Technical Matrix for Spring Force Accelerometer Design

Style	Hinge	Pickoff	Drive/Rebalance
I. Mechanics • Beam • Diaphram	Quartz Silicon Metal	Piezoelectric Piezoresistive Capacitance Inductive (magnetic)	None Electrostatic Magnetic Piezoelectric
II. Levitation	Electric Field Magnetic Field Flotation	Optical	

When designing an accelerometer one optimizes these various options to find which technique would work the best for the specific application. Ideally the suspension of a proof mass with electromagnetic fields offers the most predictable, stable technique if the electromagnetic properties of the proof mass are stable. (A mechanical hinge is less favorable because of the practical consideration of producing the defect- and impurity-free material that would be required for mechanical stability and positional repeatability of the hinge.)

Uses for Superconductivity

Superconductivity offers a unique levitation style of spring force accelerometer, where the proof mass is made of superconducting material. The superconductor, by virtue of the Meissner effect, will repel an applied magnetic field, producing a repulsive force. There are three important benefits with this levitation method. First, electrical wires, which could introduce nonlinearities and hysteresis in the spring force, do not have to be attached to the proof mass. Secondly, the dynamics of the magnetic field coupled with the superconductor form the static and dynamic equations of motion. Using an ideal superconductor, the effects from material properties would be negligible, which simplifies the accelerometer design. The third important benefit of levitation using an ideal superconductor is that there is no energy loss in the proof mass, thereby eliminating the factors of temperature sensitivity and turn-on transients.

Sensor design using non-ideal superconductors can be engineered to exploit achievable material properties. Figure 2 shows a general magnetization curve for a Type II superconductor where the permeability is plotted against an applied magnetic field. There are two critical fields, Hc_1 and Hc_2. Below Hc_1 the superconductor has ideal Miessner properties and above Hc_2 the material is no longer superconducting and is in the normal state. Between Hc_1 and Hc_2, the superconductor is in a mixed state. Designing an accelerometer where the superconductor is in the mixed state is a challenging engineering task. In the mixed state, flux penetrates the superconductor and needs to be locked to the background lattice of the material. This flux penetration phenomena impacts the benefits of using a levitated superconductor.

For high-precision applications, it is critical that the levitation field be isolated and shielded from external magnetic fields. Superconductivity would be used for both levitation and magnetic shielding, as described in the following paragraphs.
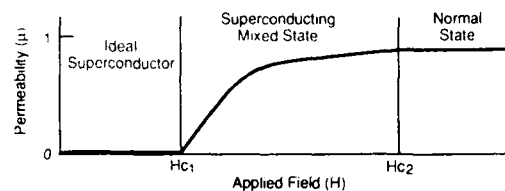
Figure 2. Typical Magnetization Curve for a Type II Superconductor
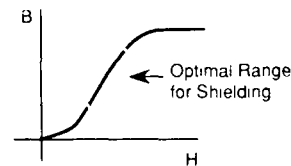
Figure 3. Typical B-H Curve for Ferromagnetic Material

Magnetic Shields

In magnetic shielding there are basically three categories for fields to be shielded. The first category is the shielding of high frequency electromagnetic fields. The common method that is used to shield these types of magnetic fields is conducting materials such as copper or aluminum. Here the attenuation is established through eddy currents being generated in the conducting materials. The performance is only limited by the skin depth of the material where $\delta \propto 1/\sqrt{\mu f \sigma}$ and μ is the permeability, f is the frequency of the incident field, and σ is the electrical conductivity.

The second category for magnetic shielding is high intensity yet low frequency fields. Here the common technique for shielding is the use of ferromagnetic materials, which have very high permeabilities. In this case one tries to design the thickness of the material and the gaps in producing the magnetic shield such that the material operates in the linear region of the B-H curve as shown in Figure 3. Here the performance is limited by the initial permeability and saturation of the material as well as demagnetization effects due to the shape of the shield.

The third category for magnetic shielding is low intensity and low frequency fields where superconducting materials have a significant advantage. For low intensity fields the ferromagnetic materials do not work well because it is difficult to make the material thin enough to get the material operating in the mid-range of the B-H curve without sacrificing strength that's needed to hold the high tolerances in the gaps of the magnetic shield. Superconductors are diamagnetic material with a permeability much less than one. Whereas a ferromagnetic material concentrates the flux, a diamagnetic material repels magnetic flux. An advantage of a diamagnetic shield is that the effect of apertures is reduced since the flux is not being concentrated across these openings.

Figure 4 shows a comparison between these three types of magnetic shields. This data was generated using finite element modeling for a geometry where the shield material was inserted between a transmitting and receiving coil. For a highly conductive material (i.e., copper) the shielding attenuation is frequency dependent, as expected. The ferromagnetic material is not as frequency dependent but requires sound engineering of gaps and operating the material at the midrange of the B-H curve. Curves for two different diamagnetic materials show that they can achieve good attenuation for good superconducting materials.

Figure 5 is an illustration and photograph of the magnetic shielding measurement set-up used in our laboratory to evaluate high-temperature superconducting shields. It consists of a sending (source) coil and a receiving (sensing) coil. Each coil, wound on a Delrin bobbin, is inserted into a circular steel E-piece. Circular disk samples are placed between the coils. The two E-pieces are used to concentrate and homogenize the magnetic field and screen leakage fields. The field strength per applied current is about 1.5 G/mA. In order to maintain constant current for the excitation (sending) signal, a voltage-to-current converter is connected to a constant voltage source with voltage-controlled gain. The pick-up signal was then fed into
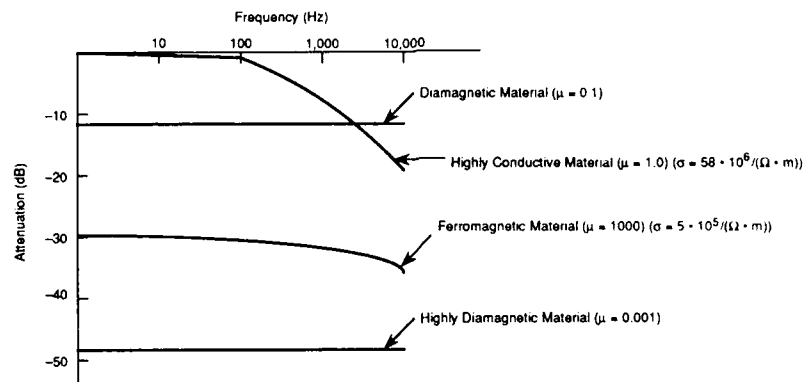
Figure 4. Shielding Attenuation vs. Sample Parameters Permeability (μ) and Conductivity (σ)
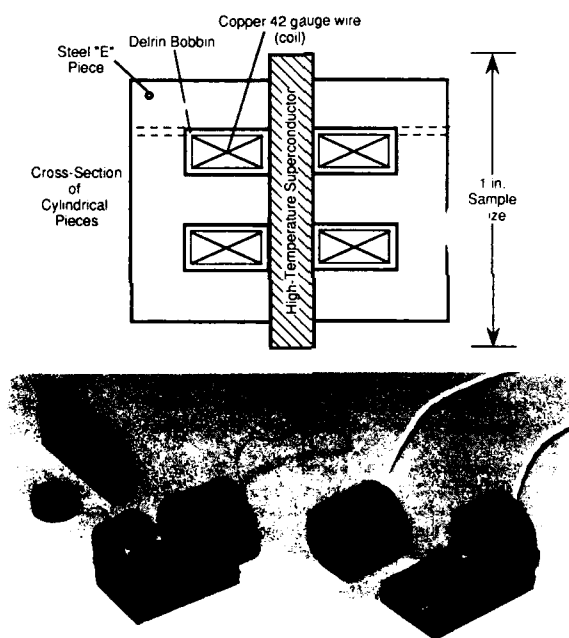
Figure 5. Sending and Receiving Coil with Sample

a lock-in amplifier. Figure 6 shows the typical magnetic shielding effectiveness for our YPaCuO samples at 77 K as a function of applied field. The attenuation is computed from S = 20 log V_0/V, where V_0 is the receiving coil voltage without the sample and V is the received voltage with the superconducting sample. This 1-in.-diameter, 1/8-in.-thick sample was sintered at 950°C for 20 hr followed by annealing for 4 hr at 550°C under oxygen atmosphere. The measuring frequency was 200 Hz where low frequency pick-up and self-resonance effect (peaked at 50 kHz) of the sensing coil are minimal. 100- to 120-dB attenuations were found to be typical of the YBaCuO superconductors. Shielding measurements were also performed on superconducting hollow cylinders. In these measurements the applied field was parallel to the axis supplied by a solenoid and the pickup coil was placed inside the hollow space. Samples are 20 mm long, 12 mm on the outer diameter and 8 mm on the inner diameter. In Figure 7 we show the shielding effectiveness of the superconducting material prepared with a procedure identical to that used in Figure 5. We see that the shielding effectiveness is approximately 72 dB at 500 Hz. The frequency dependence below 5 kHz is not fully understood. The low shielding effectiveness is due to the finite aspect ratio of a superconducting cylinder, which allows partial flux penetration into the hollow space.
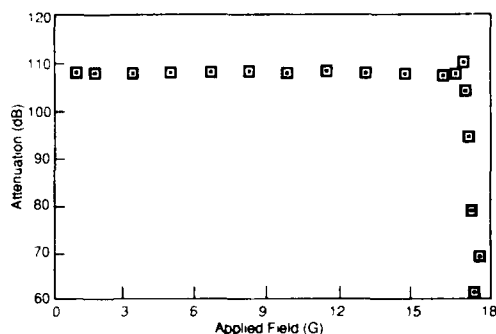
Figure 6. Magnetic Shielding of YBaCuO Material vs. Field Strength
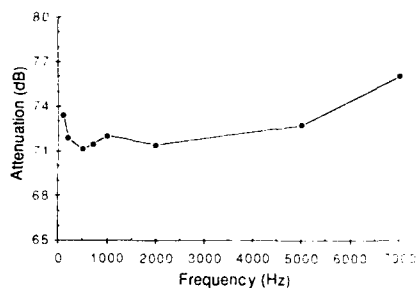
Figure 7. Frequency Dependence of YBaCuO Superconductor Tube Sample

Magnetic Levitation

Figure 8 shows the apparatus for the levitation and accelerometer experiments. The facility consists of three superconducting magnets. Magnet #1 is a solenoid with uniformity enhancement coils that produces up to 5T uniform field. Magnet #2 is a pair of oppositely wound coils that produces up to 4 kG/cm (0.4 T/cm) gradient. Magnet #3 is similar to Magnet #2. The differences are that #3 is smaller and less inductive. Magnet #2 will be used for static levitation, while #3 can be used for dynamic levitation or accelerometer experiments. It has been established that an ac oscillation of 60 amp/50 msec period over 5 min continuously is possible without quenching the magnets. 60 amp/100 msec period can last up to almost an hour. The power supplies to these magnets are regulated to compensate inductive coupling to within 0.1% stability. The sample chamber temperature can be varied from 1.5 K to 300 K. Figure 9 shows the normalized levitation force of a 1-in.-diameter superconducting sphere as a function of permeability using finite element modeling. As can be seen, as μ goes from 0 (perfect diamagnetism or Meissner effect) to $\mu = 0.5$ (intermediate state), the force drops by a factor of three. In Figure 10, we show the typical permeability change as a function of temperature and applied field for a YBaCuO superconductor. From these results it is also shown that the levitation force drops by a factor of three for an applied field of 200G when the temperature goes from 4 K to 77 K.
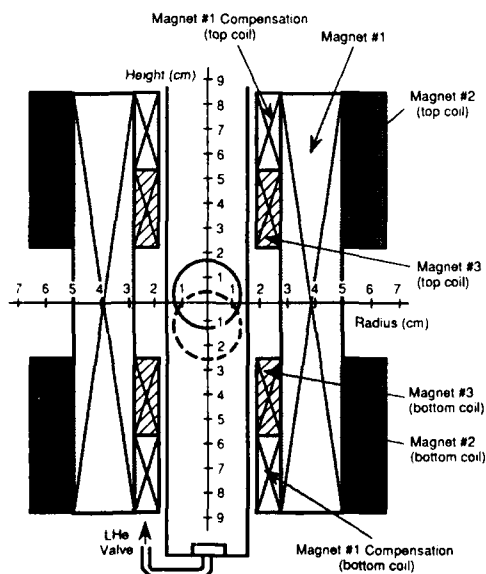
a. Illustration of Magnet System
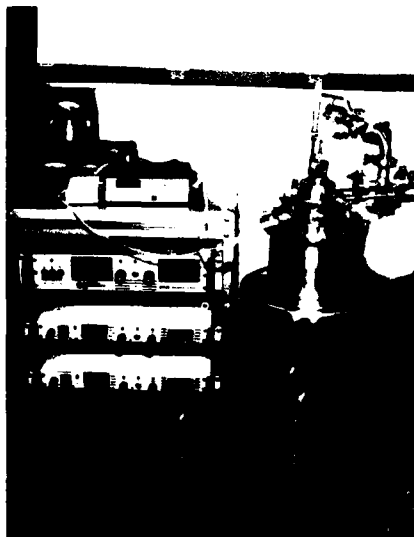
b. Photograph of Cryostat

Figure 8. Levitation Magnet System
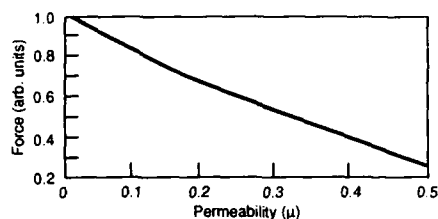
Figure 9. Levitation Force for Diamagnetic Materials
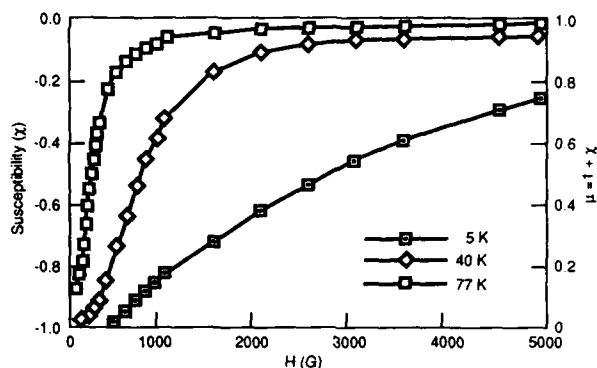
Figure 10. Susceptibility vs. Magnetic Field for YBaCuO Material

Future Directions

Superconductivity offers two unique advantages for building high-precision accelerometers: very good magnetic shields and a frictionless hinge for a spring force design. Table 4 shows a preliminary calculation for this type of sensor. Of course a critical factor in the performance of these two attributes is the idealness of the superconductor. The immediate problem in the development of high-precision accelerometers is characterizing the material, determining its impact on sensor performance, and optimizing the material further. This involves three different perspectives for the development of this sensor, namely the materials, the superconducting properties, and the sensing device. The materials perspective includes factors such as density, fracture toughness, geometric tolerance, crystal properties, and composite structures. The superconducting properties perspective includes critical temperature (T_c), critical fields (H_c), magnetization (M, χ), flux pinning and creep, magnetic shielding, and magnetic levitation. The device perspective includes the spring constant (k), the damping coefficient, and nonlinearity for the static and dynamic equations of motion. Within each perspective, compromises between what is possible and what is needed are assessed. However, only by analyzing these different perspectives simultaneously can we expect to achieve fundamental understanding of superconductive material and its full capability for high-precision accelerometers.

Table 4. Preliminary Derivation of Magnetic Field Parameters for a Superconducting Accelerometer

A. Levitation force	B. Magnetic Shield
$F_L = 1/3\ \mu\ a^3\ H\ dH/dx$ a - radius of sample (= 1 cm) μ - (permeability of gap) (= 1) H - levitation field (= 1000 Oe) dH/dx - Levitation field gradient (= 100 Oe/cm) Then $F_L = 3.3 \times 10^4$ dynes Maximum Levitation Acceleration = F_L/m m - proof mass (= $\rho\ 4/3\ \pi\ a^3$) ρ - density of HTSC (= 6 gm/cm^3) Max a = 3.3 x 10^{4}dynes/25g = 1320 cm/sec^2 (Note: 1 g = 980 cm/sec^2)	For 0.01 μg accuracy the force must be stable to: $\Delta F = 10^{-8}$ (25 gm) (980 cm/sec^2) $= 2.45 \times 10^{-4}$ dyne This leads to a specification of: $2.45 \times 10^{-4}/3.3 \times 10^4 = 0.74 \times 10^{-8}$ Thus H dH/dx must be stable to ~ 0.01 ppm If dH/dx is stable; H must be stable to this level $\Delta H = 1000G \times 10^{-8} = 10^{-5}G$ Thus the superconductors must shield external fields to better than 10^{-5}G.

Discussion

Name of Author: J. Lenz

Paper No.: 16 -- Applications of High Temperature Superconductors to High
Precision Accelerometers

Name of person asking question: John R. Vig

Question

In your introduction you mentioned that when a new technology comes along, one must look at how the promise of the new technology compares with competing technologies. What are the potential advantages of high Tc accelerometers over competing technologies, e.g., double-ended quartz tuning fork resonators, and what are the disadvantages?

Answer

The major advantage that we are concerned with is the capability to achieve very high sensitivity (~.001 µg). This benefit arises from the ideal Meissner Effect for providing a precise hinge of the proof mass. The disadvantage of the HTSC material is the low Hc_1 which will either restrict the size of the proof mass or restrict the maximum g level in which the sensor can operate.

Superconducting
Josephson Junction Gyroscope
(JJG)
Development
Program
Submitted
By

Francis A. Karwacki
Naval Air Development Center
Warminster, PA 18974-5000
United States

Abstract

This paper describes a multi-year effort to develop a Josephson Junction Gyroscope (JJG). The goal of the research project is to develop a small solid-state gyroscope that utilizes the phase coherence of Cooper-paired electrons to measure applied rotation. The research is divided into a low temperature proof of concept, high temperature material research and Josephson junction development and the development of an experimental test facility.

Introduction

The discovery of new superconducting materials with transition temperatures above the boiling point of liquid nitrogen (77K) [1,2] has generated a renewed interest in the development of various sensors fabricated from these materials. Many previously developed superconducting sensors have improved sensitivity and reduced size and cost compared to earlier sensor technologies. It is for these reasons that the inertial sensor research and development community has begun investigating these materials for potential use in inertial navigation.

This program consists of low temperature proof of concept experiment and investigations into high temperature superconducting material properties and Josephson junction applications. The proof of concept incorporates theoretical analysis and design development of gyroscope models. It also includes the design and fabrication of an experimental facility, which includes a rotational dewar probe that has the capability to experimentally evaluate magnetic shielding and perform rotation sensing measurements. The high temperature project is directed at investigating flux pinning, vortex motion, and other high critical temperature (T_c) material properties and their effect on performance. Investigations into the development of high T_c Josephson junctions will be conducted to determine the transitional feasibility for a high T_c gyroscope.

The basic theory for this unique high T_c gyroscope has been developed. Design efforts are currently under way to determine suitable techniques capable of measuring earth's rate. The design effort will be extended to include additional sensitivities as prescribed by the high T material studies that may limit the sensor capability to measure rotation.

It is the intent of the first phase of this program to extend the theoretical studies to produce a design that has the capability of measuring earth's rate. This design will then be used and develop an experimental gyro model with the express purpose of measuring an applied input rate. The second phase will be directed at analyzing new superconducting materials to determine appropriate candidate high temperature material(s). Efforts also will be directed at developing thin film deposition processes and Josephson junction fabrication techniques. These efforts will then be merged to produce a high T_c Josephson Junction Gyroscope (JJG).

Technical Risk Assessment

The first phase of the project, which is considered to be low risk, includes the completion of theoretical models, the development, selection and fabrication of an experimental model and the establishment of an experimental facility. The performance capability of each conceptual model will be analyzed to determine sensitivity. Model analysis will include, but not be limited to, minimum sensitivity as dictated by the time and temperature phase fluctuations of the Cooper-paired electrons, practical noise limits of a Josephson junction and magnetic sensitivity and shielding requirements. The design of a thin film low temperature sensor assembly will be based on this analysis.

The second phase of the project is considered to be high risk. This phase will be directed at transitioning the already proven design into a thin-film device utilizing the high temperature superconducting materials. This phase will include, but not be limited to, analysis of material characteristics to minimize/eliminate unwanted sensitivities, development of thin-film deposition processes, the patterning and development of a Josephson junction, the characterization of the developed components, and the development of suitable control/signal processing electronics.

Josephson Junction Gyroscope Theory

A JJG relies on the phase coherence of the superconducting electrons and a weak link or Josephson junction to measure rotation about a sensitive axis. This phenomenon can be achieved by producing a persistent current in a ring of superconducting material with a weak link or Josephson junction and applying a rotation to the ring. The condensate of the Cooper-paired electrons is phase coherent [3], similar to the photons in the RLG. As these electrons travel around the loop they will experience a change in phase due to the applied rotation. This change in phase can be derived by considering the Hamiltonian [4] of a particle in a rotating reference frame and placing it in the expression for the current density. Using these expressions the gradient of the quantum mechanical phase of the superconducting electrons is

$$\vec{\nabla}\phi_e = \frac{m}{\rho_e \hbar} \vec{J} + \frac{2e}{c\hbar} \vec{A} + \frac{2m}{\hbar} (\vec{\omega} \times \vec{r})$$

(1)

Integrating equation (1) around a ring broken by a Josephson junction, Figure 1, results in an expression for the integral of the change in phase given by

$$\oint \vec{\nabla}\phi_e \cdot d\vec{r} = \frac{m}{\rho_e\hbar} \int_1^2 \vec{J} \cdot d\vec{r} + \frac{2e}{c\hbar} \int_1^2 \vec{A} \cdot d\vec{r} + \frac{2m}{\hbar}\int_1^2 (\vec{\omega} \times \vec{r}) \cdot d\vec{r} + \delta\phi_j \tag{2}$$

where $\delta\phi_j$ is the phase difference across the junction and the $\int_1^2$ represents the path of integration around the ring excluding the junction. Since the wave function is single-valued this restricts the left side of equation (2) to be an integer multiple of 2π, i.e. $2\pi n$ with $n=1,2,3,\ldots\infty$. If the integration path is taken in a region where the pair density is negligible, the first term in this equation can be omitted. The gauge invariant expression for the phase difference can now be introduced to provide the missing portion of the integral. The gauge invariant phase is given by

$$\delta\phi'_j = \delta\phi_j - \frac{2e}{c\hbar} \int_1^2 \vec{A} \cdot d\vec{r} - \frac{2m}{\hbar} \int_1^2 (\vec{\omega} \times \vec{r}) \cdot d\vec{r} \tag{3}$$

If this is substituted into equation (2) (the expression for a Josephson junction [5]) and set equal to $2\pi n$ the resultant equation is

$$2\pi n = \delta\phi'_j + 2\pi \frac{\Phi}{\Phi_o} + \frac{2m}{\hbar} (\vec{\omega} \cdot \vec{A}) \tag{4}$$

where Φ and Φ_o are the total and quantum flux, respectively. Equation (4) dictates the phase behavior for the Cooper-paired electrons as they travel around the ring. The phase across the Josephson junction ($\delta\phi'_j$), when added to 2π times the enclosed flux fraction (Φ/Φ_o), and also added to the applied rotation ($\vec{\omega}$) must equal an integer multiple number of 2π. Substitution into the Josephson expression yields

$$I_o = I_c \sin (2\pi \frac{\Phi}{\Phi_o} + \frac{2m}{\hbar} (\vec{\omega} \cdot \vec{A})) \tag{5}$$

for the current in the multi-connected superconducting ring. Thus a ring with a Josephson junction carrying a current I and rotating at an angular velocity $\vec{\omega}$, will modulate the current with a period proportional to the angular velocity $\vec{\omega}$.

J. E. Mercereau, et al and J. E. Zimmerman, et al developed the basic theory and performed fundamental experiments on interference effects in Josephson junctions and on the measurement of $\hbar\cdot m$ by using a rotating superconductor. This information provided the basis for the development of the theory for this unique concept gyroscope.

Sensitivity

A diagram of a proposed concept Josephson Junction Gyroscope is presented in Figure 2. The gyro consists of a superconducting ring with a Josephson junction, two (2) pickup coils and a DC SQUID (Superconducting QUantum Interference Device) for detecting rotation. The superconducting ring is mounted with its axis of symmetry aligned with the symmetric axes of the primary windings of the pickup coils. A SQUID with its axis of symmetry perpendicular to the symmetric axis of the ring is aligned with the symmetric axes of the secondary windings of the pickup coils. An external coil will be used to produce a persistent current in the ring. This current is established by trapping flux in the ring during its transition through its critical temperature. Primary coil #1 is used to monitor the change in flux of the ring due to applied rotation. Any external fields which enter the system will be detected by the primaries of coils #1 and #2. To compensate for external fields, the secondary of coil #2 is mounted in such a way as to produce a cancellation of the external field produced by secondary #1 at the SQUID. The total flux (Φ_T) detected by the SQUID is

$$\Phi_T = \kappa_1\kappa_1'\phi_1 - \kappa_2\kappa_2'\phi_2$$

$$\Phi_T = \phi_{sr} \tag{6}$$

where $\phi_1 = \phi_{sr} + \phi_{ext}$ and $\phi_2 = \phi_{ext}$, ϕ_{sr} is the flux produced due to the rotating ring and ϕ_{ext} is the external field flux. $\kappa_1, \kappa_1', \kappa_2$ and κ_2' are the coupling factors which for the purpose of this paper will be assigned a value of one (1). The self inductance of the coils has not been considered in this calculation. The flux in the superconducting ring is given by $\phi_{sr} = B_{sr}A_{sr}$, where A_{sr} is the enclosed area and B_{sr} is its magnetic field given by

$$B_{sr} = \frac{\mu_0 I_{sr}}{2r_{sr}} \tag{7}$$

μ_0 is the permeability of free space, r_{sr} is the radius of the ring and I_{sr} is defined by equation (5). This is a first approximation which assumes a uniform magnetic field and no contribution to the field due to the persistent current. Placing the expression for ϕ_{sr}, B_{sr} and I_{sr} into equation (7) the expression for the total flux at the SQUID becomes assuming no external field contribution to equation (5)

$$\Phi_T = \frac{\mu_0 I_c A_{sr}}{2r_{sr}} \sin [\frac{2m}{\hbar} (\vec{\omega} \cdot \vec{A}_{sr})] \tag{8}$$

The minimal detectable rate (ω_{min}) is determined by defining $\omega \ll 1$ in equation (8). This reduces $\sin (\theta) \to \theta$ in equation (8) for small angular changes which yields

$$\Phi_{min} = \frac{\mu_0 m I_c A_{sr}}{r_{sr}\hbar} (\vec{\omega}_{min} \cdot \vec{A}_{sr}) \tag{9}$$

where $\Phi_T = \Phi_{min}$ and $\omega = \omega_{min}$. The minimal detectable flux for the SQUID as defined in terms of the

energy (E_{min}) is

$$\Phi_{min} = (E_{min}L)^{1/2} \tag{10}$$

where L is the inductance of the SQUID. Substituting equation (9) into equation (10) and rearranging terms to define ω_{min} in terms of the other variables yields

$$\omega_{min} = \frac{r_x \hbar}{\mu_0 \pi I_c A^2_{s}} (E_{min}L)^{1/2} \tag{11}$$

If E_{min} is defined as 10^{-34} joules, L as 10^{-9} henries, A_s as .73 cm^2 and I_c as 10^{-6} amps. The minimal detectable rate is .0054°/Hr..

PROPOSED RESEARCH AND DEVELOPMENT
Phase I: Low Temperature JJG
Gyro Modeling Studies

The modeling studies will be focused on two basic approaches: Persistent Current (dc) and Radio Frequency (rf) designs in various configurations. Specific attention will be given to configuring the sensor in such a manner as to produce a cancellation effect of average ambient magnetic fields. The sensor will thus only be sensitive to higher order moments of the local magnetic field which will effectively be eliminated using appropriate magnetic shield configurations. Preliminary investigations have focused on several potential designs.

In addition to the fundamental design studies stated above, consideration will be given to noise and its effect on gyro performance. Noise issues as related to flux stability, junction properties, and fluctuations in pair densities will be investigated to determine their effect on the fundamental sensitivity of the proposed sensor. Other issues related to fabrication methods, materials compatibility such as the substrate to superconductor interface, and environmental stability will also be included in the study.

Experimental Test Station

A rotational dewar probe will be designed and fabricated to apply rates from 1 °/sec. to > 5,000 °/sec. to the components and sub-assemblies to determine rotational sensitivity prior to final assembly. Control and signal processing electronics will be designed and fabricated to meet the requirements of the project. The electronics will be interfaced with a computer, instrumentation and data acquisition and control modules to complete the overall test station development. In conjunction with electronic design and fabrication, software will be developed to provide the necessary external control of the system and statistical analysis of the experimental data. Magnetic shielding will also be designed and fabricated to reduce the effects of external fields on gyro operation.

Phase II : High Temperature JJG
Gyro Modeling Studies

In addition to the basic sensor configuration analysis in Phase 1, other issues relating to the stability, sensitivity and compatibility of existing materials must be considered. For example, it is not known whether a stable persistent current can be produced in a JJG that utilizes high T oxides from certain materials. Current evidence indicates that the new high T superconducting oxides may be susceptible to flux slippage, due to insufficient pinning or flux melting, under conditions where conventional superconductors would be stable. This flux slippage leads to instabilities in the persistent current and hence possible degradation in performance from a JJG fabricated from these high T_c materials. Included in this study will be the use of high T materials for magnetic shielding applications.

Materials Research

Research will be directed at selecting candidate material(s) with properties to enhance gyro performance while reducing/eliminating properties that tend to degrade performance. Materials characterizations will be performed to study the stability of the proposed candidates to oxygen stoichiometry, flux pinning, vortex motion and the reactivity of materials with the environment. Deposition and patterning techniques for candidate materials will be explored to select a process that will produce thin films with identical characteristics. Techniques to be explored are: laser ablation, single gun sputtering and metalo-organic chemical vapor deposition (MOCVD).

Josephson Junction Development

Successful demonstrations of high Tc Josephson Junctions producing expected responses have been recorded. Bulk and thick film SQUIDs have also been fabricated. The extremely short coherence lengths and anisotropy characteristics of these new systems represent a new challenge to the fabrication of stable SQUID devices. The use of both bulk and film (thick and thin) SQUID configurations will be explored but particular attention will be given to epitaxial, in-situ growth of multi-layer structures and patterned weak-links in epitaxial films. For example, one proposed multilayer structure, superconductor - insulator - superconductor (SIS), composed of $YBa_2Cu_3O_7$, $PrBa_2Cu_3O_7$, $Ba_2Cu_3O_7$, with the $PrBa_2Cu_3O_7$, layer being the barrier (insulating) layer of about 20-50 Å thick, will be investigated. $PrBa_2Cu_3O_{7-x}$ is a semiconductor with an orthorhombic structure having an oxygen content similar to $YBa_2Cu_3O_7$. It is therefore ideal for the epitaxial growth of a semiconducting weak link. Epitaxial growth of such a multilayer structure has already been demonstrated in Japan. Controlled orientation of the films composing the multilayer structure can be achieved by judiciously selecting the orientation of the single crystal substrate. Sequential growth of the components of the multilayered structure will be accomplished by switching the deposition among different targets. The in-situ growth is made in a reactor with enough O_2 pressure to allow for fully oxygenated film deposition. Sequential growth of different layers can be

References

[1] M.K. Wu, J.R. Ashburn, C.J. Torng, P.H. Hor, R.L. Meng, L. Gao, A.X. Hung, Y.Q. Wang and C.W. Chu, Phys. Rev. Lett. 58, 908 (1987).

[2] H. Maeda, Y. Tanaka, M. Fukutomi and T. Asano, Jap. J. Appl. Phys 27, L209 (1988).

[3] L.N. Cooper, Phys. Rev. 104, 1189 (1956).

[4] L.D. Landau and E.L. Lifschitz, "Mechanics", Pergamon Press, New York, 1976, p. 126-129.

[5] B.D. Josephson, "Coupled Superconductors", Rev. Mod. Phy., 36, 216-220 (1964).

[6] Project Communications with Rockwell International Autonetics Division and Florida State University.

$\bar{S}$ = ENCLOSED AREA

$\bar{B}$ = FLUX LINKING RING

$\bar{\omega}$ = INPUT RATE

$$J_c = J_o \sin(\delta\phi_J)$$
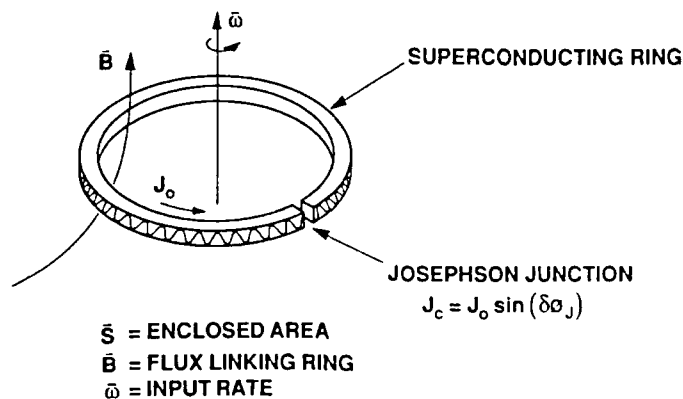
Ring with a
Junction
Figure 1
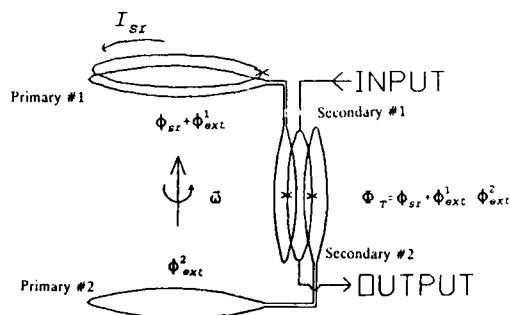
Proposed Concept
Josephson Junction Gyroscope
Figure 2

SQUIDs Devices Made From High Tc Superconductors
Results and Perspectives
by
Ronan Stéphan
THOMSON SINTRA ASM
29601 Brest Cedex
France

SUMMARY

After a brief presentation of magnetic sensoring, we will expose our own results, dealing with thick superconductive films where we used the intergranular native weak-links. We will also introduce the potential of HTSC in SQUID magnetometry, with emphasis on the utilization of thin films.

I - INTRODUCTION

The recent discovery of oxides materials which are supercon-ducting above liquid nitrogen temperature (up to 125K) has sti-mulated an extensive research effort as well on the comprehen-sion of the fundamental mechanisms involved in these materials as on the design of appropriate processes for the technical ex-ploitation of this new technology. Among the most promising devices based on these new superconductors stand the Super-conducting QUantum Interference Devices (SQUIDs), which are known to be extraordinarily sensitive magnetic field sensors, and were thought to be suited to constitute a first application of these advanced materials.

Meanwhile, the operation of high temperature superconductor SQUIDs has been demonstrated by many independant research groups, although, because of the lack of stability and homoge-neity of the superconducting samples, an advance towards a complete magnetometer or gradiometer device has not been at-tempted yet.

Besides the elaboration and characterization of the needed films from an adequately selected high temperature superconducting material (YBaCuO, BiSrCaCuO, TlBaCaCuO), the problem of patterning structures in the micrometer range must be carefully addressed. The weak-links, which constitute the key elements of a SQUID-ring, furthermore require a method to adjust their critical current density. As for the pick-up coils which senses and carries the magnetic flux and could essentially be held as a superconducting transformer loop, the feasability of long and homogeneous lines and of their points of intersection (cross-lines) are of prime importance.

II - MAGNETIC SENSORING

Most of the common magnetic sensors come along with sensi-tivities well suited for classical measurements within typical perturbated environment. This assertion means that the probes intrinsic noise level is below the fluctuations related to geomagnetism or industrial perturbations. Nevertheless new technics used in signal processing for this type of measurements (ambiant noise reference, substracter filters synthesis, differen-tial measurements, etc.) allow to get rid, to a large extent, of these parasitic signals, disclosing the need for more sensitive sensors.

As mentionned above, one of the solutions, to reduce the un-certainty related to the environmental noise, consists in measu-ring spatial derivatives of the magnetic field, which gives natu-ral rejection of space correlated perturbations. Furthermore, very sensitive gradiometric measurements on very short length require much more sensitive probes than those of the previous generation (mainly "Flux-Gate" magnetometers)

III - REQUIREMENTS FOR A SENSITIVE MAGNETOMETER

The problem of magnetic gradiometry is, therefore, the extrac-tion of minute variations due to the presence of a ferromagnetic object in the detection volume (the requirements level are around 0.5 nT/m, in an ambiant field close to 50000 nT)

What is the major reason to prefer gradient measurements rather than field measurements? The answer is threefold:

i) Gradiometry is more "localizing" than direct field measurement, because one could combine, within a *lower uncertainty*, for a given class of objects, a *distance* with a *measured value*.

ii) Besides, associated with field measurements, gradient measurements allow the resolution of the so-called *inverse problem*, i.e. the determination of the source characteristics, and, thus, the actual *magnetic identification of objects*.

iii) Finally, this technique reduces the false alarm rate due to natural fluctuations of the earth field, the latter being very homogeneous in space, and thus related to very weak gradients.

Further to these features, a convenient sensor will have to show very high sensitivity (at least two orders of magnitude below the Flux-Gate's best characteristics) and to exhibit very low intrinsic noise. As for the operational view point, the whole system will have to be easily transportable, without requiring restricting environment for proper operation.

IV – SQUIDs STATE–OF–THE–ART

IV 1 – RF and DC SQUIDs

IV.1.1 – Resistively Shunted Junction model

Figure 1 illustrates RSJC model of a real junction. The brief comments hereafter are related to main characteristics of such junctions.

i) The junction will show hysteresis if :

$$\beta_c = 2\pi I_o R^2 C/\phi_o > 1$$

$\beta_c < 1$ is needed for proper SQUID operation

ii) Resistive thermal noise induces:

– a "rounding" of the I(V) curves [1,2]

– voltage fluctuations [3,4] whose spectrum could be written:

$$S_v(f) = R_D{}^2[1 + (I_o/I)^2/2)](4k_BT/R)$$

with:

$R_D = \partial V/\partial I$ and I_o: critical current

IV.1.2 – RF SQUIDs

This device is a one junction loop RF pumped. The system shows hysteresis if:

$$\beta_L = 2\pi L I_o/\phi_o > 1$$

Its energy resolution is given by:

$$\varepsilon = [(\pi\alpha^2\phi_o{}^2/2L) + 2\pi\alpha k_B T_{aeff}]/\omega_{rf}$$

with:

α: slope of RF SQUID's "plateau" characteristics (α depends on the device noise; α = 0 if no noise)

T_{aeff}: noise temperature of the amplifier
[5]

IV.1.3 – DC SQUIDs

Figure 2 shows a DC SQUID representation.

An important parameter of the DC SQUID is :

$$\beta = 2L I_o/\phi_o$$

with:

I_o: critical current of a single junction

L: self-inductance of the loop

As for DC SQUIDs, the following features are to be optimized:

i) the transfert coefficient:

$$\partial V/\partial\phi_a = 2\beta R_D/[(1+\beta)L]$$
[6]

ii) the energy resolution, which is optimum for β = 1

$$\varepsilon_{opt} \approx 5...7k_BTL/R$$

If β = 1 in $\partial V/\partial\phi_a$,

$$(\partial V/\partial\phi_a)_{opt} = R_D/L$$

with:

R_D: SQUID dynamic resistance ≈ R/2

thus:

$$(\partial V/\partial\phi_a)_{opt} \approx R/(2L)$$

These requirements lead to the following constraints:

i) $\beta = 2L I_o/\phi_o \approx 1$

ii) $\partial V/\partial \phi_a = R/(2L)$

iii) $\varepsilon_{opt} \approx 5...7 k_B TL/R$ (in white noise region)

Thus:

i) L must be as low as possible, but...
   high enough to match the requirements of the coupling
   problem (100 pH is a "good" value)

ii) L being fixed, I_0 has te be reduced (critical current
    necessary adjustment)

iii) R should be as high as possible, but...
    a non-hysteretic behaviour requires $\beta_c < 1$.

IV 2 - Main Advances in LTSC based SQUIDs

i) RF operation:

   $\varepsilon > 10^{-30}$ J.Hz^{-1} with cooled amplifiers

ii) DC operation:

   $\varepsilon \approx 3 \, 10^{-33}$ J.Hz^{-1} at 4.2 K within the best conditions

(1/f) noise, associated with the metallic state of the junction, is
the LF limitation of the performances. The best results were
obtained by Tesche [7] and reached:

   $\varepsilon \approx 7.7 \, 10^{-32}$ J.Hz^{-1} at 0.1 Hz

V - ADVANCES RELATED TO HTSC SQUIDs

It is widely recognized that the SQUID-based magnetometers'
features match very closely the requirements for long range de-
tection and localization of magnetic objects. The main advance
from HTSC lies in the much higher temperature of operation of
a SQUID probe.

V 1 - PRELIMINARY RESULTS ON BULK HTSC SQUIDs

The observation of Josephson effect in HTSC ceramics has sti-
mulated numerous attempts to investigate the potential of this
rough material morphology in terms of superconducting devices
[8]. A large amount of SQUIDs-like devices were built (either
RF or DC biased) and exhibited rather reasonable sensitivity in
white noise region [9]. The main identified problem is the high
level of 1/f noise in such materials at 77 K, and the location of
the threshold of this noise above 1 kHz.

The following experiments and results concern thick HTSC
films made from YBaCuO composition. The oxide has been
prepared through the conventional way [10] and got thinner by
dry grinding until about 0.2 mm. The electrical contacts are

made by gold or silver pads deposition after ionic etching and
show resistivity values around 10^{-5} Ωcm^2. The pellets are then
cut out and engraved by laser (YAG, 30 W), which allows a
collective treatment of six probes at each run; the constriction
width is finally close to 0.2 mm and the laser-processing per-
turbated zone is not wider than 10 μm (Fig. 3). At that point, the
probes are characterized in terms of Shapiro steps and critical
current (Fig. 4), this latter being adjusted by the conventional
current pulses technique to fit the requirements of SQUID ope-
ration.

Table 1 gives values of $I_c R_n$ products between 10 and 100 μV,
far below the theoretical BCS prediction [11] with
$(\pi\Delta/2e) = 18$mV (Δ being close to 10 mV at 77 K). These low
values of $I_c R_n$ products could be either related to proximity
contacts rather than to proper contacts between two
superconcting grains, or to weak flux trapping in the vicinity of
the "junctions" Besides, the I(V) characteristics exhibit no
hysteresis (Fig. 5), showing that β_c (Mc Cumber parameter) is
lower than 1. From that we could deduce in RSJC model
(Resistive Shunted Junction with Capacitance) that $C < 10^{-10}$
F, and neglect the capacitance compared with the resistive
shunt.

We could underline the necessity to polarize the probes very
precisely with a current value close to critical current in order to
draw benefits from the higher value of the transfert coefficient
$(dV/d\phi)$ (Fig. 6).

Different Voltage/Flux characteristics are shown in Figure 7.

The analyse of different probes in terms of magnetic field sen-
sors, using the criteria developped by Tesche and Clarke [12],
gives the following optimal values:

i) Critical current $\approx$ 10 μA

ii) Loop inductance $\approx$ 60 pH

iii) Loop "area" $\approx$ 3000 μm^2

iv) "Junction" capacitance < 100 pF

In order to estimate the resolution of our devices, we came
down to the situation of two-junctions SQUIDs, although the
loops we used might contain more than two "junctions" We
asserted, actually, that polarization current discriminates the two
first junctions of the loop in terms of critical current. In that
case, the engraving of the constriction and the adjustment of
critical current act to decrease the number of critical paths

We get, finally, after spectral analysis of the electronic unit and
of the whole device noises, assuming the noises respectively
related to the electronics and to the probe itself are not correla-
ted, the following figures, above 100 Hz:

i) Flux noise: $\phi_n < 8 \, 10^{-6}$ V Hz$^{-1/2}$

ii) Energy resolution: $\varepsilon < 7 \, 10^{-31}$ J.Hz^{-1}

The theoretical values calculated from the experimental measurements of L, R and (dV/dϕ) are:

i) Flux noise: $\phi_n \approx 7\ 10^{-6}$ V.Hz$^{-1/2}$

ii) Energy resolution: $\varepsilon \approx 4.8\ 10^{-31}$ J.Hz^{-1}

For the best probe tested, we estimated the field sensitivity around 500 fT.Hz$^{-1/2}$ (f > 100 Hz).

These results are plotted in Fig. 8 which sums up the state-of-the-art for HTSC SQUIDs.

In view of these results, one could assess that the potential of HTSC SQUIDs are rather promising, with energy resolutions around 1000 h without flux transformer. The striking fact is the setback of 1/f noise in the reported results. If one postulates that VLF noise is related to resistivity fluctuations of Josephson's barriers at grains boundaries, probably due to erratic flux trapping, any improvement of the granular structure would reduce this flux noise. In particular, the substitution for thick ceramic films by good quality thin films will undoubtly lead to attractive devices whose sensitivities would be no more than a order of magnitude above those of conventional Helium SQUIDs.

V.2 - STATE-OF-THE-ART HTSC THIN FILMS

At this date, the best 1-2-3 films are deposited in-situ (T_c = 92 K; J_c = 10^7 A.cm^{-2} at 77 K), and result from different deposition techniques (multisource evaporation; single source off-axis sputtering; pulsed laser deposition; molecular beam epitaxy) [13,14,15].

It is important to stress the results obtained by laser deposition which are, although this technique is relatively new, associated with the best performances reported anywhere [16,17]

Data from the best films at 77 K is approaching that of Nb films for the same (T/T$_c$) reduced temperature [16]. Furthermore, new developments on tunnelling structures [18] are indicating that sandwich-type junctions could be yet made from 1-2-3.

Most of the BiSrCaCuO films are made by single target sputtering [19] and the main effort lies on the control of stoechiometry at high growth temperatures (the problem is the high volatility of Bismuth). The best films are post-annealed and give results comparable to those for 1-2-3 (T$_c$ = 108 K; J_c = 6 10^6 A.cm^{-2} at 77 K).

Thallium compounds (TlBaCaCuO) gave rise to a huge interest mainly due to the following characteristics: they come with the highest critical temperature (>125 K), and, above all, because there are a larger number of phases containing the same elements, the intergranular phase tends to provide good superconducting properties, which results in higher critical current densities even for polycrystalline badly-oriented films (J_c = 6 10^5 A.cm^{-2} at 100 K) [20].

The needs for Device fabrication could be listed as follows:

i) High T$_c$,

ii) short transition width,

iii) high critical current density (J_c > 10^5 A.cm^{-2} at 77 K)

iv) surface smoothness < 100 A

v) the oxigen stoichiometry has to be controlled in the film

At this day, in terms of reproducibility and above requirements matching, low temperature process laser deposition (with in-situ annealing) gives the best results [21].

V.3 - PATTERNING OF WEAK-LINKS
CREATION OF JOSEPHSON JUNCTIONS
CRITICAL CURRENT ADJUSTMENT

The conventional Josephson Junctions (i.e. the S.I.S. sandwich) is still not available for HTSC, because of their very short coherence length. Processing at an atomic level (a few thousands of A thickness, each atomic layer being controled) would be necessary, but is, at this date, unlikely to work out.

The S.N.S. type junction seems less difficult to fabricate and preliminary results are available at low temperature [22]. The main difficulty arising from this type of junction is the very poor dynamic resistance (R$_D$). A rough calculation gives R$_D$ around 0.1 mΩ for 1 μm^2 S.N.S. sandwich-type junction and around 10 mΩ for edge-type junction (0.1 μm wide microbridge engraved on a 1000 A thick film; J_c=10^6 A.cm^{-2}) Thus, in any case, it will hard to match these junctions to the input of the amplification stage, since the peak-to-peak SQUID signal wouls liein the 10^{-9} to 10^{-8} (V/ϕ_0) range. They would necessarily need some superconductive impedance matching circuit (LC tank circuit) which would reduce the bandwidth of operation for such a SQUID system.

Therefore, in the near future, HTSC SQUIDs will use natural weak-links of the films, as shown by the recent results of Robbes on YBaCuO thin films at Berkeley [23]. With current pulses critical current adjustment, they obtain R$_D$ around 2 Ω and I_c close to 10 μA at 77 K. Such characteristics should lead to a DC SQUID energy resolution near 10^{-30} J.Hz^{-1} at 77 K (L $\approx$ 100 pH). This method should apply to TlBaCaCuO films also which exhibit higher dynamic resistance, and would lead, in this case, to much better energy resolution (for high quality films involving low 1/f noise).

V - CONCLUSIONS

We have tried to give a brief overview on the status of SQUID magnetometry, underlining that the need for more sensitive

sensors is today a reality. HTSC SQUIDs could thus replace classical Flux–Gates and increase the spectrum of applications in magnetometric detection, matching the requirements of advanced signal processing. In view of the tremendous progress of the three past years, one could be confident in the potential of the HTSC SQUIDs, assuming that thin films quality will be improved.

Acknowledgments

The author is indebted to L.M. Mercandalli and I. Zaquine for supplying YBaCuO probes, and to P. Grégoire for technical assistance for the electronic units fabrication.

Added note

Recent results reviewed by Roger H. Koch [24] underline the striking reduction of flux noise exhibited by HTSC TlBaCaCuO SQUIDs operating at high temperature. The noise performance of these polycrystalline films–based SQUIDs is at least comparable, at very low frequencies, to those associated to LTSC commercial DC and RF SQUIDs, and the near future of these TlBaCaCuO devices appears today as extremely promising.

REFERENCES

1. Ambegaokar, Halperin – Phys. Rev. Lett. 22, 1364 (1969)
2. Ivanchenko, Zil'berman – Zh. Eksp. Teor. Fiz. 8, 189 (1968)
3. Likharev, Semenov – J.E.T.P. Lett. 15, 442 (1972)
4. Vystavkin et al. – Rev. Phys. Appl. 9, 79 (1974)
5. Clarke – IC SQUID 80, 187, W. de Gruyter, Berlin (1981)
6. Peterson, Hamilton – J. Appl. Phys. 50, 8135 (1979)
7. Tesche et al. – 17th IC Low Temp. Phys., North Holland, N.Y. (1984)
8. Esteve et al. – Europhys. Lett. 3, 1237 (1987)
9. Robbes et al. – Nature 331, 151 (1988)
10. Michel et al. – C. R. Acad. Sci. Paris 304 II, 1059 (1987)
11. Ambegaokar, Baratoff – Phys. Rev. Lett. 10, 486 (1963)
12. Tesche, Clarke – J. Low Temp. Phys. 29, 301 (1977)
13. Matijasevic et al. – Bull. Am. Phys. Soc. 34, 603 (1989)
14. Xi et al. – Z. Physik B Cond. Matt. 74, 13 (1989)
15. Terashima et al. – M2S Conf. Stanford (1989)
16. Klein et al. – Appl. Phys. Lett. 54, 757 (1989)
17. Inam et al. – Appl. Phys. Lett. 53, 908 (1988)
18. Yoshida et al. – Sc. Tech. of Thin Films SC, Plenum Press, N.Y. (1989)
19. Yoshitate et al. – Jap. J. Appl. Phys. 27, L1262 (1988)
20. Ginley et al. – Appl. Phys. Lett. 53, 406 (1988)
21. Wellstood (Berkeley) Private Communication
22. Gijs et al. – Sol. St. Comm. 71, 575 (1989)
23. Robbes (CMS Caen, F) To be published
24. Koch – Solid State Technology, 255 (May 1990)

Figure 3: SEM micrographs of a SQUID probe
(a) X20, (b) X100, (c) X300
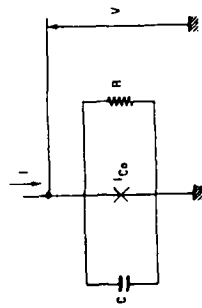
Figure 1: RSJC model of a real junction
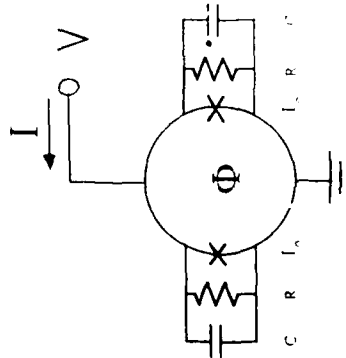
Figure 2: Schematic representation of a DC SQUID with shunt resistance R, capacitance C, junction critical current I_0, inductance L and flux Φ in the loop. I is the applied current, producing a voltage V across the SQUID

Figure 5 : I(V) characteristics of a constriction after adjustment of the critical current (H: 10 μA/div, V: 20 μV/div)
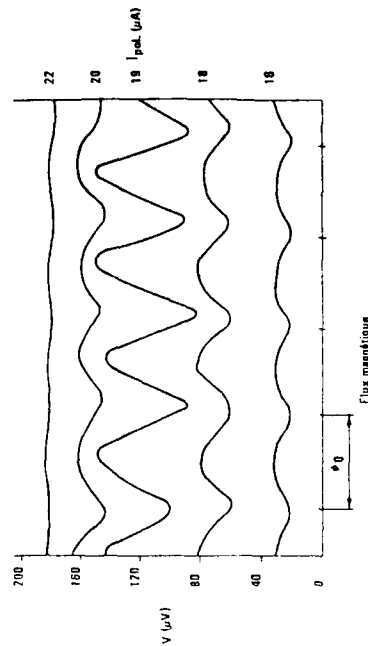
Figure 6 : V(φ) characteristics vs polarization current

Table 1 : IcRn products of the tested probes

Figure 4 : Electronic unit for preliminary characterization of the probes

Echantillon 10-9/7

f = 30 Hz, I_o = 4 µA

S_{boucle} = 4 10^4 µm²

soit φ = 225 µm

L_{boucle} = 220pH

β ...... = 19

Δ_m ...... =0.34

C_{max} ...... =50µV/φ_o

(H 9.5 nT /div
V 5 µV/div)

Echantillon 12-1/7

f = 30 Hz, I_o = 150 µA

S_{boucle} = 400 µm²

soit φ = 25 µm

L_{boucle} = 25 pH

β ...... = 3.6

Δ_m = 0.21

C_{max} ...... = 7 µV/φ_o

(H 5000 nT/div
V 10µV/div)

Echantillon 15-4-2/2

f = 3 Hz, I_o = 42µA

S_{boucle} = 90X µm²

soit φ = 100 µm

L_{boucle} = 100 pH

β = 1.2

Δ_m = 0.2

C_{max} = 15 µV/φ_o

(H 250 nT /div
V 1 µV/div)

Figure 7: Voltage / Flux characteristics of different probes

Figure 8: Energy resolution of different HTSC SQUIDs

THE WORLD OF SUPERCONDUCTIVE MACHINERY

BY
DR A D APPLETON
TECHNICAL DIRECTOR
NEI INTERNATIONAL RESEARCH AND DEVELOPMENT LIMITED
FOSSWAY
NEWCASTLE UPON TYNE
NE6 2YD
ENGLAND

SUMMARY

The development of superconducting machinery has been in progress since the early 1960's and this paper presents a summary of the progress which has been made to date together with a view on the likely developments in the future. The bulk of the work in respect of rotating machinery has been on dc homopolar motors and generators, and ac generators; the superconducting components are the stationary field windings of the dc machines and the rotating dc field windings of the ac machines.

The homopolar motors and generators are relatively simple in concept not least because the cryogenic components are stationary; however the feature which has dominated the progress in their development is current collection at the sliprings of the rotating armature and some comments on this technology are given in this presentation. The application which has been driving most of the superconducting homopolar machine projects is ship propulsion but it is of course recognised that their successful development will benefit other applications such as land based industrial drives and industrial processes requiring large quantities of dc power.

The bulk of the work on superconducting ac generators has been directed towards the requirements of large central power stations. However some of the earliest investigations were in respect of aircraft generators and this application continues to be of interest. Although some work was undertaken on 'inside out' generators in which the dc field winding (superconducting) was stationary all of the current activity is in respect of the more conventional geometry.

In the early 1980's it was discovered that by producing ultra fine wires (less than 1 micron diameter) of niobium-titanium (NbTi), these liquid helium cooled superconductors could carry current at power frequencies without prohibitive losses which had previously been the case. This discovery and the subsequent production of these wires in France and later in Japan enabled work to proceed on superconducting transformers and on totally superconducting ac generator.

The next events in this rapidly evolving technology were the discoveries in late 1986 and early 1987 that a non-metallic material was superconducting at temperatures in excess of 90K. The great significance of this development is that these ceramic materials could be cooled with liquid nitrogen instead of liquid helium and the ramifications of this upon design and cost are immense. In this presentation the likely impact of this discovery on electrical power equipment will be discussed.

DIRECT CURRENT MACHINES

Why Superconducting?

There are severe limitations to the ratings of dc motors and generators which can be constructed. These stem from the restrictions on the voltage which is permissible between commutator segments (reactance voltage effects upon commutation) and the practical limits on the size and weight of the machines. These considerations impose an upper limit on ratings of about 10-15 MW over a speed range of about 150 rev/min $\pm$ 50%. Since there are applications for variable speed dc motors and dc generators of higher ratings and higher speeds than this there is considerable interest in knowing what the technology of superconductivity can offer. It will now be shown that almost all of the work which has been undertaken is for homopolar machines.

Why Homopolar?

In 1964 when serious consideration was first given to the use of the superconductors in electrical propulsion motors the state-of-the-art was rather primative; the stability of the currents flowing in the superconductors was not well understood but it was known that time varying magnetic fields could cause losses and that superconducting wire movement under mechanical forces could cause a coil to 'quench' i.e. to revert to the non-superconducting state. It is well known that conventional type heteropolar dc machines experience 'armature reaction' effects i.e. the field of the dc excitation windings is modified by the fields produced by the time varying currents in the armature. Also it was realised that the torque reaction, which in conventional machines appears on the iron pole pieces would, for superconducting excitation windings, appear on the superconductors. Thus for two reasons - losses due to armature reaction effects and torque reaction forces - the heteropolar machine presents some difficulties. The homopolar machine on the other hand can be designed to avoid both of these problems; this is because the magnetic field of the armature can be contained within a co-axial type arrangement of the armature conductors and the torque reaction is taken on the stationary part armature conductors. The net result of this is that the superconducting field winding is isolated from any influence of the armature winding - a highly desirable situation for the state-of-the-art as it was in the 1960's.

Unlike heteropolar machines, where many turns can be made on an armature winding before connections are taken to a commutator segment, each turn of an armature conductor in a homopolar machine must be connected to a slipring. A consequence of this is that the voltage of homopolar machines is low and instead of having armature conductor wires, it is more usual to have a solid copper disc or copper bars with a slipring at the outer perimeter and a slipring near to the axis. It is often more convenient to depart from the Faraday disc concept with a single field winding to a drum type configuration with two excitation windings and two sliprings of the same diameter. This overcomes the problem of taking a high current from the small diameter slipring of a disc type geometry.

It is apparent that for a low voltage homopolar machine of significant power the current to be collected from the sliprings described above must be very high. For example a slow speed motor of about 20MW is unlikely to have an armature voltage greater than about 1kV and therefore the armature current is 20,000A. This level of current is typical for the motors which have been designed over the past 25 years. It follows that one of the earliest considerations in a development programme is the method to be employed for current collection.

The UK programme based at NEI started by consideration of liquid metal systems but changed after a short time to solid metal graphite brushes. In the USA at the David Taylor Naval Ship Research and Development Center (DTRC), Annapolis, most of the work has been based upon the use of liquid metals. The state of the art of both approaches has been greatly advanced over the many years of development and both are still under active consideration.

Although the original reasons for choosing homopolar machines namely armature reaction and torque reaction effects are no longer valid because of the very substantial improvements which have been made in the performance of superconductors it is still the case that this choice is the most appropriate for large dc motors and generators. The reasons for this are beyond the scope of this review paper but they are related to the extreme robustness of homopolar machines; a good example of this is a design which was undertaken by NEI for a 60 MW, 80 rev/min superconducting motor for an icebreaker which had to be capable of providing twice full load torque at zero speed when the ship was stuck in ice.

Some examples of machines that have been constructed

The first superconducting homopolar motor[1] was designed and constructed, on behalf of the Ministry of Defence, at NEI International Research and Development Limited and was first operated in June 1966. This machine, which is now in the Science Museum in London, is shown in Figure 1 as it was under test; it employed a niobium-zirconium (NbZr) superconductor and developed 50 horse power at 2000 rev/min. The armature consisted of two Faraday discs made of cupro-nickel supported on either side of a stainless steel disc. The peak magnetic flux density was 2.5 tesla and the two discs connected in series generated a voltage (back emf) of 10.7 V; the armature current was 3500 A. The current collection was by conventional brushes of copper graphite (Morganite CMIS); it is noted that these commercially available brushes, the performance of which was demonstrated on test rigs for this first motor in 1965, is still one of the preferred options in modern superconducting motors.

A major step change in rating was then made at NEI when it was decided in 1967 to construct, with the support of the National Research and Development Corporation, a 3250 horse power, 200 rev/min superconducting motor[2]; this motor was designed and built in just over two years and first tested in October 1969. One of the features of this motor was a new idea[3] to increase the armature voltage by segmenting the slipring; this can be seen in the photograph of Figure 2. The voltage was increased from 40V to 440V by this concept and the brushes employed were the Morganite CM2 a slight variation on the Morganite CMIS. The motor is shown in Figure 3 under test at Fawley power station in the South of England where it was used to drive a main cooling water pump for a 500 MW turbo generator.

A programme for the development of superconducting homopolar machines was started in the USA at the DTRC in 1969; the first motor which was constructed was rated at 300 kW and employed a drum type geometry with liquid metal current collection. This machine employed an iron casing to shape the direction of the magnetic flux and to contain it within the machine. A 300 kw superconducting homopolar generator to power the motor was also constructed. This work was followed by the construction of two 3000 HP superconducting motors shown under test at DTRC in Figure 4. These machines, constructed by General Electric, were also tested in a small ship in Chesapeake Bay; see Figure 5.

A complete marine propulsion system i.e. motor and generator, of 1MW rating is shown in Figure 6; this was constructed by NEI, on behalf of the Ministry of Defence, in the mid 1970's and employed additional superconducting windings to screen the environment from the magnetic flux of the motor excitation windings. The generator was driven by at 1500 rev/min by a Deltic diesel engine and employed a new type of current collection developed at NEI; this was a metal plated carbon fibre brush. The motor was loaded by a water brake at a speed of 375 rev/min. This project led onto a major programme which was started at NEI in 1979 to construct the field systems for a 25 MW, 200 rev/min motor and to undertake an exhaustive programme of experimental investigations into the performance of a range of electrical brushes on a range of different slipring materials; this programme was completed in 1983.

Some Observations on the dc Machines Programmes - Past and Future

(i)   The dc machines development programme

        The bulk of the world activity in respect of dc motors and generators has been carried out in the UK and the USA; this has been described briefly. In many respects the two programmes have been complementary in that they adopted rather different approaches but both have made a significant contribution to the technology.

(ii)   Refrigeration

No reference has yet been made to the helium refrigeration systems which are required for the machines that have been built to date. It must be noted that in the 1960's helium refrigeration technology was in its infancy as far as stand alone small scale systems were concerned. The major difficulties were linked to the need to maintain a very high purity of the helium particularly during the gas compression. Over the years most of the problems have been resolved but it remains a fact that refrigeration at 4 degrees Kelvin (269°C) is an engineering challenge in respect of design complexity, cost and reliability.

(iii)   Current Collection

This technology has been the subject of large investment over the past 26 years and, by and large, the design engineer can now obtain the performance which he requires from one of the alternative systems i.e. solid brushes or liquid metal systems.

(iv)   Future Developments

The emerging technology of superconductors which can be cooled with liquid nitrogen will have an enormous impact upon the progress which can be made with superconducting dc machines. Designs are greatly simplified because nitrogen is much more tolerant to heat ingress and costs of refrigeration are reduced by nearly two orders of magnetude. Nitrogen can be obtained free of charge from the atmosphere which, apart from other considerations, is an important factor for a ship at sea.

The development of the technology for homopolar machines is now very advanced and with the lower cost and greater reliability of nitrogen refrigeration there is no barrier to these machines achieving a full commercial status for industrial drives of the highest powers that are likely to be required and dc generators of 100 MW or higher for the electro-chemical industry.

AC GENERATORS

Why Superconducting?

The ratings of ac generators in central power stations has risen from about 60 MW in the 1940's to well over 1000 MW in the 1980's. The reason for this increase is economy of scale - imagine the cost of power stations and hence the cost of electrical energy if 60 MW was the highest rating available. While it is true that in recent years there is less pressure, for a variety of reasons, for producing the highest raings, there remains a need to reduce costs and improve efficiency.

It has been shown, beyond doubt, that the length, weight and losses can each be reduced by 50% by the use of superconducting windings. By the use of liquid helium cooled superconductors for the excitation windings of a 660 MW generator the efficiency can be increased from 98.6% to 99.2% i.e. a saving of 3960 kW. The capitalised value of these losses over the life of the generator is about £2500/kW (depends upon load factor) which is a saving of nearly £10M. In addition there are savings in manufacturing, transport and turbine hall costs. It must be noted that these savings are realistic only if the reliability of the equipment is at least as good as the system which it replaces. The rating at which a superconducting generator breaks even with a conventional generator on the basis of first costs alone (i.e. neglecting the efficiency savings obtained by using superconductors) is about 500MW. With liquid nitrogen cooling it is estimated that this will fall to less than 100MW.

The Rotating Field System

In a conventional type ac generator the rotating field winding consists of copper bars located in deep axial slots cut into a solid steel forging. The bars are usually locked into position by steel wedges fitted to the tops of the slots. At the ends of the slots the conductors are bent round curved slots and these end windings are supported by 'end bells'. The most common method of cooling is by hydrogen gas but more advanced designs are moving towards water cooling.

For the development of superconducting ac generators it is usual to follow this general approach but the major differences are that the forging is operating at 4K and because of this it is necessarty for it to be made of an austenitic steel (it is no longer necessary to rely upon the magnetic properties of the forging). Since the forging and its superconducting winding are at this low temperature it is necessary to reduce heat transfer from ambient surroundings by locating it in a vacuum, by providing thermal radiation shields and by careful design of the supports at the ends of the forging. These supports must however retain the capability of transmitting the full load and short circuit machine torques. The vacuum is achieved by providing an outer cylindrical rotor which may, or may not be designed to transmit the machine torque. According to the design philosophy which is adopted. The liquid helium coolant is introduced by a vacuum insulated tube along the axis of the rotor from the non-drive end. The helium is made to flow in the slots and, in many designs, it is then used to counterflow cool the inner rotor support system and the current leads which must take the excitation current from the long temperature winding to the ambient temperature slip rings.

The Armature Winding

In a conventional design the stator or armature winding is located in slots in a laminated iron core. The winding is usually water cooled with appropriate end windings to form the 3 phase connections.

In a superconducting generator the arrangement is generally the same except that in principle there is no need to employ the laminated iron core because sufficient mmf (magneto-motive-force) is available to make this redundant. However, it is usual to retain the iron core, because it serves the dual purpose of

enhancing the generator output and keeping the magnetic flux contained within the machine. Use is made of the lack of need for the iron by taking the armature conductors out of the slots into the air gap. This has the double benefit of allowing more copper to be used and reducing the reactance of the armature winding by a significant amount.

An Example of the Machine Concept

The general arrangement of the NEI design of a large superconducting generator[4] is shown in Figure 7. The rotor arrangement is as described above but, in this design, the armature winding is contained within a monolithic structure of epoxy-concrete. This arrangement was adopted to ensure adequate support for the large mechanical forces that appear on the armature winding and also to facilitate the use of a helical armature winding[5] which was evolved at NEI to reduce the complexity of the end windings.

Some Examples of Machines That Have Been Constructed

The first superconducting ac generator[6] was designed and constructed at MIT in 1969; it had a rating of 45 kVA. During the next 20 years machines were built in a number of countries as shown in the following table.

MANUFACTURER	COUNTRY	RATING	TEST
MIT	USA	45 kVA	1969
All Unions Inst.	USSR	65 kVA	1970
MIT	USA	3000 kVA	1972
Westinghouse	USA	5000 kVA	1972
All Unions Inst.	USSR	1500 kVA	1973
Peri, Shanghai	China	400 kVA	1974
Karkov	USSR	200 kW	1975
Electrosila	USSR	2000 kW	1975
Fuji, Mitsubishi	Japan	6250 kVA	1977
Crt BT, Grenoble	France	500 kVA	1980
TU, Munich	Germany	300 kVA	1980
General Electric	USA	20 MVA	1981
Electrosila	USSR	20 MVA	1981
Fuji	Japan	20 kVA	1982
Hitachi	Japan	50 MVA	1984
Skoda	CSSR	5000 kVA	1984
Mitsubishi	Japan	30 MVA	1984
Toshiba	Japan	3000 kVA	1984
Elin-Union	Austria	2000 kVA	1986
CRTBT	France	20 kvA	1988
Toshiba	Japan	100 kVA	1989
Electrosila	USSR	300 MW	1989

NOTES:

(1)   GEC-ALSTHOM built the superconducting rotor of a 250 MW generator in 1980.

(2)   EPRI-WESTINGHOUSE made considerable progress with a 300 MW generator until 1984 when the project was cancelled.

(3)   SIEMENS-KWU[7] have nearly completed a 400 MW generator which will be under test in 1991 and will have a 850 MW commercial prototype in 1996.

(4)   Mitsubishi, Toshiba and Hitachi are each building a 70 MW machine and will have a 200 MW commercial prototype in 1997.

(5)   Electrosila is projecting a 1000 MW generator by 1998.

Figure 8 shows a 20 MW generator constructed by General Electric in the mid 1970's, and Figure 9 shows the rotor of a 400 MW generator which is nearly ready for test by Siemens.

Some Observations on the ac Generator Programmes - Past and Future

It has been shown that a large number of superconducting ac generators have been constructed all of which have employed helium cooled NbTi superconductors. In the USA, UK and to a degree in France the development of these machines has been put into low gear. However work is continuing in Germany, Japan and the USSR and we may expect to see commercial prototypes under test; 850 MVA in Germany (1996); 200 MVA in Japan (1997) and 1000 MW in USSR (1998).

In France and Japan work is proceeding on small ac generators which are totally superconducting; in those designs the armature winding employs the new ultra-fine NbTi wires in which the 'ac' losses are reduced to acceptable levels. If this work is successful the machine efficiencies will be increased further - typically from 99.2% for a partially superconducting machine to about 99%.

The availability of the liquid nitrogen cooled superconductors will allow considerable simplifications in the design of the rotor, without the need to be forced to meet difficult and expensive design arrangements. For a totally superconducting generator there can be no doubt that liquid nitrogen cooling

will be more tractable than is the case with helium cooling. Perhaps more importantly the increase in reliability which will accompany liquid nitrogen cooling may be the spur to the re-instatement of development programmes which have been subject to curtailment.

SUPERCONDUCTIVITY AND THE ELECTRICAL POWER INDUSTRY

Superconducting power equipments which are not included within the scope of this presentation but which nevertheless form an important part of the general infrastructure are;

(i)   Transformers

Although a lot of excellent design work was undertaken in the 1960's and 1970's it was not until the advent of ultra-fine NbTi wires that a realistic design could be considered. A 200 kW transformer has been constructed in France and a 100 kVA 60 Hz coil has been built in Japan. If a suitable liquid nitrogen cooled superconductor can be developed the prospects for building large power transformers are greatly enhanced.

(ii)   Cables

A large amount of development work has taken place over the last 25 years notably in USA[8], UK, Austria, Germany and Japan but also in numerous others. The cables are technically feasible but one of the problems is that in order to be economically attractive the rating must be between about 1000 and 3000 MVA (according to the different programmes). There is evidence that as a result of the development of liquid nitrogen cooled superconductors a degree of international collaboration is now building up so that more progress may be made during the next few years.

(iii)   Fault Current Limiters

The limiting of the level of fault currents is an important aspect of the operation of power systems and to meet this need NEI designed and constructed[9] a 5MVA fault current limiter about 10 years ago. This was based upon the use of an iron core with two windings one ac and one dc, the latter being superconducting. When energised the dc winding saturates the core with flux and the impedance of the ac winding is low. Under fault conditions the iron core is automatically taken out of magnetic saturation, the ac winding develops a higher impedance and the fault current is limited. This device was completely successful technically and is applicable mainly to HV transmission systems; it is however rather expensive at distribution voltage level where the potential market is large. The liquid nitrogen superconductors will reduce the costs and this could be one of the first applications for superconductors in power engineering.

CONCLUSIONS

1.   A considerable amount of development work has taken place over the past 25 years in respect of superconducting rotating machines. Even without the advent of the new liquid nitrogen superconductors progress will continue to be made but with the availability of these new materials there will be a spur to greater activity and good progress may be expected.

2.   Developments for many of the applications for superconductors in power engineering are likely to be undertaken and this will enhance the general industrial infrastructure for this technology.

3.   It is noticable that for most of the applications described there has been a good measure of international collaboration and all of the signs are that this will continue.

REFERENCES

1   Appleton A D., Design of Superconducting Machines. PhD Thesis, University of London, 1977.

2   Appleton A D., Motors, Generators and Flux Pumps. Commission 1 London Annex 1969-1 Bull.11h pp 261-269.

3   Appleton A D., and MacNab R B., British Patent No.1285026, 15.9.69.

4   Appleton A D., Ross J S H., Mitcham A J., Bumby J R., Superconducting AC Generators: Progress on the Design of a 1300MW, 300 rev/min Generator ASC, San Francisco, 1976.

5   Anderson A F., Bumby J R., Hassall B I., Analysis of Helical Armature Windings with Particular Reference to Superconducting AC Generators, IEE Proc. Vol.127, Pt.C No.3, May 1980.

6   Woodson H H., Stekly Z J J., Halas E., IEEE Transactions on Power Apparatus and Systems, Vol.PAS-85, No.3, March 1966, P 264.

7   Lambrecht D., Superconducting Turbogenerators; Status and Trends, Cryogenics 1985, Vol.25 November.

8   Forsyth E B., Thomas R A., Performance Summary of the Brookhaven Superconducting Power Transmission System. Cryogenics 1986, Vol.26, November.

9   Raju B P., Parton K C., Bartram T C., Fault Current Limiting Reactor with Superconducting DC Bias Winding CIGRE Paper 23-03, 1982, Session 1-9 September.

10   Forsyth E B., Thomas R A., Performance Summary of the Brookhaven Superconducting Power Transmission System. Cryogenics 1986 Vol.26, Nov.

Fig. 1

Fig. 2
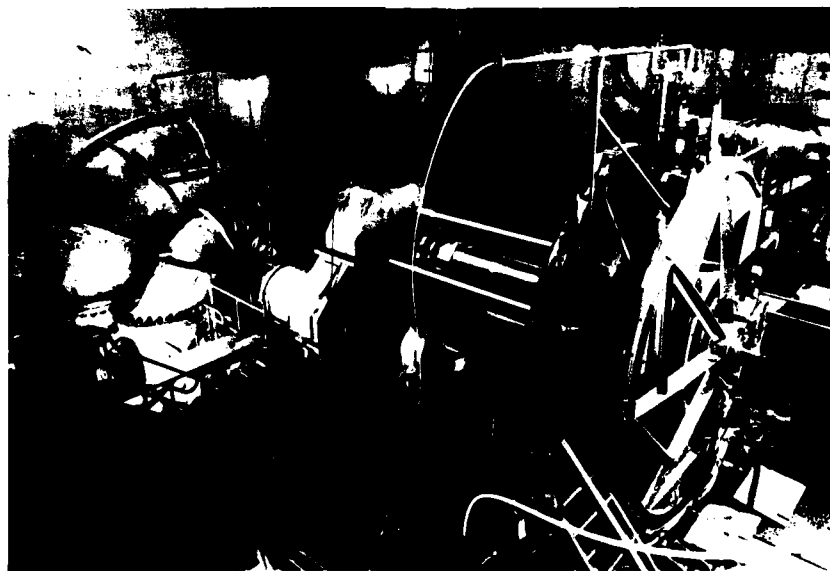
Fig. 3
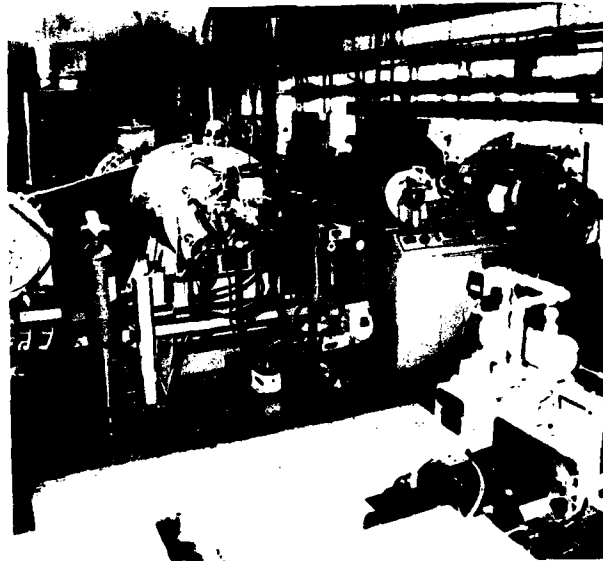
Fig. 4
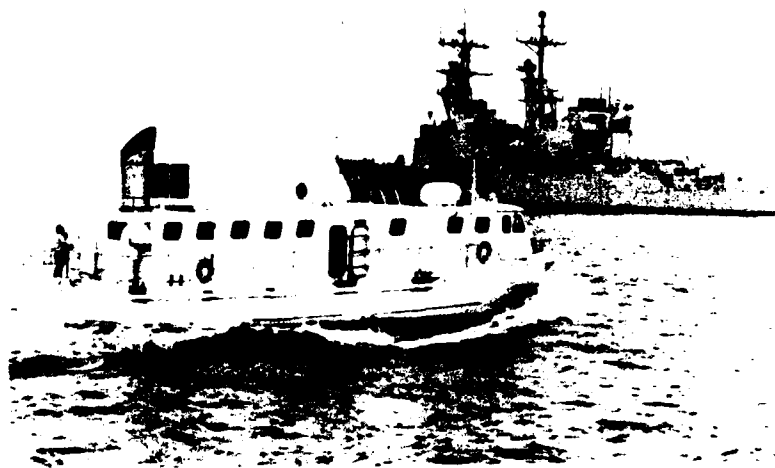
Fig. 5
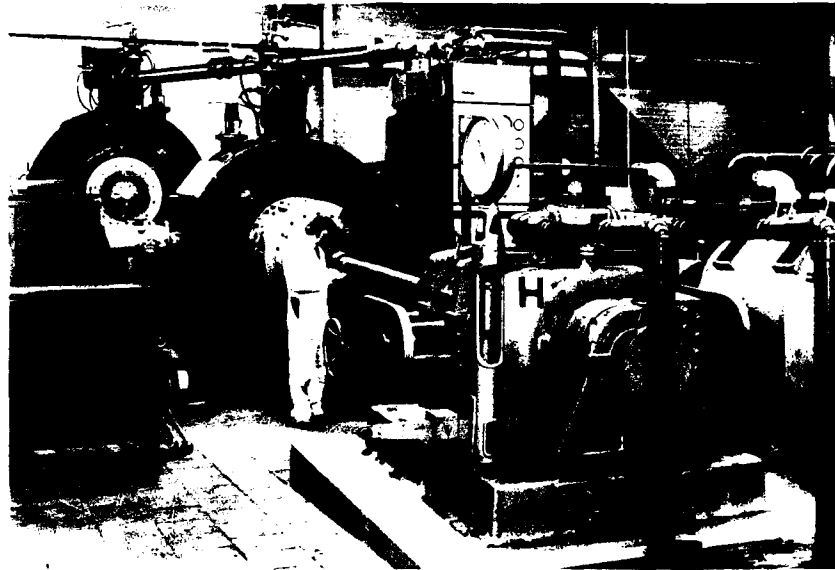
Fig. 6
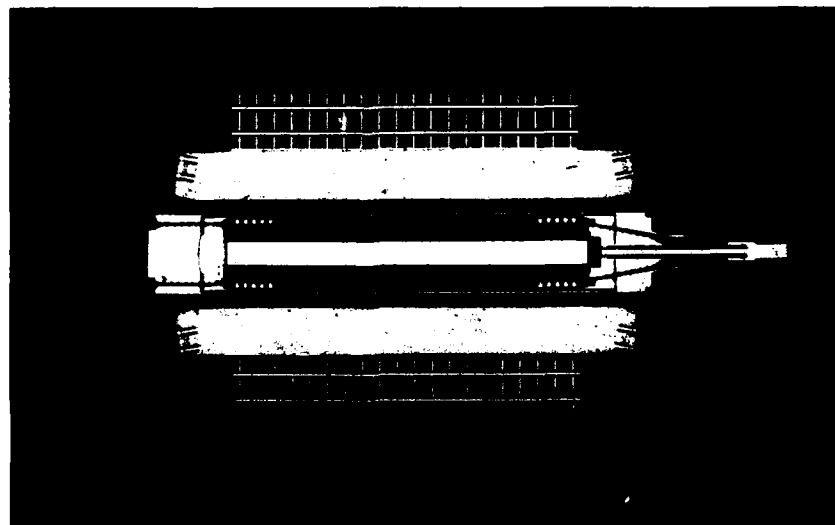
Fig. 7
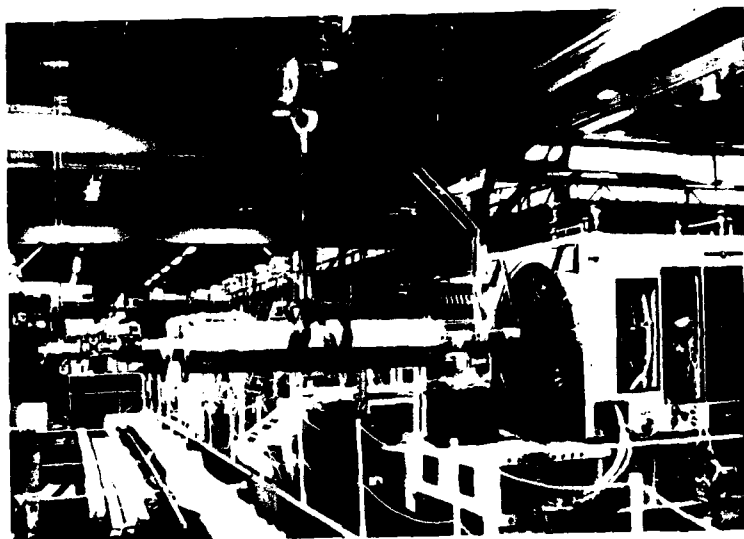
Fig. 8
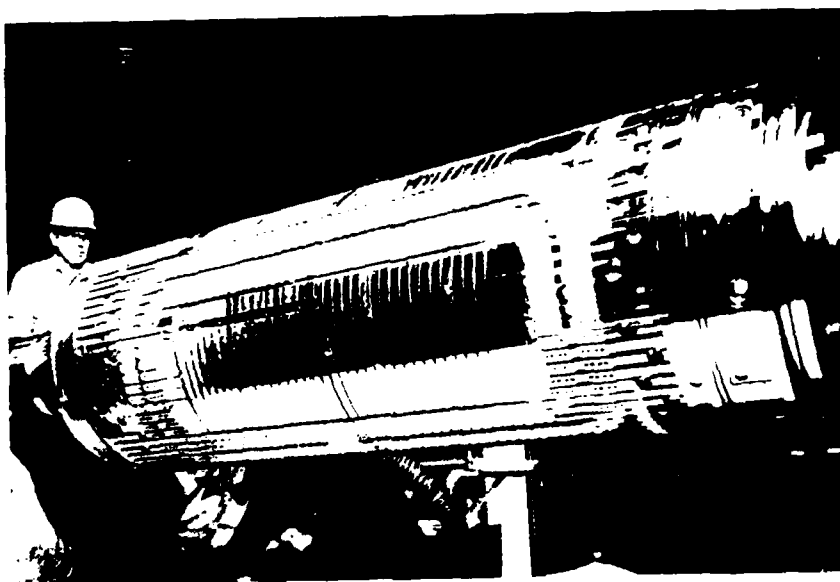
Fig. 9

Discussion

Name of Author: Dr. A. Appleton

Paper No.: 19 -- The World of Superconductive Machinery

Name of person asking question: Andrew Smith

Question

How low a resistivity material do you need?

Would cryogenic copper do almost as well?

Answer

The problem with using copper at low temperatures is the cost of providing the power for the necessary refrigeration. The resistance ratio of good quality copper increases with reducing temperature but the total losses (i.e., I^2R and refrigeration) is never better then a superconductor.

The study which came closest to solving this problem was to use the cooling capacity of LNG (liquefied natural gas) at 112 K to reduce the cost of making liquid nitrogen. The latter was used, in the study, for cooling a cryogenic power cable around London; the results showed possibilities for advances but it failed to gain support.

Perhaps this question could be examined again if we ever have a "liquid hydrogen economy", i.e., by the use of liquid hydrogen for energy transmission.

OXIDE SUPERCONDUCTOR COILS - PRESENT SUCCESSES, FUTURE CHALLENGES

Carl J. Russo
American Superconductor Corp
149 Grove Street
Watertown, Massachusetts USA 02172-2828
telephone 617-923-1122

Abstract

Coils are a fundamental building block for large-scale applications. Successful application of oxide super-conductor coils in these applications requires: high quality, superconducting-oxide wire forms; an insulation technology compatible with processing; a mandrel material compatible with processing and operational requirements; a compatible, high-strength, mechanical-support material; ability to maintain superconducting properties while being strained; and compatibility with other subsystems which are part of the application.

The present state of coil development will be dis-cussed in terms of several applications. Predictions for the future of oxide superconductor coils will be examined in terms of several figures of merit and an-ticipated operational criteria.

Introduction

Coil sets are normally built to detect or create mag-netic fields. Two general classes of air-core, coil sets are important in most applications. These classes are coil sets with the magnetic field: parallel to the axis of symmetry (solenoids, toroids, and flat spirals); and perpendicular to the axis of symmetry (racetrack and saddle field coils). The combination of these coil sets can be used to create other magnetic field geometries.

Properties of the Superconductor/Normal Metal Composite and their Relationship to Applications

In the companion wire paper, "Success Criteria for Oxide Superconductor Wires - Measuring the Present, Predicting the Future," the issues related to making good quality wires for a variety of applica-tions are discussed. For a majority of power applica-tions, the combination of a superconductor and a normal-metal composite will give optimum results, as it does for the existing metallic superconductors operating at liquid helium temperatures[1] However, for some signal coil applications, pure oxide superconductor may be a more appropriate approach.

Many of the reasons for using metal composites with oxide superconductors and with metal-based super-conductors are the same: cryostability, normal-zone propagation, ductility etc. A few, including thermo-mechanical properties at higher operating temperatures, are different. The rich literature which has evolved for the use of metal-based superconductors is a useful guide for applications involving oxide superconductors.

Critical Current Density

The critical current performance of the supercon-ductor often drives a given application. The values of the critical current are based on the total cross-section of the active filaments, including the normal conductor between the filaments but excluding the outer sheaths and insulation. This has been normal practice in the low-temperature superconductors industry.

To date, bulk, polycrystalline, $YBa_2Cu_3O_{2-x}$ (YBCO) coils, have had poor performance in magnetic fields. Critical current typically drops an order of magnitude in fields of 10-20 gauss range, independent of temperature, and the critical current usually drops to unacceptably low values when the fields reach 100 gauss.

Bulk, polycrystalline $Bi_2Sr_2CaCu_2O_{8-x}$ (BSCCO) with currents higher than 10,000 A-cm^{-2} in fields higher than 20 tesla enable the production of very high field magnets.

The Importance of Wire Length

While critical current is an important operating parameter for coils, the ability to economically make long lengths of wire with high critical currents is a better measure of performance. Therefore the $J_c \times L$ criteria is usually more useful when considering applications where reasonable lengths of wire are required. While melt-textured and single-crystal materials have provided the best J_c performance to date, they are usually not of practical value for coil applications due to limitations on length which can be made.

AC Power Applications

Currently, $J \times L \approx 10^6$ A-cm^{-1} is achievable at 77 K in low magnetic fields with AC loss substantially better than copper operating at the same temperature $J \times L$ may increase as fast as a few orders of magnitude per year. Therefore, low-field, commercial AC applica-tions should have oxide superconductor wire avail-able for use in the early to mid 1990s. Figure 1 shows the evolution of these low-field applications

BSCCO materials have sufficient properties for oper-ation even at 77K. In carefully chosen, low-field

applications, YBCO has adequate properties in modest magnetic fields to be useful The lack of a solution to the YBCO, weak-link problem does not stop the development of AC applications. If the weak-link problem is solved earlier than the late 1990s in bulk-processed, YBCO material, then progress in AC applications will accelerate.

The low fields associated with most AC applications allow the oxide ceramics to operate with good J_cs at temperatures in the 50-80K range. The low, stored energy and low, magneto-mechanical stresses in low-field AC applications remove several of the wire-formation and coil- design challenges apparent in high-field applications. These challenges include cryostability and burnout protection.

All superconductors operating in an alternating current environment have losses. Higher operating temperature makes heat removal and thermal stability in the presence of AC losses easier to control. At present, AC losses in unoptimized materials are approximately an order of magnitude better than high-purity copper operating at the same temperature.

Figure 1. Evolution of high-T_C superconductors for low field AC applications
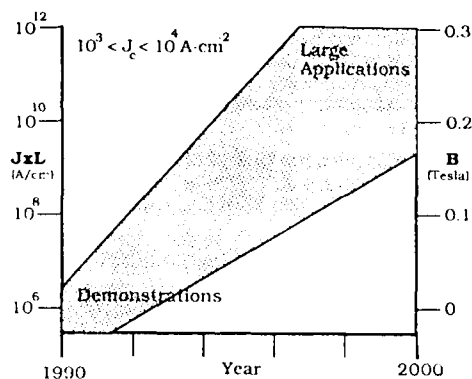
Process Control

The issue of process control is important in long-length applications. The wire industry in general and the superconducting wire industry in particular have been limited in their abilities to consistently produce high quality materials with tight control over all important specifications. These specifications include: conductor and insulation, cross-section uniformity, filament sausaging, mechanical properties, normal state resistivity over the length, and losses under AC and high-field conditions. Typically, the wire manufacturer measures the parameters of a conductor, wire, or cable at the beginning and end of the run and assumes that the process has sufficient control to give similar properties along the entire length.

Few high-quality, in-situ process control tools are available to the superconductor industry at present. This lack of process control tools limits the ability to make large coils without joints and offer standardized products which can be specified across the industry. The metal superconductor industry is beginning to reach these goals in the fabrication of materials used for the magnetic resonance imaging (MRI) magnet business when the materials are NbTi. However, the industry is still plagued by the need to select material for applications where high performance is required.

Operational Requirements

Oxide superconductor wire will have several requirements which are similar to copper and metal superconductor wire. These will include compatibility with processing as well as uniformity of electrical and mechanical properties along the entire useful length of material.

Processing Compatibility

Compatibility with subsequent processing has been a major issue with all wire forms. In the silver- and tin-plated wire industry, for example, plating nonuniformities and porosity are exacerbated when the wire must be insulated with very thin, high-temperature polymer insulation. This processing is done at elevated temperatures, is often sufficient to cause the interdiffusion of the plating and base wire metals, and is often accompanied by the release of trapped gases due to poor plating.

Similarly, Nb_3Sn must have all of its mechanical processing completed before conversion to superconducting form. When a wind-and-react approach is used, the wire needs an insulation technology compatible with the winding of the material into a magnet and subsequent firing at temperatures beyond the range of polymer insulations. When a react-and-wind approach is used, the mechanical properties of the superconductor must be sufficient to survive the winding process. As a result, Nb_3Sn and related compounds are only used in situations where NbTi cannot be used. The resulting Nb_3Sn magnets are substantially more expensive than NbTi magnets mostly due to process compatibility problems.

Oxide superconductors will be no different in requiring compatibility with subsequent processing. For materials which require a wind-and-react approach, mineral insulations like $Y_2 Ba Cu O_5$ 2-1-1 are being developed for direct contact with YBCO materials. To date, polymer insulations in contact with oxides containing alkali earth materials such as Sr, Ba, or Ca do not show promise of long-term lifetimes. Materials which are sheathed in silver are much less problematic in that they can be coated with conventional polymer insulations.

Mechanical Properties

Once the basic issues of sufficient critical current are addressed, most of the issues with coils will be related to their mechanical and thermal properties. In high-field coils, the magnetic stresses are close to the limits of high-strength steels. In the simple case of solenoids, the stress is proportional to B^2r. Therefore, producing high-field magnets with large bores will be an extremely difficult problem. Since the oxide superconductors do not appear to have high mechanical strength, some form of strengthening member needs to be introduced. This strengthening member needs to have a thermal expansion match close to that of the oxide superconductor and must be compatible with the processing of the superconductor if wind-and-react processing is to be used. The mechanical support of superconducting windings in epoxy-based materials is a conventional process for metal superconductors. It is expected that oxide superconductors will build on this existing expertise.

Systems Issues for Low Field or Signal Coils

Low-field coils have relatively modest mechanical property requirements, and in small sizes they will require a relatively small amount of material. Therefore, these coils will be the first to see application with oxide superconductors. A few of these coils will be used in DC applications. In this case the J_c properties in field will be the only other issue to tackle. Most small coils will be used in signal and AC applications where the AC properties, residual noise, and residual resistance under field conditions will be important considerations.

AC Properties

Since most of the oxide wires used in coil applications will be metal, superconducting-oxide composites of one form or another, they will have loss properties in AC fields similar to metal superconductors. There is rich literature concerning the AC properties behavior of metal superconductors in the presence of magnetic field.

If normal metal is used in small quantities for improved mechanical properties, then interconnectivity of the normal metal is avoided and eddy current losses at higher frequencies can be reduced. Unoptimized wires have demonstrated over an order of magnitude improvement in 50-100 Hz AC losses at 77K compared to silver operating at 77K. Further progress is expected as AC loss issues are further addressed.

Residual Resistance

There is usually some residual resistivity in superconductors. This is especially the case under AC conditions. Simple pinning models show that in a field reversal, the flux must be depinned to change direction under the influence of the alternating field.

This depinning is a nonconservative event and leads to thermal losses.

The residual resistance under low field conditions is typically very low at DC, and is often connected with the losses in the normal metal under AC conditions. For signal applications the residual resistance is a major source of noise.

Noise

Noise is a major issue for signal coils like SQUID coupler coils. Since these must be closed, superconducting loops which often operate in persistent mode, the sources of resistance must be identified. Typically, there is some resistance due to the wire itself, and a large component of loss is due to the joints as well. The ability to make high quality superconducting joints will be important for low-noise applications. A chart of applications as a function of noise level and residual resistance is shown in figure 2. Note that ε = noise energy per bandwidth, and R = AC surface resistance.

Figure 2. Evolution of bulk oxide superconductors for signal applications
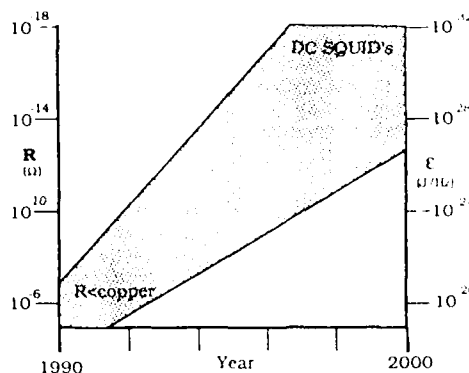
At present, the residual resistance in oxide superconductors[2] even at DC is too high for use in persistent-mode coils. As the material becomes better pinned, persistent-mode applications will evolve.

Systems Issues for High Field Coils

If sufficient critical current in high field can be obtained in a superconductor, then the issues involved in building high-field coils are nearly totally thermal and mechanical in nature. The fields and the resulting forces in a high-field, high-T_c superconductor magnet are the same as in a low-T_c superconductor material. Magnet stability at 4K is more difficult than at higher temperatures, but magnet protection is more difficult at elevated temperatures than at 4K

Figure 3 Time evolution of high field applications at low temperatures using oxide superconductors.
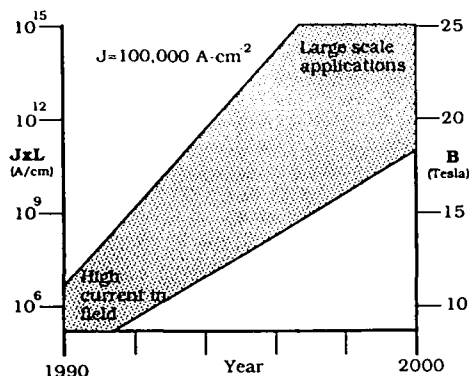
Stability

If any microscopic motion of the conductors occurs at high fields, then a significant amount of energy is released. A motion of a single, metal superconductor wire by 0.0001" can be sufficient to produce enough heat locally to drive the magnet normal at 4K. Since the heat capacity rises quickly above 4K, it is much easier to keep these small perturbations from driving the magnet unstable at elevated temperatures.

Protection

If a perturbation in the wire causes the magnet instability and allows the formation of a normal zone, then the normal zone must either propagate quickly through the magnet (quench) or shrink fast enough so that the stored energy in the magnet cannot burnout the normal zone. Studies by Iwasa[3] indicated that the thermal properties of the coil winding tend to dominate normal zone propagation. Based on these findings, the optimum operating temperature for an adiabatic, oxide superconductor magnet appears to be 20-40K.

Driven vs Persistent-Mode

Superconducting magnets which do not require frequent changes in field are often run in persistent-mode. For magnetic resonance imaging magnets at liquid helium temperature, this is often done with retractable current leads so that thermal loss can be reduced. Magnets which must change field frequently keep the leads firmly connected to the magnet and sustain a higher liquid helium loss. Lead loss is usually a major source of helium boil-off in low-T_c superconductor magnets. Lead loss is a particularly serious problem in large, energy storage magnets.

Two properties of the superconductor determine if the material can be run in persistent mode: the index and the residual resistance.

The index represents the exponent n in the equation

$$V = V_c[I/I_c]^n$$

where V is the voltage and I the current flowing through the coil. This model adequately describes the I-V characteristic of most superconductors in the transition from superconductor to normal conductor. The measurement is performed at operating magnetic field. The subscripted variables are measured at the critical current with the given criteria. The residual resistance, R=V/I, and the inductance of the coil determine the time constant for a magnet in persistent mode. If the index of the wire is low, then only a relatively small fraction of the current density can be used to keep an acceptable value of residual resistance. Values of n=30 are desirable for magnets operating in persistent-mode since nearly all of the critical current can be used before the resistance begins to rise.

The residual resistance is directly related to the index in the transition region since

$$R = V/I = [V_c/I] [I/I_c]^n$$

Present oxide superconductor materials have residual resistances which are too high to allow most magnets to run in persistent-mode for acceptable times. This problem will be solved as flux pinning methods are improved for oxide superconductors.

$J_c V = Br^2$

The time frame for the construction of large solenoidal magnets will be related to the volume of superconductor which can be produced with a specific critical current. For a specific wire size, $J_c V = Br^2$ is closely related to JxL. It also points out that the production of high magnetic fields over large areas requires very large quantities of material with good properties. Therefore, based on the development of adequate production capacity for high quality material, large-bore, high-field magnets will take the longest to develop. This is why applications like SMES and MHD ship propulsion are placed near the end of the decade in figure 3.

Maximum vs Average Field

A great deal of effort has been expended in the existing superconducting magnet community to minimize the amount of magnetic field in the windings of high-field magnets. Part of the reason is related to the decrease in J_c as B increases, and part is related to increase in mechanical stress due to JxB effects. Minimizing the field in the coil usually leads to magnet designs where the maximum-to-average

field ratio in the magnet is as close to one as possible. This trend will continue for oxide superconductor magnets.

Joints

High quality, superconducting joints are required for any viable, superconducting wire form. The use of a silver-bearing microcomposites allows the formation of superconducting joints which can maintain high critical currents. Normal, metal-to-oxide superconductor joints are also readily made in silver-bearing microcomposites.

Insulation Technology

Metal-sheathed, oxide superconductor wire can use conventional polymer insulation as long as the material can be reacted before winding. The ability of microcomposites to remain superconducting with reasonable strains is demonstrated in the companion paper "Success Criteria for Oxide Superconductor Wires - Measuring the Present, Predicting the Future."

In cases where small radius coils need to be constructed with large diameter wire, a wind-and-react technique, similar to the one used for Nb3Sn, can be applied. This requires a high-temperature, insulation technology which is either compatible with the sheathing material or the oxide superconductor itself if no sheathing material is used.

Mechanical Considerations

Once a superconducting wire technology is in hand, most of the constraints on a magnet design are mechanical and thermal in nature. These constraints include the support materials for the wire, the magneto-mechanical stresses due to the fields generated in the coil, and the ability to properly cool the coil.

Support Materials

Three types of support materials are required: mandrels for winding the coil, spacers for cryogen passages, and an epoxy-like material for bonding together the wires and preventing motion. All of these materials must be able to withstand the thermal cycling characteristic of cryogenic operation and all must have thermal expansion coefficients reasonably well matched to the superconducting wire.

B^2r = radial stress in solenoids

In large magnets operating at high fields, the induced stresses require a substantial amount of support material to prevent the deformation of the superconducting wire. Now that BSCCO will allow the production of high-field magnets, the next challenge will be to manufacture high-field (~20 tesla) solenoid magnets with reasonably large bores. In solenoidal designs B^2r~radial stress, and the magnet tends to compress axially

Cryogenics

The advent of oxide superconductors has rekindled thoughts of practical devices at temperatures higher than liquid helium temperatures. Most researchers think of operating coils made from these materials at one of the liquid cryogen operating temperatures. for example liquid nitrogen at 77K, liquid neon at 27K, or liquid hydrogen at 21K.

The range of temperatures available to liquids and gases used as heat transfer media is shown in figure 4. Liquids have a limited operating range when the partial pressure above the liquid is changed either by pumping or by adding other gases such as neon Gas mixtures can also be used for improved heat transfer characteristics, especially at high pressures

Figure 4. Closed Cycle refrigeration with gases as the heat transfer medium
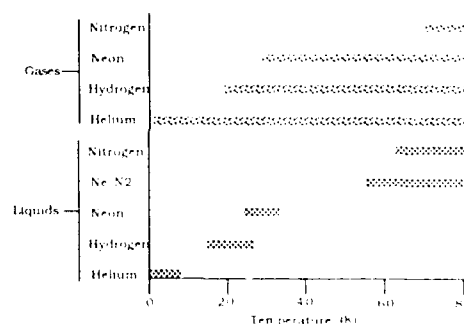
While these cryogenic liquids are convenient for laboratory experiments, these fixed temperatures may stifle creative solutions using closed-cycle refrigeration with the new oxide superconductors. Storage and shipment of large quantities of cryogenic fluids is also costly and inconvenient for commercial applications.

Freon-based refrigerators have replaced ice as the commercial cooling method of choice. It is expected that cryocoolers, which can be integrated with superconducting applications, will replace liquid cryogens in commercial applications. Combining cryocoolers with oxide superconductors optimizes the systems performance by selecting the best operating temperature rather than limiting systems performance by selecting one of a few, liquid operating temperatures.

A LIQUID NITROGEN COOLED SUPERCONDUCTIVE ELECTRON BEAM FOCUSING SYSTEM FOR IMPROVED PERFORMANCE ECM HELIX TRAVELING WAVE TUBES

by

M.C.Green
Varian Associates, Inc.
611 Hansen Way
Palo Alto, CA 94303-0883
United States

ABSTRACT

In avionics, the focus of attention in recent years has been upon the development of solid state devices for low-level signal processing. Device development based upon the new high-temperature superconductors has mirrored this, with concentration upon thin film systems as a basis for the eventual fabrication of delay lines, resonators and the like. However, large numbers of avionics systems, particularly in the electronic countermeasures (ECM) area, employ traveling wave tubes (TWTs) as final power amplifiers.

Broad-band ECM helix TWTs utilizing periodic permanent magnet (PPM) focusing systems are particularly suitable for the application of superconductive focusing systems, since despite the relatively low magnetic fields employed along the electron beam axis in a typical PPM stack, the PPM configuration is limited to less-than-optimum axial fields by the local saturation of polepiece material between the adjacent ring magnets of the stack. In a typical I-J band ECM helix TWT, the axial field does not exceed 2.5 KG despite the use of exotic polepiece materials, which in turn means a lower-than-optimum perveance electron beam. This impacts adversely upon TWT bandwidth, stability and gain.

The relatively low field requirement for this application means that a solenoidal field generated by a high-temperature super-conductor flux trap is potentially practical with today's level of materials development.

INTRODUCTION

In the avionics world, as in the world of electronics in general, the majority of research effort and attention is directed toward the development of solid state devices. This has been reflected in the proportion of effort devoted to thin film device development in the area of high-temperature superconductor (HTS) material, with the intent to produce delay lines, resonators, and eventually mixers for low-level signal processing. HTS-based devices possess the potential for lower loss and disperson, higher Q, and lower noise coupled with higher frequency capability when compared to devices using conventional conductor materials.

The concentration on solid state components tends to ignore the fact that at higher power levels and frequencies in the microwave and millimeter-wave bands fundamental physical constraints (for example, the electric field gradients that can be supported in semiconductor structures) set limits to the power output of solid state devices. The area of high-power microwave sources and amplifiers is dominated by linear beam electron tubes such as traveling wave tubes and klystrons, and will remain so for the foreseeable future. These devices too can benefit in performance capability from the employment of high-temperature superconductors in portions of their structures where the limitations of normal conductors currently constrain their performance.

In avionics systems, helix traveling wave tubes are widely employed as final power amplifiers. In the electronic countermeasures area, they are used in both radars and jammers. Helix traveling wave tubes are broad-band, (1-3 octave) low-noise, medium-power (50 watts to a few kilowatts) devices.

The key component of a helix TWT is a helical microwave transmission line wrapped closely around a small-diameter cylindrical electron beam (Fig. 1). The electron gun typically operates at around 10 KV. The pitch of the helix is chosen so that the component of velocity of the rf wave along the electron beam axis is approximately matched to the electron velocity. Under these conditions, microwave energy can be transferred from the helix to the electron beam, and vice versa. The coupling is via the electric field which exists between the turns of the helix. This interacts with the electron beam to cause velocity modulation of the electrons. Under the correct conditions, this process enables transfer of the kinetic energy of the electrons to augment the microwave energy on the helix, and we have a microwave amplifier. Since the helix is a nonresonant transmission line, the TWT is a broad-band amplifier. This is particularly useful in an ECM situation.
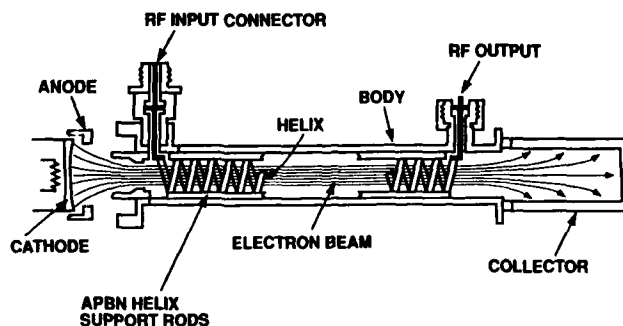
Fig. 1   Helix traveling wave tube structure.

For efficient operation of the TWT, the electron beam must pass as closely as possible to the inner surface of the helix without actually impacting upon it. The electron beam has to be confined magnetically to counteract radial expansion, due to the mutual space charge repulsion of the electrons; in airborne TWTs, an engineering tradeoff exists between energy consumed to confine the electron beam and performance capability as a microwave amplifier.

HELIX TWT FOCUSING TECHNIQUES

The most effective focusing is achieved by wrapping a solenoid around the body of the TWT and rigidly confining the electron beam. However, the weight of the solenoid is typically ten times the weight of the TWT itself, and it requires more than a kilowatt of C.W. electrical power to maintain the magnetic field, All of this power is dissipated as heat. In modern military aircraft, the extra weight, prime power drain and cooling load associated with the focusing solenoid carries an unacceptable performance penalty. As a result, the vast majority of airborne TWTs use periodic permanent magnet focusing systems.

A PPM stack (Fig. 2) consists of a series of ring magnets sandwiched between polepiece disks. The magnetic field directions alternate from magnet to magnet. High-energy product materials such as $SmCo_5$ and Sm_2Co_{17} are used in the magnets to minimize size and weight.
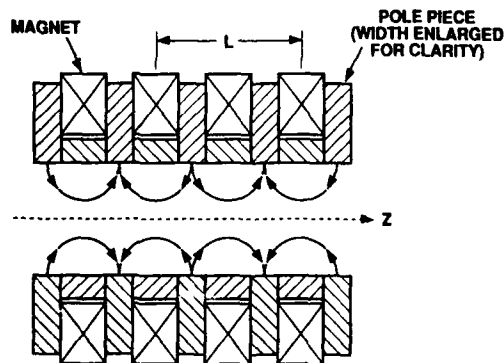
Fig. 2   Magnetic field components in a PPM stack.

PPM stacks suffer from three constraints in terms of electron beam focusing efficiency. First, the alternating magnetic fields of the magnetic cells provide a periodic focusing action strongest at the cell center. Thus, the electron beam periodically diverges and reconverges in a rippling action. This reduces the helix filling factor that can be employed, and hence lowers the coupling efficiency between the electron beam and the rf circuit. Second, except for low current, low microperveance

electron beams, confined flow focusing in which the magnetic field lines thread through the cathode and match the electron trajectories cannot be employed with PPM focusing systems. This is because the magnetic field reversals between PPM cells would impart too much rotational energy to the electron beam in alternate cells, leading to instabilities if there were B-field threading the cathode.

Third, despite the high-energy product magnet materials available, the r.m.s. magnetic field that can be attained on the beam axis with a PPM stack is lower than desired. This arises because the polepieces between the magnets in the PPM stack must be kept short in order to minimize the overall magnetic cell length, L (see Fig. 2). If L becomes comparable to the plasma wavelength of the beam λ_p, then severe beam oscillations can occur. Design guidelines for stability require that

$$\frac{\lambda_p}{L} = 2.5 .$$

In a typical I-J band helix TWT used in large numbers in airborne ECM systems, the rms axial magnetic field does not exceed 2.5 KG due to polepiece saturation. This is in spite of the use of exotic magnetic materials such as vanadium permendur for the polepieces. (The field within the polepiece itself can exceed 20 KG when vanadium permendur is used.)

The lower-than-optimum axial field impacts adversely upon the beam filling factor that can be achieved, and hence upon rf efficiency, bandwidth and stability against backward wave oscillations. Additionally, the lack of stiffness of the beam results in excessive helix interception and body current under conditions of high rf drive. This further limits the maximum permissible power output of the TWT.

The adverse effects of lack of sufficient axial magnetic focusing field become more severe at higher operating frequencies. PPM focusing constraints are a primary performance limiter for millimeter-wave helix TWTs. Herein lies the potential for the application of a superconducting solenoid, which can be conceptually regarded as a "permanent electro-magnet", to TWT focusing. Figure 3 illustrates the improved electron beam quality obtainable with a solenoidal focusing field. Obviously, the use of low-temperature superconductors in military airplanes, which are liable to be deployed anywhere in the world, is not practical because of logistical difficulties in supplying liquid helium in the field. But the recent advent of high-temperature superconductors capable of operating at liquid nitrogen temperature changes the picture completely. Liquid oxygen is already a standard consumable in modern military aircraft, and both nitrogen and oxygen are readily liquified and available worldwide.

PPM FOCUSED BEAM

**<50% Helix Filling Factor, Beam Is
Soft And Scalloping**

SOLENOID FOCUSED BEAM

**67% Helix Filling Factor, Beam Is Stiff
And Laminar, Can Use Hollow Beam**
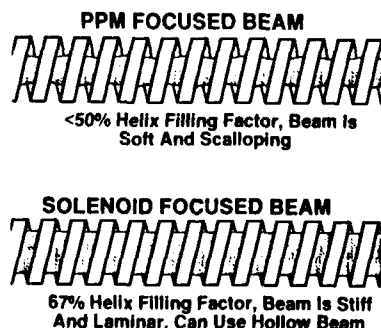
Fig. 3   Beam focusing comparison.

When a superconducting cylinder at a temperature above its transition temperature is immersed in a solenoidal field generated by an external magnet, the field will thread through the material and the bore of the cylinder with only minor perturbations. When the super-conductor is cooled through its transition temperature, flux will be expelled from the body of the cylinder into the bore and the surrounding volume. For a Type I super-conductor such as lead, the flux exclusion from the material will theoretically be complete below the critical magnetic field. For a Type II superconductor such as NbTi (and including all the new high-temperature superconductor materials), the expulsion of flux is only partial. This is because it is energetically favorable for Type II materials to exist in the "mixed state" with single quanta of magnetic flux (fluxoids) threading through the super conducting material in tubular volumes of normal material of negligible cross-sectional area.
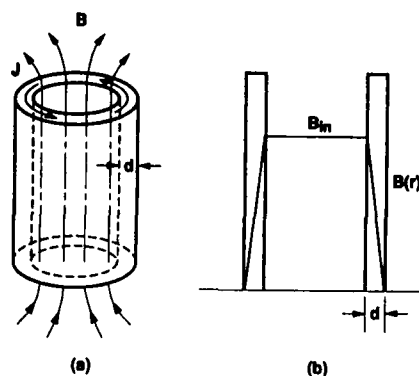
Fig. 4   Flux trapped in hollow cylinder of Type II superconductor: (a) sketch of overall geometry;
(b) local flux-density profile.

If the external source of magnetic field is now removed, a circulating current is induced in the
cylinder, which opposes the change in the flux threading through the bore.   This process would also
occur if the cylinder were made of normal conducting materials such as copper, but in this case the
induced current would rapidly die away due to resistive losses.   In the superconductor, the induced
transport current around the cylinder is persistent and lossless, and the opposition to the change in
flux is therefore 100% efficient.   The flux threading the bore is maintained indefinitely as long as the
transport current continues to flow and can be said to be trapped within the superconducting
cylindrical bore.   The procedure   just described   for   inducing   a   transport   current   in   the
superconductor is often described as "charging" the flux trap.   It is one of a number of methods that
may be employed for this purpose.

Considering the superconducting cylinder as a solenoid, the field that can be trapped on axis is
a function of two things: the magnitude of the transport current that can be supported, and the
maximum magnetic field gradient that can be maintained through the cylindrical wall (see Fig. 4b).

FLUX MOTION IN TYPE II SUPERCONDUCTORS

One of the most difficult materials engineering problems with existing low-temperature
Type-II superconductors in practical solenoids has been to ensure that fluxoids penetrating the
mixed state material do not move through the body of the material during high-current, high-field
operation.   Returning to the idealized cylindrical flux trap of Fig. 4, we see that when a transport
current J flows around the cylinder in the y direction, the fluxoids penetrating the material in the
z direction along the cylinder axis experience a Lorentz force, which pushes them in a direction
transverse to the current flow and out of the wall of the cylinder.

Maxwell's equations are valid within the body of a superconducting material, and the Maxwell
equation relating the current density to the curl of the field may be written:

$$\mathrm{Curl}\ H \ = \ 4\pi\,\frac{J}{c}$$

where J represents the externally-imposed transport current.

If the wall thickness of the cylinder d is small compared to the radius R, we may reduce the
problem to a one-dimensional one by neglecting the curvature.   In this case, the equation may be
rewritten

$$\frac{dH}{dx} \ = \ -4\pi\,\frac{J}{c}$$

with H in the z direction and J in the y direction.   There is an outward force on each fluxoid of

$$f \ = \ \frac{\phi o}{4\pi}\left|\frac{dH}{dx}\right|$$

per unit length. Summed over all fluxoids, this gives a force per unit volume of

$$\alpha = \frac{B}{4\pi}\left|\frac{dH}{dx}\right|$$

Unless this force α is balanced by some other force, we must expect the fluxoids to move outward through the wall, each carrying one quantum of flux with it, reducing the trapped flux inside the cylinder and resulting in a corresponding decrease in J. Eventually, the internal field in the ring falls below Hc1 and the material is no longer in the mixed state.

The motion of the fluxoids transverse to the transport current generates an electric field which is parallel to J. This manifests itself as a resistive voltage, power is dissipated and local heating of the superconductor occurs.

Summing up, the motion of the fluxoids makes the superconductor appear to have resistance. The persistent current decays, the trapped field diminishes and energy is dissipated in the material.

FLUX PINNING

In practical engineering superconductors, the motion of the fluxoids is prevented by trapping at pinning centers. These are inhomogeneities in the material which cause a large local variation in surface energy. They can be voids, dislocations, impurity segregations, etc., and they furnish potential wells in which it is energetically favorable for fluxoids or bundles of fluxoids to reside. The stabilization of the fluxoids at pinning centers provides an effective pinning force which resists the Lorentz force α up to some critical value of magnetic field and pins the fluxoids so that they remain stationary up to large values of α.

In HTS materials at 77K, the lattice vibrational energy is much higher than in LTS materials at 4.2K. Hence fluxoids are more readily activated thermally to jump from one pinning point to another in HTS material. Considerable development effort is currently being directed toward improving the flux pinning properties of HTS materials by preparing material with pinning centers having deeper potential energy wells.

APPROACHES TO FLUX TRAP

For a solenoidal magnetic focusing field for a helix TWT, only axial magnetic field components are required in the body of the tube. Hence only azimuthal currents are required to flow in the cylindrical flux trap. Thus the flux trap can be built up from a stack of separate rings or disks without compromising performance.

The magnetic field requirement on axis is quite modest. 600 Gauss would suffice for a medium-power E-F band tube and 2.5 KG for an I-J band ECM TWT. Ignoring end effects on the flux trap, the former field requirement could be met by a transport current J of 600 amperes per centimeter length of the flux trap. If the flux trap wall thickness d is 1 centimeter, the HTS material must be able to support a transport current density J_c of 600 A/cm^2 in the self magnetic field at 77K. This is a moderate requirement and is within a factor of three of the present performance capability of magnetically-oriented bulk YBCO immersed in a magnetic field of 1 Tesla [1]. Epitaxial thin films of YBCO can support transport current densities up to four orders of magnitude higher than this, which would greatly reduce the amount of superconductor needed . However, in the case of thin films, there are problems in achieving good film properties over a sufficiently large area for a macroscopic application like a flux trap. There are also issues of substrate cost and availability.

PROGRESS AND PLANS

Work on the preparation and characterization of YBCO flux trap rings for microwave tube focusing was initiated more than two years ago by Varian [2]. Present activity is being expanded to encompass a thin film based approach with the demonstration of a HTS flux trap for an E-F band helix TWT targeted for the end of 1991.

CONCLUSIONS

Many present-day helix TWTs which employ PPM focusing systems because of weight and electric power consumption constraints are limited in their rf performance by polepiece saturation in the PPM stack. This imposes an upper limit on the axial focusing field that can be attained, which in

turn means a lower-than-optimum perveance electron beam. This impacts adversely upon TWT bandwidth, stability and gain. The lack of stiffness in the beam focusing forces the use of a relatively small filling factor, which lowers the efficiency of the tube. The high body current under large-signal conditions limits the maximum power that can be achieved.

In addition to their maximum field limitations, PPM focusing systems generally cannot employ confined-flow focusing, in which the focusing field threads through the cathode in the electron gun with the flux tubes conforming optimally to the converging electron trajectories. In a PPM focusing system, the cathode is generally in a field-free region; this results in beam nonlaminarity as the electrostatic electron trajectories interact with the magnetic flux when the beam enters the first PPM cell. This in turn sets a limit to the area convergence which can be used in the gun (a maximum of around 20:1) for acceptable beam-entry conditions to the PPM stack. This low-area convergence increases the emission current density (amperes per cm^2) drawn from the cathode and results in a more highly stressed cathode with shorter operating life.

Because of their modest axial field requirement and small diameter, helix traveling wave tubes present an unusually favorable potential application where high-temperature conductors might be employed to furnish the focusing field.

The capability to fabricate HTS wire is not yet sufficiently advanced to permit the construction of a wire-wound superconducting solenoid (operating at 77K) able to generate the required magnetic field. However, the J_c properties of both magnetically-oriented bulk and epitaxial thin film HTS material indicate that fabrication of a cylindrical flux trap capable of maintaining an suitable solenoidal field is possible with only a small advance in the present state of the art.

The ability to operate a helix TWT with a solenoidal magnetic field and with confined flow focusing in the electron gun should yield substantial improvements in rf performance. The zero electric power consumption and heat dissipation of the HTS flux trap when charged at 77K removes one of the primary constraints which have hitherto prevented the use of conventional copper-wound solenoids for TWT focusing in airborne applications.

References

1.   R. H. Arendt, A. R. Gaddipati, M. F. Garbauskas, E. L. Hall, H. R. Hart, Jr., K. W. Lay, J. D. Livingston, F. E. Luborsky and L. L. Schilling, Mat. Res. Soc. Symp. Proc., **99**, 203 (1988).

2.   C. A. Shiffman, S. Sridar and G. E. Thomas, IEDM Tech. Digest, p. 530 (1988).

SYNTHESIS AND CHARACTERIZATION OF HIGH TEMPERATURE SUPERCONDUCTOR MATERIALS

W. A. Ferrando, A. P. Divecha, S. D. Karmarkar, A. N. Mansour, and P. W. Hesse
Research and Technology Department
Naval Surface Warfare Center
Silver Spring, MD 20903-5000
United States

SUMMARY

High temperature superconductors are oxides and, therefore, inherently brittle. A process involving thermal decomposition of silver nitrate in the presence of $YBa_2Cu_3O_7$ (123) powder has been developed which shows promise for synthesis of fine diameter wires. The silver deposits uniformly on the 123 powder as indicated by optical and scanning electron microscopy. The composite powder can be formed into rods (.4 mm diameter) via drawing and swaging through conical converging dies. Finer diameter wires (.1 mm) have been produced by slurry extrusion of the composite powder in a polymeric vehicle. The current carrying capacity, J_c, continues to rise due to better understanding of the Ag/superconductor interface. J_c values of a typical wire has now reached 400 A/cm^2 at 77 K and zero magnetic field, with a superconducting transition temperature of 93 K. In addition, the $AgNO_3$ decomposition process can be employed with fine HTS powder and ethylene glycol as a suitable vehicle to produce an adherent, stable high temperature superconducting paint. The composition, chemistry, and uniformity of dispersion of Ag was investigated by X-ray diffraction, X-ray photoelectron spectroscopy, and scanning electron microscopy.

INTRODUCTION

The recent discovery of high temperature superconductors (HTS) with critical temperature (T_c) exceeding 90 K[1-7] has inspired many researchers to develop generic processes for the production of an HTS material suitable for potential applications requiring high current carrying capacities. The most technologically desirable forms of a superconducting material are a wire (with a round or rectangular cross section which can be conveniently made into a coil), a ribbon, or a thin film of superconducting paint. Being oxides, these materials are inherently brittle, and thus their conversion to wire form presents a real challenge. The most advanced existing techniques are expected to be inadequate to convert the HTS material into wires or coilable forms needed for large scale military and industrial applications. Highly innovative and entirely new processes will be needed to induce ductility or formability in these oxides.

During the past several years, many efforts have focused attention on this issue with varying degrees of success.[8-15] Most of the approaches, have been successful to a reasonable extent. These include dispersion of HTS particles in metallic matrices such as silver[8,9] and gold,[10] diffusion bonding in carbon fiber reinforced tin-superconductor composite,[11] tape casting,[12] metal cladding,[13] metal core composites,[14] and melt-processible superconductors.[14,15]

At NSWC, initially, we have prepared HTS wires via mechanical mixing of fine metallic Ag powder with HTS powder and also by the method rapid solidification of metallic precursors (Yb, Ba, and Cu with Ag).[16] In both cases, it was possible to attain zero resistance, but with negligible current carrying capacity. To date, NSWC's most promising approach entails thermal decomposition of $AgNO_3$ with HTS powder. We have discovered that silver nitrate, with its low melting point (222 °C) and decomposition temperature (444 °C) permits achievement of a relatively homogeneous aggregates of the two components for further processing into a coilable superconducting composite of high quality. The silver coated HTS powder mass can be converted into a wire via swaging, drawing, and extrusion. The silver matrix is utilized to impart ductility or formability to the HTS oxide. Furthermore, silver is a preferred matrix because it does not react with the superconductor even above its melting point (956 °C).[8,9,17] This approach because of its versatility, simplicity, and scale-up potential, holds potential for future implementation. Equally importantly, the approach is generic and may be applicable to all present oxide superconductors and those yet to be invented. It is noteworthy that the $AgNO_3$ process has the unique feature that the silver coating provides environmental protection unlike almost all other processes and products which degrade upon exposure to atmospheric moisture and thermal cycling to liquid nitrogen temperature. NSWC's product's properties remain stable even after repeated thermal cycling and months of ambient exposure in a laboratory atmosphere.

While the desirability of producing high temperature superconducting materials in wire or ribbon form is undeniable, the performance of a substantial set of electronic devices can be improved significantly if the superconducting materials are made available in the form of a thick film or paint. The $AgNO_3$ process, with slight modification, can produce a thick film of a superconducting paint on flat and curved surfaces. Paint coatings under discussion here fall within the range of about 10-100 μm thickness, compared with coatings of only several microns which are normally produced by sputtering, CVD and the like for electronic device applications.[18] Potential applications of thick film coatings include infrared detectors, magnetic field sensors, magnetic shielding and microwave cavities.

This report describes in detail the synthesis of superconducting wire and superconducting paint, and includes a summary of surface and bulk analyses made using XRD, XPS, and SEM to determine the critical factors controlling the current carrying capacity. Major emphasis is placed on $YBa_2Cu_3O_7$ (123) due to its commercial availability.

EXPERIMENTAL PROCEDURE

Sample Preparation:

The superconducting powder of YBa_2Cu_3O (thereafter referred to as 123), initially, was obtained for the most part from W.R. Grace Corp. (Grace Specialty 778 Chemicals, Davison Chemical Division, Dept. TR, P. O. Box 2117, Baltimore, MD 21203) and, as the program progressed, from two other laboratories, Argonne National Laboratory (Materials and Components Technology Division, Argonne, IL 60439) and Ceramic Process Systems Corp. (155 Fortune Blvd., Milford, MA 01757). Research grade silver nitrate reagent was procured from Fisher Scientific Company (Chemical Manufacturing Division, Fair Lawn, New Jersey 07410).

The Ag/HTS composite powder was prepared (Figure 1) by mixing appropriate amounts of $AgNO_3$ and HTS powder (123 was used in this case, but another HTS compound can be substituted) in a mortar and pestle, to produce approximately 15 w/o Ag concentration after decomposition. For low Ag concentration (i.e., less than 5 w/o Ag), it is found that sufficient amount of ethylene glycol must be added to the $AgNO_3$ and 123 mixture to increase the wettability and, thus, to produce a uniform dispersion of the Ag coating in the composite powder. The ethylene glycol is inert to the 123 compound and dissolves the $AgNO_3$, spreading it uniformly through the entire mass of the 123 powder. Solubility of $AgNO_3$ in ethylene glycol was found to be at least 7.5 gm/10 cc. However, if ethylene glycol is added, it must be slowly evaporated at 50 °C prior to firing. The mixture is then heated on a hot plate in a glass beaker to melt the nitrate completely (> 222 °C) while stirring. After cooling to room temperature, the mixture is ground to break up the aggregates into a fine powder, transferred to an alumina crucible and heated to approximately 500 °C to decompose the nitrate to metallic silver.

The composite powder was converted into a wire via swaging. Typically, the powder is packed into a copper or silver tube as shown schematically in Figure 1. Tube size and drawing die size sequences are shown in Table 1. The copper tubes, which require intermediate annealing during the swaging process, proved reactive towards 123 even at the relatively low annealing temperatures (e.g. - 400 °C). This mandates the use of silver tubes to avoid degradation of the 123 powder.
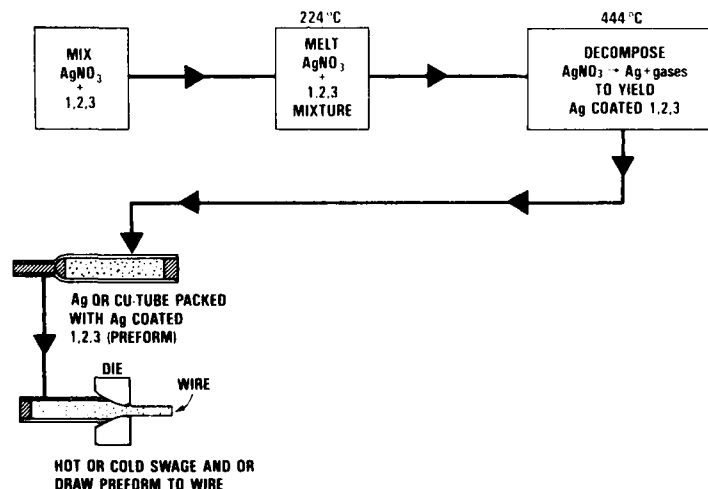
Fig. 1 HTS Wire Processing Flow Chart

Table I
Details of Ag/HTS Preform Preparation

	Ag tube preforms	Cu tube preforms
powder weight (gms)	12	15
tube length inches (mms)	6(152.4)	6(152.4)
outside diameter inches (mms)	0.290(7.36)	0.365(9.27)
inside diameter inches (mms)	0.245(6.22)	0.300(7.62)
die sequence diameter inches (mms)	0.250(6.35)	0.335(8.50)
	0.234(5.94)	0.299(7.59)
	0.203(5.15)	0.250(6.35)
	0.187(4.74)	0.234(5.94)
		0.203(5.15)
		0.187(4.74)
after jacket removal inches (mms)	0.155(3.93)	0.155(3.93)

The formulation of an HTS paint using $AgNO_3$ is outlined in Figure 2. The $AgNO_3$ powder is ground and added to the HTS powder (123 was used in this case, but another HTS compound could be substituted), to produce 15 w/o Ag after decomposition. A sufficient quantity of pure ethylene glycol is added to the HTS/$AgNO_3$ mixture to uniformly disperse the $AgNO_3$ particles through the HTS mass. The 123/$AgNO_3$ /glycol mixture (in the form of a slurry) is applied to the substrate (e.g., Al_2O_3 and ThO_2) by brushing or spray, and the ethylene glycol is evaporated slowly at 50 °C. Careful evaporation of the ethylene glycol is essential because at temperatures significantly higher than 50 °C, ethylene glycol may combust and alter the final product properties. Finally, the substrate with the superconducting paint is heated at 460 °C, sintered at 900 °C in 3 % O_2 atmosphere, and then annealed at temperatures in the range 400-600 °C in 100% O_2. In order to attain smooth and uniform film surface, the HTS powder particle size should be very fine (. 10 μm). The minimum thickness of the paint or film produced by this method is equal to the average HTS powder particle size.

The choice of a substrate is critical for successful coating. The substrate must be able to tolerate the sintering temperature without cracking or chemically reacting with the HTS matrix. Its thermal expansion must match that of the superconductor, such that the film remains under compression during thermal cycling. This retards the formation of microcracks which impair J_c and broaden the superconducting transition. The substrate must not produce too large of a compressive stress, however, or separation of the film could occur. Various substrates have been tested in the course of several HTS thin film efforts.[17-19] These include Ba-Ti, Ni-Al-Ti, Al_2O_3, spinel, MgO, SiO_2, and $SrTiO_3$, and YSZ (yttria stabilized zirconia). Those containing Ni or Ti experienced some degree of chemical reaction. The most successful substrates were those of spinel and YSZ. These yielded complete superconducting transitions with T_c of about 81 K and transition widths of less than 10 K.

Typically, the 123/$AgNO_3$/glycol was brush painted on an Al_2O_3 and ThO_2 (thoria) tube sections. In each case the ethylene glycol was slowly evaporated at 50 ° C. The tubes were subsequently fired at 460 °C to decompose the $AgNO_3$. This operation was carried several times to produce desired coating thickness generally 0.0005-0.003" (0.0127-0.0762 mm). Finally, the tubes were sintered overnight at 900 °C and annealed at 400 °C in air.
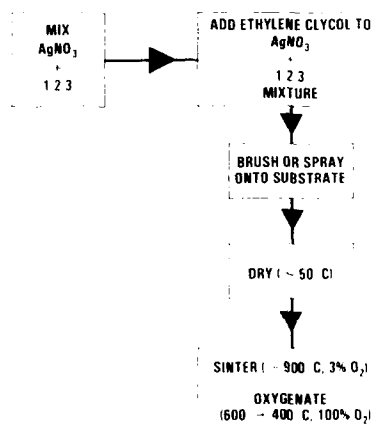
```
       ┌─────────┐        ┌──────────────────────┐
       │  MIX    │        │ ADD ETHYLENE GLYCOL TO │
       │ AgNO₃   │──────▶ │        AgNO₃          │
       │   ·     │        │         ·             │
       │  123    │        │        123            │
       └─────────┘        │      MIXTURE          │
                          └──────────────────────┘
                                    │
                                    ▼
                          ┌──────────────────────┐
                          │   BRUSH OR SPRAY      │
                          │   ONTO SUBSTRATE      │
                          └──────────────────────┘
                                    │
                                    ▼
                               DRY ( ~ 50 C)
                                    │
                                    ▼
                          SINTER ( ~ 900 C, 3% O₂)

                             OXYGENATE
                          (600 → 400 C, 100% O₂)
```

Fig. 2. HTS Paint Processing Flow Chart

T_c and J_c measurements:

Transition temperature and current carrying capacity were measured by the standard, 4-point method. Silver paste was utilized for connecting copper wire leads to the superconductor. In some later work, the copper wire leads were joined to the superconductor using $AgNO_3$ decomposition process. It was observed that the presence of very low resistance Ag sheath both prevented proper O_2 anneal after swaging and rendered measurement difficult because of current requirements and instrumental sensitivity. The silver sheath, therefore, was removed by machining to facilitate T_c and J_c measurements on the core, composed entirely of the Ag/123 composite superconductor. The J_c measurements were made at 77 K and zero magnetic field. A Keithly model 503 milliohmmeter was used.

Sample Characterization:

A combination of bulk and surface analytical techniques such as X-ray diffraction (XRD), X-ray photoelectron spectroscopy (XPS), and scanning electron microscopy (SEM) were used to investigate the structure, chemistry, and morphology of the Ag/123 composite material.

The X-ray diffraction patterns were collected by means of a Siemens Theta-Theta D500 diffractometer over the range of 2θ values between 10° and 80° using copper K_a X-ray radiation (= 1.5405 Å) with diffracted beam monochromator. The 123 control sample and Ag/123 composite powder were ground into fine powder and mounted onto a zero-back-ground quartz support via petroleum type jelly.

XPS spectra were obtained with a Physical Electronics 5400 photoelectron spectrometer under computer control. All spectra were obtained with an unmonochromatized Mg x-ray source (h = 1253.6 eV) operated at 15 KV with the anode drawing a current of 27 mA. The analysis chamber pressure was kept below $5x10^{-9}$ Torr. The XPS analysis area was 1x3 mm^2 for all samples. The resolution of the analyzer was set to give a full-width-at-half-maximum (FWHM) of 1.00 eV for the sputter-cleaned Ag $3d_{5/2}$ transition line. Binding energies were referenced to adventitious carbon (C 1s at 284.6 eV) which puts the Ag $3d_{5/2}$ transition line at 368.2 eV. For binding energy and quantitative concentration information, the photoelectron peaks were fit with a Gaussian line shape except for the Ag 3d lines where a combined Gaussian-Lorentzian line shape was employed.

SEM was used to investigate the grain boundary structure, the uniformity of dispersion and morphology of the Ag crystallites, and composition. An Amray 1000A SEM operated at an electron beam voltage of 20 KeV, current of 0.01 na, and a diameter of the order of 100 Å was used in this investigation. Experiments were performed at a system pressure better than 10^{-6} Torr.

RESULTS AND DISCUSSION

Silver nitrate is a white crystalline solid with a melting point to a liquid phase at 222 °C. The liquid decomposes as its temperature is raised to 444 °C according to

$$AgNO_3 \longrightarrow AgNO_3 \text{ (liquid) } @ 222 °C$$

and
$$2AgNO_3 \longrightarrow 2Ag + 2NO_2 + O_2 @ 444 °C$$
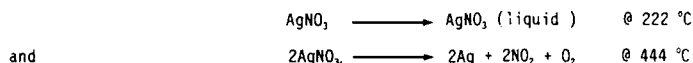
evolving nitrogen dioxide and oxygen, leaving high purity Ag deposit. The $AgNO_3$ liquid formed at > 222 °C is observed to have very low viscosity. As a consequence, it spontaneously flows and wets the 123 powder. After further heating above its melting point, the nitrate decomposes leaving a uniform and adherent deposit of Ag on the 123 powder.

The effort thus far has concentrated on material containing 15 wt/o Ag based primarily on the knowledge that "Percolation" effect is operative up to ~ 35 wt/o Ag.[20] For these concentrations, the volume of AgNO, liquid is sufficient to adequately encapsulate the 123 powder mass. The 123/Ag powder was prepared in batches of 10 to 15 grams. A small portion of the composite powder (approximately 2 grams) was pressed into a pellet. Once it was determined that the pellet exhibited the Meissner effect, the composite material was processed into a wire or rod configuration via swaging (Figure 1). Initial swaging experiments were very ambitious. The preform is reduced from the starting outside diameter of 0.250" (6.35 mm) to as low as 0.030" (0.762 mm) without intermediate annealing. As mentioned previously, the high conductivity of Ag interfered with T_c and J_c measurements. The Ag/123 powder had suffered deformation beyond its formability limits and 'sausaging' familiar in the low temperature superconductor processing was encountered.[21] Swaging, therefore, was terminated at a convenient stage where the removal of the Ag Sheath was possible by machining and the core material 0.155" (3.93 mm) was free from sausaging effects.

Typical curves of resistance and magnetic susceptibility vs. temperature for such rods are shown in Figure 3. The relatively high density (~ 90-95 %) of the swaged rod probably contributes to the sharpness of the transition. The J_c values at this early stage, however, did not exceed 200 A/cm^2. Increasing sintering temperature to more than 950 °C and increasing the annealing time from 18 hours to 72 hours did not affect J_c.
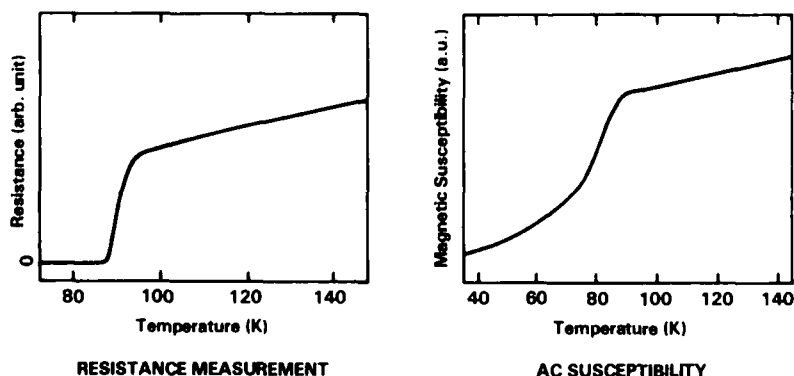

RESISTANCE MEASUREMENT   AC SUSCEPTIBILITY

Fig. 3. Superconducting Transition of $YBa_2 Cu_3 O_x$ - 15 w/o Ag Composite

The sensitivity of the 123/Ag composite powder to environmental degradation is well documented.[17,22] To determine the protection provided by the coating, one sample exposed to laboratory air was tested several times in a period of three months. The J_c values remained constant (~150 A/cm²) indicating that the silver coating is responsible for the stability of the sample.

Recent experiments in collaboration with Dr. Poeppel of the Argonne National Laboratory, Argonne, IL, led to a cooperative effort in which both their 123 powder was coated with Ag by NSWC using the $AgNO_3$ process. Argonne then extruded the powders into fine diameter wires by the slurry extrusion method. A photograph of a wire fabricated by the slurry extrusion method and a coil made from this wire is shown in Figure 4. The J_c values on a straight wire 0.050" (0.127 mm) prepared thus was 400 A/cm². In a coil configuration, this value dropped to 250-300 A/cm².

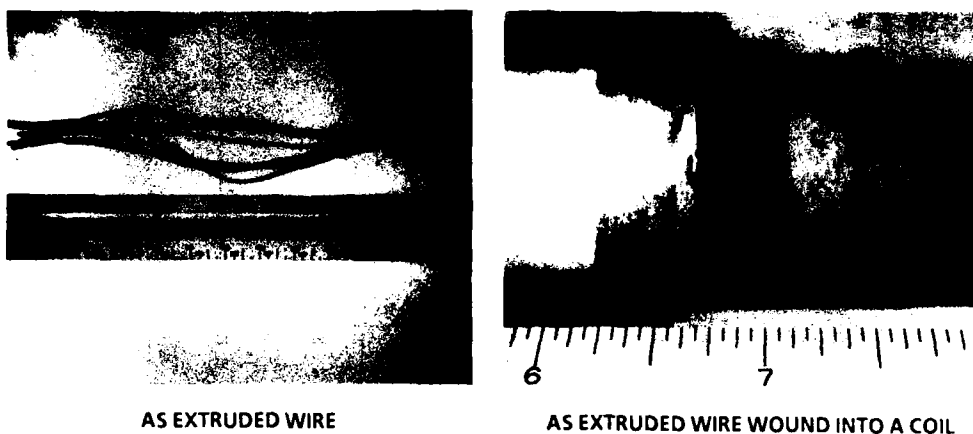**AS EXTRUDED WIRE**   **AS EXTRUDED WIRE WOUND INTO A COIL**

Fig. 4. A photograph of a wire fabricated by the slurry extrusion method

T_c and J_c measurements for the superconducting paint were also made. A quite sharp drop in resistance was observed at about 81 K, however, a small residual resistance remained at 77 K for the superconducting paint on the Al_2O_3 substrate. The curve remained unchanged with further annealing in O_2. This indicated the possibility of unhealed microcracks in the coating due to mismatch in thermal expansion of the superconducting paint and the substrate. For the superconducting paint on the ThO_2 substrate, on the other hand, a complete superconducting transition at T_c of about 81 K with several degrees width was observed (Figure 5). After thermal cycling and several months exposure to ambient conditions, during which no particular precautions to protect the superconducting paint were taken, a second measurement of T_c was made (Figure 5). The new measurement indicates essentially the same superconducting behavior. Hence, a reasonably stable and fully superconducting paint film at 77 K was successfully produced. J_c measurements on this film indicates a value of only 0.30 Amps/cm² at 77 K. While some applications of HTS coatings might not need a substantial J_c, most involving microwave handling will require at least moderately high J_c. Proper choice of substrate and sintering/oxygenation heat treatment should produce the improvement required for many applications.
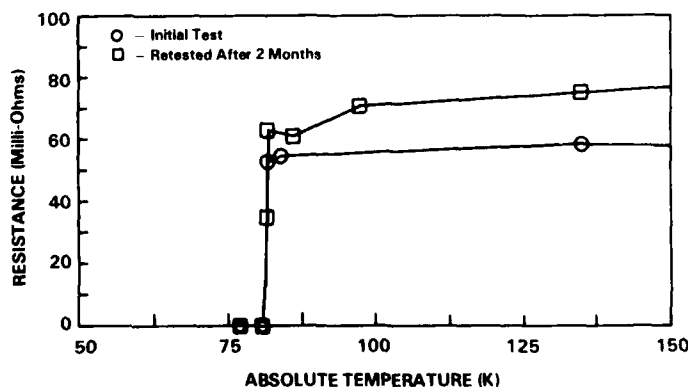

Fig. 5. Super Conducting Transition For HTS Paint

X-ray diffraction analysis is used to detect if there are any compositional changes occurring during the fabrication process. Figure 6 displays the XRD pattern of the as received 123 superconductor material indicating the material consists mainly of the 123 phase and of only a small quantity of $BaCuO_2$ impurity. After decomposition of the $AgNO_3$ step, the XRD pattern (Figure 7) consist mainly of Bragg diffraction lines which correspond to the 123 phase and metallic silver as expected.
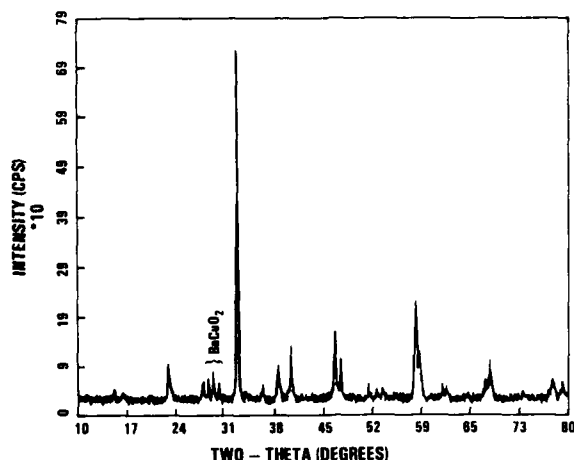

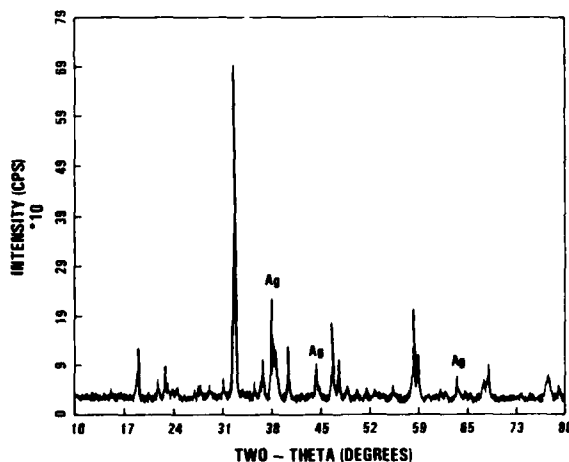Fig. 6. X-Ray Diffraction Pattern of As Received 1 2 3 Powder with Bragg Lines

Fig. 7. X-Ray Diffraction Pattern after $AgNO_3$ Decomposition onto 1 2 3 Powder

After each of the swaging and the final sintering steps the XRD pattern is qualitatively similar to that taken after the $AgNO_3$ decomposition step with no change in composition except for a reduction in the amount of metallic Ag present. The percent ratio of intensity for the most intense Bragg line of Ag to that of the most intense line of 123 has dropped from 30 (value after the $AgNO_3$ decomposition) to 17 after swaging and to 13 after sintering. A reduction and quite possibly agglomeration of Ag after sintering at 925 °C is expected due to a high vapor pressure of Ag which has a melting point of 960 °C. Furthermore, results of analysis of the XRD data presented in Table II indicate that significant changes are induced in the full-width-at-half-maximum (FWHM) and/or peak positions of the Bragg diffraction lines after the $AgNO_3$ decomposition, swaging, and sintering steps. The origin of these variations is not yet understood, but may be related to a change in the oxygen content of the 123 lattice or stresses introduced during processing. More work must be undertaken to correlate the physical state of the 123 material (with respect to strain, degree of shear, etc.) during mechanical processing with its degree of retention for the superconducting properties.

Table II
Summary of XRD Results of 123 coated with 15 w/o Ag Via AgNO₃ Process

Preparation Procedure Step	Peak Position , 2θ	FWHM
123 Argonne as received	32.550	0.272
	32.865	0.312
123 coated with AgNO₃	32.550	0.255
	32.865	0.328
123 after AgNO₃ decomposition at 470 °C	32.538	0.203
	32.844	0.243
123/15 w/o Ag swaged in Ag tube	32.486	0.260
	32.817	0.296
123/15 w/o Ag swaged in Ag tube sintered at 925 °C	32.522	0.254
	32.834	0.305

Chemical state identification and atomic percent determination were made from high resolution XPS scans of regions corresponding to the C 1s, O 1s, Cu $2p_{3/2}$, Y 3d, Ba $3d_{5/2}$, and Ag 3d lines. XPS analysis shows that the near surface region composition contains significant amounts of Ba carbonate and probably $BaCuO_2$ in addition to the 123 phase and Ag. The x-ray photoelectron spectrum of the 3d transition lines for Ag in the 123/15 w/o Ag composite powder is compared with that of a clean-sputtered surface of metallic silver in Figure 8. The binding energy of the Ag $3d_{5/2}$ and $3d_{3/2}$ lines for the composite powder were each shifted by 0.4 eV to lower binding energy relative to metallic silver. Furthermore, the Ag $3d_{5/2}$ and Ag $3d_{3/2}$ for the composite powder were significantly broader than those of metallic silver. The Ag $3d_{5/2}$ and $3d_{3/2}$ transition lines of the composite powder had each a full-width-at-half-maximum of 1.4 eV compared to 1.0 eV for metallic silver. These observations were similar for composite material with current carrying capacity of 200 or 400 A/cm^2 and were also similar for Ag on the cylindrical outside surface or an air-fractured cross sectional area of the superconducting wire. Based on a shift of 0.4 eV to lower binding energy and a broadening in the full-width-at-half-maximum, we conclude that the chemistry of Ag in the composite is similar to that of Ag_2O. It is to be noted here that XPS only probes the near surface region of up to 50 Å deep. This observation when combined with those of XRD indicates that the metallic Ag particles in the composite material are encapsulated with a film of Ag_2O.
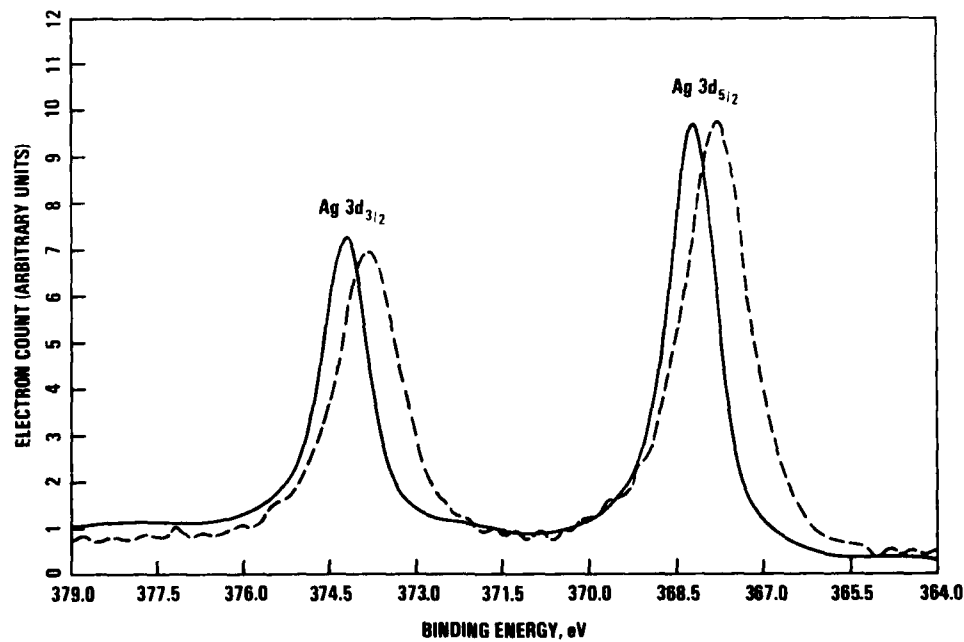

Fig. 8. XPS of Ag 3d Transition from Ag Metal (Solid) and 1 2 3/15 w/o Ag Composite Powder

The optical microstructure of an agglomerate of 123 particles (dark areas) in a silver matrix is presented in Figure 9. The silver coating is continuous with no readily observable porosity. Under higher magnification SEM examination, a typical 123 particle in the as received state is characterized by high surface area (Figure 10, left photo). After treatment with silver nitrate (Figure 9, right photo) the surface is devoid of all the surface asperities and morphological features, indicating that the process is capable of depositing Ag on large as well as fine particles. This feature of the process is very important because the coating is necessary to permit Cooper pairs to travel from one superconducting grain to the next. This phenomenon is commonly referred to as the "Proximity" effect,[23] and is necessary to enhance the coupling between the grain boundaries of the 123 particles. Comparison of silver maps indicates that samples with current carrying capacity of 400 A/cm^2 has better Ag uniformity on the surface than those with current carrying capacity of 200 A/cm^2. This indicates the need for improvements in the Ag coating process in order to enhance the coupling between the grain boundaries of the 123 phase and Ag and, thus, attain higher critical currents.
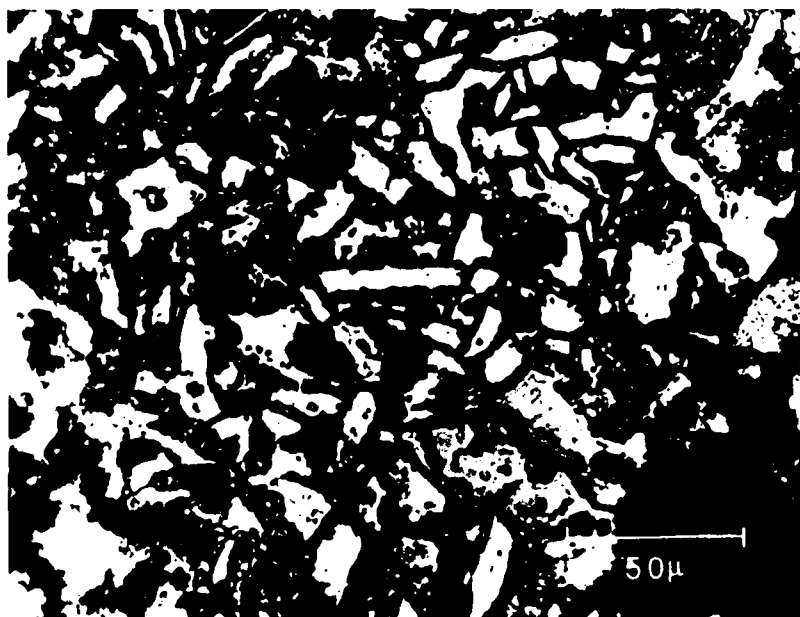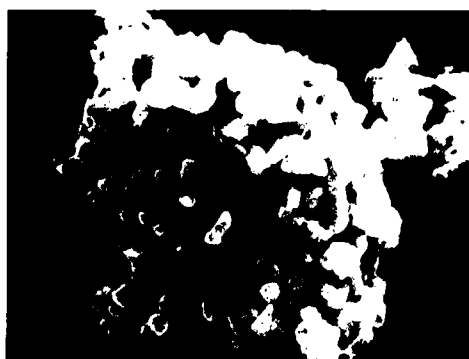

Fig. 9. Microstructure of YBCO Powder Mass Infiltrated with Ag from AgNo$_3$
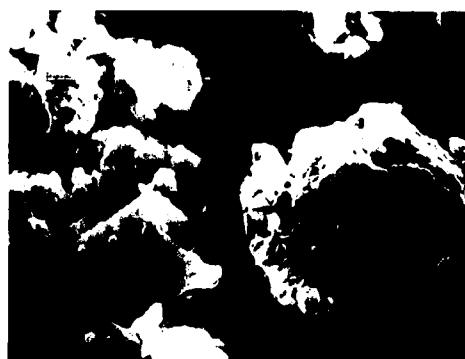
AS RECEIVED   **Ag COATED**

MAG: 10,000 X   1 μm   MAG: 10,000 X   1 μm

Fig. 10. SEM Photo of YBCO (123) Powder

Large area (1mm x 1mm) EDAX elemental analysis of a sample with current carrying capacity of 200 A/cm² after the various preparation procedure steps are summarized in Table III. The depth of EDAX analysis is approximately 2 μm. The data in Table III indicates that the composition of the near surface region (approximately, 2μm deep) of the as received 123 material, 123 coated with $AgNO_3$, 123 after $AgNO_3$ decomposition, and 123 after swaging but no sintering is deficient in Y. This observation is qualitatively consistent with those of XRD and XPS which indicates the presence of $BaCuO_2$ and Ba carbonate species, respectively. The data in Table III also indicates that the Ag content is approximately 50 % of its nominal value. After the swaging process, a reduction in the Ag content is observed, in agreement with the XRD results, which may be due to the break up of the 123 particles and the production of fresh, Ag uncoated surfaces. Further reduction in the Ag content is also observed after the sintering step, in agreement with the XRD results. As mentioned earlier, this observation may be due to a high vapor pressure of Ag at the high sintering temperature. Small area (of the order of 1μm x 1μm) EDAX analysis of various spots showed significant variations in the Ag content ranging form almost zero to fifty atomic percent indicating the presence of Ag rich and Ag poor spots on the surface. It is noteworthy to mention here that an Ag coating of thickness less than 500 Å will give a very weak signal and may not be detected with EDAX.

Table III
Summary of EDAX Elemental Analysis of 123 and 123/15 w/o Ag

Preparation Procedure Step	Atomic percent of				Empirical Formula
	Y	Ba	Cu	Ag	
123 Argonne as received	09.37	36.28	54.06		$Y_{0.52}Ba_{2.01}Cu_3$
123 coated with $AgNO_3$	09.22	31.63	49.44	09.71	$Y_{0.56}Ba_{1.92}Cu_3Ag_{0.59}$
123 after $AgNO_3$ decomposition at 470 °C	09.93	32.57	48.15	09.35	$Y_{0.62}Ba_{2.03}Cu_3Ag_{0.58}$
123/15 w/o Ag swaged in Ag tube with no sintering	10.90	33.20	50.08	05.82	$Y_{0.65}Ba_{1.99}Cu_3Ag_{0.35}$
123/15 w/o Ag swaged in Ag tube sintered at 925 °C	16.61	36.08	43.81	03.50	$Y_{1.14}Ba_{2.47}Cu_3Ag_{0.24}$
Nominal Composition for 123 with 15 w/o Ag	14.11	28.21	42.30	15.37	$Y_{1.00}Ba_{2.00}Cu_3Ag_{1.09}$

SUMMARY AND CONCLUSIONS

A novel, yet simple process, has been developed to enable silver coating of 123 high temperature superconductor powder precursor for the preparation of wires and rods via swaging, extrusion or other wire-making procedures. The swaging of Ag/123 powder filled silver tubes have been carried out successfully at NSWC. Atmospherically stable rods and wires of 0.1-0.25" (2.5-6.4 mm) outside diameter have been produced. Some difficulties has been encountered with heat treatment and wire property measurements in the presence of the sheath. Measurements on short wire segments indicate a T_c of 92 K with relatively sharp transition region (with only 2-3 degrees width). The maximum J_c measured was 400 A/cm². The rods were found to maintain their superconducting properties in laboratory ambient for at least several months. A series of microscopic studies on the composite powder by XRD, XPS, and SEM revealed a reduction in the Ag content from its nominal value with significant variations in the Ag content between various spots on the surface of the sample.

A recent collaborative effort with Argonne National Laboratory has led to the production of straight and coiled lengths of high temperature superconductor wire from the $AgNO_3$ composite powder process by an extrusion method. These wires have a relatively fine diameter of 0.05" (1.27 mm). J_c measurements performed at 77 K on the wires indicate typically 400 A/cm² on straight sections and 250-300 A/cm² in the coiled form. Prospects for near term improvement in the J_c capacity appear good as the process is optimized for the composite powder.

A process has also been developed at NSWC for production of superconducting paint which may have potential for many electronic device applications.

REFERENCES

1. Wu, M. K.; Ashburn, J. R.; Torng, C. J.; Hor, P. H.; Meng, R. L.; Gao, L. Huang, Z. J.; Wang, Y. Q.; Chu, C. W.: Superconductivity at 93 K in a New Mixed-Phase Y-Ba-Cu-O Compound System at Ambient Pressure, Phys. Rev. Lett. 58(9), 908 (1987).

2. Moodenbaugh, A. R.; Suenaga, M.; Asano, T.; Shelton, R. N.; Ku, H. C.; McCallum, R. W.; Klavins, P.: Superconductivity near 90 K in the Lu-Ba-Cu-O System, Phys. Rev. Lett. 58 (18), 1885 (1987).

3. Murphy, D. W.; Sunshine, S.; van Dover, R. B.; Cava, R. J.; Batlogg, B.; Zahurak, S. M.; Scheemeyer, L. F.: New Superconducting Cuprate Perovskites, Phys. Rev. lett. 58(18), 1888 (1987).

4. Hor, P. H.; Meng, R. L.; Wang, Y. Q.; Gao, L.; Huang, J.; Bechtold, J. Forste, K.; Chu, C. W.: Superconductivity Above 90 K in the Square-Planar System $ABa_2Cu_3O_{6+x}$ with A=Y, La, Nd, Sm, Eu, Gd, Ho, Er, and Lu, Phys. Rev. Lett. 58(18), 1891 (1987).

5. Sheng, Z. Z.; Hermann; A. M.: Bulk Superconductivity at 120 K in the Tl-Ca/Ba-Cu-O, Nature 332, 138 (1988).

6. Sheng, Z. Z.; Hermann, A. M.; El Ali, A. El; Almasan, C.; Estrada, J.; Datta, T.; Matson, R. J.: Superconductivity at 90 K in the Tl-Ba-Cu-O System, Phys. Rev. Lett. 60(10), 937 (1988).

7. Chu, C. W.; Bechtold, J. J.; Gao, L.; Hor, P. H.; Huang, Z. J.; Meng, R. L.; Sun, Y. Y.; Wang, Y. Q.
    Xue, Y. Y.: Superconductivity up to 114 K in the Bi-Al-Ca-Sr-Cu-O Compound System without Rare-Earth
    Elements, Phys. Rev. Lett. 60(10), 941 (1988).

8. Snow, D. B.; Weinberger, B. R.; Peterson, G. G.; Lynds, L.; Eaton, H., Jr.; Burila, C. T.; Potrepka
    D. M.; Kuwabara, M.: Processing, Microstructure and Properties of $YBa_2Cu_3O_{7-x}$, Proceedings of the 1989
    Symposium on High Temperature Superconductor Compounds: Processing and Related Properties, Edited by
    Whang, S. H. and DasGupta, A., the 118th Annual Meeting of The Minerals, Metals & Materials Society,
    Las Vegas, NV, 27-28 February 1989, A Publication of TMS, pp. 121-134.

9. Curreri, P. A.; Peters, P. N.; Leong, P. T.; Chou, H.; Wu, M. K.; Husng, C. Y.: Processing and
    Properties of high T_c oxide/silver matrix composite superconductors, Proceedings of the 1989 Symposium
    on High Temperature Superconductor Compounds: Processing and Related Properties, Edited by Whang, S.
    H. and DasGupta, A., the Annual Meeting of The Minerals, Metals & Materials Society, Las Vegas, NV,
    27-28 February 1989, A Publication of TMS, pp. 143-154.

10. Streitz, F. H.; Cieplak, M. Z.; Xiao, G; Gavrin, A.; Bakhshai, A.; Chien, C. L.: Superconducting Au-
    YBa_2Cu_3O, Composites, Appl. Phys. Lett. 52(11), 927 (1988).

11. Ho, C. T.; Chung, D. D. L.: Carbon Fiber Reinforced Tin-Superconductor Composites, J. Mater. Res.
    4(6), 1339 (1989).

12. Singh, J. P.; Shi, D.; Capone, D. W.: Mechanical and Superconducting Properties of Sintered Composite
    $YBa_2Cu_3O_{7-x}$ Tape on Silver Substrate, Appl. Phys. Lett. 53(3), 237 (1988).

13. Tiefel, T. H.; Sherwood, R. C.; Jin, S.; Fastnacht, R. A.: Fabrication of High T_c Superconductor Wires,
    Proceedings of the 1989 Symposium on High Temperature Superconductor Compounds: Processing and Related
    Properties, Edited by Whang, S. H. and DasGupta, A., the 118th Annual Meeting of The Minerals, Metals
    & Materials Society, Las Vegas, NV, 27-28 February 1989, A Publication of TMS, pp. 465-470.

14. Hojaji, H.; Micheal, K. A.; Barkatt, A.; Thorpe, A. N.; Ware, M. F.; Talmy, I.; Haught, D. A.;
    Alterescu, S.: A Comparative Study of sintered and Melt-Grown Recrystallized YBa_2Cu_3O, J. Mater. Res.
    4(1), 28 (1989).

15. Hermann, A. M.; Sheng, Z. Z.; EL Ali, A.; Mooney, G. D.; Nelson, A. J.; Goral, J.; Kazmerski, L. L.:
    Structural and Elemental Analysis of Melt-Processible High-Temperature Superconductors by Surface
    Science and X-Ray Diffraction Measurements, J. Appl. Phys. 64(10), 5056 (1988).

16 Shin, K. H.; Whang, S. H.; Karmarkar, S.; Divecha, D.: Preparation and Properties of Yb-Ba-Cu-O-Ag
    Superconductors Via Melt Spinning-Oxidation Route, Proceedings of the 1989 Symposium on High
    Temperature Superconductor Compounds: Processing and Related Properties, Edited by Whang, S. H. and
    DasGupta, A., the 118th Annual Meeting of The Minerals, Metals & Materials Society, Las Vegas, NV,
    27-28 February 1989, A Publication of TMS, pp. 495-502.

17. Chang, C.: Reduced Moisture-Induced Degradation of YBaCuO Superconducting Films by Silver and High
    Deposition Temperatures, Appl. Phys. Lett. 53(12), 1113 (1988).

18. Leskela, M.; Truman, J. K.; Mueller, C. H.; Holloway, P. H.: Preparation of Superconducting Y-Ba-Cu-
    O Thin films, J. Vac. Sci. Technol. A 7(6) 3147 (1989).

19. Bansal, N. P.; Simons, R. N.; Farrell, D. E.: High T_c Screen-Printed $YBa_2Cu_3O_{7-x}$: Effect of the Substrate
    Material, Appl. Phys. Lett. 53(7), 603 (1988).

20. Singh, J. P.; Leu, H. J.; Poeppel, R, B.; van Voorhees, E.; Goudey, G. T.; Winsley, K.; Shi, D.:
    Effect of Silver and Silver Oxide Additions on the Mechanical properties and Superconducting Properties
    of $YBa_2Cu_3O_{7-x}$, J. Appl. Phys. 66(7), 3154 (1989).

21. Collings, E. W.; Editor, Design and Fabrication of Conventional and Unconventional Superconductors,
    Noyes Publication, 1984.

22. Chen, K.; Maheswaran, B.; Liu, Y. P.; Giessen, B. C.; Chan, C.; Markiewicz, R. S.: Critical Current
    Enhancement in Field Oriented $YBa_2Cu_3O_{7-x}$, Appl. Phys. Lett. 55(3), 289 (1989).

23. Chen, I; Sen, S.; Stefanescu, D. M.: Production of Stabilized Superconducting Metal/YBa_2Cu_3O Composites
    by Conventional Metallurgical Techniques, in "Processing and Applications Of High T Superconductors:
    Status and Prospects," Proceedings of the 4th Annual Northeast Regional Meeting, TMS, 9-11 May 1988,
    pp. 151-160.

ACKNOWLEDGEMENT

REPORT DOCUMENTATION PAGE

1. Recipient's Reference	2. Originator's Reference	3. Further Reference	4. Security Classification of Document
	AGARD-CP-481	ISBN 92-835-0586-7	UNCLASSIFIED

5. Originator	Advisory Group for Aerospace Research and Development North Atlantic Treaty Organization 7 rue Ancelle, 92200 Neuilly sur Seine, France

6. Title	APPLICATIONS OF SUPERCONDUCTIVITY TO AVIONICS

7. Presented at	the Avionics Panel Specialists' Meeting held in Bath, England, 7th—8th May 1990.

8. Author(s)/Editor(s)	9. Date
Various	October 1990

10. Author's/Editor's Address	11. Pages
Various	166

12. Distribution Statement	This document is distributed in accordance with AGARD policies and regulations, which are outlined on the Outside Back Covers of all AGARD publications.

13. Keywords/Descriptors

Avionics	Low Tc superconductors
Closed cycle refrigerators	Superconductors
High Tc superconductors	Superconductivity

14. Abstract

Recent advances in developing high temperature superconductors have renewed interest in the entire superconductivity field. Modern techniques in materials preparation are making it possible to fabricate a number of new superconducting components which promise significant improvements in the performance of avionics systems. The almost daily revelation of advances in this area attests to its importance as an emerging technology. This Specialists' Meeting brought together device scientists and avionics engineers to explore the possibilities for exploiting all aspects of superconductivity in avionics systems.

AGARD Conference Proceedings No.481
Advisory Group for Aerospace Research and Development, NATO
APPLICATIONS OF SUPERCONDUCTIVITY TO AVIONICS
Published October 1990
166 pages

Recent advances in developing high temperature superconductors have renewed interest in the entire superconductivity field. Modern techniques in materials preparation are making it possible to fabricate a number of new superconducting components which promise significant improvements in the performance of avionics systems. The almost daily revelation of advances in this area attests to its importance as an emerging technology.

P.T.O.

AGARD-CP-481

Avionics
Closed cycle
  refrigerators
High Tc superconductors
Low Tc superconductors
Superconductors
Superconductivity

AGARD Conference Proceedings No.481
Advisory Group for Aerospace Research and Development, NATO
APPLICATIONS OF SUPERCONDUCTIVITY TO AVIONICS
Published October 1990
166 pages

Recent advances in developing high temperature superconductors have renewed interest in the entire superconductivity field. Modern techniques in materials preparation are making it possible to fabricate a number of new superconducting components which promise significant improvements in the performance of avionics systems. The almost daily revelation of advances in this area attests to its importance as an emerging technology.

P.T.O.

AGARD-CP-481

Avionics
Closed cycle
  refrigerators
High Tc superconductors
Low Tc superconductors
Superconductors
Superconductivity

AGARD Conference Proceedings No.481
Advisory Group for Aerospace Research and Development, NATO
APPLICATIONS OF SUPERCONDUCTIVITY TO AVIONICS
Published October 1990
166 pages

Recent advances in developing high temperature superconductors have renewed interest in the entire superconductivity field. Modern techniques in materials preparation are making it possible to fabricate a number of new superconducting components which promise significant improvements in the performance of avionics systems. The almost daily revelation of advances in this area attests to its importance as an emerging technology.

P.T.O.

AGARD-CP-481

Avionics
Closed cycle
  refrigerators
High Tc superconductors
Low Tc superconductors
Superconductors
Superconductivity

AGARD Conference Proceedings No.481
Advisory Group for Aerospace Research and Development, NATO
APPLICATIONS OF SUPERCONDUCTIVITY TO AVIONICS
Published October 1990
166 pages

Recent advances in developing high temperature superconductors have renewed interest in the entire superconductivity field. Modern techniques in materials preparation are making it possible to fabricate a number of new superconducting components which promise significant improvements in the performance of avionics systems. The almost daily revelation of advances in this area attests to its importance as an emerging technology.

P.T.O.

AGARD-CP-481

Avionics
Closed cycle
  refrigerators
High Tc superconductors
Low Tc superconductors
Superconductors
Superconductivity

This Specialists' Meeting brought together device scientists and avionics engineers to explore the possibilities for exploiting all aspects of superconductivity in avionics systems.

Papers presented at the Avionics Panel Specialists' Meeting held in Bath, England 7th and 8th May 1990.

ISBN 92-835-0586-7

This Specialists' Meeting brought together device scientists and avionics engineers to explore the possibilities for exploiting all aspects of superconductivity in avionics systems.

Papers presented at the Avionics Panel Specialists' Meeting held in Bath, England 7th and 8th May 1990.

ISBN 92-835-0586-7

This Specialists' Meeting brought together device scientists and avionics engineers to explore the possibilities for exploiting all aspects of superconductivity in avionics systems.

Papers presented at the Avionics Panel Specialists' Meeting held in Bath, England 7th and 8th May 1990.

ISBN 92-835-0586-7

This Specialists' Meeting brought together device scientists and avionics engineers to explore the possibilities for exploiting all aspects of superconductivity in avionics systems.

Papers presented at the Avionics Panel Specialists' Meeting held in Bath, England 7th and 8th May 1990.

ISBN 92-835-0586-7